Long-term interactions between shrub growth and soil nitrogen availability in the Western Siberian tundra:

application of mechanistic modelling approaches using wood-ring data

Andrew C Martin

Thesis submitted for the degree of Doctor of Philosophy

Department of Zoology, University of Oxford

68,000 words

Trinity Term 2019

St Edmund Hall
University of Oxford

Abstract

Rationale. Shrub growth and expansion is occurring in the Arctic, with implications for global climate. Multiple strands of evidence demonstrate an important role of recent increases in tundra air temperatures in enhanced growth of deciduous shrubs at the expense of graminoids and mosses, commonly termed 'shrubification'. However, shrub growth responses are heterogeneous through both space and time, as evidenced by: (a) meta-analyses of the climate-sensitivity of shrub wood production through time; and (b) progressive declines in the strength of the relationship between remotely sensed vegetation productivity and warming air temperatures. It is plausible that – over decades – soil nitrogen (N) availability may contribute to the observed heterogeneity of shrub growth sensitivity to climate. My key aim was to quantify and identify the presence of N-limitation to shrub growth and its variability in space and through time in Western Siberia, Russia.

Method. First, to determine the status of the evidence base for alternative controls on shrub growth, including soil N, I created and followed an evidence mapping protocol to generate a spatial-temporal evidence map. Second, I analysed stable nitrogen isotope ratios ($\delta^{15}N$) in *Salix lanata* L. shrub wood rings, which provided annually resolved time-series to indicate local-scale N availability. I created annual resolution $\delta^{15}N$ time series for ten individuals at Yuribei (1980-2013), Yamal Peninsula, and three-yearly resolution time-series for ten shrub individuals at each of three sites within Western Siberia (1940-2013). I interrogated the $\delta^{15}N$ and ring width time-series for shrub individuals by creating mechanistic representations of shrub-nitrogen dynamics; I then identified the most appropriate representations of N-dependency and other environmental constraints on individual shrub growth. Third, I assessed the role of snow dynamics in controlling the relations between nitrogen and shrub growth by extending the modelling approach to incorporate seasonality. Here, snow variability was proxied at a regional scale by earth observation and a local scale by the investigation of $\delta^{18}O$ and $\delta^{13}C$ isotope time series from wood rings. A software library, *Bristlecone*, was developed and used to conduct model-fitting and model-selection of mechanistic models.

Results. First, the evidence map identified that there were spatial-temporal limitations within the recent evidence for controls on Arctic shrubification processes, including constraints on the temporal extent and resolution of N-limitation effects on shrub growth. Second, reconstructed $\delta^{15}N$ time-series indicated that declines in N availability to the *Salix lanata* shrubs have occurred over

decades. Although declines in soil N were observed in Arctic bioclimatic subzones D and E, different trajectories occurred at fine spatial resolution. Interrogation of the $\delta^{15}N$ and ring width time-series indicated that the growth of all shrub individuals assessed has been N-limited; and for a majority of these, plant-soil litter feedbacks were a significant determinant of shrub-nitrogen dynamics. Model-inferred dynamics also suggested that the ratio of shrub N uptake to soil N supply has increased over decades. I identified summer air temperature as an important control on individual shrub growth rates in Western Siberia but that this has declined over recent decades. In addition, the growth of shrub individuals at Yuribei was sensitive to the length and timing of the snow-free growing season, but analysis of nitrogen-shrub dynamics did not identify snow depth effects to soil N replenishment rates nor shrub biomass protection.

Implications. The findings challenge a key assumption that rising air temperatures have led to universal increases in N availability within tall shrub-dominated Arctic tundra environments. Although all *Salix lanata* individuals studied were N-limited over decades, the strength and form of limitation varied, with implications for modelling of these dynamics in Earth System Models. The presence of strong litter feedbacks and relative insensitivity of shrub-nitrogen relations to snow-induced microclimatic effects suggest that shrub establishment and maturation provides a greater long-term control on N availability than climatic controls.

Author Contributions

Paper 1 (Chapter 2). Dr Macias-Fauria, Dr Myers-Smith, Dr Jeffers, and I developed the conceptual approach, I developed and conducted the evidence protocol and analysis, Dr Petrokofsky provided advice on research coding, and I led the writing of the manuscript.

Paper 2 (Chapter 3). I developed the nitrogen isotope method, determined mathematical models, implemented, and conducted the mathematical modelling method, and led the writing of the manuscript. Dr Jeffers and Dr Macias-Fauria conceptualised the research. Prof Bonsall provided guidance on the modelling approach. Prof Forbes, and Dr Macias-Fauria completed field work, and Pentti Zetterberg created original ring width chronologies. I contributed the nitrogen isotope time series. I led the writing of the manuscript and all authors contributed to this.

Paper 3 (Chapter 4). I developed the nitrogen isotope method, determined mathematical models, implemented, and conducted the mathematical modelling method, and led the writing of the manuscript. Dr Jeffers and Dr Macias-Fauria conceptualised the research. Prof Forbes, and Dr Macias-Fauria completed field work, and Pentti Zetterberg measured and cross-dated ring widths. I contributed the nitrogen isotope time series. I led the writing of the manuscript and all authors contributed to this.

Paper 4 (Chapter 5). I conceptualised the research. I contributed the stable oxygen and carbon isotope time series. Model hypotheses were developed with advice from Dr Jeffers and Dr Macias-Fauria. I led the writing of the manuscript and all authors contributed to this.

Paper 5 (Chapter 6). I am the sole author of this manuscript.

Appendix 1. William Harvey and I developed the concept for the Global Pollen Project; I implemented the ideas into a database and web app. Continued revision of the framework was conducted by myself and William Harvey. The authors contributed equally to the manuscript.

Acknowledgements

This work would not have been possible without the continued support of my parents. We have had many discussions about the technicalities of willow growth while at the same time rooting them out of broken stone field drains. Rachel Mary Martin (née Gwynn) probably knows the details of this research as well as I do myself, having had to put up with sustained whirring of computer fans over multiple years, and having listened to seemingly endless model-fitting and mathematical concerns. I thank Ffinlo Moore and Dr William Harvey for being constant support especially during the final year of the DPhil for being understanding and caring friends. William's model-themed best man's speech may have confused some of the elderly relatives but was a much-appreciated light-hearted take on my time in Oxford.

I would like to thank my co-supervisors Dr Lizzy Jeffers and Dr Marc Macias-Fauria for their continued support and engagement with this research. I thank my third supervisor Prof Kathy Willis for opening up additional opportunities. I would also like to give a special mention to Dr Peter Long and Dr Gillian Petrokofsky who have provided substantial support, guidance, and encouragement over a number of years, and this research would not have been the same without them.

I would like to thank my examiners, Dr Rob Salguero-Gómez (University of Oxford) and Prof Howard Epstein (University of Virginia) who have provided valuable contributions to the final work and subsequent papers.

Thanks also go to support over four years to colleagues at the Oxford Long-Term Ecology Lab, including fellow DPhil old-hands Dr Catherine Gretsy, Dr Heri Andrianandrasana, Dr Heinrik Hannerman, and fresh faces Matthew Jordon and Francesco Pelizza. Danielle Sinclair provided

outstanding support and help with the technical lab parts of this thesis. Thanks also to Dr Susanna Vogel, Alistair Yeomans, Eva Macias-Fauria, and Dr Sandra Nogué for their support.

I thank the Natural Environment Research Council of the UK for funding my DPhil research, and the Isle of Man Government for the annual Gubay Award for additional research costs. St Edmund Hall also provided funding for fieldwork in Finnish Lapland and course fees for a wood anatomy course in the Swiss Alps.

Table of Contents

Table of Figures

List of Tables

Abbreviations

AGR	Absolute Growth Rate
AM	Arbuscular Mycorrhizae
CF-IRMS	Continuous Flow Mass Spectrometer
CRU-TS	Climate Research Unit Time Series
DON	Dissolved Organic Matter
ECM	Ectomycorrhizal [fungi]
GDD	Growing Degree Days
GPP	Gross Primary Production
IAEA	International Atomic Energy Agency
ITEX	International Tundra Experiment
MaxNDVI	Maximum Normalised Difference Vegetation Index
MFMS	Model-Fitting and Model-Selection
MLE	Maximum Likelihood Estimate
NDVI	Normalised Difference Vegetation Index
NPK	Nitrogen Phosphorus Potassium [Fertiliser]
PDB	Pee Dee Belemnite
PNL	Progressive Nitrogen Limitation
RGR	Relative Growth Rate
RMSE	Root Mean Square Error
SMOW	Standard Mean Ocean Water
TI-NDVI	Time-Integrated Normalised Difference Vegetation Index

1

Chapter 1

Introduction

1.1 Background

Recent increases in Arctic shrub growth are altering global climate and regional ecosystem processes. Yet there is significant heterogeneity in shrub growth dynamics across space and time. Climate change ecologists are searching for the underlying drivers of so-called 'shrubification' of the Arctic. Much attention has focused on the role of increased temperatures but until recently, broader ecological factors (i.e. biotic interactions; belowground processes) have been largely overlooked. Here I describe research conducted to quantify the potential role of soil available nitrogen in constraining decadal growth dynamics of *Salix lanata* L., a deciduous shrub, in Arctic Russia.

1.1.1 Shrubification of the Arctic tundra

The Arctic tundra is a globally significant terrestrial biome due to its large role in climate regulation. Tundra soils contain 50% of global soil organic carbon stores frozen within permafrost (Hugelius et al. 2014). The dominance of low vegetation - such as creeping dwarf shrubs, graminoids, and mosses – that are easily snow covered provides high albedo (Epstein et al. 2013). Ground-based observations demonstrate that an increase in woody shrub biomass – 'shrubification' – has occurred in the Arctic tundra over recent decades via three processes:

a) **increasing shrub height** (from dwarf or low to tall forms);

b) **shrub infilling** of non-shrub (e.g. graminoids and moss) areas in patchy landscapes; and

c) **northward/upward movement** of shrub species' ranges (Myers-Smith et al. 2011).

Shrubification may play a pivotal role in climate warming through shrub-climate feedback mechanisms (Loranty & Goetz 2012). Evidence from Alaska indicates that lengthening of the snow-free growing season and shrub expansion have both contributed to regional warming over the recent past, although the warming effect arising from shrubification is expected to increase substantially if recent shrubification trends continue (Chapin et al. 2005). Shrub cover is also an important mediator in the regulation of soil carbon stocks: shrub cover can reduce permafrost thaw through shading effects (Blok et al. 2010) but can also extend rooting depth to enable shrubs to access and breakup thawing organic deposits (Blume-Werry et al. 2019). Shrubification occurs primarily through increased deciduous shrub species performance and at the expense of evergreen and dwarf shrubs, graminoids, lichens, and mosses (Frost & Epstein 2014). Ground-based evidence for this ecological change is derived from repeat photography (Sturm et al. 2001; Frost & Epstein 2014; Lantz et al. 2012), the International Tundra Experiment (ITEX) plots (Elmendorf et al. 2011; Epstein et al. 2013), dendrochronological research (Young et al. 2016), and indigenous knowledge (Forbes et al. 2009). Shrubification has been observed across the entire Arctic, with similar observations occurring in North American, and Eurasian Arctic tundra. However, shrub expansion is not uniform at local and regional scales (Tape et al. 2012), infilling landscapes from riparian corridors, retrogressive thaw slumps, and other favourable topographic positions. At a regional scale, shrubification processes do not occur equally throughout the tundra biome, but have greater sensitivity within the southern bioclimatic subzones (Myers-Smith, Elmendorf et al. 2015). At the local scale, Frost et al (2013) showed that, although the overall zonation of the Arctic tundra is controlled by temperature gradients (Walker, Reynolds et al. 2009), smaller scale landscape processes dominate at a finer spatial grain (Frost et al. 2013). Shrub establishment has been observed on newly exposed substrates related to periglacial processes, such as after retrogressive thaw slumping (Lantz et al. 2009), patterned ground (Frost et al. 2013), drying lake basins (Marsh et al. 2009), and degraded pingos (Mackay and Burn 2011).

At the biome scale, the Arctic tundra has become significantly more productive over recent decades with increases in above-ground plant biomass. Satellite observations (1982-2017) indicate a

widespread '*greening*' of the Arctic tundra (Piao et al. 2006; Lucht et al. 2002). Greening is defined as an increase in the quantity of photosynthetically active vegetation as indicated by the Normalised Vegetation Difference Index (NDVI). NDVI is calculated from the absorption and reflectance of vegetation in red and near-infrared bands: plants absorb red wavelengths when photosynthetic pigments are present, while also reflecting much of the near-infrared spectrum (Gonsamo & Chen 2016). Formally, NDVI = (NIR/VIS)/(NIR+VIS), where NIR is near-infrared reflectiveness and VIS is red reflectiveness at the Earth's surface (Tucker 1977). NDVI has been shown to have a strong relationship with aboveground biomass in the Arctic tundra (Raynolds et al. 2011). Since the start of the pan-Arctic, comprehensive satellite-observation period in the Arctic (1982), the maximum growing season NDVI (MaxNDVI) has been increasing (**Figure 1–1**). 'Greening' trends have been directly linked to an increase in deciduous shrub biomass in multiple locations (Boelman et al. 2011; Macias-Fauria et al. 2012), suggesting that recent increases in NDVI may reflect shrubification processes.

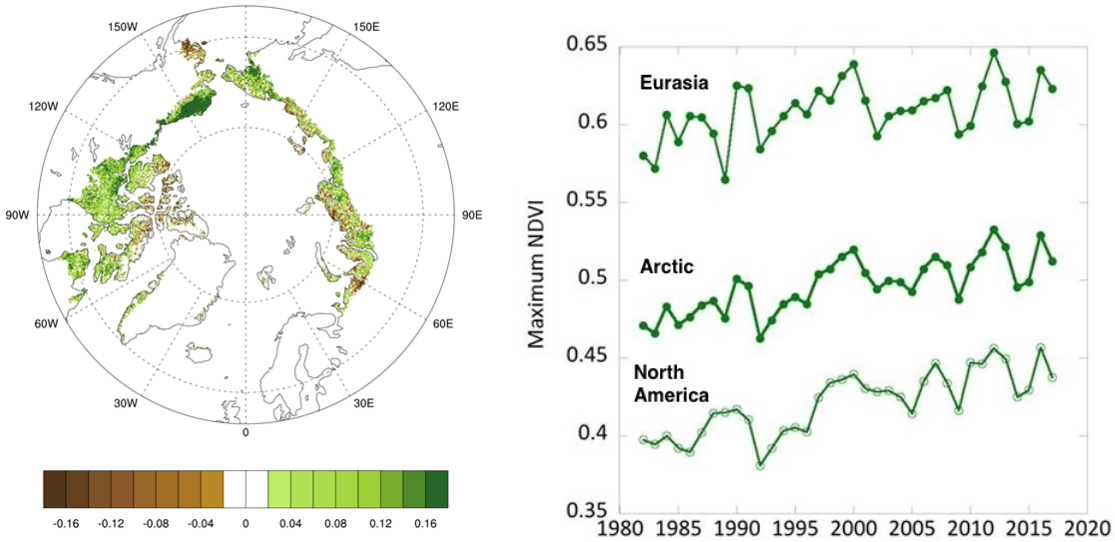

Figure 1–1 Magnitude of the overall trend in MaxNDVI (Maximum Normalized Difference Vegetation Index) for the period 1982-2017 (*left*) and annual MaxNDVI from 1982 to 2017 (*right*). *Source: Epstein 2018.*

Greening has been linked to increased air temperatures (and to a lesser extent changing precipitation regimes), but a progressive decoupling has been reported over the recent period (Piao et al. 2014). Growing season temperature exerts substantial control over remotely sensed greening trends, and ground-based observations of shrub growth and expansion. The Arctic as a whole has experienced

the largest recent temperature increases of any terrestrial biome, driven by the Arctic Amplification (e.g. Serreze & Barry 2011), an umbrella term used to group a suite of processes that result in several positive feedbacks and thus higher temperature sensitivity in the Arctic. Among these, the high albedo and thermal insulation properties of ice and snow play a significant role, and thus the recent high Arctic temperature trends have been linked to significant declines in sea ice extent in the Arctic Ocean and changes in snow seasonality (Epstein et al. 2018), among other processes such as the lapse-rate feedback (Pithan & Mauritsen 2014; Stuecker et al. 2018). Experimental warming studies in recent decades of between 5 – 20 years in length have led to stimulated shrub growth at the expense of graminoids and mosses (Elmendorf et al. 2011). Longer-term observational evidence using shrub wood rings also indicate a dominant role of summer temperature on individual-based shrub growth over the past two centuries: a Pan-Arctic meta-analysis of ring width data found that 36% of individuals showed significant summer temperature dependence (Myers-Smith, Elmendorf, et al. 2015).

The relationship between tundra productivity and climate is heterogeneous both in time and space. Spatially, shrubs are responding positively to rapidly warming summer air temperatures, but with high heterogeneity at the biome scale (Bjorkman et al. 2019). Although 56% of the variance in annual Arctic shrub ring widths can be explained by air temperature data (Myers-Smith, Elmendorf, et al. 2015), shrub ring width data also indicated high spatial heterogeneity in shrub-temperature responses. Temporally, over the past few years, 'browning' trends – decreases in greening – have increased their frequency in the Arctic tundra. Time-integrated (TI-) NDVI, the sum of the biweekly growing season NDVI and a proxy for productivity, has declined since 2005 in Eurasia (Bhatt et al. 2013) and since 2011 across the pan-Arctic (Epstein et al. 2018), suggesting that there may even have been a recent reversal of the long-term 'greening' trend. At the same time, there is evidence to suggest a progressive decoupling of temperature and remotely sensed vegetation productivity over recent decades. Analyses of the partial correlation between TI-NDVI and summer (May – September) air temperature at a Pan-Arctic scale (above 60°N) indicate that the role of temperature

on vegetation productivity has declined over the last 30 years (1982-2011), from 0.80 to 0.56 (Piao et al. 2014), and that this trend is insensitive to variability in precipitation (**Figure 1–2**).

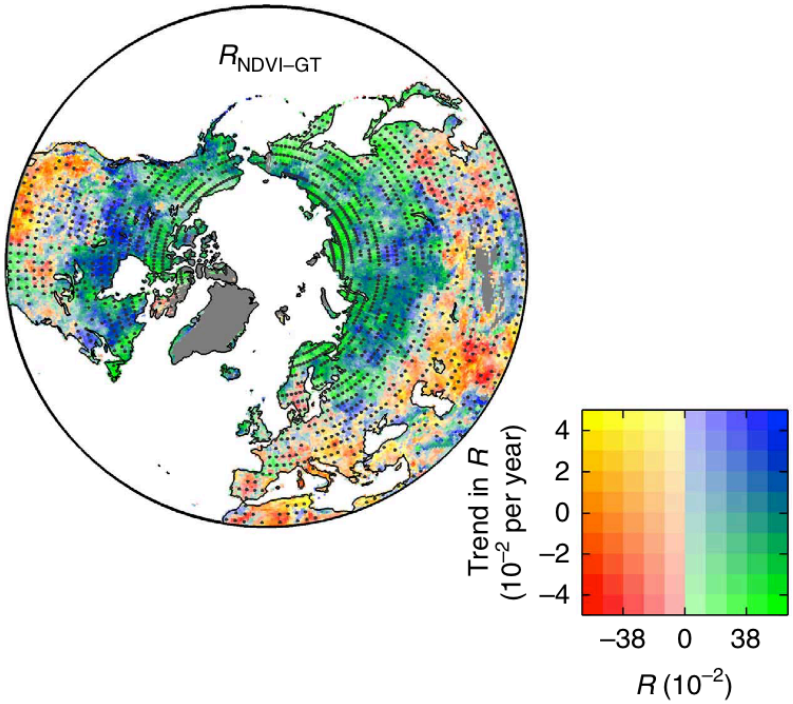

Figure 1–2 Partial correlation coefficient ($R_{NDVI-GT}$) between growing season NDVI (Normalized Difference Vegetation Index) and growing season temperature. F*rom Piao et al (2014).*

The above findings suggest that, as temperature increases in the Arctic, other significant control(s) on shrub productivity may be increasing in importance at the Pan-Arctic scale. There therefore appears to be a key knowledge gap emerging in the understanding of controls of Artic shrub growth and expansion; whilst temperatures are increasing, Arctic vegetation appears to be limited by other factors. Key questions that need to be addressed include:

1. what alternative ecological processes could best explain decoupling between climatic drivers and productivity over the medium- to long-term; and

2. can these ecological processes explain Pan-Arctic declines in temperature *vs*. productivity coupling, or in some cases in overall productivity, over the recent period?

Without such an assessment, we cannot understand the processes that control Arctic shrub growth and expansion, thus our predictive capacity for future shrubification and its impact on climate regulation is limited. Woody shrubs are projected to expand in cover in the Arctic tundra by as

much as 52% by 2050 when projected with climate-based niche modelling (Pearson et al. 2013), but this does not account for the observed heterogeneity in shrub responses to climate. To fully understand the mechanisms driving shrubification, we must (a) expand our outlook to alternative controls beyond basic climatic parameters that could explain Pan-Arctic variability in productivity over the medium- to long-term, and (b) assess which associated ecological processes could best explain recently observed trends.

1.1.2 An Alternative Contributing Factor to Observed Trends: Nutrient Status

Nitrogen (N) is essential for plant growth and is one of the most limiting macronutrients to growth in high latitudes (Bobbink et al. 2010). Fertilisation experiments from the ITEX network of experimental plots indicate that shrub growth in a number of tundra environments is N-limited: experimental addition of N has been observed to increase shrub biomass production over years to decades (Bouskill et al. 2014). Plot-scale evidence suggests that woody deciduous shrubs are able to dominate environments subjected to nutrient fertilisation: nutrient addition of N and Phosphorus (P) in Alaskan moist tundra for example led to substantial increases in wood mass, as community composition shifted towards a dominance of the deciduous shrub *Betula nana* (Shaver et al. 2001). However, growth release has been constrained at some sites by simultaneous N and P limitation (Gordon et al. 2001; Street et al. 2017), and reindeer grazing has been observed to shift the nutrient balance tundra vegetation from N-limitation towards P-limitation (Sitters et al. 2019). At an ecosystem level, the proposed mechanisms for herbivore-induced shifts between N and P limitation are (a) the direct effect of variability in the N:P stoichiometry of animal nutrient status and subsequent waste products (Sitters et al. 2017); and (b) indirect effects on litter production and soil compaction (Bardgett and Wardle 2003).

The magnitude of growth release after fertilisation varies between deciduous shrub species and floristic regions. For example, *Betula nana* has substantial physiological advantages in Alaska that can enable rapid change from a dwarf to tall shrub growth form after N addition (Heskel et al. 2013); however, *Betula nana* is genetically fixed with dwarf growth form in Fennoscandia. Shrub

expansion can also be accelerated by elevated N availability: *Betula nana* has been observed to increase seed production after fertilisation (Moulton & Gough 2018).

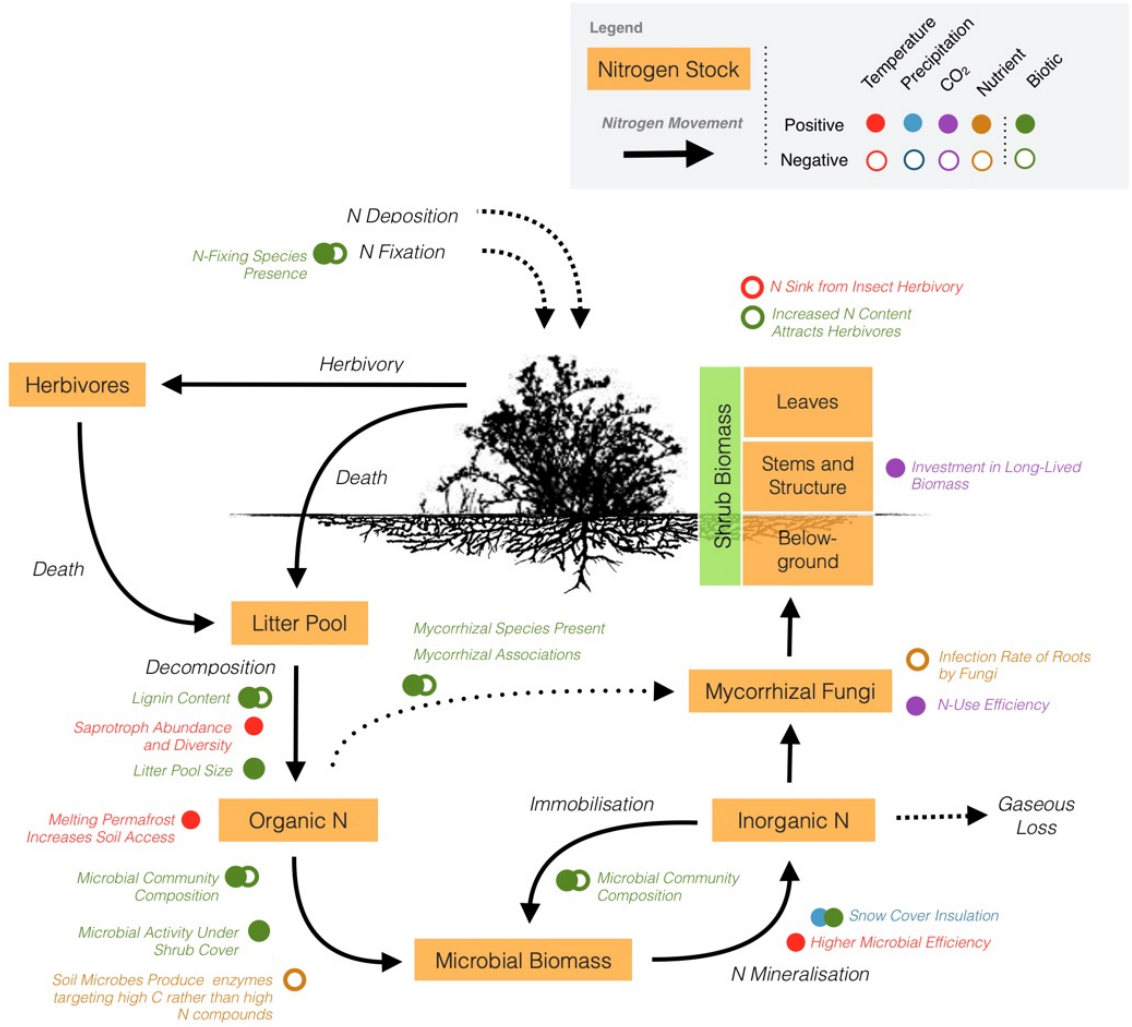

Figure 1–3 Key stocks (boxes) and flows (arrows) that may dictate nitrogen availability to Arctic shrubs. The diagram includes (a) controls on the rate of nitrogen cycling processes (*red = temperature effects; blue = moisture effects*), (b) properties of biodiversity that mediate N cycling processes (*green*), and (c) the role of atmospheric CO_2 concentration in regulating nitrogen availability (*purple*). Hollow circles indicate negative effects, and solid circles positive effects.

Although experimental research has focused on nutrient addition and the effects of N deposition, future trajectories of N availability, rates of change, and spatial differences are highly uncertain. Biogeochemical feedbacks to climate may arise from long-term N trajectories, with increasing N availability driving increasing air temperature in a broad biogeochemical feedback (Arneth et al. 2010). There are biotic and abiotic mechanisms within Arctic ecosystems that may influence the

direction and rate of change in N availability to shrubs (**Figure 1–3**). Broadly, the following mechanisms have been proposed:

a) **Climate-related mechanisms:** elevated soil temperatures causing increased efficiency of N-mineralising microbes (Mikan et al. 2002); temperature-induced permafrost thaw releasing presently locked-up soil organic matter (Schuur et al. 2008); changes to snow depths modifying soil insulation during winter (Sturm et al. 2005).

b) **Shrub-feedback mechanisms:** shrub establishment shades soils thus reducing the rate of permafrost melt and slowing the rate of access of soil roots to new soil organic matter sources (Juszak et al. 2014).

There are two primary external inputs of N into Arctic systems: fixation of atmospheric N_2 and deposition of reactive forms of N. N_2 fixation appears more important in the tundra biome than N deposition. N enters Arctic ecosystems primarily by fixation of atmospheric N_2 by microbes associated with (a) diazotrophs, both free-living and associated with mosses and lichens (Stewart et al. 2011); and (b) microbial symbionts of the deciduous shrub *Alnus spp*. and legumes (e.g. *Astralagus*). Mosses provide the greatest overall N_2 sink in sub-Arctic tundra (Gavazov et al. 2010). Although global deposition of reactive N has increased dramatically over the 20th century (Vitousek et al. 1997), Arctic environments are relatively pristine (Galloway 2005; Peñuelas et al. 2013) and loads of N deposition to Arctic tundra environments are very low (Bobbink et al. 2010). Ensemble modelling indicates that that reactive N deposition was below 0.2gN/m^2/year (standard deviation range of 0.2 – 0.5 gN/m^2/year) within the high-latitude Arctic tundra (Lamarque et al. 2005).

Experimental studies have focused on addition of N or NPK fertilisers, to assess how increased N may affect shrub productivity. However, the standardised study designs focus on N inputs of orders of magnitude greater than proposed natural rates of increase in N availability, and by their nature cannot examine the effects of declining N on shrub productivity. Yet records of terrestrial N availability from natural archives suggest declining soil N availability over recent decades and centuries (McLauchlan et al. 2013). Stable N isotope analysis of sediment cores can provide a proxy

of catchment-scale N availability (McLauchlan et al. 2013). Analysis of the stable N isotope composition of lake sediments (a proxy of catchment-scale N availability) from high-latitude sites contained in McLauchlan et al. (2013) indicate that sedimentary $\delta^{15}N$ has been stationary or declining over the last 150 years (Jeffers, unpublished data); therefore catchment-scale N availability may be progressively declining. Palaeoecological records have also indicated a positive relationship between shrub growth and N availability; in Alaska there is sedimentary evidence to suggest that *Alnus* expansion led to increased N availability during the mid-Holocene (Hu et al. 2001).

1.1.2.1 The Progressive Nitrogen Limitation Hypothesis

Recently observed heterogeneity in the responses of shrub growth to a warming climate (Myers-Smith, Elmendorf et al. 2015) and declines in the greenness-temperature relationship (Piao et al. 2014) suggest that shrub growth and expansion is increasingly limited by processes operating at local to regional scale. It is plausible that – given substantial increases in aboveground woody biomass over recent decades – scarce nutrients may be increasingly 'locked up' in plant biomass; such a mechanism could in theory occur throughout the tundra, but also incorporate the substantial spatial heterogeneity within soil resources. As an evidence gap exists for recent trajectories of soil N availability, a key hypothesis to test is Progressive Nitrogen Limitation (PNL – Luo et al. 2004). The PNL hypothesis suggests that – driven by increased atmospheric carbon dioxide or another environmental stimulus – plant growth may become increasingly N-limited after initial fertilisation effects from increased atmospheric carbon dioxide drive declines in soil N availability over the long-term. Multiple mechanisms underpin PNL (**Figure 1–4**). First, enhanced growth locks nitrogen into longer-lived stores, which slows the rate of litter production causing a *transactional nitrogen limitation*. Second, the C:N ratio of plant litter may increase. Above a critical ratio of C:N in the litter pool soil microbes begin to consume N for their own growth. Net N-mineralisation is thus displaced by net N-immobilisation by microbes representing *sink-driven PNL*.

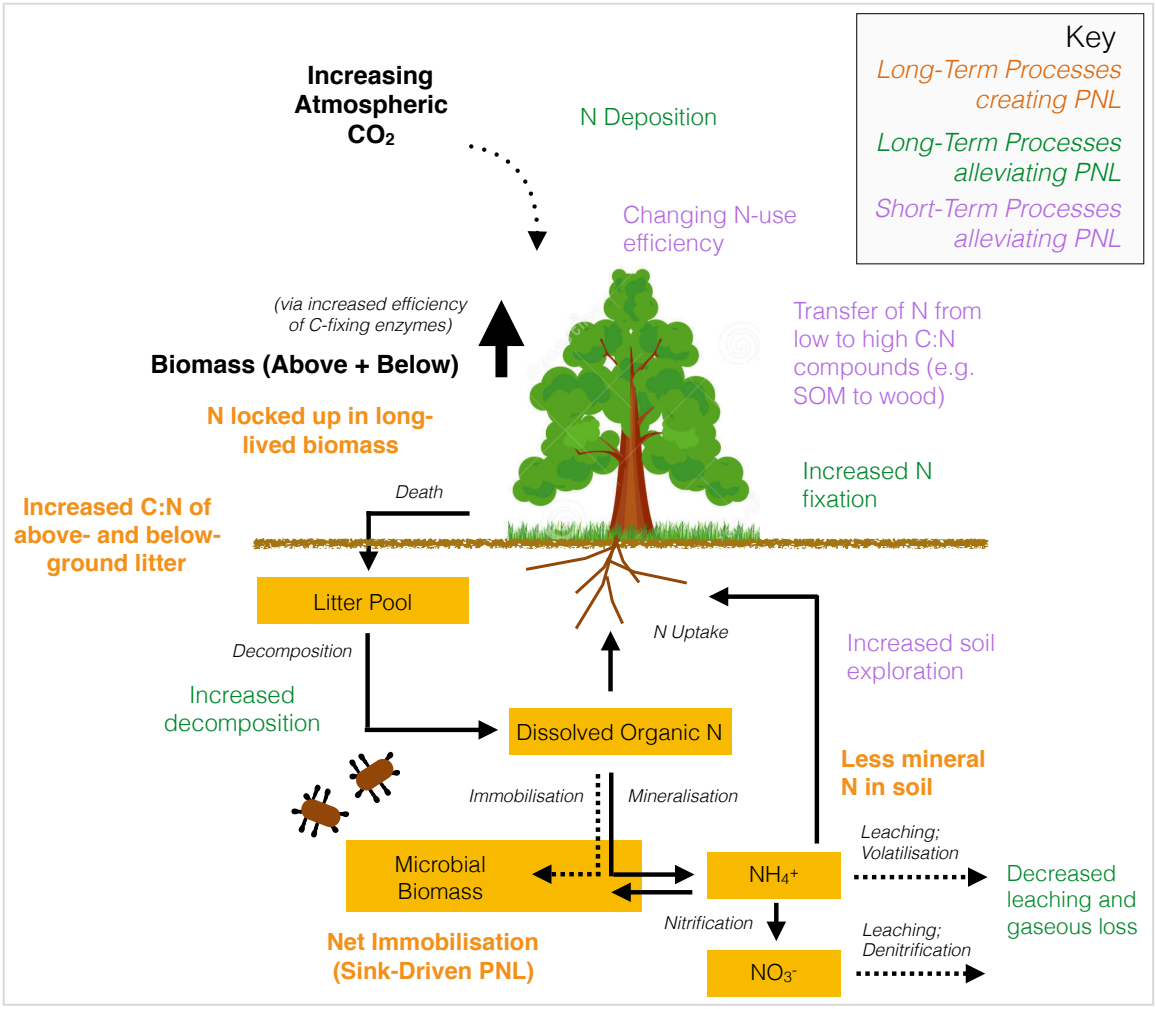

Figure 1–4 Schematic of ecological processes that determine if Progressive Nitrogen Limitation (PNL) occurs in an ecosystem. Over long timescales CO_2 fertilisation will lead to PNL (orange processes) unless N inputs increase, or N losses decrease (green processes). Over short timescales the long-term processes may be masked by physiological responses (purple processes).

PNL may be alleviated by increased external N inputs (i.e. deposition of reactive N, increased N_2 fixation) or decreased N losses (i.e. leaching, gaseous loss) from an ecosystem. When assessed over short time periods, PNL can also be masked by physiological responses that overcome low N (Johnson 2006), which may make PNL undetectable within the temporal frame of current experimental research. For example, rooting behaviour may adapt to increase exploration by fine roots and mycorrhizal hyphae. Alternatively, N uptake may increase alongside increases in N-use efficiency, in effect transferring N from low C:N pools to high C:N pools. The medium- to long-term temporal dynamics are dictated by the size of N and C stocks within an ecosystem: C stocks are large within the Arctic tundra, and it has been observed that it can take decades for the impact of nutrient and warming changes to become apparent in Arctic tundra systems, as observed at

Alexandra Fjord (Lamb et al. 2011). Microbial biomass has also been observed to increase only slowly in response to environmental manipulations with no perceivable effects for longer than a decade (Rinnan et al. 2007), indicating that indirect mechanisms over the longer-term may be important.

Evidence from other ecosystems suggests that PNL may be occurring there. A meta-analysis of global foliar $\delta^{15}N$ data suggests that N demand may be increasing relative to N supply across all environments (Craine et al. 2018). Soil N availability has also been declining across the continental US since at least 1850 (McLauchlan et al. 2017). In the Arctic there is evidence to suggest that CO_2 fertilisation has had a greater effect on vegetation productivity than previously thought, as Earth System Models (ESMs) have underestimated the CO_2 fertilisation effect on GPP in high latitudes (Winkler et al. 2019). CO_2 fertilisation effects have also been constrained by N and moisture limitation in lower latitudes (Reich et al. 2014; Norby et al. 2010).

As the dominant mechanisms of PNL operate on decadal to centennial timescales, the occurrence of PNL or otherwise may not have been fully observed with current experimental and observational methods. PNL's role in long-term arctic greening therefore remains largely unquantified. ESMs represent N-limitation through considerably different and increasingly complex mechanisms (Thomas et al. 2015); there is a need to identify the most important mechanisms with their spatial-temporal scales to best focus efforts of model development (Thomas et al. 2015). Given uncertainty surrounding the rates of change in tundra soil N availability, the broad question to address is to what extent N limits shrub growth over the long-term, whether this is progressive or alleviating, and if N-limiting effects are driven by plant-soil feedbacks. This therefore provides the impetus for the current research.

1.2 Key Aims and Objectives

The ***overarching aims*** of this DPhil are to:

a) identify recent evidence for alternative controls on Arctic shrub growth;

b) determine trends in soil N availability to tundra shrubs over recent decades in North-Western Siberia;

c) establish the mechanism, strength, and variability of N limitation to shrub growth; and

d) compare the role of N limitation to the direct role of climate.

McLauchlan et al. (2007) demonstrated the potential to use stable N isotopes from tree rings as an indicator of point-based N availability (McLauchlan et al. 2007). This DPhil adopts this method to create novel time-series of N availability in the tundra from arctic shrubs, which have rings suitable for the use of dendrochronological techniques (Myers-Smith, Hallinger, et al. 2015). The DPhil has been organised into the five core chapters as outlined in **Table 1–1**:

Table 1–1 Chapter summaries with methods indicated by spatial and temporal characteristics

Ch.	Method Group	Geographical Extent	Temporal Resolution	Temporal Extent	n	Explanatory Variables
2	Evidence Map	Biome: Arctic and Oro-Arctic tundra	NA	NA	429 included research items	24 proximal controls to shrub growth
3	Data and Modelling	Site: Yuribei, Yamal Peninsula	Annual	1980 – 2013	10 $\delta^{15}N$ time-series	N availability
4	Data and Modelling	Region: North-Western Siberia (Varandei, Yuribei, Mordy Yaha)	Three-yearly N; annual growth	1941 – 2013	30 $\delta^{15}N$ time-series	N availability, air temperature, topography
5	Data and Modelling	Site: Yuribei, Yamal Peninsula	Annual (modelled monthly)	1980 – 2013	10 $\delta^{15}N$, 5 $\delta^{13}C$ & $\delta^{18}O$ time-series	N availability, snow, air temperature, moisture, elevation
6	Scientific Software	NA	NA	NA	NA	NA

I have limited the study to Arctic and high-latitude alpine tundra. Shrub expansion has also occurred in alpine environments globally (Brandt et al. 2013) predominantly through the expansion of dwarf shrub heathland (Kullman 2010). Although the expansion of shrubs in alpine tundra may appear to occur through similar mechanisms to shrub expansion in the Arctic tundra, there are fundamental differences in ecological context that change key assumptions of the drivers of change. First, the species composition of vascular plants is lower in diversity and more homogeneous within Arctic than alpine tundra. Second, seed dispersal need only occur over short distances to reach alpine environments, whereas migration distance to reach warming Arctic tundra may be thousands of kilometres.

1.3 Study Region: The Western Siberian tundra

Western Siberia has warmed rapidly over recent decades and has experienced some of the highest rates of the terrestrial Arctic, especially during the winter (**Figure 1–5**). Declines in the extent and thickness of sea ice since the 1980s have pronounced effects on the Yamal and Taymyr Peninsulas, as summer ice has withdrawn from their coastlines (Macias-Fauria et al. 2012). The Western Siberian Arctic spans the bioclimatic range of the Arctic (**Figure 1–7**), and for this reason has previously been studied as a transect of tundra bioclimates (Walker, Leibman, et al. 2009). Our research focuses on bioclimate subzones D and E, covering the low and middle Arctic tundra. At the southern margin (subzone E), woody shrubs are the dominant vegetation type. The Arctic biome is relatively species-poor, with few dominant woody species. The dominant woody genera are *Betula* and *Salix*, although *Alnus* has encroached in some locations on the taiga-tundra ecotone. At the southern margins of the Arctic tundra, tall shrubs are prevalent. The dominant tall shrub species in Yamal is *Salix lanata* L. The dominant soil types are peat and peaty gley soils of bogs with shallow ice-rich permafrost (cryic histosols). There are significant organic carbon stores present in the permafrost of Yamal (Hugelius et al. 2014; Schirrmeister et al. 2011). The *cryic* temperature regime indicates that soils are very cold in winter but warm up slightly in summer.

There are regionally specific stressors to ecosystems in Western Siberia. First, reindeer herding controls the distribution of vegetation, as Nenets nomadic reindeer herders have the greatest reindeer herds and longest ongoing migration on Earth (Forbes et al. 2009). The same herding routes have been used for generations and tend to avoid shrubby lowland areas where mosquitos are prevalent; however, routes have become progressively disrupted by the proliferation of tall shrub thickets over recent years (Forbes et al. 2009). Grazing routes contribute substantially to observed vegetation dynamics (Kryazhimskii et al. 2011) although climate warming appears to exert a dampening effect (Yu et al. 2011). Second, there are signs that climate extremes are becoming more common: during the period over which this DPhil has been conducted (2014 – 2018), a series of major dry heatwaves have occurred during summer months on the Yamal Peninsula, which have had serious consequences for nomadic reindeer herders: these recent events are out of the temporal span of the material analysed in this study. Third, there has been a recent increase in economic activity and development alongside an expansion of the oil and gas industry (Forbes et al. 2009), which affect nomadic migration patterns and may increasingly contribute to environmental pollution in the future.

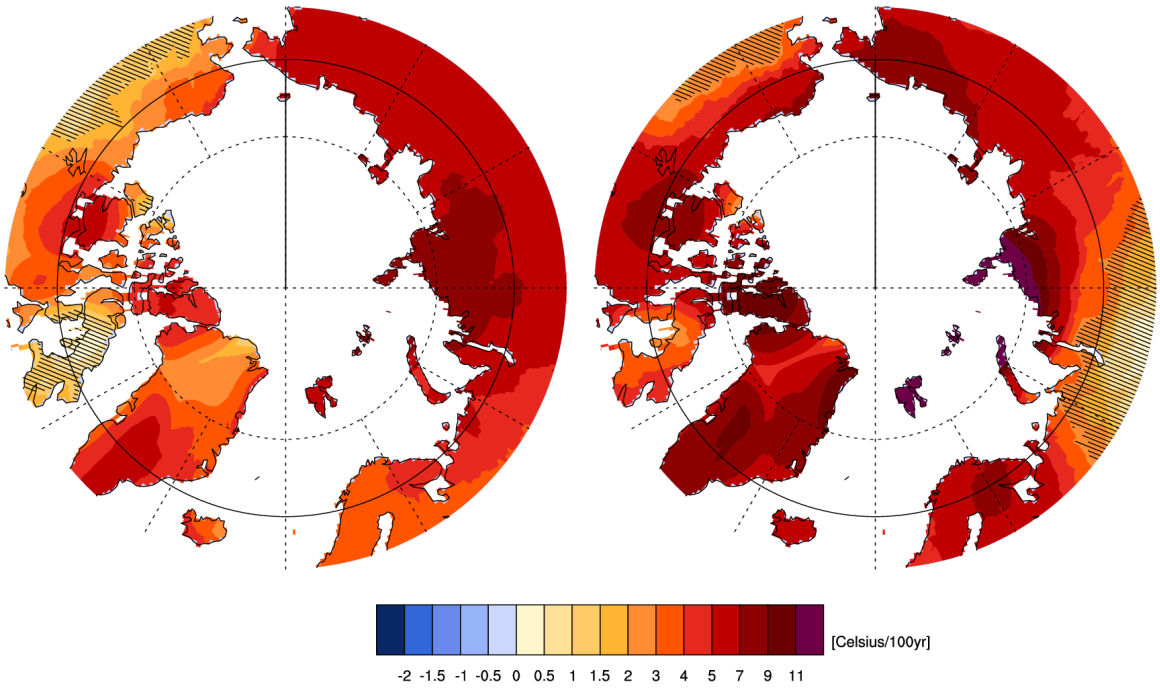

Figure 1–5 Mean regression temperature on time 1980-2019 CRU TS 4.1: April – September (left) and October – March (right). The hatching represents areas where the signal is smaller than one standard deviation of natural variability. *Data source: KNMI Climate Explorer.*

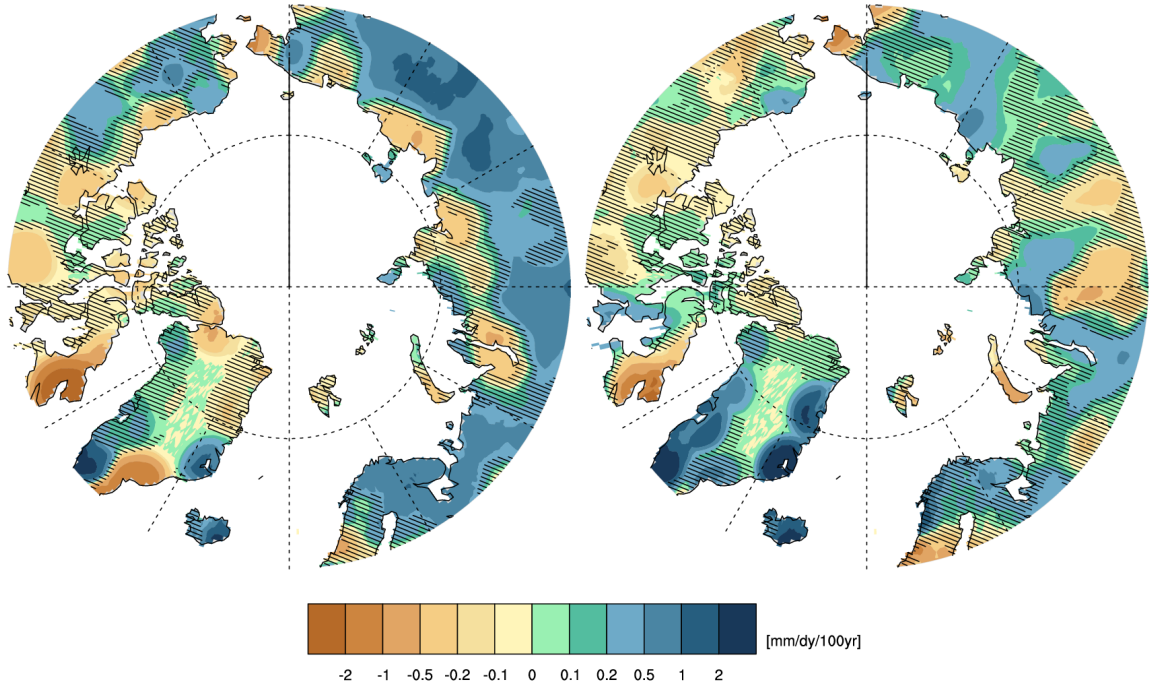

Figure 1–6 Mean regression precipitation on time 1980-2019 CRU TS 4.1: April – September (left) and October – March (right). The hatching represents areas where the signal is smaller than one standard deviation of natural variability. *Data source: KNMI Climate Explorer.*

A series of five field campaigns have been previously conducted in the *Nenets* and *Yamalo-Nenets*

Autonomous Okrugs by a research group led by Prof Bruce Forbes at the Arctic Centre, University

of Lapland (Finland). The Okrugs are administrative regions of Russia with autonomy for the indigenous *Nenets*. The five field campaigns were: Varandei (2005), Laborovaya (2007), Yuribei (2013), and Mordy Yaha / Bovanenko (2013). During each field campaign, between 30 and 60 tall shrubs were destructively harvested to obtain stem discs from ground level, with the aim of generating ring-width series. The sampled shrubs occurred in common topographic positions. In terms of the Circumpolar Arctic Vegetation Classification, Varandei falls within non-tussock sedge, dwarf shrub, moss tundra; Laborovaya within erect dwarf-shrub tundra; Yuribei at the intersection of low-shrub tundra and sedge, moss, low-shrub wetland; and Mordy Yaha within low-shrub tundra (**Figure 1–7**).

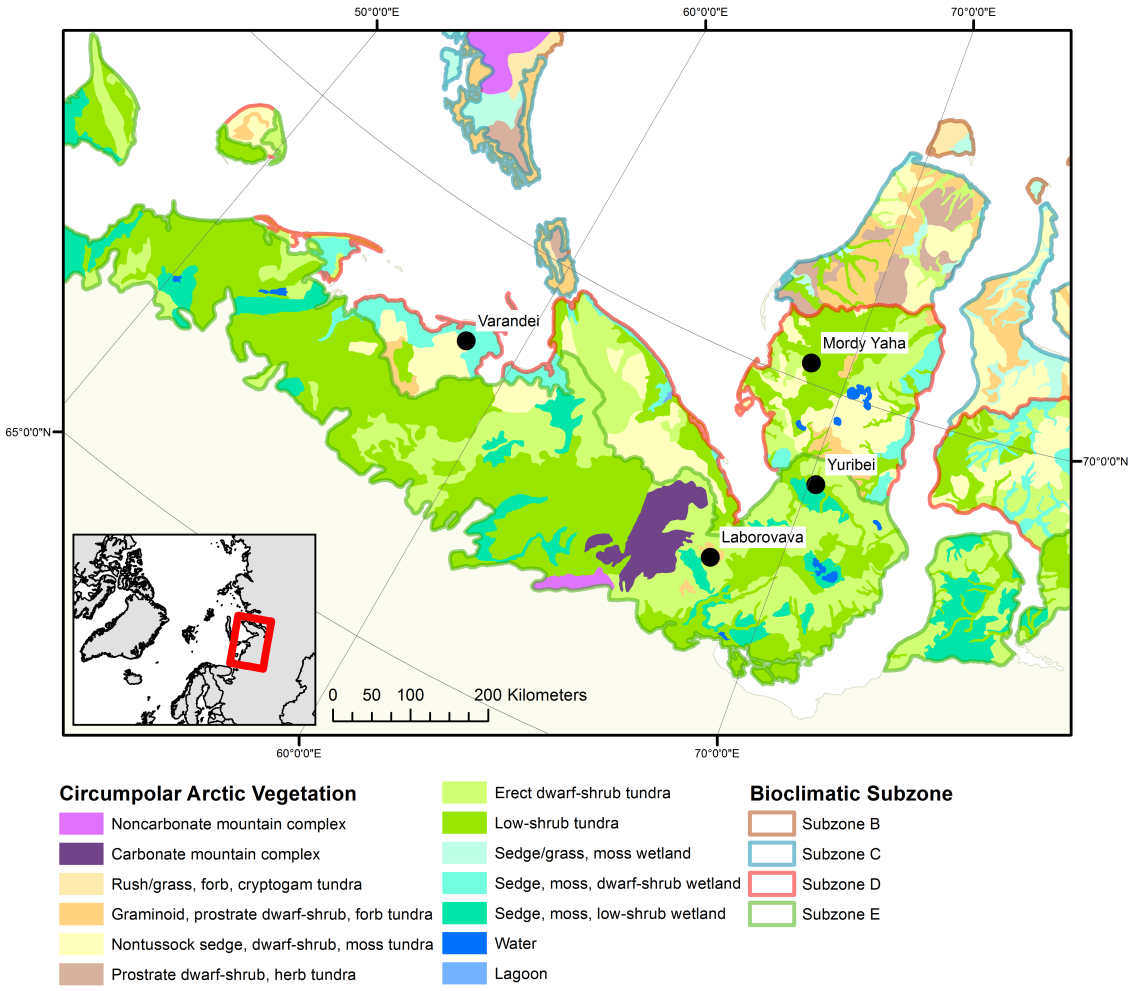

Figure 1–7 Map of Western Siberia showing shrub sampling areas, vegetation types, and bioclimate subzones as defined by the Circumpolar Arctic Vegetation Map (CAVM) (Walker, Raynolds, et al. 2009).

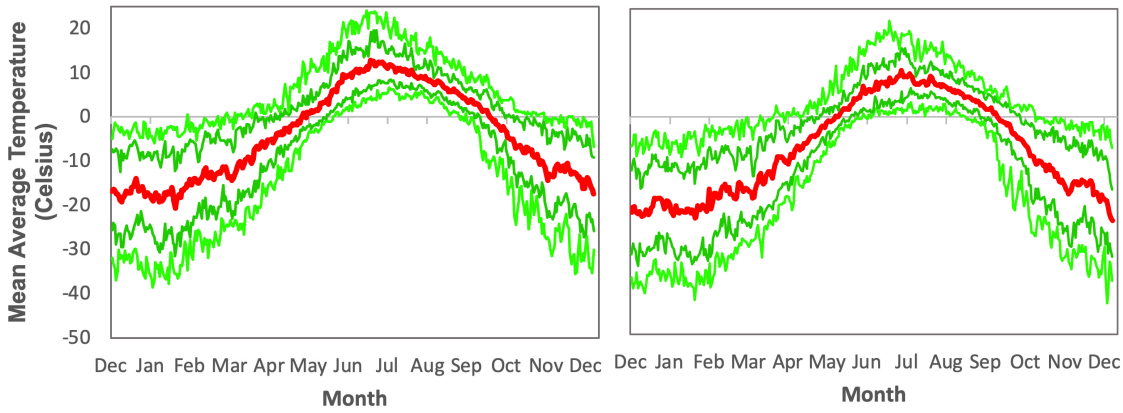

Figure 1–8 Mean 1980 – 2013 climatology for Varandei (**left**) and Yuribei / Mordy Yaha (**right**) derived from close-by weather station data in the GHCN-D v2 database. Red line = mean daily temperature; dark green lines = 17% and 83% percentiles; light green lines = 2.5% and 97.5% percentiles. The nearest weather station for Varandei was *Mys Konstantinovskii* (68.55N, 55.50E) and for Yuribei / Mordy Yaha was *Marre Sale* (69.72N, 66.82E). Source: *KNMI Climate Explorer*.

Soil type and soil conditions are a key determinant of nutrient availability and thus trajectories of change. Our sampling locations are of relatively consistent soil conditions and are representative of the Cryic Histosols that occur throughout most of the region (**Figure 1–9**). Soils at Varandei, Laborovaya, Yuribei, and Mordy Yaha are non-carbonate acidic (Walker, Raynolds, et al. 2009). There are two key sources of information on Russian Arctic soils: (a) covariates from global soil models that are inferred using machine-learning approaches; and (b) national- and local-level maps created by the Soviet Union. At the global scale, SoilGrids250m uses global models to predict local soil conditions at a series of soil depths (Hengl et al. 2017). For Russia, there are local resources that incorporate additional Soviet / Russian data sources. These include the *Land Resources of Russia* soil maps (Stolbovoi & McCallum 2002) at a scale of 1:25 million, and the *State Soil Map of the Russian Federation* at 1:1 million (Rukhovich et al. 2013; Mikhailov 2016; Mikhajlov 2017). Key predicted soil properties for regions in which shrubs were sampled are shown in **Table 1–2**:

Table 1–2 Key soil properties for shrub locations from *Land Resources of Russia*

Soil Property	Varandei	Laborovaya	Yuribei	Bovanenkovo / Mordy Yaha
Land Resources of Russia				
World Reference Base (WRB 1998) Soil Class	Histosols Histosols Fibric	Cryosols Cryosols Histic	Cryosols Cryosols Histic	Cryosols Cryosols Gleyic
Soil Carbon Density at 0-10cm Depth (kg/m^2)	178.00	295.02	295.02	53.00

Soil Respiration ($kg/m^2/year$)	0.25	0.06	0.06	0.04
Cation Exchange Capacity for Topsoil (mg-equivalent/100g)	99.0	18.1	18.1	18.3
Total Nitrogen Content (% - Kjeldahl method)	0.49	0.11	0.11	0.40
Acidity (pH – H_2O)	5.9	6.0	6.0	6.9
Soil Drainage Class	Very Poor	Poor	Poor	Very Poor
Fertility Class	Moderate	Moderate	Moderate	Moderate
SoilGrids 250m				
World Reference Base (WRB 1998) Soil Class (predicted probability for occurrence of soil class)	Cryic Histosols (26%), Haplic Gleysols (23%), Haplic Cambisols (21%)	Cryic Histosols (40%), Haplic Cambisols (31%), Haplic Gleysols (5%)	Cryic Histosols (48%), Haplic Cambisols (26%), Haplic Gleysols (16%)	Cryic Histosols (38%), Haplic Cambisols (33%), Haplic Cambisols (Dystric) (8%)
Depth to Bedrock (cm)	196	200	200	200
Clay: Silt: Sand Fraction	12:46:42	16:47:37	24:35:41	23:39:38
CEC (cmolc/kg) @0cm	73	45	58	66
Soil pH (H_2O) @0cm	5.3	5.5	5.6	6.2
Soil Organic Carbon Stock (tonnes/ha)	~400	~500	~800	~700

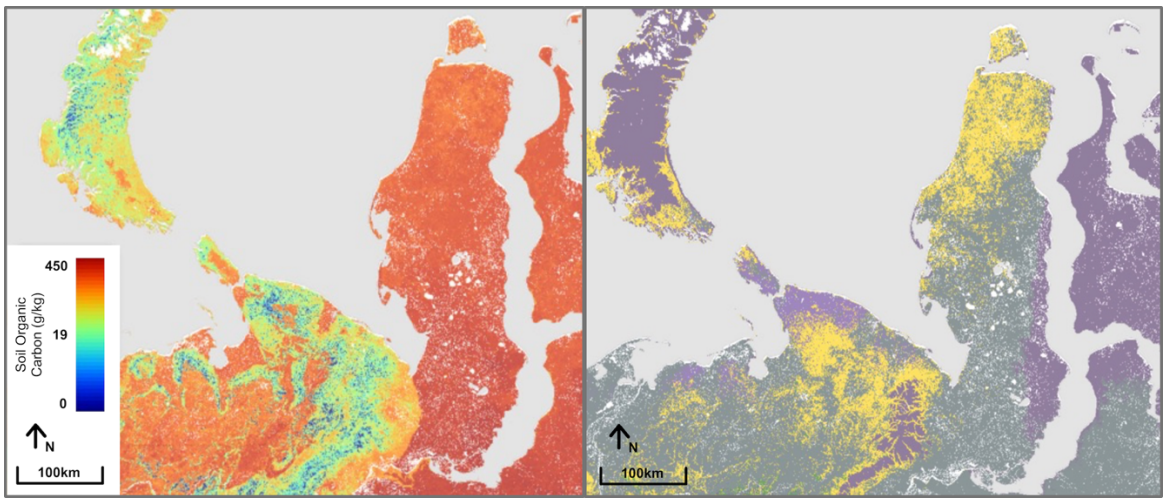

Figure 1–9 Maps of key soil properties in Western Siberia as predicted by the global SoilGrids 250m model (Hengl et al 2017). *Left*: Soil organic carbon content in the fine earth fraction at 100cm depth (g/kg). *Right*: Most likely TAXNWRB soil classification given global soil covariate data, as predicted by SoilGrids 250m. Colours indicate cyric histosols (grey), haplic cambisols (yellow) and haplic cryosols (purple).

1.4 Primary Methods

The research in three of the papers presented for this DPhil thesis focuses on the combination of long-term ecological proxies from wood rings with a model-based hypothesis testing approach (Bonsall and Hastings 2004), through which we identify the most plausible suite of mechanisms that best explain the observed data (*see Section 1.4.3*).

1.4.1 Dendroecology of Arctic Shrubs

Arctic deciduous shrubs produce annual rings that can be cross dated (Myers-Smith, Hallinger, et al. 2015). Standard dendrochronological approaches can be applied for cross-dating and chronology development (Speer 2010). Ring widths indicate the absolute growth rate of stems through time, and thus growth sensitivity to climate may be assessed by computing correlations with climate variables. Beyond this, the cumulative basal diameter can be related to total stem or plant biomass through the use of allometric equations (see Section 1.4.3.1 for such modelling approaches). In addition, wood anatomical features can provide quantitative and qualitative detail of the life history of individuals (Fonti et al. 2009; Braun et al. 2013; Wimmer 2002).

1.4.2 Stable N isotopes in wood as a proxy of N availability

The stable nitrogen isotope ratio ($\delta^{15}N$) of wood rings is used as a measurement of point-based soil nitrogen availability (McLauchlan et al. 2007). Wood $\delta^{15}N$ records the $\delta^{15}N$ of N taken up by plants, and the value corresponds to multiple metrics of N availability at the time of wood formation (Gerhart & McLauchlan 2014; Craine et al. 2015). $\delta^{15}N$ is defined as:

$$\delta^{15}N(‰) = 1000\left(\frac{R_{sample}}{R_{standard} - 1}\right)$$

Here, *R* represents the abundance of ^{15}N with respect to ^{14}N. Fractionation occurs when a biotic or abiotic process discriminates towards ^{15}N (enrichment) or ^{14}N (depletion). Within the nitrogen cycle, there are three major processes that inflict a relatively large fractionation effect: (1) gaseous loss, (2) conversion of NH_4^+ to NO_3^-, and (3) processing of N by mycorrhizal fungi (Craine et al.

2015). As the standard used for $\delta^{15}N$ is air, N fixed from the atmosphere is approximately 0.00‰. For woody plants with ectomycorrhizal (ECM) fungal symbionts, $\delta^{15}N$ is thus interpreted as bioavailable N directly available to the plant (i.e. point-based) (Gerhart & McLauchlan 2014).

Wood $\delta^{15}N$ has been used as an indicator of natural variability of N cycling in ecosystem N from tropical (Hietz et al. 2010), temperate (McLauchlan et al. 2007; Bukata & Kyser 2007), and alpine (Dijkstra et al. 2008) trees. Regional studies indicate increases and declines in soil N through time. For example, for West Canadian Douglas Fir (ECM-associated) wood $\delta^{15}N$ has been correlated to site productivity along an edaphic gradient (Kranabetter et al. 2013). A meta-analysis of wood $\delta^{15}N$ in North America suggests that N availability has been declining within the last 200 years (McLauchlan et al. 2017). In the Arctic, wood and foliar $\delta^{15}N$ have been used in natural abundance and tracer studies to: identify the timing of N uptake between plant species (McKane et al. 2002); partition the contribution of mycorrhizal N-supply to total plant N (E. A. Hobbie & Högberg 2012); and reveal N-competition between shrub species (Gundale et al. 2012). Globally, plant $\delta^{15}N$ systematically decreases with decreasing mean annual temperature (MAT) and increases with mean annual precipitation (MAP) (Amundson et al. 2003). Plants and soil in warm and dry ecosystems have the greatest $\delta^{15}N$, as greater losses of N occur from soils alongside greater N availability. To date, no long-term wood $\delta^{15}N$ time-series had been created within the Arctic tundra.

Wood $\delta^{15}N$ can be explained in terms of N cycling in Arctic tundra environments. Wood $\delta^{15}N$ reflects N availability to the plant at the time of wood formation. Isotope mixing models have shown that N losses exert the greatest fractionation effect on soil N (Bai & Houlton 2009). As N availability increases relative to biotic demand, increasing soil N losses preferentially remove ^{14}N from soils, which increases the $\delta^{15}N$ of the remaining soil N. In addition, at elevated N availability the proportion of N acquired from mycorrhizal associates decreases; mycorrhizae transfer ^{15}N-depleted N into plants (Hobbie and Colpaert 2003) thus this pathway induces lower plant (thus wood) $\delta^{15}N$ at lower soil N availability (**Figure 1–10**). There are two key features of Arctic tundra plant-soil relations, neither of which changes the wood $\delta^{15}N$ interpretation: (a) the greater role of organic N sources; and (b) temporal partitioning of N availability:

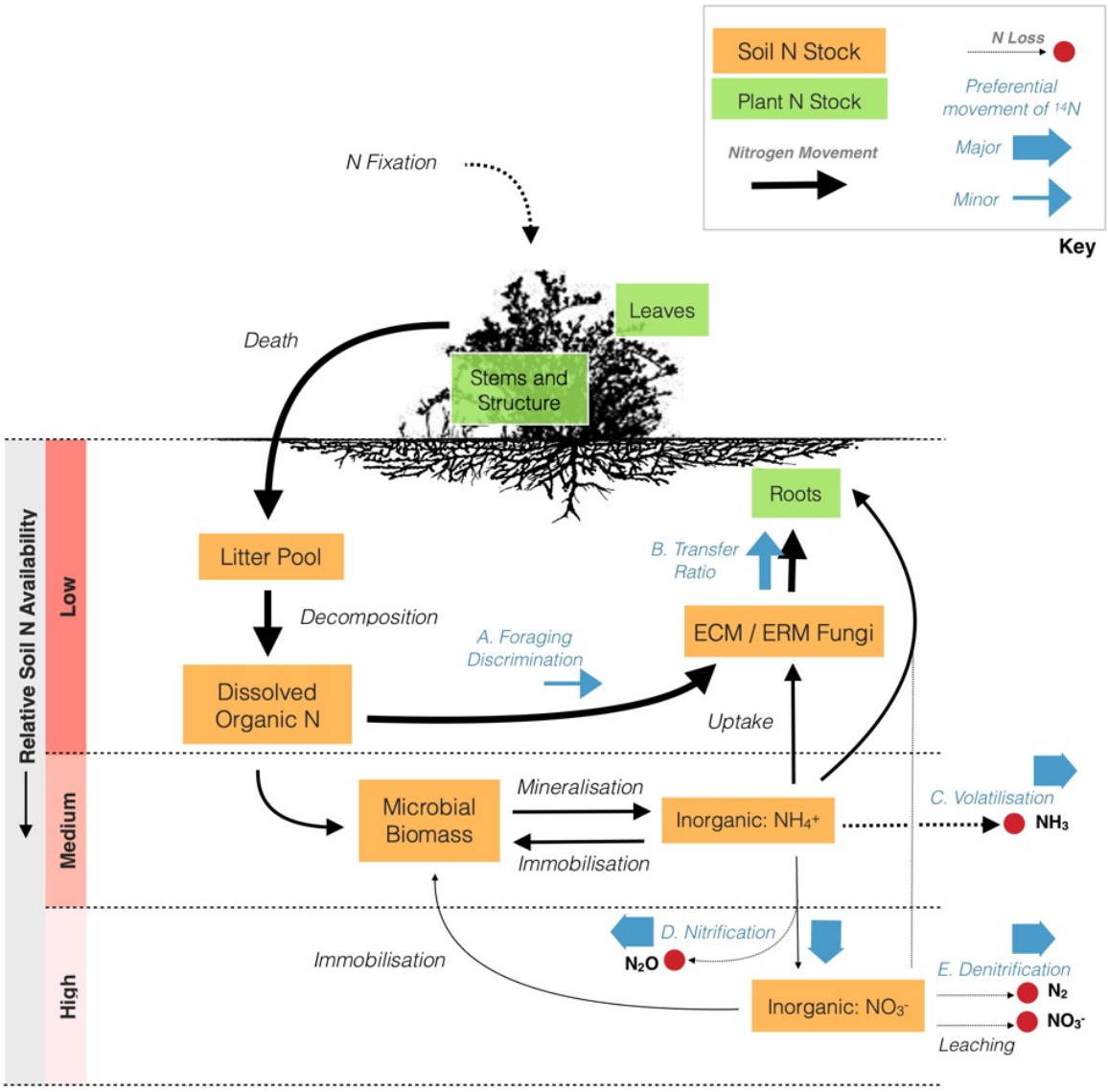

Figure 1–10 Diagram of key stocks and flows in the nitrogen cycle of Arctic tundra environments, and key N isotope fractionating effects. Black arrows indicate N flows, and boxes N stocks. Blue arrows indicate preferential movement of the lighter N isotope ^{14}N, enriching the previous stock in ^{15}N. The gradient of N availability (left) indicates how greater N availability aligns with greater plant $\delta^{15}N$. **Low N:** There is strong N recycling as plants rely on mycorrhizal fungi for uptake of dissolved organic N; preferential transfer of ^{14}N (***A***+***B***) lowers plant $\delta^{15}N$. **Greater N:** Direct uptake of mineralised N (NH_4^+) reduces plant dependence on mycorrhizal uptake, thus lowering the importance of ***A*** and ***B*** (increasing plant $\delta^{15}N$); in addition, volatilisation may occur (**C**), further increasing the $\delta^{15}N$ of the remaining inorganic N. **High N:** Gaseous losses occurring from nitrification of NH_4^+ (**D**) and denitrification of resultant NO_3^- (**E**) enrich the mineral soil pool as ^{14}N is preferentially lost, which is reflected in greater plant $\delta^{15}N$. N deposition (not represented) can imprint its own signature on mineral soil N pools.

(a) the greater role of organic N sources. Harsh environmental conditions and poor soils are responsible for a different N-cycling regime in Arctic tundra environments. The temperature-efficiency of soil microbial processes are exponential, with mean annual temperatures below 5°C constraining their efficiency and thus slowing the rates of N mineralisation and decomposition

(Mikan et al. 2002). At low N availability, fine roots become a more expensive investment than fungal hyphae; plants thus invest carbon into mycorrhizal associates to maximise N returns per unit of C investment, with up to 86% of N in plants derived from mycorrhizae (E. A. Hobbie & J. E. Hobbie 2008). Not all N is directed to the plant however, as some is kept by fungi to meet its own requirements depending on the transfer ratio. In environments where N is even more limited (either via a reduced rate of supply or low concentration of N), there is evidence that plants lower their N demand due to a high C requirement per unit N from mycorrhizae; a trade-off curve has been empirically derived to capture this process (E. A. Hobbie & Högberg 2012). Plants and their mycorrhizal associates use Dissolved Organic Nitrogen (DON) to meet their nitrogen requirements, rather than inorganic forms of N (NH_4^+ and NO_3^-). The inorganic pathway therefore becomes irrelevant for most purposes. In temperate deciduous forests and most other low-latitude ecosystems, plant nitrogen is predominantly obtained directly by roots as NH_4^+ (Cairney 2000). In Arctic environments, where soil nitrogen availability is inherently lower, the role of plant and mycorrhizal uptake of DON is greater and may even exceed the role of inorganic N (Koyama et al. 2014). The type of mycorrhizal associates (ECM, EM, AM) can have varying fractionation effects, with a meta-analysis of 9,000 plant samples demonstrating that fungi type accounted for 29% of the variation in global foliar $\delta^{15}N$ (Craine et al. 2009). West Siberian *Salix lanata* shrubs are ECM-associated (Akhmetzhanova et al. 2012); ECM fungi preferentially transfer ^{14}N to plants in a consistent manner (Taylor et al. 2003).

(b) temporal partitioning of N availability. Arctic tundra ecosystems exhibit strong temporal partitioning of N availability, with net N immobilisation occurring during the growing season. Evidence supports the theory that N mineralisation does not stop during the Arctic winter, but occurs at low rates throughout, owing to snow insulation of the soil (Sistla & Schimel 2013). The build-up of mineral N is 'pulsed' across the landscape with snowmelt – the deeper winter snow depth, the greater the pulse. N availability is thus greatest during the first month of the growing season. As N-mineralising microbes are metabolically limited by low temperatures, they are near as competitive as plants and mycorrhizae for DON. Thus, net N mineralisation becomes prominent

during the height of the growing season, as microbes and plants compete directly against each other for limited DON.

1.4.3 Statistical versus mechanistic approaches to ring width analysis

Relationships between environmental change and wood ring time-series are often interrogated using empirical methods. Wood rings provide direct and annually resolved observations of plant growth through time. Standard dendrochronological techniques involve correlation to assess the sensitivity of ring-width series to environmental variables such as air temperature and precipitation (Fritts 1976), primarily because researchers aim to use growth rings as a proxy for past environmental change. These traditional dendrochronological approaches are not however able to determine the environmental causes (or underlying mechanisms) of observed trends and variability.

An alternative approach involves interrogation of data using models to represent the hypotheses under consideration. As the functional form of ecological processes is often non-linear (e.g. plant growth), causation may be determined by codifying ecological hypotheses as simple mathematical representations and fitting these to observed datasets. An information-theoretic approach can thus be used to determine the most appropriate ecological hypothesis given the data: a 'model-fitting and model-selection' (MFMS) approach (Burnham & Anderson 2007). This approach is applied to a broad suite of ecological problems in 'The Ecological Detective' (Hilborn & Mangel 1997).

A key advantage of the MFMS approach is that subjectivity arising from model selection can be minimised by choosing to start a high level of abstraction where only key basic assumptions are modelled; MFMS of increasingly complex models may then guide model development within a systematic approach that both reflects the underlying data structure and avoids increasing in complexity beyond the ability of the dataset. Related techniques exist to ensure objectivity in model development; box-cox transforms may be used to 'tease out' underlying functional forms from the observations, which can then influence the selection of further ecological mechanisms for assessment (Hossain 2011). When using time-series data and if this is of suitable length, local likelihood methods may be used investigate whether hidden or missing mechanisms may be

identified given the observations; patterns in the variability of estimated parameters through time indicate that further complexity may better explain the data (Tibshirani and Hastie 1987).

A model selection approach has been recently applied to determine the functional form of relationship between climate and shrub growth at Toolik Lake, Alaska (Ackerman et al. 2017). In this thesis I apply such approaches to ascertain mechanisms of N-limitation of Arctic shrub growth based on ecological theory.

1.4.3.1 Modelling approaches for wood ring research

Mechanistic models can be used to interrogate plant growth time-series in two alternative paradigms: (1) the process-based ("bottom-up") paradigm; and (2) the systematic ("top-down") paradigm (Poorter et al. 2013). In the bottom-up paradigm (1), levels of interlinked physiological mechanisms are simulated such that the results of fine-grained processes are integrated within higher level models. For example, 'light use efficiency' models quantify light interception by plants, then propagate this to a light-limited biomass growth model (Poorter et al. 2013). Bottom-up approaches have been used to simulate the production of annual wood ring increments through the climate-dependency of xylogenesis (Guiot et al. 2014). Alternatively, in the top-down paradigm (2) a systematic approach is applied to identify mechanisms of increasing complexity from the original growth time-series. A suite of top-down models has been developed to simulate wood ring production of varying complexity for assessing the climate sensitivity of individual trees, and competitive effects, which are discussed below. Bottom-up models of xylogenesis (Guiot et al. 2014) are not covered here as they are too complex for model-fitting and model-selection for tree ring isotope time-series.

The direct climate-dependence of wood growth is most simply represented in the top-down VS-Lite model (Tolwinski-Ward et al. 2010), which contains only four parameters to estimate. This model is a simplified version of the Vaganov-Shashkin conceptual model of conifer xylem development and resultant ring width (Vaganov et al. 2011). Monthly-resolution growth simulations respond to monthly temperature and precipitation data, and account for insolation based

on latitude. The VS-Lite model incorporates temperature and moisture limitation to plant growth using a mathematical representation of Liebig's law of the minimum. Given a stressing temperature below which no growth can occur (T_1), and a saturating temperature level above which ring width is no longer sensitive to temperature (T_2), temperature's limitation effect (g_T) is defined as:

$$g_T(m,y) = \begin{cases} 0 & T(m,y) \leq T_1 \\ \dfrac{T(m,y) - T_1}{T_2 - T_1} & T_1 \leq T(m,y) \leq T_2 \\ 1 & T_2 \leq T(m,y) \end{cases}$$

Here, *T(m,y)* is the current month and year air temperature, where all temperature values may be substituted for any environmental factor. Growth is simply therefore the minimum of the temperature and soil moisture limiting effects at any time. Model-fitting has been used to assess climate-sensitivity of individual trees and for identifying seasonal drought effects of tree growth (Mina et al. 2016). The VS-Lite model has been used in a Bayesian framework to capture uncertainties within the model's processes (Tolwinski-Ward et al. 2013).

Alternatively, approaches that relate wood rings to biomass or carbon thus representing whole-plant performance rather than mechanistic limits on cambium development can be used to incorporate broader hypotheses and mechanisms that dictate plant-environment interactions. I determined that this approach is necessary for this DPhil research, as the amount of N used at any time is directly related to whole-plant growth. A relatively complex example for climate-dependence is the "T" model (Li et al. 2014); this assumes that that gross primary production (GPP) drives individual tree growth, which in turn dictates wood production using functional geometric relationships that require species-specific parameters. GPP is modelled as dependent on local climate and light availability using first-principles representations (Li et al. 2014).

There are two important considerations when relating wood rings to whole-plant performance: (1) geometry and (2) age-related trends:

(1) First, the relation between plant size (e.g. stem radius) and mass depends on geometrical relations, often defined using allometric equations. Equations are commonly constructed in production forestry (Picard et al. 2012), but shrub forms are understudied. Recently, allometric equations were established for *Betula* and *Salix* shrubs in Yakutia and Alaska (Berner et al. 2015); however, significant differences were found between these regions, indicating that they are not currently generalisable to other tundra locations. Region-specific relations are required as tissue allocation is controlled by species and phenotypic plasticity to environmental conditions (Poorter et al. 2012). The allometric model can be defined independently of the growth model, or an alternative approach with wood ring data is to estimate allometric and growth model parameters simultaneously (Pommerening & Muszta 2015). The choice depends on the complexity of the allometric model.

(2) Second, plants often exhibit age-related (*ontogenetic*) declines in their Relative Growth Rate (RGR) defined as the rate of growth per unit of current mass (Pommerening & Muszta 2016). It is therefore appropriate to consider non-linear models of asymptotic growth (Paine et al. 2011).

I chose to only examine mechanistic rather than empirical models within this DPhil, as empirical models are not formulated from biological process (Burkhart & Tomé 2012). To my knowledge, no other study has used top-down modelling approaches to relate wood ring widths and time-series of soil nutrient availability. To achieve this, I seek to integrate this approach with plant-resource modelling approaches.

1.4.3.2 Approaches to model individual plant-nutrient interactions

A key conceptual approach when considering top-down mechanistic modelling of plant-nutrient interactions is the *resource economy* approach (or ***'Tilman theory'***). This formulation assumes that plant functions such as photosynthesis and respiration have per-unit resource costs; when a resource is 'perfectly essential', processes cannot occur without it (Tilman 1990; Tilman 1988). In a resource-rich environment where resources are not limiting, plant growth may be defined as:

$$\mathrm{RGR}_{\max} = P_{\max}\left[1 - \frac{S+R}{B}\right] - r$$

Here, $\mathrm{RGR}_{\max}$, the maximum relative growth rate, is a function of the resource-unlimited photosynthetic rate ($P_{\max}$) multiplied by the leaf fraction (where allocation is represented by stem S and root R fraction), minus the maintenance cost of respiration r. The Tilman theory thus represents trade-off between leaf physiology and biomass allocation that occurs between species-specific traits (Hunt & Cornelissen 1997). Tilman's approach assumes that plant competition occurs primarily belowground for soil resources. A 'nutrient requirement' per unit biomass – defined as the amount of nutrient required to both maintain and produce a unit of biomass – can be the ultimate determinant of a plant species' ability to outcompete others (Huisman 1994).

Nitrogen (N) availability may limit shrub growth via two mechanisms. First, nutrient deficiency is known to limit the maximum biomass yield of plants. Tilman (1990) suggests that this follows a Monod-type response of growth rate to the limiting nutrient, given the maximum attainable growth rate. Second, uptake rates are a function of N availability, thus N available within a time period may be restricted by the foraging capability of the root system. Removing tissue partitioning between stems, roots, and leaves, this may be represented by continuous time differential equations:

$$\text{Rate of biomass change} = \text{growth} - \text{loss}$$

$$\text{Rate of nitrogen change} = \text{supply rate} - \text{consumption rate}$$

or

$$\frac{dB}{dt} = f(N)B - mB$$

$$\frac{dN}{dt} = y(N) - QBf(N)$$

Here, $f(N)$ is a monotonically increasing function that represents the nutrient-limited maximum growth rate, and m represents a resource- and density-independent loss rate; the parameter Q

indicates the nutrient content required per unit of biomass production; and the function $y(N)$ is again a monotonically increasing function that represents nutrient supply (Tilman 1990). Using this approach, the biomass of plant populations or individuals may be interrogated to determine their competitive ability against others. Although the ability of Tilman's basic theory in predicting competitive ability for nutrients has been debated (Craine 2007; Craine 2005; Tilman 2007), predictions are supported by field experiments (Miller et al. 2005) and it provides a mathematical representation from which to begin to interrogate dendro-isotope time-series. It has also been demonstrated that the other major paradigm – CSR (*Competitor-Stress-Ruderal*) theory (Grime 2007), where trade-offs occur within plant organs rather than from allocation (Craine 2005) – may be reproduced within Tilman's theory (Jabot & Pottier 2012).

For this DPhil, I apply the resource economy approach to interrogate annually resolved time series of growth and nitrogen over decades. To achieve this, I modified the base equations to incorporate additional fundamental considerations in a naturally observed environment:

$$\frac{dB}{dt} = rf(N)B - \gamma_B$$

$$\frac{dN}{dt} = y(N) - f(N)B - \gamma_N N + \alpha\gamma_B B$$

Here, I have simply rearranged the previous equations such that the nutrient requirement of plant biomass Q is replaced by an incorporation factor r. An important process of soil N balance is N loss through leaching and gaseous loss; here I represent this using a density-dependent loss term γ_N whereby losses are greater the more that is available. I also renamed m to γ_B for consistency. Within the model-fitting and model-selection approach, I examine hypotheses of root foraging strategies by substituting $f(N)$. The ArcVeg model of plant-nutrient dependence in the Arctic tundra uses a linear model of continuous uptake, suggesting that even the simplest representation may be appropriate for low N tundra soils (Yu et al. 2009; Yu et al. 2011). In later chapters, I modify $f(N)$ and $y(N)$ to account for environmental forcing (or *time varying*) parameters that test the role

of independent environmental factors on the mechanisms represented here. Finally, previously identified high use of organic N uptake via mycorrhizae may be reflected by litter feedbacks that work against the microbial bottleneck (Chapman et al. 2006). I examine the role of plant feedbacks to soil N by using an optional feedback (in green above), where α is a litter quality factor. I explored the use of biomass partitioning between roots and stems but determined that this could not be inferred with the available time series information.

As the Arctic vegetation is primarily N-limited, P-limitation is unlikely to occur. Using this assumption, in this DPhil I seek to examine the role of N in shrub growth as a single limiting resource. In addition, there is no environmental proxy from wood rings or otherwise that can quantify P availability through time. As N is a perfectly essential nutrient, if P limitation were to occur in shrub-nutrient models it would simply be represented by a lack of response to variability in N.

1.5 Synthesis

The overarching aim of this DPhil is to identify the role of N limitation in the growth of individual Arctic shrubs in Western Siberia. There are key lines of evidence to suggest that N limitation may explain recently observed trends in shrub growth and expansion, including: heterogeneous responses to climate; decoupling between Arctic greening and air temperature increase; recent browning events; and stronger responses of Arctic vegetation to CO_2 fertilisation than previously identified. In addition, there are key data gaps in our understanding of the long-term (decadal) processes that may lead to N limitation in Arctic tundra shrubs. Here I have outlined the primary methods that will be used to address key research questions throughout the following chapters:

In **Chapter 2** I design and complete an evidence-mapping protocol to contextualise N limitation within the recent evidence for controls to shrub growth and expansion.

In **Chapter 3** I demonstrate the use of the combined wood ring and modelling methods at Yuribei and on a timescale coincident with the remote sensing record (1980-2013). I reconstruct the first

ten $\delta^{15}N$ reconstructions from *Salix lanata* wood rings and design a theoretical model of shrub growth and nutrient interactions. Using the model-fitting and model-selection approach, I determine the most likely functional form of N limitation, the role of plant-soil feedbacks, and estimate asymptotes to growth.

In **Chapter 4** I apply the methods developed in the previous chapter to create a $\delta^{15}N$ dataset of greater spatial and temporal extent and conduct a similar modelling exercise. $\delta^{15}N$ time-series extend as far back as 1940 and are produced from three locations. I expand the modelling approach to account for temperature limits on photosynthesis.

In **Chapter 5** I examine the role of temporal resolution, seasonality, and snow dynamics, which I identified as important considerations in tundra shrub-nitrogen relations. I reconstruct regional snow depths using remote sensing. I adapt the previous modelling approach to contain internal dynamics at monthly temporal resolution and use these to assess the role of snow protection effects to shrubs and the role of snow insulation on temperature-dependent soil microbial processes. I also determine if $\delta^{18}O$ and $\delta^{13}C$ isotopes are related to snow variability and assess if these may be used as indicators of local-scale snow dynamics.

In **Chapter 6** I explain *Bristlecone*, a software library and tool for conducting model-fitting and model-selection that was developed as part of this research and used to produce Chapters 3, 4, and 5.

Finally, in **Chapter 7** the results are synthesised highlighting further questions raised by the research.

In addition, the **Appendices** contain associated research that was conducted during the time of this DPhil. The Global Pollen Project (GPP – first author) is a crowdsourcing platform that aims to establish a global pollen morphology key with taxonomic uncertainty, with the aim of increasing the robustness of palaeoecological research. At the time of writing, the GPP contains 2,750 digitised reference slides for 239 plant families (37% of global diversity) and 1,307 genera. The *Thalloo*

evidence mapping tool enables interactive visualisations for spatial-temporal evidence maps and was used to make the figures in Chapter 2. The Local Ecological Footprinting Tool (third author) provides ecological assessments at a landscape-scale for environmental decision making.

1.6 References

Ackerman, D. et al., 2017. Arctic shrub growth trajectories differ across soil moisture levels. *Glob Change Biol*, 23(10), pp.4294–4302.

Akhmetzhanova, A.A. et al., 2012. A rediscovered treasure: mycorrhizal intensity database for 3000 vascular plant species across the former Soviet Union. *Ecology*, 93(3), pp.689–690.

Amundson, R. et al., 2003. Global patterns of the isotopic composition of soil and plant nitrogen. *Global biogeochemical cycles*, 17(1), p.220.

Arneth, A. et al., 2010. Terrestrial biogeochemical feedbacks in the climate system. *Nature Geoscience*, 3(8), pp.525–532.

Bai, E. & Houlton, B.Z., 2009. Coupled isotopic and process-based modeling of gaseous nitrogen losses from tropical rain forests. *Global biogeochemical cycles*, 23(2), pp.n/a–n/a.

Bardgett, R.D. & Wardle, D.A., 2003. Herbivore-Mediated Linkages between Aboveground and Belowground Communities. *Ecology*, 84(9), pp.2258–2268.

Berner, L.T. et al., 2015. Biomass allometry for alder, dwarf birch, and willow in boreal forest and tundra ecosystems of far northeastern Siberia and north-central Alaska. *Forest Ecology and Management*, 337, pp.110–118.

Bhatt, U.S. et al., 2013. Recent Declines in Warming and Vegetation Greening Trends over Pan-Arctic Tundra. *Remote Sensing*, 5(9), pp.4229–4254.

Bjorkman, A.D. et al., 2019. Status and trends in Arctic vegetation: Evidence from experimental warming and long-term monitoring. *Ambio*, 23, pp.4294–15.

Blok, D. et al., 2010. Shrub expansion may reduce summer permafrost thaw in Siberian tundra. *Global Change Biology*, 16(4), pp.1296–1305.

Blume-Werry, G. et al., 2019. Dwelling in the deep - strongly increased root growth and rooting depth enhance plant interactions with thawing permafrost soil. *The New phytologist*, p.nph.15903.

Bobbink, R. et al., 2010. Global assessment of nitrogen deposition effects on terrestrial plant diversity: a synthesis. *Ecol Appl*, 20(1), pp.30–59.

Boelman, N.T. et al., 2011. Does NDVI reflect variation in the structural attributes associated with increasing shrub dominance in arctic tundra? *Environmental Research Letters*, 6(3), p.035501.

Bouskill, N.J., Riley, W.J. & Tang, J.Y., 2014. Meta-analysis of high-latitude nitrogen-addition and warming studies implies ecological mechanisms overlooked by land models. *Biogeosciences*, 11(23), pp.6969–6983.

Brandt, J.S. et al., 2013. Regime shift on the roof of the world: Alpine meadows converting to shrublands in the southern Himalayas. *Biological Conservation*, 158, pp.116–127.

Braun, S. et al., 2013. Evaluating the wood anatomical and dendroecological potential of arctic dwarf shrub communities. *IAWA Journal*, 34(4), pp.485–497.

Bukata, A.R. & Kyser, T.K., 2007. Carbon and Nitrogen Isotope Variations in Tree-Rings as Records of Perturbations in Regional Carbon and Nitrogen Cycles. *Environ Sci Technol*, 41(4), pp.1331–1338.

Burkhart, H.E. & Tomé, M., 2012. Growth Functions. In *Modeling Forest Trees and Stands*. Dordrecht: Springer Netherlands, pp. 111–130.

Burnham, K.P. & Anderson, D.R., 2007. *Model Selection and Multimodel Inference*, Springer Science & Business Media.

Cairney, J.W.G., 2000. Evolution of mycorrhiza systems. *Naturwissenschaften*, 87(11), pp.467–475.

Chapin, F.S. et al., 2005. Role of land-surface changes in arctic summer warming. *Science*, 310(5748), pp.657–660.

Chapman, S.K. et al., 2006. Plants actively control nitrogen cycling: uncorking the microbial bottleneck. *New Phytologist*, 169(1), pp.27–34.

Craine, J.M., 2007. Plant strategy theories: replies to Grime and Tilman. *Journal of Ecology*, 95(2), pp.235–240.

Craine, J.M., 2005. Reconciling plant strategy theories of Grime and Tilman. *Journal of Ecology*, 93(6), pp.1041–1052.

Craine, J.M. et al., 2015. Ecological interpretations of nitrogen isotope ratios of terrestrial plants and soils. *Plant and Soil*, 396(1-2), pp.1–26.

Craine, J.M. et al., 2009. Global patterns of foliar nitrogen isotopes and their relationships with climate, mycorrhizal fungi, foliar nutrient concentrations, and nitrogen availability. *New Phytologist*, 183(4), pp.980–992.

Craine, J.M. et al., 2018. Isotopic evidence for oligotrophication of terrestrial ecosystems. *Nature ecology & evolution*, 2(11), pp.1735–1744.

Dijkstra, P. et al., 2008. 15N enrichment as an integrator of the effects of C and N on microbial metabolism and ecosystem function. *Ecol Letters*, 11(4), pp.389–397.

Elmendorf, S.C. et al., 2011. Global assessment of experimental climate warming on tundra vegetation: heterogeneity over space and time. *Ecology Letters*, 15(2), pp.164–175.

Epstein, H.E., 2018. *Tundra Greenness*,

Epstein, H.E., Myers-Smith, I. & Walker, D.A., 2013. Recent dynamics of arctic and sub-arctic vegetation. *Environmental Research Letters*, 8(1), p.015040.

Fonti, P. et al., 2009. Studying global change through investigation of the plastic responses of xylem anatomy in tree rings. *New Phytologist*, 185(1), pp.42–53.

Forbes, B.C. et al., 2009. High resilience in the Yamal-Nenets social-ecological system, West Siberian Arctic, Russia. *Proc Natl Acad Sci U S A*, 106(52), pp.22041–22048.

Fritts, H.C., 1976. *Tree Rings and Climate*, Academic Press.

Frost, G.V. et al., 2013. Patterned-ground facilitates shrub expansion in Low Arctic tundra. *Environmental Research Letters*, 8(1), p.015035.

Frost, G.V. & Epstein, H.E., 2014. Tall shrub and tree expansion in Siberian tundra ecotones since the 1960s. *Glob Change Biol*, 20(4), pp.1264–1277.

Galloway, J.N., 2005. The global nitrogen cycle: past, present and future. *Sci China C Life Sci*, 48 Spec No, pp.669–677.

Gavazov, K.S. et al., 2010. Isotopic analysis of cyanobacterial nitrogen fixation associated with subarctic lichen and bryophyte species. *Plant and Soil*, 333(1-2), pp.507–517.

Gerhart, L.M. & McLauchlan, K.K., 2014. Reconstructing terrestrial nutrient cycling using stable nitrogen isotopes in wood. *Biogeochemistry*, 120(1-3), pp.1–21.

Gonsamo, A. & Chen, J.M., 2016. Circumpolar vegetation dynamics product for global change study. *Remote Sensing of Environment*, 182, pp.13–26.

Gordon, C., Wynn, J.M. & Woodin, S.J., 2001. Impacts of increased nitrogen supply on high Arctic heath: the importance of bryophytes and phosphorus availability. *The New phytologist*, 149(3), pp.461–471.

Grime, J.P., 2007. Plant strategy theories: a comment on Craine (2005). *Journal of Ecology*, 95(2), pp.227–230.

Guiot, J.L., Boucher, E. & Gea-Izquierdo, G., 2014. Process models and model-data fusion in dendroecology. *Frontiers in Ecology and Evolution*, 2, p.L04705.

Gundale, M.J. et al., 2012. Nitrogen niches revealed through species and functional group removal in a boreal shrub community. *Ecology*, 93(7), pp.1695–1706.

Hengl, T. et al., 2017. SoilGrids250m: Global gridded soil information based on machine learning B. Bond-Lamberty, ed. *PLOS ONE*, 12(2), p.e0169748.

Heskel, M. et al., 2013. Differential physiological responses to environmental change promote woody shrub expansion. *Ecology and evolution*, 3(5), pp.1149–1162.

Hietz, P., Dünisch, O. & Wanek, W., 2010. Long-Term Trends in Nitrogen Isotope Composition and Nitrogen Concentration in Brazilian Rainforest Trees Suggest Changes in Nitrogen Cycle. *Environ Sci Technol*, 44(4), pp.1191–1196.

Hilborn, R. & Mangel, M., 1997. *The Ecological Detective*, Princeton University Press.

Hobbie, E.A. & Colpaert, J.V., 2003. Nitrogen availability and colonization by mycorrhizal fungi correlate with nitrogen isotope patterns in plants. *The New phytologist*, 157(1), pp.115–126.

Hobbie, E.A. & Hobbie, J.E., 2008. Natural Abundance of 15N in Nitrogen-Limited Forests and Tundra Can Estimate Nitrogen Cycling Through Mycorrhizal Fungi: A Review. *Ecosystems*, 11(5), pp.815–830.

Hobbie, E.A. & Högberg, P., 2012. Nitrogen isotopes link mycorrhizal fungi and plants to nitrogen dynamics. *New Phytologist*, 196(2), pp.367–382.

Hossain, M.Z., 2011. The use of box-cox transformation technique in economic and statistical analyses. *Journal of Emerging Trends in Economics and Management Sciences*, 2(1), pp.32–39.

Hu, F.S., Finney, B.P. & Brubaker, L.B., 2001. Effects of Holocene Alnus Expansion on Aquatic Productivity, Nitrogen Cycling, and Soil Development in Southwestern Alaska. *Ecosystems*, 4(4), pp.358–368.

Hugelius, G. et al., 2014. Estimated stocks of circumpolar permafrost carbon with quantified uncertainty ranges and identified data gaps. *Biogeosciences*, 11(23), pp.6573–6593.

Huisman, J., 1994. The Models of Berendse and Tilman: Two Different Perspectives on Plant Competition? *Functional Ecology*, 8(3), p.282.

Hunt, R. & Cornelissen, J.H.C., 1997. Physiology, Allocation, and Growth Rate: A Reexamination of the Tilman Model. *The American naturalist*, 150(1), pp.122–130.

Jabot, F. & Pottier, J., 2012. A general modelling framework for resource-ratio and CSR theories of plant community dynamics J. Fridley, ed. *Journal of Ecology*, 100(6), pp.1296–1302.

Johnson, D.W., 2006. Progressive N limitation in forests: review and implications for long-term responses to elevated CO2. *Ecology*, 87(1), pp.64–75.

Juszak, I. et al., 2014. Arctic shrub effects on NDVI, summer albedo and soil shading. *Remote Sensing of Environment*, 153, pp.79–89.

Koyama, A. et al., 2014. Soil bacterial community composition altered by increased nutrient availability in Arctic tundra soils. *Frontiers in Microbiology*, 5(e34842), p.1071.

Kranabetter, J.M. et al., 2013. An Assessment of Contemporary and Historic Nitrogen Availability in Contrasting Coastal Douglas-Fir Forests Through δ15N of Tree Rings. *Ecosystems*, 16(1), pp.111–122.

Kryazhimskii, F.V. et al., 2011. System analysis of biogeocenoses of the Yamal Peninsula: Simulation of the impact of large-herd reindeer breeding on vegetation. *Russian Journal of Ecology*, 42(5), pp.351–361.

Kullman, L., 2010. A richer, greener and smaller alpine world: review and projection of warming-induced plant cover change in the Swedish Scandes. *AMBIO: A Journal of the Human Environment*, 39(2), pp.159–169.

Lamarque, J.F. et al., 2005. Assessing future nitrogen deposition and carbon cycle feedback using a multimodel approach: Analysis of nitrogen deposition. *Journal of Geophysical Research: Atmospheres*, 110(D19), p.20573.

Lamb, E.G. et al., 2011. A High Arctic soil ecosystem resists long-term environmental manipulations. *Global Change Biology*, 17(10), pp.3187–3194.

Lantz, T.C. et al., 2009. Relative impacts of disturbance and temperature: persistent changes in microenvironment and vegetation in retrogressive thaw slumps. *Glob Chang Biol*, 15(7), pp.1664–1675.

Lantz, T.C., Marsh, P. & Kokelj, S.V., 2012. Recent Shrub Proliferation in the Mackenzie Delta Uplands and Microclimatic Implications. *Ecosystems*, 16(1), pp.47–59.

Li, G. et al., 2014. Simulation of tree-ring widths with a model for primary production, carbon allocation, and growth. *Biogeosciences*, 11(23), pp.6711–6724.

Loranty, M.M. & Goetz, S.J., 2012. Shrub expansion and climate feedbacks in Arctic tundra. *Environmental Research Letters*, 7(1), p.011005.

Lucht, W. et al., 2002. Climatic control of the high-latitude vegetation greening trend and Pinatubo effect. *Science*, 296(5573), pp.1687–1689.

Luo, Y. et al., 2004. Progressive nitrogen limitation of ecosystem responses to rising atmospheric carbon dioxide. *Bioscience*, 54(8), pp.731–739.

Macias-Fauria, M., Forbes, B.C., Zetterberg, P. & Kumpula, T., 2012. Eurasian Arctic greening reveals teleconnections and the potential for structurally novel ecosystems. *Nature Climate Change*, 2(8), pp.613–618.

Mackay, J.R. & Burn, C.R., 2011. A Century (1910–2008) of Change in a Collapsing Pingo, Parry Peninsula, Western Arctic Coast, Canada. *Permafrost and Periglacial Processes*, 22(3), pp.266–272.

Marsh, P. et al., 2009. Changes in thaw lake drainage in the Western Canadian Arctic from 1950 to 2000 T. D. Prowse, ed. *Hydrological Processes*, 23(1), pp.145–158.

McKane, R.B. et al., 2002. Resource-based niches provide a basis for plant species diversity and dominance in arctic tundra. *Nature*, 415(6867), pp.68–71.

McLauchlan, K.K. et al., 2017. Centennial-scale reductions in nitrogen availability in temperate forests of the United States. *Scientific Reports*, 7(1), p.7856.

McLauchlan, K.K. et al., 2013. Changes in global nitrogen cycling during the Holocene epoch. *Nature*, 495(7441), pp.352–355.

McLauchlan, K.K. et al., 2007. Changes in nitrogen cycling during the past century in a northern hardwood forest. *Proc Natl Acad Sci U S A*, 104(18), pp.7466–7470.

Mikan, C.J., Schimel, J.P. & Doyle, A.P., 2002. Temperature controls of microbial respiration in arctic tundra soils above and below freezing. *Soil Biology and Biochemistry*, 34(11), pp.1785–1795.

Mikhailov, I.S., 2016. Soil map of the Russian Arctic on a 1 : 1 M scale: Contents and compilation methods. *Eurasian Soil Science*, 49(4), pp.377–385.

Mikhajlov, I.S., 2017. The expirience of creation of soil-ecological map of Yamal-Nenets autonomous district. *Bulletin of V.V. Dokuchaev Soil Science Institute*.

Miller, T.E. et al., 2005. A critical review of twenty years' use of the resource-ratio theory. *The American naturalist*, 165(4), pp.439–448.

Mina, M. et al., 2016. Forward modeling of tree-ring width improves simulation of forest growth responses to drought. *Agricultural and Forest Meteorology*, 221, pp.13–33.

Moulton, C.A. & Gough, L., 2018. Effects of Soil Nutrient Availability on the Role of Sexual Reproduction in an Alaskan Tundra Plant Community. *Arctic, Antarctic, and Alpine Research*, 43(4), pp.612–620.

Myers-Smith, I.H. et al., 2011. Shrub expansion in tundra ecosystems: dynamics, impacts and research priorities. *Environmental Research Letters*, 6(4), p.045509.

Myers-Smith, I.H., Elmendorf, S.C., et al., 2015. Climate sensitivity of shrub growth across the tundra biome. *Nature Climate Change*, 5(9), pp.887–891.

Myers-Smith, I.H., Hallinger, M., et al., 2015. Methods for measuring arctic and alpine shrub growth: A review. *Earth-Science Reviews*, 140, pp.1–13.

Paine, C.E.T. et al., 2011. How to fit nonlinear plant growth models and calculate growth rates: an update for ecologists. *Methods in Ecology and Evolution*, 3(2), pp.245–256.

Pearson, R.G. et al., 2013. Shifts in Arctic vegetation and associated feedbacks under climate change. *Nature Climate Change*, 3(7), pp.673–677.

Peñuelas, J. et al., 2013. Human-induced nitrogen-phosphorus imbalances alter natural and managed ecosystems across the globe. *Nature Communications*, 4(1), pp.2934–10.

Piao, S. et al., 2006. Effect of climate and CO2 changes on the greening of the Northern Hemisphere over the past two decades. *Geophysical Research Letters*, 33(23).

Piao, S. et al., 2014. Evidence for a weakening relationship between interannual temperature variability and northern vegetation activity. *Nature Communications*, 5, p.5018.

Picard, N., Saint-André, L. & Henry, M., 2012. *Manual for building tree volume and biomass allometric equations: from field measurement to prediction*, FAO/CIRAD.

Pithan, F. & Mauritsen, T., 2014. Arctic amplification dominated by temperature feedbacks in contemporary climate models. *Nature Geoscience*, 7(3), pp.181–184.

Pommerening, A. & Muszta, A., 2015. Methods of modelling relative growth rate. *Forest Ecosystems*, 2(1), p.5.

Pommerening, A. & Muszta, A., 2016. Relative plant growth revisited: Towards a mathematical standardisation of separate approaches. *Ecological Modelling*, 320, pp.383–392.

Poorter, H. et al., 2012. Biomass allocation to leaves, stems and roots: meta-analyses of interspecific variation and environmental control. *The New phytologist*, 193(1), pp.30–50.

Poorter, H., Anten, N.P.R. & Marcelis, L.F.M., 2013. Physiological mechanisms in plant growth models: do we need a supra-cellular systems biology approach? *Plant, Cell & Environment*, 36(9), pp.1673–1690.

Raynolds, M.K. et al., 2011. A new estimate of tundra-biome phytomass from trans-Arctic field data and AVHRR NDVI. *Remote Sensing Letters*, 3(5), pp.403–411.

Rinnan, R. et al., 2007. Fifteen years of climate change manipulations alter soil microbial communities in a subarctic heath ecosystem. *Glob Chang Biol*, 13(1), pp.28–39.

Rukhovich, D.I. et al., 2013. State soil map of the Russian federation: An ArcInfo version. *Eurasian Soil Science*, 46(3), pp.225–240.

Schuur, E.A.G. et al., 2008. Vulnerability of Permafrost Carbon to Climate Change: Implications for the Global Carbon Cycle. *Bioscience*, 58(8), pp.701–714.

Serreze, M.C. & Barry, R.G., 2011. Processes and impacts of Arctic amplification: A research synthesis. *Global and Planetary Change*, 77(1-2), pp.85–96.

Shaver, G.R. et al., 2001. Species Composition Interacts With Ferlilizer To Control Long-Term Change In Tundra Productivity. *Ecology*, 82(11), pp.3163–3181.

Sistla, S.A. & Schimel, J.P., 2013. Seasonal patterns of microbial extracellular enzyme activities in an arctic tundra soil: Identifying direct and indirect effects of long-term summer warming. *Soil Biology and Biochemistry*, 66, pp.119–129.

Sitters, J. et al., 2017. The Stoichiometry of Nutrient Release by Terrestrial Herbivores and Its Ecosystem Consequences. *Frontiers in Earth Science*, 5, p.2640.

Sitters, J. et al., 2019. Long-term heavy reindeer grazing promotes plant phosphorus limitation in arctic tundra. *Functional Ecology*, pp.1365–2435.13342.

Speer, J.H., 2010. *Fundamentals of tree-ring research*, Tucson: University of Arizona Press.

Stewart, K.J. et al., 2011. Bryophyte-cyanobacterial associations as a key factor in N2-fixation across the Canadian Arctic. *Plant and Soil*, 344(1-2), pp.335–346.

Stolbovoi, V. & McCallum, I., 2002. Land Resources of Russia.

Street, L.E., Mielke, N. & Woodin, S.J., 2017. Phosphorus Availability Determines the Response of Tundra Ecosystem Carbon Stocks to Nitrogen Enrichment. *Ecosystems*, 21(6), pp.1155–1167.

Stuecker, M.F. et al., 2018. Polar amplification dominated by local forcing and feedbacks. *Nature Climate Change*, 8(12), pp.1076–1081.

Sturm, M. et al., 2005. Winter Biological Processes Could Help Convert Arctic Tundra to Shrubland. *Bioscience*, 55(1), p.17.

Sturm, M., Racine, C. & Tape, K., 2001. Increasing shrub abundance in the Arctic. *Nature*, 411(6837), pp.546–547.

Tape, K.D. et al., 2012. Landscape Heterogeneity of Shrub Expansion in Arctic Alaska. *Ecosystems*, 15(5), pp.711–724.

Taylor, A.F.S. et al., 2003. Species level patterns in 13C and 15N abundance of ectomycorrhizal and saprotrophic fungal sporocarps. *The New phytologist*, 159(3), pp.757–774.

Thomas, R.Q., Brookshire, E.N.J. & Gerber, S., 2015. Nitrogen limitation on land: how can it occur in Earth system models? *Glob Change Biol*, 21(5), pp.1777–1793.

Tibshirani, R. & Hastie, T., 1987. Local Likelihood Estimation. *Journal of the American Statistical Association*, 82(398), pp.559–567.

Tilman, D., 1990. Mechanisms of Plant Competition for Nutrients: The Elements of a Predictive Theory of Competition. In *Perspectives on Plant Competition*. Elsevier, pp. 117–141.

Tilman, D., 1988. *Plant Strategies and the Dynamics and Structure of Plant Communities*, Princeton University Press.

Tilman, D., 2007. Resource competition and plant traits: a response to Craine et al. 2005. *Journal of Ecology*, 95(2), pp.231–234.

Tolwinski-Ward, S.E. et al., 2010. An efficient forward model of the climate controls on interannual variation in tree-ring width. *Climate Dynamics*, 36(11-12), pp.2419–2439.

Tolwinski-Ward, S.E., Anchukaitis, K.J. & Evans, M.N., 2013. Bayesian parameter estimation and interpretation for an intermediate model of tree-ring width. *Climate of the Past*, 9(4), pp.1481–1493.

Tucker, C.J., 1977. Asymptotic nature of grass canopy spectral reflectance. *Applied optics*, 16(5), pp.1151–1156.

Vaganov, E.A., Anchukaitis, K.J. & Evans, M.N., 2011. How Well Understood Are the Processes that Create Dendroclimatic Records? A Mechanistic Model of the Climatic Control on Conifer Tree-Ring Growth Dynamics. In *Dendroclimatology*. Developments in Paleoenvironmental Research. Dordrecht: Springer, Dordrecht, pp. 37–75.

Vitousek, P.M. et al., 1997. Human Alteration Of The Global Nitrogen Cycle: Sources And Consequences. *Ecological Applications*, 7(3), pp.737–750.

Walker, D.A., Leibman, M.O., et al., 2009. Spatial and temporal patterns of greenness on the Yamal Peninsula, Russia: interactions of ecological and social factors affecting the Arctic normalized difference vegetation index. *Environmental Research Letters*, 4(4), p.045004.

Walker, D.A., Raynolds, M.K., et al., 2009. The Circumpolar Arctic vegetation map. *Journal of Vegetation Science*, 16(3), pp.267–282.

Wimmer, R., 2002. Wood anatomical features in tree-rings as indicators of environmental change. *Dendrochronologia*, 20(1-2), pp.21–36.

Winkler, A.J. et al., 2019. Earth system models underestimate carbon fixation by plants in the high latitudes. *Nature Communications*, 10(1), p.885.

Young, A.B. et al., 2016. Species and site differences influence climate-shrub growth responses in West Greenland. *Dendrochronologia*, 37, pp.69–78.

Yu, Q. et al., 2011. Modeling dynamics of tundra plant communities on the Yamal Peninsula, Russia, in response to climate change and grazing pressure. *Environmental Research Letters*, 6(4), p.045505.

Yu, Q., Epstein, H. & Walker, D., 2009. Simulating the effects of soil organic nitrogen and grazing on arctic tundra vegetation dynamics on the Yamal Peninsula, Russia. *Environmental Research Letters*, 4(4), p.045027.

Chapter 2

Shrub growth and expansion in the Arctic tundra: an assessment of controlling factors using an evidence-based approach

This paper was published in the journal **Environmental Research Letters** in August 2017.

Martin, A.C. et al., 2017. Shrub growth and expansion in the Arctic tundra: an assessment of controlling factors using an evidence-based approach. *Environmental Research Letters*, 12(8), p.085007. doi: 10.1088/1748-9326/aa7989

Shrub growth and expansion in the Arctic tundra: an assessment of controlling factors using an evidence-based approach

Andrew C. Martin[1], Elizabeth S. Jeffers[1], Gillian Petrokofsky[1], Isla Myers-Smith[2], and Marc Macias-Fauria[3]

1. Oxford Long-Term Ecology Laboratory, Department of Zoology, University of Oxford, OX1 3PS
2. School of GeoSciences, University of Edinburgh, EH9 3FF
3. School of Geography and the Environment, University of Oxford, OX1 3QY

2.1 Abstract

Woody shrubs have increased in biomass and expanded into new areas throughout the Pan-Arctic tundra biome in the last decades, which has been linked to a biome-wide observed increase in productivity. Experimental, observational, and socio-ecological research suggests that air temperature – and to a lesser degree precipitation – trends have been the predominant drivers of this change. However, a progressive decoupling of these drivers from Arctic vegetation productivity has been reported, and since 2010, vegetation productivity has also been declining. We created a protocol to (a) identify the suite of controls that may be operating on shrub growth and expansion, and (b) characterise the evidence base for controls on Arctic shrub growth and expansion. We found evidence for a suite of 23 proximal controls that operate directly on shrub growth and expansion; the evidence base focused predominantly on just four controls (air temperature, soil moisture, herbivory, and snow dynamics). Sixty-five percent of evidence was generated in the warmest tundra climes, while 24% was from only one of 28 floristic sectors. Temporal limitations beyond 10 years existed for most controls, while the use of space-for-time approaches was high, with 14% of the evidence derived via experimental approaches. The findings suggest the current evidence base is not sufficiently robust or comprehensive at present to answer key questions of Pan-Arctic shrub

change. We suggest future directions that could strengthen the evidence, such increased attention for the collection of time-series and palaeoecological sources of evidence, and lead to an understanding of the key mechanisms driving changes in Arctic shrub environments.

2.2 Introduction

The Arctic tundra biome provides essential regulatory effects to global climate, in particular albedo (Juszak et al 2014), storage of organic carbon in its living biomass (Nauta et al 2014), and permafrost dynamics (Blok et al 2010). Over at least the last three decades, changes in vegetation composition have occurred that have significant consequences for the regulatory capability of tundra environments. Specifically, the ability of woody shrub species to produce biomass has increased, leading to shrubs of greater maximum height (Epstein et al 2012). Spatial expansion has also occurred: latitudinal 'shrublines' have advanced (Myers-Smith and Hick 2017), and new recruitment has enabled progressive filling of patchy landscapes (Tape et al 2006; Myers-Smith et al 2011; Frost, & Epstein 2014), both at the expense of mosses and lichens (Elmendorf et al 2012b). Such '**shrubification**' has been a Pan-Arctic trend since the 1980s, supported by data from experimental plots (Elmendorf et al 2012a), remote sensing and repeat photography (Sturm et al 2001; Walker et al 2006; Epstein et al 2012; Frost, & Epstein 2014; Tape et al 2012; Tremblay et al 2012), dendrochronologies (Macias-Fauria et al 2012; Forbes et al 2010), and indigenous knowledge (Cuerrier et al 2015; Henry et al 2012; Forbes et al 2009).

Air temperature and growing season lengths have increased in tundra ecosystems more than at lower latitudes, due to positive feedbacks that snow and ice (both on land and at sea) have with climate (Serreze, & Barry 2011). Shrubification can be attributed primarily to air temperature changes (Myers-Smith et al 2015), and to a lesser extent soil moisture (Myers-Smith et al 2015; Ackerman et al 2017), although shrub responses are heterogeneous. Data from the International Tundra Experiment (ITEX) long-term plot network demonstrates regional differences in the responses of tundra vegetation to summer air temperatures (Elmendorf et al 2012a). Similarly, shrub ring chronologies indicate heterogeneous long-term responses to mean summer temperature, with maximum sensitivity in warmer and wetter tundra sites (Myers-Smith et al 2015). The

observed heterogeneity suggests that other processes are important in controlling shrubification trends.

Shrubification has been linked to satellite-derived observations of widespread **'greening'** (increases in vegetation productivity, as measured by the Normalised Difference Vegetation Index – NDVI). Recently, the NDVI index has shown widespread negative trends across the Arctic tundra for the first time in decades (Epstein et al 2015; Ju and Masek 2016). NDVI has been demonstrated as a correlative proxy for shrubification (e.g. Forbes et al 2010), but predictions based on NDVI assume that (a) correlations between plot-scale productivity and NDVI holds across Arctic regions, despite local-scale factors introducing uncertainty (Jorgenson et al 2015), and (b) the relationship holds under future conditions (e.g. increased landscape shrub biomass). Recognising these uncertainties, the recent negative NDVI trends could be driven by complex environmental controls on shrubs beyond simple temperature metrics, such climatic extremes, and/or discrete disturbance events (Phoenix and Bjerke 2016). A progressive decline in the relationship between air temperature and NDVI since 1982 (Piao et al 2014; Kremers et al 2015) further supports the role of controls beyond air temperature.

Rapidly increasing air temperatures or increased growing season lengths appear responsible for shrubification trends, but with significant roles for other controls that contribute to heterogeneity in shrub-temperature responses. Without a robust assessment of these controls, one cannot ascertain their relative importance, the adequacy of current study designs, or the evidence required to reveal mechanisms driving shrubification processes. We conducted an evaluation of the current evidence base to answer the following questions:

1. What is the suite of controls that may act upon shrub growth and expansion in the Arctic tundra?
2. Do study designs take account of controls to shrubification and the mechanisms that may drive them, and are there spatial gaps in the evidence base that may limit our ability to detect their significance?

3. Do study designs take account of temporal characteristics sufficiently comprehensively to enable inferences to be drawn about likely mechanisms?

2.3 Methods

2.3.1 Protocol

To establish the controls that may be operating on Arctic shrub growth and expansion, the quantitative evidence base for each control, and gaps in current research directions, we systematically mapped recently published literature (full protocol in **Supplementary Material**). Briefly, we searched the online database Web of Science Core Collection for "topic= Arctic AND Shrub*", limited to publication years January 2012-January 2017. The following inclusion criteria were then applied:

1. **Shrub Response.** The study carried out statistical analysis within which at least one direct measure of shrub growth or expansion was used as a response variable (see **Supplementary Material**).
2. **Control.** Within the statistical test(s), an environmental control external to the shrub was used as a predictor to test against shrub response(s) identified in 1.
3. **Location.** At least one site for which the statistical test was completed must occur within the Arctic tundra. We defined the Arctic tundra as any land north of the Arctic treeline (Walker et al 2002) and 'Oro-Arctic' areas (Virtanen et al 2016).

For each included source, we identified every environmental control used as a predictor, at every independent site. The many-to-many relationship between sources, controls, and sites was multiplied out to form source-control-site data points, hereafter referred to as **evidence points**.

2.3.1.1 Delineation of Methodologies

Methodology was characterised for each evidence point as non-experimental or experimental, then into subclasses depending on temporal characteristics. Following best practice in evidence synthesis (Collaboration for Environmental Evidence 2013), we characterised the data used within statistical

analyses and not the data collected. For non-experimental evidence, **observational** controls had measurements taken through time to form a time-series of two or more time points. **Spatial gradients** used multiple measurements across space to substitute for time, while **chronosequences** attributed such variation across space to specific previous times to form a retrospective time-sequence. For environmental controls that had been manipulated, we defined four broadly distinct forms of experimental design based on the temporal nature of the data used within statistical analysis:

(i) A **time-series factorial** was defined as an experiment in which measurements of both the environmental control and shrub response(s) were taken through time and included in statistical analysis.

(ii) A **response-only factorial** only included time-series for the response variable, with no predictor time-series.

(iii) A **non-temporal factorial** contrasted the effect of a manipulation with a control plot, but no time series was present. For example, a nutrient addition experiment that tests for an effect on budding date after 18 years, with no 'before' point, and using differences between control and manipulation plots as a substitution for time, would fit this category.

(iv) An **experimental chronosequence** used multiple plots through space with varying treatment lengths to assess the role of treatment on shrub response(s).

2.3.2 Classification of Controls

We classified the environmental controls found in the evidence base into two major categories – **ultimate** and **proximal** – to provide scope and rigour to the systematic analysis via this underlying framework (**Figure 2–1**). **Proximal controls** are defined as environmental state parameters that directly impact the ability of a shrub individual to increase in biomass, reproduce or establish, without the need for any intermediate environmental properties (e.g. soil moisture, fire). Proximal controls provide the minimal degree of complexity from which to characterise the underlying mechanisms controlling shrub growth and expansion. Where a proxy measure was used that could

be directly attributed to a proximal control (e.g. thaw degree days, for ice and frost), this was included as an evidence point for the proximal control (all proxy measures listed in **Supplementary Table 2–3**). Proximal controls are driven ultimately by further environmental properties that influence their occurrence in space and time (**ultimate controls**), such as the role of sea ice on local air temperature, but without support for any direct mechanistic relationship to shrub performance. Shrub traits (e.g. leaf size and properties, reproductive strategy, wood and vessel structure, metabolic adaptations, growth form, species-related symbiotic relations, etc.) are significant determinants of plant-environment interactions, and can vary between genera, species, populations, ecotypes, and functional type (Chapin et al 1996). As we did not consider effect sizes in this analysis, we do not formally characterise internal controls here, and leave this for discussion and as a future avenue for research.

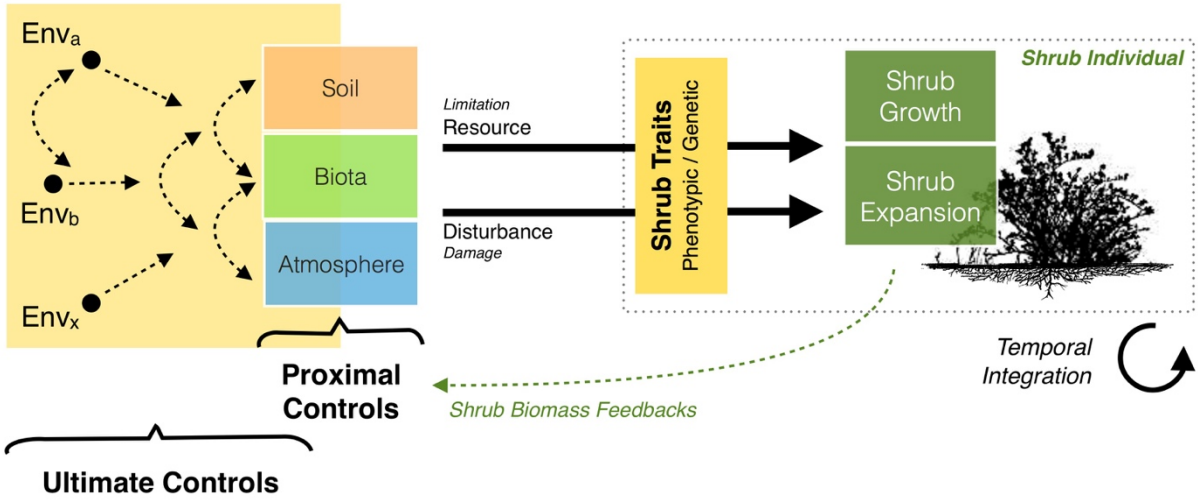

Figure 2–1 Conceptual overview of the framework used for the analysis. **Proximal controls** are state parameters that directly influence the performance of shrub individuals, without any intermediary role of other environmental parameters. These controls may be resources that can become limiting (e.g. soil moisture, nutrients), or disturbance drivers that can cause damage (e.g. gall mites, storm damage). The effectiveness of proximal controls is mediated by **shrub traits** (leaf size and properties, reproductive strategy, wood and vessel structure, metabolic adaptations, growth form, species-related symbiotic relations). The occurrence of proximal controls depends on additional environmental parameters – **ultimate controls** (Env$_a$, Env$_b$ … Env$_x$).

2.3.3 Analysis of Spatial Characteristics

To assess the degree to which the evidence points were spatially clustered or dispersed, we computed spatial autocorrelation using the Global Moran's I statistic (using an inverse distance spatial relationship over Euclidean distance). This approach was additionally utilised to identify

spatial clustering for control categories, controls, and experimental designs. To identify specific hotspots of evidence production, we calculated the Getis-Ord Gi* statistic (Getis and Ord 1992).

To identify research gaps in terms of broad environmental / ecological variability, we computed intersections between available Pan-Arctic layers and all evidence points, calculating Getis-Ord Gi* for each resultant landscape component:

a) for **climatic gradients**, we used bioclimate subzones, as defined in the Circumpolar Arctic Vegetation Map (CAVM) (Walker et al 2005);

b) for **plant functional forms**, we used the Arctic physiognomic classification from the CAVM (Walker et al 2005), which reflects variability in above-ground ecosystem structure; and

c) for **biodiversity**, we used Arctic floristic groups and sectors (Elvebakk et al 1999; Yurtsev 1994), which represent broad patterns of plant species diversity (occurring due to regional differences in glacial and landscape history).

2.4 Results

135 of the 432 sources identified met the inclusions criteria and were included in the final analysis.

We found 1,140 source-control-site evidence points reported during the period January 2012 – January 2017 (inclusive), derived from the 135 sources.

2.4.1 Suite of Controls

We identified 23 proximal controls (1,029 evidence points), presented in **Table 2–1**. Despite the range of potential proximal controls, there was predominant focus on just five: air temperature (including mean, maximum, minimum, above-freezing mean, growing degree days, and diurnal regional temperature proxies - 429 evidence points, or 41.69% of all proximal evidence points), soil moisture (including precipitation mean and sum, groundwater level, water track presence, and soil drainage proxies- 263, 25.56%), active layer depth (124, 12.05%), and to a lesser extent

herbivory (66, 6.41%), and snow depth / cover (including snow-free date - 37, 3.56%). We also identified analysis of 24 ultimate controls within the evidence base, outlined in **Table 2–2**.

Table 2–1 Proximal controls to Arctic shrub growth / expansion assessed within the evidence base (Jan. 2012 – Jan. 2017 inclusive).

Category		Control	Form / Duration Variants
Plant/Atmosphere Interface		Air Temperature	Winter Warming Event
		Atmospheric Carbon Dioxide Concentration	
		Fire	Occurrence, Burn Intensity
		Humidity	-
		Ice and Frost	Ice Encasement (Rain-on-Snow) Events
		Insolation	UV-B, Photoperiod
		Snow Depth / Cover	-
Biotic Interactions		Fungal Infection	-
		Herbivory (includes trampling and other biomass removal processes)	Bird, Mammal, Gall Mites, Leaf Miners, Defoliators, Other Invertebrates
Soil	Surface Conditions	Cryoturbation	-
		Erosion	Aeolian, Thermo-Erosion
		Soil Stability	Thaw Slump
	Belowground Conditions	Active Layer Depth	-
		Acidity	-
		Soil Moisture	Drought, Flooding
		Soil Salinity	Saline Incursion
		Soil Temperature	-
		Soil Texture	
	Belowground Resources	Organic Matter	-
		Mineral Content	-
		Nitrogen	-
		Phosphorus	-
		Potassium	-

Table 2–2 Ultimate controls utilised during the period Jan. 2012 – Jan. 2017.

Category	Ultimate Control(s)
Climatic teleconnections	Sea ice extent/concentration.
Glacial and Periglacial Geomorphology	Time since glacial retreat; blockfields; ice-wedge polygons; pingos; palsas; patterned ground; physiographic unit; thermokarst; water tracks.
Topography	Altitude; aspect; elevation; exposure; physiographic unit; slope
Ecosystem Structure	Plant functional forms; total above-ground biomass; canopy height; competitive intensity; distance from current shrub range.
Human Activity	Proximity to human infrastructure; replacement by human infrastructure.

2.4.2 Spatial Characteristics of the Evidence Base

Spatial analysis revealed areas of research focus, and spatial gaps (full results in Appendix A.2.3). Analysis of the spatial structure of all evidence points revealed global clustering (*Moran's Index = 0.237, z = 2.13, p = 0.033*). Hotspot analysis indicated six significant ($p<0.05$) hotspots of evidence production, centred in Alaska (Toolik Lake, Barrow, and Atqasuk), Alexandra Fiord (Canada), Endalen (Svalbard), and Abisko (Sweden).

Patterns of spatial clustering were significantly different between study designs, and controls (**Figure 2–2** and **Figure 2–3**). Clustering was greater for proximal control evidence points alone ($z = 2.43$, $p = 0.015$), with ultimate control evidence points displaying no significant clustering or dispersal, being widespread around the circumpolar Arctic. Experimental research was focused around long-term ITEX experimental plots at Toolik Lake (23 points), Daring Lake (13 points), Svalbard (14 points), and in the Fennoscandian Oro-Arctic (55 points). Only two experimental evidence points occurred in non-Fennoscandian Eurasia above the altitudinal treeline. There were no significant global patterns for any individual proximal control, or proximal control category, aside from the air-plant interface (clustering, $z = 3.85$, $p = 0.00$), and air temperature ($z = 2.11$, $p = 0.03$).

Spatial analysis identified evidence gaps when intersecting by environmental / vegetation variability:

A. **Climatic Gradient.** Arctic climatic bands were not equally represented within the dataset. Evidence points were weighted to the low Arctic in bioclimate subzone E (**Figure 2–2 and Figure 2–3**), the warmest of the Arctic's zonal bands. 64.84% of evidence points occurred in areas with > 9°C July temperatures: 37.46% of evidence points intersected subzone E, while 27.39% intersected Oro-Arctic regions (**Supplementary Figure 2–9**). Only 121 evidence points (10.69%) occurred in Subzones A and B (the highest latitude and climatically harshest regions), where some prostrate shrubs (i.e. *Salix arctica*) occur.

B. **Plant Functional Form.** The evidence base was clustered significantly into the 'tussock sedge, dwarf shrub, moss tundra' physiognomic unit, in which Toolik Lake is located (full results in **Supplementary Table 2–6**).

C. **Biodiversity.** For floristic diversity, significant clustering occurred within the 'Alaskan Tundra' sector of the Beringia group. This sector accounted for 33.5% of all evidence points, despite only being 3.96% of the total tundra area, and only one of 28 floristic regions. Outside these regions, we identified evidence gaps in areas for which there few of no evidence points. During this period, no results were published for six floristic sectors (10.5% tundra area): Anabar – Olenyek, East Chukotka, Kharaulakh, and Wrangell Island (Russia), Jan Mayen (Iceland), and North Beringian Islands (Alaska).

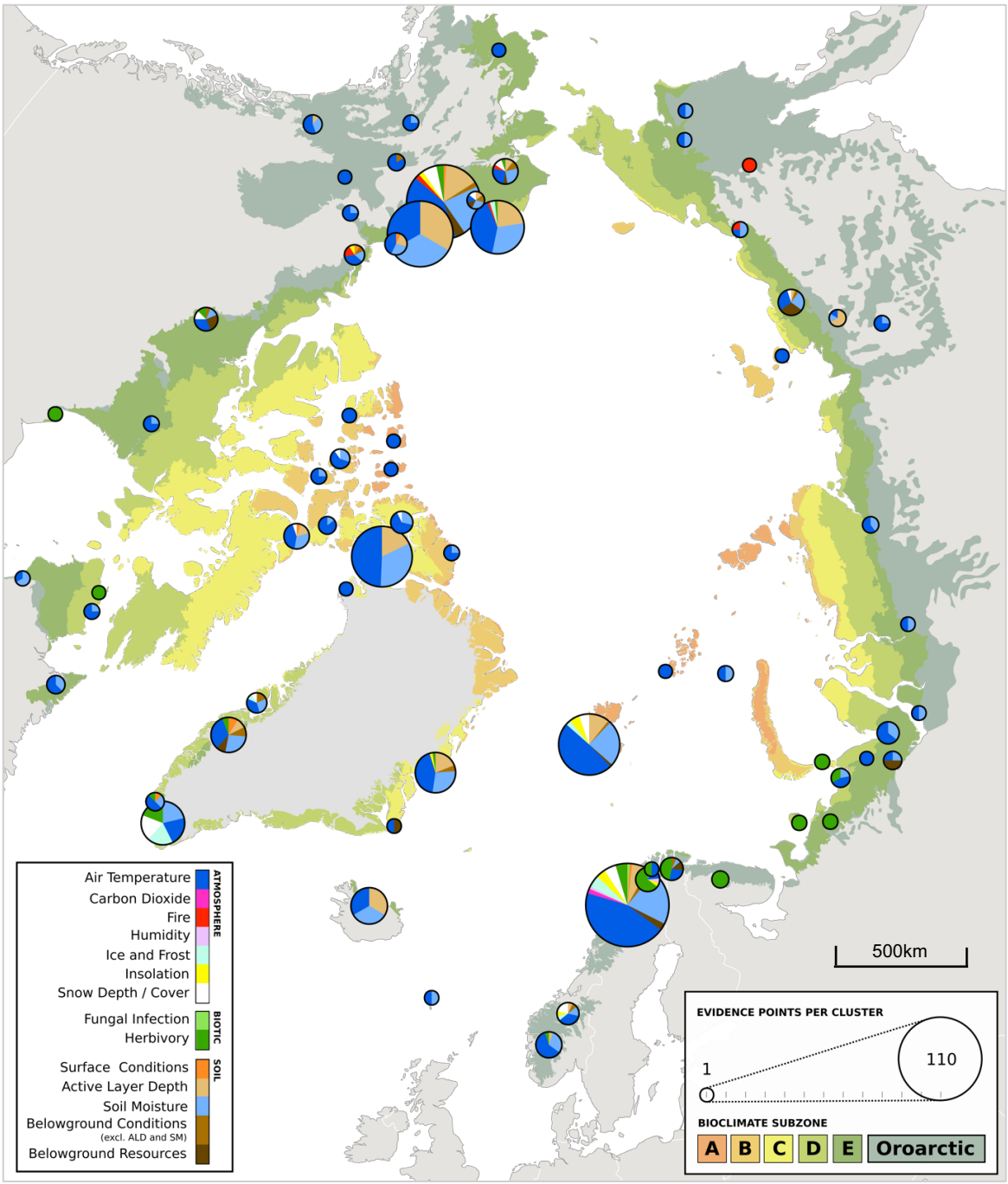

Figure 2–2 Pan-Arctic map showing evidence points generated for proximal controls on Arctic shrub growth and expansion (reported in peer-reviewed literature during the period 1 January 2012 – 31 January 2017). Each circle represents one location at which an evidence point was generated, or a regional cluster if more than one location occurred within 150km. Circle size represents the count of evidence points that occurred at the location. Pie segments represent a percentage of the evidence points at a location for each control type, represented by colour. Landmass colouring indicates bioclimatic subzone (Walker et al 2005), or Oro-Arctic (defined in ***Section 2a***). Continental and Pan-Arctic evidence points are not represented in this figure. ALD = Active Layer Depth; SM = Soil Moisture.

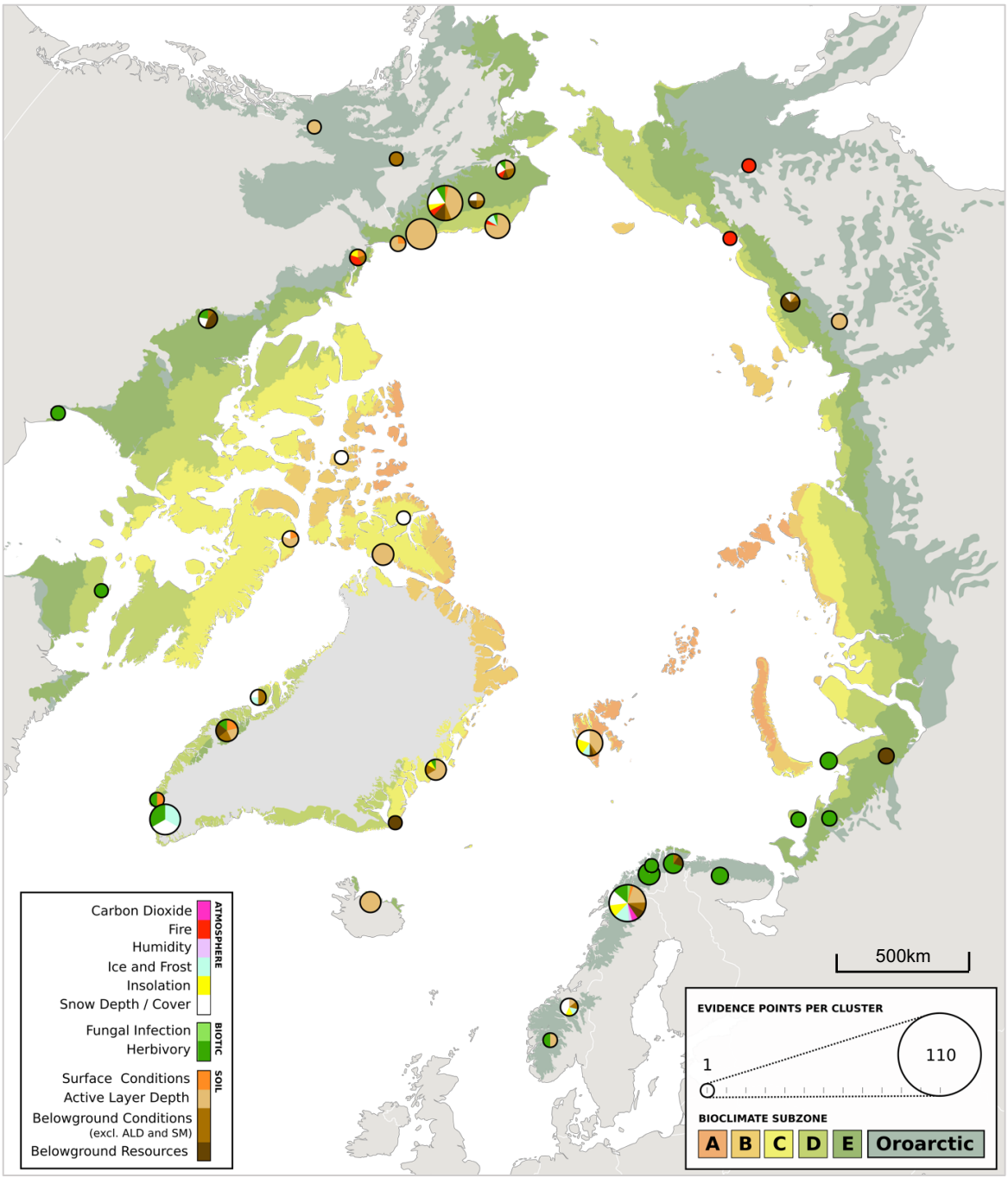

Figure 2–3 Pan-Arctic map showing evidence points generated for proximal controls on Arctic shrub growth and expansion (reported in peer-reviewed literature during the period 1 January 2012 – 31 January 2017), with air temperature and soil moisture sites removed from site pies to emphasise alternative controls. Each circle represents one location at which an evidence point was generated, or a regional cluster if more than one location occurred within 150km. Circle size represents the count of evidence points that occurred at the location. Pie segments represent a percentage of the evidence points at a location for each control type, represented by colour. Landmass colouring indicates bioclimatic subzone (Walker et al 2005), or Oro-Arctic (defined in ***Section 2a***). Continental and Pan-Arctic evidence points are not represented in this figure. ALD = Active Layer Depth; SM = Soil Moisture.

2.4.3 Methodological and Temporal Characteristics of the Evidence Base

In total, 86% of evidence points were derived from observation, with 14% derived from experimental data. For proximal controls, we found the greatest use of spatial gradient approaches for air temperature (14%), herbivory (5%), and soil belowground conditions (soil moisture (40%), and active layer depth (28%)) predictors (**Figure 2–4A**). Spatial gradient evidence points constituted 40% of the total. Soil belowground resources were assessed for a median timespan of eight years, biotic interactions for ten years, air-plant interface controls for 29 years, soil belowground conditions for 50 years, and soil surface conditions for 240 years.

Evidence was generally limited to no more than 25 years, aside from certain controls and study designs where long-term observational data could be obtained (**Figure 2–4B**). Decadal to centennial evidence was dominated by weather-station-derived proxy measures (coupled with dendroecological and repeat photography response variables): gridded, interpolated data products enabled numerous long-term studies of air temperature (proxy: regional air temperature), and soil moisture (proxy: regional precipitation). Space-for-time substitution was used widely, specifically for soil moisture, air temperature, and to a lesser extent herbivory, and snow dynamics. While observational evidence was used for all proximal controls aside from atmospheric CO_2 and insolation (including UV-β), manipulations were limited to 13 out of the 23: air temperature, snow dynamics, herbivory, nutrient availability, ice formation, insolation, CO_2, and soil abiotic conditions. Experimental design and the resulting evidence was weighted towards the use of non-temporal analyses (**Figure 2–4B**). This was especially pronounced for certain controls: for soil macronutrients, 10 of 11 experimental analyses used this approach.

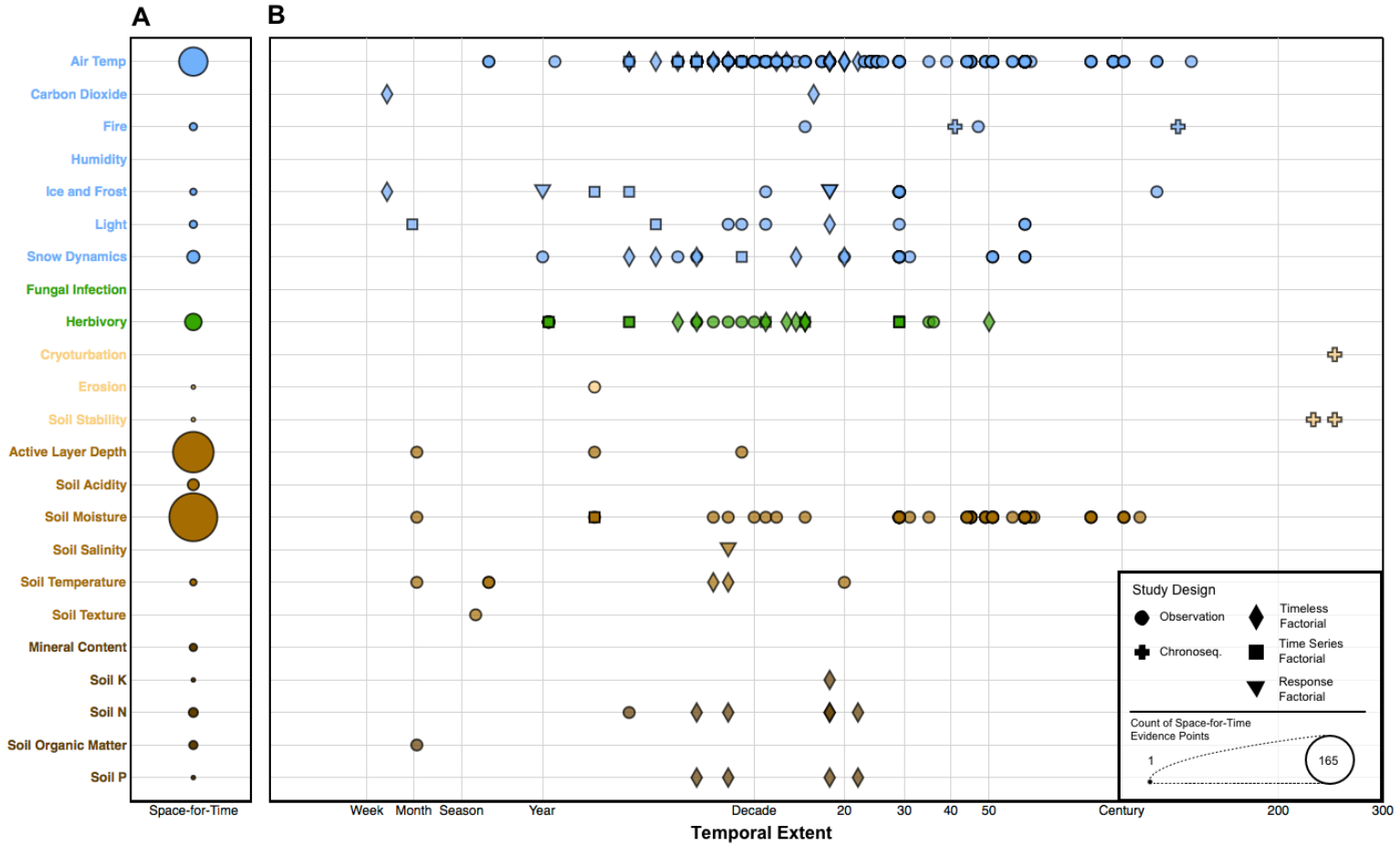

Figure 2–4A) Number of **space-for-time evidence points** per proximal control represented by circle size, excluding chronosequence approaches. **B)** Temporal extent of evidence points per proximal control (reported in peer-reviewed literature during the period 01 Jan 2012 – 31 Jan-2017). Temporal extent is defined as time series duration (observational and full factorial studies), time between newest and oldest phenomena (chronosequence), and length of prior manipulation before test ('non-temporal' factorial). Chronosequence is included here, despite being a space-for-time approach, as a concrete temporal extent is defined and used for analysis. Experimental design classifications are fully defined in Supplementary Material.

2.5 Discussion

2.5.1 Current Evidence Base

2.5.1.1 Suite of Controls

A predominant **focus on air temperature, soil moisture, and herbivory** controls suggests that other proximal controls – that may explain recent shrubification trends – are being overlooked. A scoping exercise (Supplementary Material 2.8.3.1) identified additional proximal controls that were not included in the compiled evidence base: abrasion by snow and ice crystals (Sonesson and Callaghan 1991), wind damage, microbial (Sedlacek et al 2014) and mycorrhizal (Deslippe and Simard 2011) associations, pollinators (Rich et al 2013), allelopathy (Bråthen et al 2010), soil micronutrients, and soil texture (Frost et al 2014). These proximal controls, alongside those that made a low proportion of the evidence base (atmospheric CO_2, insolation, cryoturbation, erosion (including aeolian and thermo-erosion), and fungal infection), may have been overlooked.

2.5.1.2 Spatial Gaps

Strong spatial clustering of the evidence base towards Alaska and Fennoscandia (**Figure 2–2**), as well as spatial gaps in the Eurasian Arctic (**Figure 2–5**), indicate that full spatial variability may not be captured for each proximal control. 65% of the evidence was generated within the warmest parts of the Arctic tundra biome, where summer (July) temperatures average above 9°C. Consequently, any controls and their mechanisms occurring exclusively, or with greater strength, in colder regions may be missed. Dominant processes driving shrubification vary between warmer tall shrub-dominated tundra (spatial infilling), and northernmost shrublines (increasing height and northward expansion). As these processes differ by biological mechanism, responses to controlling factors are likely different. The elevation gradient at Brooks Range has been used as a proxy for bioclimatic subzone, with elevation as a proxy for latitudinal space; however, the non-carbonate bedrock and acidic soils of the range do not account for the variability of plant functional forms and environmental conditions within higher latitude bioclimatic subzones.

Although shrubification trends appear to be driven by key species with Pan-Arctic distributions (*Betula nana*, *Salix* sp.), there are indications of regional genotypic variation in these, and other, shrub species (Abbott, & Brochmann 2003; Eidesen et al 2007; Eidesen et al 2013; Jørgensen et al 2012). Similarly, there is evidence for significant phenotypic plasticity within shrub species in response to some proximal controls (Edwards et al 2005; Berner et al 2015), such as within-species spatial gradients from prostrate to erect growth forms. Significant focus of evidence in the 'Alaskan Tundra' floristic sector (Tkach et al 2010), and the Fennoscandian Oro-Arctic, may limit coverage of unique Eurasian ecotypes, species, and thus adaptations, resilience and/or vulnerabilities (**Figure 2–5**). Spatial focus on long-term ITEX plots at Toolik Lake and Daring Lake (Alaska, USA) has provided comprehensive evidence for moist, low shrub tundra environments; however, this habitat does not account for the breadth of tundra physiognomies (aside from tussock sedge, dwarf shrub, moss tundra'), where other mechanisms may be significant.

2.5.1.3 Temporal Limitations

We noted temporal limitations to soil controls, where the extent of temporal evidence (aside from chronosequence) was generally limited to below 25 years (**Figure 2–4B**), while hypothesised drivers (e.g. changes in carbon and nitrogen cycling) may occur over decadal to centennial timescales. The mechanisms through which controls may operate vary by their timescales, from diurnal to centennial timescales. The lower temporal resolutions for soil-based controls (**Figure 2–13**) also limits inference of within-season and inter-annual control variability, such as how seasonal variability may impact different life-stages (budding, flowering).

Without time series, one can establish the directionality of response, but not the functional form (linear, non-linear) of the mechanism(s) at work. As 42% of experimental evidence utilised non-temporal approaches, these evidence points cannot be used independently to ascertain temporal dynamics, but may only be useful when combined in meta-analyses (e.g. Elmendorf et al 2012b), assuming methodologies can be compared. Similarly, climatic gradients, and the Finland-Norway herbivory gradient, provided a large fraction of evidence. Such space-for-time substitution approaches do mask the rate and order of temporal processes, and have been empirically proven to

overestimate the effects of air temperature on tundra shrub growth compared to experimental and observational data (Elmendorf et al 2015).

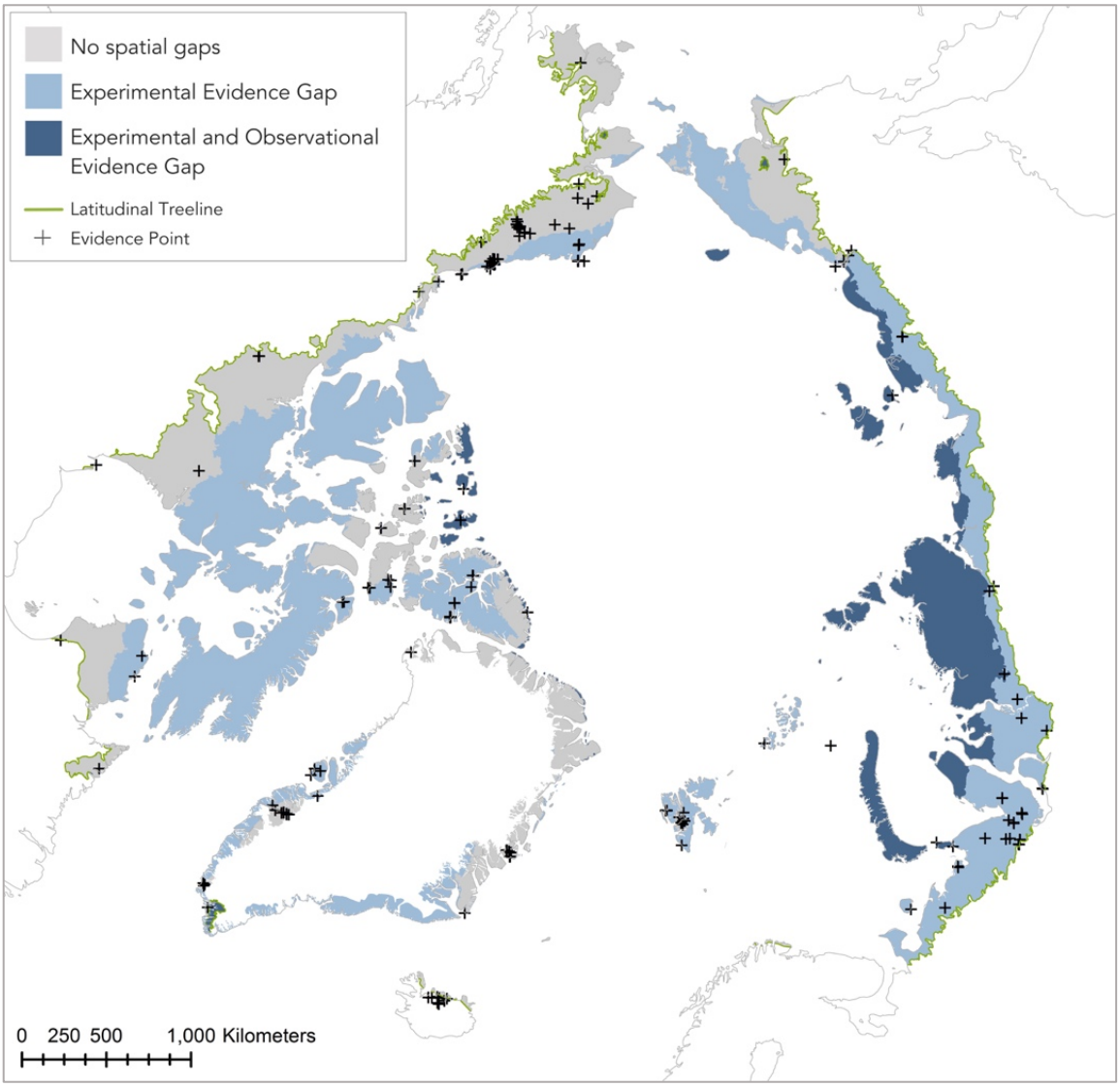

Figure 2–5 Map demonstrating regions of the Arctic for which there were evidence gaps during the period January 2012 to January 2017. The regional delineation displayed is bioclimatic subzone further split by floristic group. An evidence gap was defined as a bioclimate x floristic group region where there were five or less evidence points (equivalent to one or less point per year on average). Differentiation is made between evidence points derived from experimental evidence versus observational evidence (defined in 2.3.1.1).

2.5.2 Applications and Limitations of our Approach.

One or more mechanism(s) may be responsible for the aggregate effects of a proximal control on shrub growth and expansion through space and time. In the context of global change, these mechanisms need characterisation if we aim at predicting future changes in shrub performance, habitat, and distribution. Our methods of metadata collection can be used as a tool to assess the

suitability of the evidence base to support or refute possible mechanistic hypotheses. This approach is demonstrated for soil nutrients in **Box 2-1**.

We acknowledge limitations in our approach. First, the evidence gap between the Eurasian and North-American Arctic represents a publication bias; our search strategy does not cover Russian-language or other non-English scientific literature: spatial gaps in Eurasia may therefore have been accentuated. Second, we did not attempt to characterise the importance and strength of proximal controlling factors (resource limitations and discrete events) in space and time, but only the nature of the recent evidence base. Third, as our aim was to characterise the current trends in, and direction, of research, our analysis only represents the most recent five years of research, while older research may display different research quantities and priorities. We extended our search protocol to cover past research, finding that our study analysed 37.5% of all research captured by the search criteria (Supplementary Section 2.8.3.1).

Box 2 – 1. Soil Nitrogen and Shrubification

Soil macronutrients – including nitrogen (N), phosphorus (P), and potassium (K) – are essential resources for plant survival and fitness. Their availability is spatially heterogeneous at all scales (CAVM Team 2003; Walker et al 2005; DeMarco et al 2011), as a result of geology, glacial history, landscape processes, abiotic microhabitats, and plant community composition. Nitrogen is one of the most limiting macronutrients to growth in high latitudes (Bobbink et al 2010). There are multiple hypotheses for trajectories of tundra N availability, including: (1) increasing N availability as elevated soil temperatures increase the efficiency of N-mineralising microbes (Sturm et al 2005); (2) sequestration of N into long-lived woody biomass, reducing plant-available N in soils over decadal to centennial timescales (Progressive Nitrogen Limitation – PNL) (Luo et al 2004); and (3) increasing anthropogenic N deposition (Bobbink et al 2010).

Elevated N increases shrub aboveground biomass and shrub cover, with combined N-P limitation occurring in certain locations (Zamin, & Grogan 2012). Evidence was limited to 25 years, which is not long enough to support or refute some shrub-N interactions such as PNL: short-term mechanisms can distort long-term (decadal to centennial) processes (Johnson 2006). Exclusive use of non-temporal experimental approaches (**Figure 2–4B**) limits our understanding of rates of change, providing only single measures of 'length and strength of manipulation' to elevated response. The predictors do not quantify soil bioavailable N, essential to infer starting conditions and stressing and limiting levels of N, nor its forms, essential for understanding mechanisms of uptake and their variability between taxa and environments (i.e. organic versus inorganic forms). Manipulations often do not reflect the rates of change hypothesised for bioavailable N, fertilising at levels beyond expected quantities and rates of change (Bouskill et al 2014).

Past and future trajectories of N, thus N-shrub interactions, may be determined with alternative methodologies. Spatial variability in N or shrub traits (mycorrhizal associates, N-use efficiency) may explain the differences in observed N limitation across space, requiring measures of N and shrubification beyond ITEX plots. Temporal data could allow partitioning of short- and long-term responses that are difficult to differentiate using non-temporal approaches. Ideally, time-series measurements of bioavailable N on the same timescales as shrub responses would enable researchers to characterise rates of change within and between years whilst accounting for background N variability. Such time series could be interrogated using statistical modelling techniques, to infer the model and parameters of N-dependent growth.

2.5.3 Mechanisms Driving Recent and Future Shrubification Trends

To reduce uncertainty and increase predictive capability of future shrubification trends, we require mechanistic rather than correlative understandings of the underlying processes. We suggest three key knowledge gaps that must be reduced to gain such an understanding:

1. **Spatio-Temporal Trends of Shrubification.** Properties beyond biomass and cover that receive lesser attention, such as phenology (Prevéy et al 2017), and advancing shrublines (Myers-Smith et al 2017), could be measured for enhanced clarity over Pan-Arctic shrubification trends.
2. **Effectiveness of Proximal Controls.** Study designs may be sought that can assess the effectiveness per-unit variability within controlling factors on the identified mechanisms of shrubification, within the present range of environmental variability.
3. **Past and Future Variability of Control(s).** Each proximal control will vary through time due to a suite of underlying ultimate controls. Establishment of variability for the recent period, over which shrubification has occurred, and linking this to effect sizes, could enable establishment of (a) controls that are varying over the recent period, and (b) controls that may be responsible for observed changes.

We suggest four methodological directions through which tundra ecologists could enhance their study designs to address the above knowledge gaps:

1. **Incorporation of Time Series,** to establish the directionality and functional forms of shrub responses to environmental controls.
2. **Direct Measurement of Proximal Controls.** Many factorial studies did not measure the environmental control being studied, but rather measured the size and rate of perturbation. These methods assume that there is a direct link between perturbation and control (e.g. addition of 5g nitrogen fertiliser raises bioavailable nitrogen by a linear quantity). Inference of mechanisms could be enhanced by measuring the proximal control(s) directly, for example using automatic continuous loggers rather than gridded climate products. For time

series, this will require creative solutions to overcome control-specific difficulties. Soil belowground resources, for example nutrients, require measurements by field researchers, but new technologies should be sought to increase automatic data collection capabilities.

3. **Use of Environmental Archives.** Palaeo-ecological and palaeo-environmental data from environmental archives can provide long-term indications of shrub response and environmental control. Fossil pollen accumulation rate data could be modelled as shrub biomass response (Seppä et al 2009) to a range of proximal controls. For the long-term, dendroecological or pollen data could be coupled to long-term proxies of nutrient availability (McLauchlan et al 2013), herbivory (Baker et al 2016), and/or local climate (Jeffers et al 2012), from sedimentary archives.

4. **Mechanistic modelling.** Modelling approaches can be used to test competing hypotheses regarding the mechanisms underpinning plant-environment and biotic interactions through time (Jeffers et al 2012) and across space (Damgaard et al 2016); however, these approaches were rarely used in the evidence base.

2.6 Conclusions

Whereas there is significant evidence for an important role of air temperature and precipitation as drivers of Arctic shrubification, our systematic approach identified 23 proximal controls (those operating directly on the individual shrub and potentially affecting its growth and/or expansion) reported between January 2012 and January 2017, spanning soil properties, biotic interactions, and the plant-atmosphere interface. The focus of shrubification research has prominently been on air temperature and precipitation, while evidence suggesting a progressively declining role of climate requires us to consider other potential controls. We found spatial gaps in the evidence for all proximal controls, with research concentrated in the warmest bioclimatic zones of the tundra, and spatial gaps in Western and Central Arctic Siberia. These regions of research concentration already have a high percentage of tall shrub cover, while regions in the intermediate-latitude tundra (bioclimatic subzones B-D) were sparsely covered.

There is a basic mechanistic understanding of many of the controls on tundra shrubification, mostly derived from experiments conducted in acidic, low shrub, low latitude tundra, where shrubs are already a major component of the vegetation. In comparison, there is little focus on the mechanisms of range expansion and northward dispersal, operating at the northernmost range limit. In the studies included here, we found limitations in the temporal extent and resolution of evidence used, although this varied considerably depending on the proximal control considered. Study designs were in general found to be insufficient for investigating the mechanistic relationship between controls and shrubification, due to frequent use of non-temporal approaches. Reliance on space-for-time and non-temporal approaches risks not accurately reflecting the true rate and order of processes operating within the system.

We identify three knowledge gaps and four recommendations that tundra ecologists can consider to enhance the value of their data and future research. If progress is to be made toward predicting future spatial-temporal shrubification trends, more emphasis must be placed on the mechanisms underpinning shrubification.

The map is available as an online visualisation at: https://oxlel.github.io/evidencemaps/arcticshrub.

2.7 References

Abbott, R.J. & Brochmann, C., 2003, History and evolution of the arctic flora: in the footsteps of Eric Hulten, Molecular Ecology, 12(2), pp. 299-313.

Ackerman, D., Griffin, D., Hobbie, S.E. & Finlay, J.C., 2017, Arctic shrub growth trajectories differ across soil moisture levels, *Global Change Biology*.

Baker, A.G., Cornelissen, P., Bhagwat, S.A., Vera, F.W.M. & Willis, K.J., 2016, Quantification of population sizes of large herbivores and their long-term functional role in ecosystems using dung fungal spores, *Methods in Ecology and Evolution*, 7(11), pp. 1273-81

Barrio, I.C., Hik, D.S., Jónsdóttir, I.S., Bueno, C.G., Mörsdorf, M.A. & Ravolainen, V.T., 2016, Herbivory Network: An international, collaborative effort to study herbivory in Arctic and alpine ecosystems, Polar Science, 10(3), pp. 297-302.

Berner, L.T., Alexander, H.D., Loranty, M.M., Ganzlin, P., Mack, M.C., Davydov, S.P. & Goetz, S.J., 2015, Biomass allometry for alder, dwarf birch, and willow in boreal forest and tundra ecosystems of far northeastern Siberia and north-central Alaska, Forest Ecology and Management, 337, pp. 110-8.

Blok, D., Heijmans, M.M.P.D., Schaepman-Strub, G., Kononov, A.V., Maximov, T.C. & Berendse, F., 2010, Shrub expansion may reduce summer permafrost thaw in Siberian tundra, Global Change Biology, 16(4), pp. 1296-305.

Bobbink, R., Hicks, K., Galloway, J., Spranger, T., Alkemade, R., Ashmore, M., Bustamante, M., Cinderby, S., Davidson, E., Dentener, F., Emmett, B., Erisman, J.W., Fenn, M., Gilliam, F., Nordin, A., Pardo, L. & De Vries, W., 2010, Global assessment of nitrogen deposition effects on terrestrial plant diversity: a synthesis, Ecol Appl, 20(1), pp. 30-59.

Bouskill, N.J., Riley, W.J. & Tang, J.Y., 2014, Meta-analysis of high-latitude nitrogen-addition and warming studies implies ecological mechanisms overlooked by land models, Biogeosciences, 11(23), pp. 6969-83.

Bråthen, K.A., Fodstad, C.H. & Gallet, C., 2010, Ecosystem disturbance reduces the allelopathic effects of Empetrum hermaphroditum humus on tundra plants, Journal of Vegetation Science, 21(4), pp. 786-95.

Cuerrier, A., Brunet, N.D., Gérin-Lajoie, J., Downing, A. & Lévesque, E., 2015, The Study of Inuit Knowledge of Climate Change in Nunavik, Quebec: A Mixed Methods Approach, Human Ecology, 43(3), pp. 379-94.

Chapin, F.S., Bret-Harte, M.S., Hobbie, S.E. & Zhong, H., 1996, Plant functional types as predictors of transient responses of arctic vegetation to global change, Journal of Vegetation Science, 7(3), pp. 347-58.

Collaboration for Environmental Evidence. (2013). Guidelines for systematic reviews in environmental management. Retrieved from http://environmentalevidence.org/wp-content/uploads/2014/06/Review-guidelines-final-print.pdf.

Damgaard, C., Raundrup, K., Aastrup, P., Langen, P.L., Feilberg, J. & Nabe-Nielsen, J., 2016, Arctic resilience: no evidence of vegetation change in response to grazing and climate changes in South Greenland, Arctic, Antarctic, and Alpine Research, 48(3), pp. 531-49.

Deslippe, J.R. & Simard, S.W., 2011, Below-ground carbon transfer among Betula nana may increase with warming in Arctic tundra, New Phytologist, 192(3), pp. 689-98.

DeMarco, J., Mack, M.C. & Bret-Harte, M.S., 2011, The effects of snow, soil microenvironment, and soil organic matter quality on N availability in three Alaskan arctic plant communities, Ecosystems, 14(5), pp. 804-17.

Edwards, M.E., Brubaker, L.B., Lozhkin, A.V. & Anderson, P.M., 2005, Structurally novel biomes: A response to past warming in Beringia, Ecology, 86(7), pp. 1696-703.

Eidesen, P.B., Carlsen, T., Molau, U. & Brochmann, C., 2007, Repeatedly out of Beringia: Cassiope tetragona embraces the Arctic, Journal of Biogeography, 34(9), pp. 1559-74.

Eidesen, P.B., Ehrich, D., Bakkestuen, V., Alsos, I.G., Gilg, O., Taberlet, P. & Brochmann, C., 2013, Genetic roadmap of the Arctic: plant dispersal highways, traffic barriers and capitals of diversity, New Phytologist, 200(3), pp. 898-910.

Elmendorf, S.C., Henry, G.H., Hollister, R.D., Fosaa, A.M., Gould, W.A., Hermanutz, L., Hofgaard, A., Jónsdóttir, I.S., Jorgenson, J.C. & Lévesque, E., 2015, Experiment, monitoring, and gradient methods used to

infer climate change effects on plant communities yield consistent patterns, Proceedings of the National Academy of Sciences, 112(2), pp. 448-52.

Elmendorf, S.C., Henry, G.H.R., Hollister, R.D., Björk, R.G., Bjorkman, A.D., Callaghan, T.V., Collier, L.S., Cooper, E.J., Cornelissen, J.H.C., Day, T.A., Fosaa, A.M., Gould, W.A., Grétarsdóttir, J., Harte, J., Hermanutz, L., Hik, D.S., Hofgaard, A., Jarrad, F., Jónsdóttir, I.S., Keuper, F., Klanderud, K., Klein, J.A., Koh, S., Kudo, G., Lang, S.I., Loewen, V., May, J.L., Mercado, J., Michelsen, A., Molau, U., Myers-Smith, I.H., Oberbauer, S.F., Pieper, S., Post, E., Rixen, C., Robinson, C.H., Schmidt, N.M., Shaver, G.R., Stenström, A., Tolvanen, A., Totland, O., Troxler, T., Wahren, C.-H., Webber, P.J., Welker, J.M. & Wookey, P.A., 2012a, Global assessment of experimental climate warming on tundra vegetation: heterogeneity over space and time, Ecol Lett, 15(2), pp. 164-75.

Elmendorf, S.C., Henry, G.H.R., Hollister, R.D., Björk, R.G., Boulanger-Lapointe, N., Cooper, E.J., Cornelissen, J.H.C., Day, T.A., Dorrepaal, E., Elumeeva, T.G., Gill, M., Gould, W.A., Harte, J., Hik, D.S., Hofgaard, A., Johnson, D.R., Johnstone, J.F., Jónsdóttir, I.S., Jorgenson, J.C., Klanderud, K., Klein, J.A., Koh, S., Kudo, G., Lara, M., Lévesque, E., Magnússon, B., May, J.L., Mercado-Dı´az, J.A., Michelsen, A., Molau, U., Myers-Smith, I.H., Oberbauer, S.F., Onipchenko, V.G., Rixen, C., Schmidt, N.M., Shaver, G.R., Spasojevic, M.J., Þórhallsdóttir, E., Tolvanen, A., Troxler, T., Tweedie, C.E., Villareal, S., Wahren, C.-H., Walker, X., Webber, P.J., Welker, J.M. & Wipf, S., 2012b, Plot-scale evidence of tundra vegetation change and links to recent summer warming, Nature Climate Change, 2(6), p. 453.

Elvebakk, A., Elven, R. & Razzhivin, V.Y., 1999, Delimitation, zonal and sectorial subdivision of the Arctic for the Panarctic Flora Project, The species concept in the High North-A Panarctic Flora Initiative, pp. 375-86.

Epstein, H.E., Raynolds, M.K., Walker, D.A., Bhatt, U.S., Tucker, C.J. & Pinzon, J.E., 2012, Dynamics of aboveground phytomass of the circumpolar Arctic tundra during the past three decades, Environmental Research Letters, 7(1), p. 015506.

Epstein, H. E., Bhatt, U. S., Raynolds, M. K., Walker, D. A., Bieniek, P. A., Tucker, C. J., et al. (2015). *Tundra greenness*. Arctic Report Card 2015.

Forbes, B.C., Fauria, M.M. & Zetterberg, P., 2010, Russian Arctic warming and 'greening' are closely tracked by tundra shrub willows, Global Change Biology, 16(5), pp. 1542-54.

Forbes, B.C., Stammler, F., Kumpula, T., Meschtyb, N., Pajunen, A. & Kaarlejärvi, E., 2009, High resilience in the Yamal-Nenets social–ecological system, West Siberian Arctic, Russia, Proceedings of the National Academy of Sciences, 106(52), pp. 22041-8.

Frost, G.V. & Epstein, H.E., 2014, Tall shrub and tree expansion in Siberian tundra ecotones since the 1960s, Global Change Biology, 20(4), pp. 1264-77.

Frost, G.V., Epstein, H.E. & Walker, D.A., 2014, Regional and landscape-scale variability of Landsat-observed vegetation dynamics in northwest Siberian tundra, Environmental Research Letters, 9(2), p. 025004.

Getis, A. & Ord, J.K., 1992, The Analysis of Spatial Association by Use of Distance Statistics, Geographical Analysis, 24(3), pp. 189-206.

Henry, G.H.R., Harper, K.A., Chen, W., Deslippe, J.R., Grant, R.F., Lafleur, P.M., Lévesque, E., Siciliano, S.D. & Simard, S.W., 2012, Effects of observed and experimental climate change on terrestrial ecosystems in northern Canada: results from the Canadian IPY program, Climatic Change, 115(1), pp. 207-34.

Jeffers, E.S., Bonsall, M.B., Watson, J.E. & Willis, K.J., 2012, Climate change impacts on ecosystem functioning: evidence from an Empetrum heathland, New Phytologist, 193(1), pp. 150-64.

Johnson, D.W., 2006, Progressive N limitation in forests: review and implications for long-term responses to elevated CO2, Ecology, 87(1), pp. 64-75.

Jorgenson, J.C., Raynolds, M.K., Reynolds, J.H. & Benson, A.-M., 2015, Twenty-five year record of changes in plant cover on tundra of northeastern Alaska, Arctic, Antarctic, and Alpine Research, 47(4), pp. 785-806.

Juszak, I., Erb, A.M., Maximov, T.C. & Schaepman-Strub, G., 2014, Arctic shrub effects on NDVI, summer albedo and soil shading, Remote Sensing of Environment, 153, pp. 79-89.

Jørgensen, T., Kjær, K.H., Haile, J., Rasmussen, M., Boessenkool, S., Andersen, K., Coissac, E., Taberlet, P., Brochmann, C., Orlando, L., Gilbert, M.T.P. & Willerslev, E., 2012, Islands in the ice: detecting past vegetation on Greenlandic nunataks using historical records and sedimentary ancient DNA Meta-barcoding, Molecular Ecology, 21(8), pp. 1980-8.

Ju, J. & Masek, J. G. (2016). The vegetation greenness trend in canada and US alaska from 1984–2012 landsat data. Remote Sensing of Environment, 176, 1-16.

Kremers, K.S., Hollister, R.D. & Oberbauer, S.F., 2015, Diminished response of arctic plants to warming over time, PLoS One, 10(3), p. e0116586.

Luo, Y., Su, B.O., Currie, W.S., Dukes, J.S., Finzi, A., Hartwig, U., Hungate, B., McMurtrie, R.E., Oren, R.A.M. & Parton, W.J., 2004, Progressive nitrogen limitation of ecosystem responses to rising atmospheric carbon dioxide, Bioscience, 54(8), pp. 731-9.

Macias-Fauria, M., Forbes, B.C., Zetterberg, P. & Kumpula, T., 2012, Eurasian Arctic greening reveals teleconnections and the potential for structurally novel ecosystems, Nature climate change, 2(8), pp. 613-8.

Mazier, F., Nielsen, A.B., Broström, A., Sugita, S. & Hicks, S., 2012, Signals of tree volume and temperature in a high-resolution record of pollen accumulation rates in northern Finland, Journal of Quaternary Science, 27(6), pp. 564-74

McLauchlan, K.K., Williams, J.J., Craine, J.M. & Jeffers, E.S., 2013, Changes in global nitrogen cycling during the Holocene epoch, Nature, 495(7441), p. 352.

Myers-Smith, I.H., Elmendorf, S.C., Beck, P.S.A., Wilmking, M., Hallinger, M., Blok, D., Tape, K.D., Rayback, S.A., Macias-Fauria, M., Forbes, B.C., Speed, J.D.M., Boulanger-Lapointe, N., Rixen, C., Lévesque, E., Schmidt, N.M., Baittinger, C., Trant, A.J., Hermanutz, L., Collier, L.S., Dawes, M.A., Lantz, T.C., Weijers, S., Jørgensen, R.H., Buchwal, A., Buras, A., Naito, A.T., Ravolainen, V., Schaepman-Strub, G., Wheeler, J.A., Wipf, S., Guay, K.C., Hik, D.S. & Vellend, M., 2015, Climate sensitivity of shrub growth across the tundra biome, Nature Climate Change, 5(9), pp. 887-91.

Myers-Smith, I.H., Forbes, B.C., Wilmking, M., Hallinger, M., Lantz, T., Blok, D., Tape, K.D., Macias-Fauria, M., Sass-Klaassen, U. & Lévesque, E., 2011, Shrub expansion in tundra ecosystems: dynamics, impacts and research priorities, Environmental Research Letters, 6(4), p. 045509.

Myers-Smith, I. & Hik, D.S., 2017, Climate warming as a driver of tundra shrubline advance, Journal of Ecology.

Nauta, A.L., Heijmans, M.M.P.D., Blok, D., Limpens, J., Elberling, B., Gallagher, A., Li, B., Petrov, R.E., Maximov, T.C., van Huissteden, J. & Berendse, F., 2014, Permafrost collapse after shrub removal shifts tundra ecosystem to a methane source, Nature Climate Change, 5(1), pp. 67-70.

Orshan 1989, Shrub as a Growth Form, in The Biology and Utilization of Shrubs, pp. 249-65.

Oulehle, F., Rowe, E.C., My\vska, O., Chuman, T. & Evans, C.D., 2016, Plant functional type affects nitrogen use efficiency in high-Arctic tundra, Soil Biology and Biochemistry, 94, pp. 19-28.

Phoenix, G.K. & Bjerke, J.W., 2016, Arctic browning: extreme events and trends reversing arctic greening, Global Change Biology.

Piao, S., Friedlingstein, P., Ciais, P., Zhou, L. & Chen, A., 2006, Effect of climate and CO2 changes on the greening of the Northern Hemisphere over the past two decades, Geophysical Research Letters, 33(23).

Piao, S., Nan, H., Huntingford, C., Ciais, P., Friedlingstein, P., Sitch, S., Peng, S., Ahlström, A., Canadell, J.G., Cong, N., Levis, S., Levy, P.E., Liu, L., Lomas, M.R., Mao, J., Myneni, R.B., Peylin, P., Poulter, B., Shi, X., Yin, G., Viovy, N., Wang, T., Wang, X., Zaehle, S., Zeng, N., Zeng, Z. & Chen, A., 2014, Evidence for a weakening relationship between interannual temperature variability and northern vegetation activity, Nat Commun, 5, p. 5018.

Prevéy, J., Vellend, M., Rüger, N., Hollister, R.D., Bjorkman, A.D., Myers-Smith, I.H., Elmendorf, S.C., Clark, K., Cooper, E.J., Elberling, B., Fosaa, A.M., Henry, G.H.R., Høye, T.T., Jónsdóttir, I.S., Klanderud, K., Lévesque, E., Mauritz, M., Molau, U., Natali, S.M., Oberbauer, S.F., Panchen, Z.A., Post, E., Rumpf, S.B., Schmidt, N.M., Schuur, E.A.G., Semenchuk, P.R., Troxler, T., Welker, J.M. & Rixen, C., 2017, Greater temperature sensitivity of plant phenology at colder sites: implications for convergence across northern latitudes, Global Change Biology.

Rich, M.E., Gough, L. & Boelman, N.T., 2013, Arctic arthropod assemblages in habitats of differing shrub dominance, Ecography, 36(9), pp. 994-1003

Schirrmeister, L., Grosse, G., Wetterich, S., Overduin, P.P., Strauss, J., Schuur, E.A.G. & Hubberten, H.-W., 2011, Fossil organic matter characteristics in permafrost deposits of the northeast Siberian Arctic, Journal of Geophysical Research: Biogeosciences, 116(G2), pp. G00M02-.

Sedlacek, J.F., Bossdorf, O., Cortés, A.J., Wheeler, J.A. & van Kleunen, M., 2014, What role do plant--soil interactions play in the habitat suitability and potential range expansion of the alpine dwarf shrub Salix herbacea? *Basic and Applied Ecology*, 15(4), pp. 305-15

Seppä, H., Alenius, T., Muukkonen, P., Giesecke, T., Miller, P.A. & Ojala, A.E., 2009, Calibrated pollen accumulation rates as a basis for quantitative tree biomass reconstructions, The Holocene, 19(2), pp. 209-20.

Serreze, M.C. & Barry, R.G., 2011, Processes and impacts of Arctic amplification: A research synthesis, Global and Planetary Change, 77(1-2), pp. 85-96.

Sonesson, M. & Callaghan, T.V., 1991, Strategies of survival in plants of the Fennoscandian tundra, Arctic, pp. 95-105.

Sturm, M., Racine, C. & Tape, K., 2001, Climate change: increasing shrub abundance in the Arctic, Nature, 411(6837), pp. 546-7.

Sturm, M., Schimel, J., Michaelson, G., Welker, J.M., Oberbauer, S.F., Liston, G.E., Fahnestock, J. & Romanovsky, V.E., 2005, Winter Biological Processes Could Help Convert Arctic Tundra to Shrubland, BioScience, 55(1), pp. 17-26.

Tape, K.D., Hallinger, M., Welker, J.M. & Ruess, R.W., 2012, Landscape Heterogeneity of Shrub Expansion in Arctic Alaska, Ecosystems, 15(5), pp. 711-24.

Tape, K., Sturm, M. & Racine, C., 2006, The evidence for shrub expansion in Northern Alaska and the Pan-Arctic, Global Change Biology, 12(4), pp. 686-702.

Tkach, N.V., Hoffmann, M.H., Röser, M. & Hagen, K.B.V., 2010, Temporal patterns of evolution in the Arctic explored in Artemisia L. (Asteraceae) lineages of different age, Plant Ecology & Diversity, 1(2), pp. 161-9.

Tremblay, B., Lévesque, E. & Boudreau, S., 2012, Recent expansion of erect shrubs in the Low Arctic: evidence from Eastern Nunavik, Environmental Research Letters, 7(3), p. 035501.

Virtanen, R., Oksanen, L., Oksanen, T., Cohen, J., Forbes, B.C., Johansen, B., Käyhkö, J., Olofsson, J., Pulliainen, J. & Tømmervik, H., 2016, Where do the treeless tundra areas of northern highlands fit in the global biome system: toward an ecologically natural subdivision of the tundra biome, Ecology and Evolution, 6(1), pp. 143-58.

Walker, D.A., Daniëls, F.J.A., Alsos, I., Bhatt, U.S., Breen, A.L., Buchhorn, M., Bültmann, H., Druckenmiller, L.A., Edwards, M.E., Ehrich, D., Epstein, H.E., Gould, W.A., Ims, R.A., Meltofte, H., Raynolds, M.K., Sibik, J., Talbot, S.S. & Webber, P.J., 2016, Circumpolar Arctic vegetation: a hierarchic review and roadmap toward an internationally consistent approach to survey, archive and classify tundra plot data, Environmental Research Letters, 11(5), p. 055005.

Walker, D.A., Gould, W.A., Maier, H.A. & Raynolds, M.K., 2002, The Circumpolar Arctic Vegetation Map: AVHRR-derived base maps, environmental controls, and integrated mapping procedures, International Journal of Remote Sensing, 23(21), pp. 4551-70.

Walker, D.A., Raynolds, M.K., Daniëls, F.J., Einarsson, E., Elvebakk, A., Gould, W.A., Katenin, A.E., Kholod, S.S., Markon, C.J., Melnikov, E.S., Moskalenko, N.G., Talbot, S.S., Yurtsev, B.A. & The other members of the CAVM Team, 2005, The Circumpolar Arctic vegetation map, Journal of Vegetation Science, 16(3), pp. 267-82.

Walker, M.D., Wahren, C.H., Hollister, R.D., Henry, G.H.R., Ahlquist, L.E., Alatalo, J.M., Bret-Harte, M.S., Calef, M.P., Callaghan, T.V., Carroll, A.B., Epstein, H.E., Jónsdóttir, I.S., Klein, J.A., Magnússon, B., Molau, U., Oberbauer, S.F., Rewa, S.P., Robinson, C.H., Shaver, G.R., Suding, K.N., Thompson, C.C., Tolvanen, A., Totland, Turner, P.L., Tweedie, C.E., Webber, P.J. & Wookey, P.A., 2006, Plant community responses to experimental warming across the tundra biome, Proceedings of the National Academy of Sciences, 103(5), pp. 1342-6.

Yurtsev, B.A., 1994, Floristic division of the Arctic, Journal of Vegetation Science, 5(6), pp. 765-76.

Zamin, T.J. & Grogan, P., 2012, Birch shrub growth in the low Arctic: therelative importance of experimental warming, enhanced nutrient availability, snow depth and caribou exclusion, Environmental Research Letters, 7(3), p. 034027.

1

2.8 Supplementary Material

2.8.1 Method for Systematic Protocol

2.8.1.1 Classification of Shrub Responses

The biological mechanisms through which shrubification occurs encompass increased shrub height, patch infilling, and range expansion (Myers-Smith et al 2011). These components of shrubification may thus have very different controlling factors. We assessed the evidence base for shrub responses by including shrub responses for two broadly defined classes:

i. **Shrub Growth.** Modification of above- and below-ground biomass, and / or improved physiological performance of an individual shrub.

ii. **Shrub Expansion.** Modification of reproductive effort (sexual or asexual), reproductive success, or successful establishment of an individual shrub; or modification of species assemblage to reflect changing spatial configuration of shrub biomass.

A shrub species was defined as a woody vascular plant species that is known to grow in a shrub form (Orshan 1989). We excluded response variables that did not include sufficient support as a proxy (while recognising the possible connection between these variables and shrubification). This led to the exclusion of pollen data and NDVI, where a connection to shrubification processes was not established in the paper (e.g. many of the 'greening' studies).

2.8.2 Systematic Protocol

To determine research sources to include, we searched the online database Web of Science Core Collection for "topic= Arctic AND Shrub*", limited to publication years January 2012-January 2017 (inclusive). This resulted in 432 publications. The following inclusion criteria were then applied:

1. **Shrub Response.** The study carried out statistical analysis within which at least one direct measure of shrub growth of expansion was used as a response variable (as defined in 2.8.1.1).

2. **Control.** Within statistical test(s), an environmental control external to the shrub was used as a predictor to test against shrub response(s) identified in 1.

3. **Location.** At least one site for which the statistical test was completed must occur within the Arctic tundra. We defined the Arctic tundra as any land north of the Arctic treeline, as defined by Walker et al (2002). We also included 'Oro-Arctic' alpine tundra in this definition, as these areas are botanically more like Arctic than Alpine tundra, sharing common Arctic components of biodiversity (Virtanen et al 2016). Higher elevations in these areas, however, do create specific environmental conditions, including deeper permafrost, and differing climatic seasonality, but these create opportunity for environmental gradient study. We defined the Oro-Arctic as WWF ecoregions that make up the Arctic biome, minus land above the altitudinal treeline, following Virtanen et al 2016. This resulted in the inclusion to the high-altitude Scandinavian tundra and others, shown in **Figure 2–2**. Locations that did not fall within the area itself or a 50km buffer were excluded.

For each included source, we identified every environmental control used as a predictor, and every site. Sites were separated out where they could be analysed independently in terms of the control in question. This precludes, for instance, sites that form part of a chronosequence or spatial gradient. Regional or Pan-Arctic studies were flagged as such. For meta-analyses, we used the site-control data 'second hand' (i.e. as published by the authors in the publication), unless the required data was not provided. The many-to-many relationship between controls and sites was multiplied out to form source-control-site data points.

For each control data point, we characterised the nature of the evidence in terms of methodology, and temporal resolution and extent. Following best practice in evidence synthesis (Collaboration for Environmental Evidence 2013), we characterised the data used in the statistical analysis and not the data collected. We identified the data type (Boolean, continuous, integer, ordinal) and units of the input data for the control. The temporal extent, resolution, and length of any prior manipulations were recorded. Methodology was classified into non-experimental or experimental, then into

subclasses depending on temporal characteristics. For non-experimental evidence, **observational** controls had measurements taken through time to form a time-series of two or more time points. **Spatial gradients (or space-for-time)** used multiple measurements across space to substitute for time, while **chronosequences** attributed such variation across space to specific previous times to form a retrospective time-sequence. For environmental controls that had been manipulated, we defined four broadly distinct forms of experimental design based on the temporal nature of the data used within statistical analysis:

(i) A **time-series factorial** was defined as an experiment in which measurements of both the environmental control and shrub response(s) were taken through time, and included in statistical analysis. This includes before-after-control-intervention (BACI) designs, as well as those with more than two time points.

(ii) A **response-only factorial** only included time-series (> one time point) for the response variable, with no predictor time-series (Boolean - manipulated / not manipulated). This includes studies that provided, for example, one summer validation of the effect of an open-top-chamber, but did not include measurements of temperature in their statistical analysis.

(iii) A **non-temporal factorial** contrasted the effect of a manipulation with a control plot, but no time series was present. For example, a nutrient addition experiment that tests for an effect on budding date after 18 years, with no 'before' point, and using differences between control and manipulation plots as a substitution for time, would fit this category.

(iv) An **experimental chronosequence** used multiple plots through space with varying treatment lengths to assess the role of treatment length on shrub response(s).

2.8.3 Supplementary Results

2.8.3.1 Inclusion Criteria

We found 432 publications using our search criteria, of which 135 were included inclusion criteria was applied. The phenomenon of Arctic greening was, however, first fully recognised in the early 2000s, although satellite indices of Arctic vegetation productivity have been available since 1982. Similarly, 'shrubification' research has occurred over the past two decades or more, with other shrub-based research occurring prior to this period. Our study was designed to detect spatial gaps and methodological limitations within current research, although we recognise the importance of prior research for defining current research foci and methodological approaches.

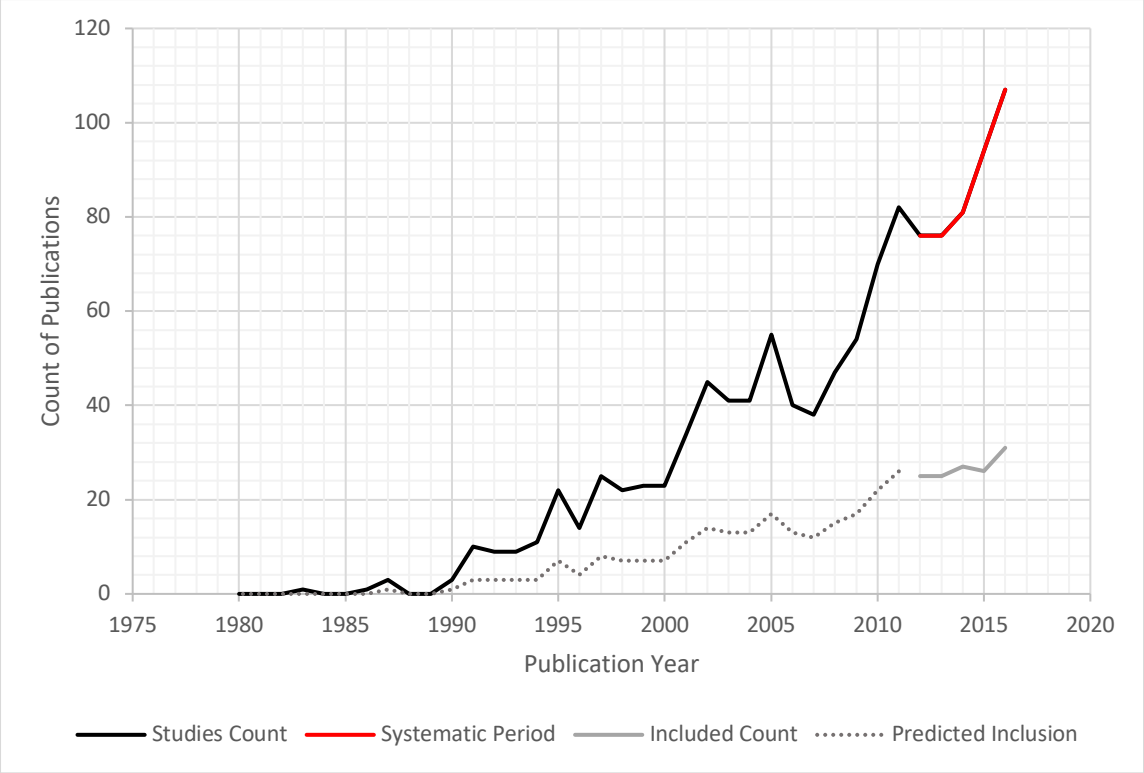

Figure 2–6 Number of publications per year on Arctic shrub research since 1980, using search criteria defined in our systematic protocol. Back-prediction of inclusion prior to 2012 calculated using inclusion rate for 2012-2017 and provided for indicative purposes only.

To assess the effect of assessing a five-year window (Jan. 2012 – Jan. 2017), we completed our search for all time. We found only one publication before 1980 ("Transpiration Rates of Arctic and Alpine Shrubs" – Bliss 1960). The period of our systematic approach accounts for 37.5% of all publications since 1980 (434 of 1,157 publications). For the five-year period, there was a mean

inclusion rate per year of 31.15% (28.97% for 2016, 27.66% for 2015, 33.33% for 2014, 32.89% for 2013, 32.89% for 2012). We constructed an indicative back-prediction to estimate the count of publications that may have been included from the past period, has it been assessed. This suggested that 37.29% of relevant evidence since 1980 was included in our analysis.

2.8.3.2 Proxy Measures

We established links between proximal controls and any proxy measures used to represent them. These are shown in **Table 2–3**.

Table 2–3 Proximal controls to Arctic shrub growth / expansion derived from the evidence base (Jan. 2012 – Jan. 2017 inclusive).

Category		Control	Form / Duration Variants	Proxy Measures Used
Canopy-Plant Interface		Atmospheric Carbon Dioxide Concentration		
		Air Temperature	Winter Warming Event	Above-freezing mean, Air Temperature (Mean, Sum), Diurnal Air Temperature (mean, min., max.), Growing Degree Days
		Fire	Occurrence, Burn Intensity	Fire scar (burn severity)
		Humidity		Water Balance
		Ice and Frost	Ice Encasement (Rain-on-Snow) Events	Thaw Degree Days, Frost Days
		Insolation	UV-B, Photoperiod	Cloudiness, Photosynthetically Active Radiation (PAR), Sunshine Duration, Total Radiation
		Snow Depth / Cover		Snow-free date
Biotic Interactions		Fungal Infection		
		Herbivory (including trampling and other biomass removal processes)	Bird, Mammal, Gall Mites, Leaf Miners, Defoliators, Other Invertebrates	
Soil	Surface Conditions	Cryoturbation		
		Erosion	Aeolian, Thermo-Erosion *(running water on permafrost)*	
		Soil Stability	Thaw Slump	
	Belowground Conditions	Active Layer Depth		
		Acidity		
		Soil Moisture	Drought (e.g. SPEI), Flooding	Groundwater Level, Precipitation (Mean, Sum), Soil Drainage, Water Tracks
		Soil Salinity	Saline Incursion	
		Soil Temperature		
		Soil Texture		
	Belowground Resources	Organic Matter		
		Mineral Content		Bedrock type
		Phosphorus		
		Nitrogen		Exchangable NH4+, NO3-, and N
		Potassium		

Key: *Red lettering indicates controls that occur as disturbance events, rather than resource limitations.*

2.8.3.3 Spatial Intersects

Global clustering within the dataset was established using the Global Moran's I statistic. The null hypothesis is that there is complete randomness in the count of evidence points at each spatial

location. The final dataset of evidence points was imported into ArcMap and projected at an equidistant Arctic projection. The data was treated such that evidence points that were spatially overlapped (occurred at the same site) were aggregated to a single point, so that each point represented the count of evidence points that occurred at that spatial location. Global Moran's I was calculated for the whole dataset using the ArcMap Spatial Analyst toolbox. Additionally, Global Moran's I was calculated for proximal controls only, ultimate controls only, each proximal control category defined in Table 1, and all individual proximal controls with an evidence point count greater than 30. The results of these analyses are summarised in **Table 2–4**.

Table 2–4 Results of global clustering analysis conducted using Global Moran's I statistic.

Evidence Points Included	n	Moran's Index	Variance	z-Score	p-Value
All evidence points	1132	0.237	0.0127	2.13	0.0333*
Proximal controls only	1020	0.271	0.0127	2.43	0.0150*
Ultimate controls only	112	-0.174	0.0127	-1.51	0.130
Experimental designs only	176	0.713	0.0126	6.38	0.000000**
Observational designs only	956	0.0657	0.0129	0.608	0.543
Atmosphere-plant interface (proximal)	510	0.435	0.0130	3.85	0.000118**
Biotic (proximal)	66	0.179	0.0128	1.61	0.107
Soil – All (proximal)	444	0.118	0.0127	1.07	0.283
Soil belowground conditions (proximal)	405	0.0992	0.0125	0.915	0.360
Soil belowground resources (proximal)	30	-0.00371	0.0101	-0.00504	0.996
Active Layer Depth	123	0.189	0.0125	1.72	0.0852
Air Temperature	427	0.236	0.0128	2.11	0.0348*
Herbivory	65	0.179	0.0128	1.61	0.108
Snow Dynamics	37	0.103	0.0130	0.931	0.352
Soil Moisture	260	0.0792	0.0125	0.736	0.462

All figures to three significant figures. Neighbour distance was 1,000km for all analyses. * = 95% significance; ** = 99% significance. Z-Score indicates strength of clustering (positive) or dispersal (negative) of evidence point counts within the dataset, when contrasted to the null hypothesis of complete randomness.

The specific locations of significant evidence point clustering were calculated using the Getis-Ord Gi* statistic. An inverse distance spatial relationship was used, calculated on Euclidean distance, using a neighbour threshold of 1000km. For this analysis, sites within 15km were collapsed to summed counts at a centroid to remove duplicate matches at the same research location. **Table 2–5** shows the eight sites that were detected as significant hotspots.

Table 2–5 Hotspots that indicate significant sites at which evidence points were clustered, with non-significant locations removed for brevity.

Site Name	Latitude (DD)	Longitude (DD)	Gi Score	p-Value
Toolik Lake, Alaska, USA	68.65	-149.56	7.994	0.000**
Abisko, Sweden	68.34	18.67	6.791	0.000**
Alexandra Fiord, Canada	78.88	-75.82	6.59	0.000**
Endalen, Svalbard, Norway	78.19	15.85	3.684	0.000**
Barrow, Alaska, USA	71.31	-156.64	2.782	0.005**
Alaska, USA	69.97	-144.01	2.18	0.029*
Zackenberg, Greenland	74.28	-20.33	1.88	0.060
Atqasuk, Alaska, USA	70.47	-157.38	1.88	0.060

* = 95% significance; ** = 99% significance. Gi-score indicates strength of clustering at a location.

Local clustering was also assessed within the context of land divisions of interest in the Arctic terrestrial environment. We intersected the full evidence points dataset with metrics of environmental variability, as described in the main text: bioclimate (including Oro-Arctic), physiognomy, and floristic province. For physiognomy and floristic province, Oro-Arctic evidence points were excluded, as the Artic designations of interest do not designate areas below the northern treeline. Individual evidence points were stacked by spatial location, as in the global clustering analysis. To account for coordinate inaccuracies in the literature, such as points occurring marginally off coasts, each site was associated with its nearest environmental unit via proximity

analysis (using geodesic measurements). Each site was then joined to its nearest environmental unit, to give evidence point counts per designation. The results of the analyses are shown in **Table 2–6**.

Table 2–6 Research intensity in relation to environmental variability, computed using Getic-Ord Gi* statistic.

Zonation	Evidence Points Included	N	Zone	Gi-Score	p-Value
Bioclimate Subzone	All evidence points	15	Bioclimate A	-1.242	0.214
		106	Bioclimate B	-0.591	0.554
		189	Bioclimate C	0.002	0.998
		88	Bioclimate D	-0.720	0.471
		424	Bioclimate E	1.684	0.092
		310	Oro-Arctic	0.868	0.385
Bioclimate Subzone X Floristic Group	All evidence points (excl. Oro-Arctic)	210	E – Beringia	50.81	0.000**
		105	C – North Atlantic	2.320	0.020*
		102	E – North Atlantic	2.241	0.025*
		92	B – Canada	1.978	0.048*
		NB Non-significant results excluded for brevity			
Floristic Sector	All evidence points (excl. Oro-Arctic)	16	Kanin-Pechora	-0.252	0.801
		18	Polar Ural	-0.214	0.830
		25	Yamal-Gydan	-0.082	0.934
		6	Taimyr	-0.441	0.659
		0	Anabar-Olenyek	-0.554	0.579
		0	Kharaulakh	-0.554	0.579
		26	Yana-Kolyma	-0.06	0.949
		0	Wrangell Island	-0.554	0.579
		0	West Chukotka	-0.554	0.579
		1	East Chukotka	-0.536	0.592

		3	South Chukotka	-0.498	0.619
		20	Beringian Alaska	-0.177	0.860
		0	North Beringian Islands	-0.554	0.579
		268	Northern Alaska	4.505	0.000**
		47	Central Canada	0.331	0.739
		14	West Hudsonian	-0.290	0.772
		110	Ellesmere-North Greenland	1.522	0.128
		14	Baffin-Labrador	-0.290	0.772
		86	West Greenland	-0.177	0.860
		49	East Greenland	0.333	0.739
		38	North Iceland-Jan Mayen	0.163	0.870
		0	North Fennoscandia	-0.554	0.579
		81	Svalbard-Franz Josef Land	0.975	0.330
Physiognomic Unit	All evidence points (excl. Oro-Arctic)	83	Carbonate Mountain Complex	0.936	0.350
		0	Cryptogram Barren Complex	-0.918	0.359
		6	Crypogram, Herb Barren	-0.784	0.433
		73	Erect Dwarf-Shrub Tundra	0.712	0.476
		13	Glaciers	-0.650	0.516
		12	Graminoid, Prostrate Dwarf-Shrub, Moss Tundra	-0.650	0.516
		0	Lagoon	-0.918	0.359
		125	Low-Shrub Tundra	1.873	0.061
		99	Non-Carbonate Mountain Complex	1.293	0.196
		5	Non-Tussock Sedge Dwarf-Shrub, Moss Tundra	-0.806	0.420
		8	Nunatak Complex	-0.739	0.460
		26	Prostrate Dwarf-Shrub, Herb Tundra	-0.337	0.736

	75	Prostrate / Hemiprostrate Dwarf-Shrub Tundra	0.757	0.449
	9	Rush / Grass, Forb, Cryptogram Tundra	-0.717	0.474
	71	Sedge, Moss, Dwarf-Shrub Wetland	0.668	0.504
	6	Sedge, Moss, Low-Shrub Wetland	-0.784	0.433
	67	Sedge / Grass, Moss Wetland	0.578	0.563
	141	Tussock-Sedge Dwarf-Shrub, Moss Tundra	2.231	0.026*
	3	Water	-0.828	0.407

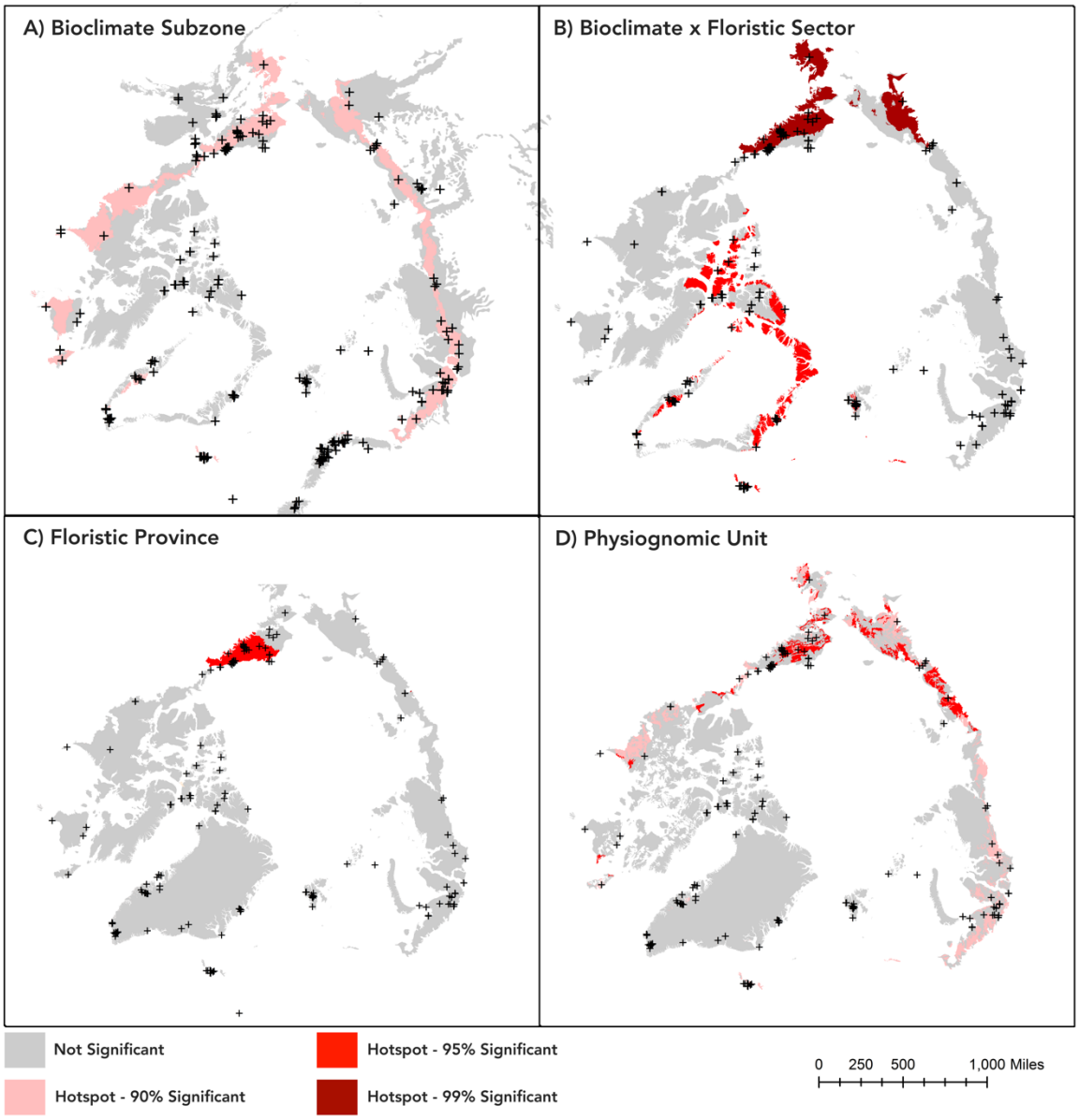

Figure 2–7 Maps showing results of hotspot analysis for all evidence points (A), or all evidence points not in the Oro-Arctic (B, C, and D), indicating statistically significant hotspots for A) Bioclimate subzones, B) Physiognomic units, and C) floristic provinces. Crosses represent evidence points.

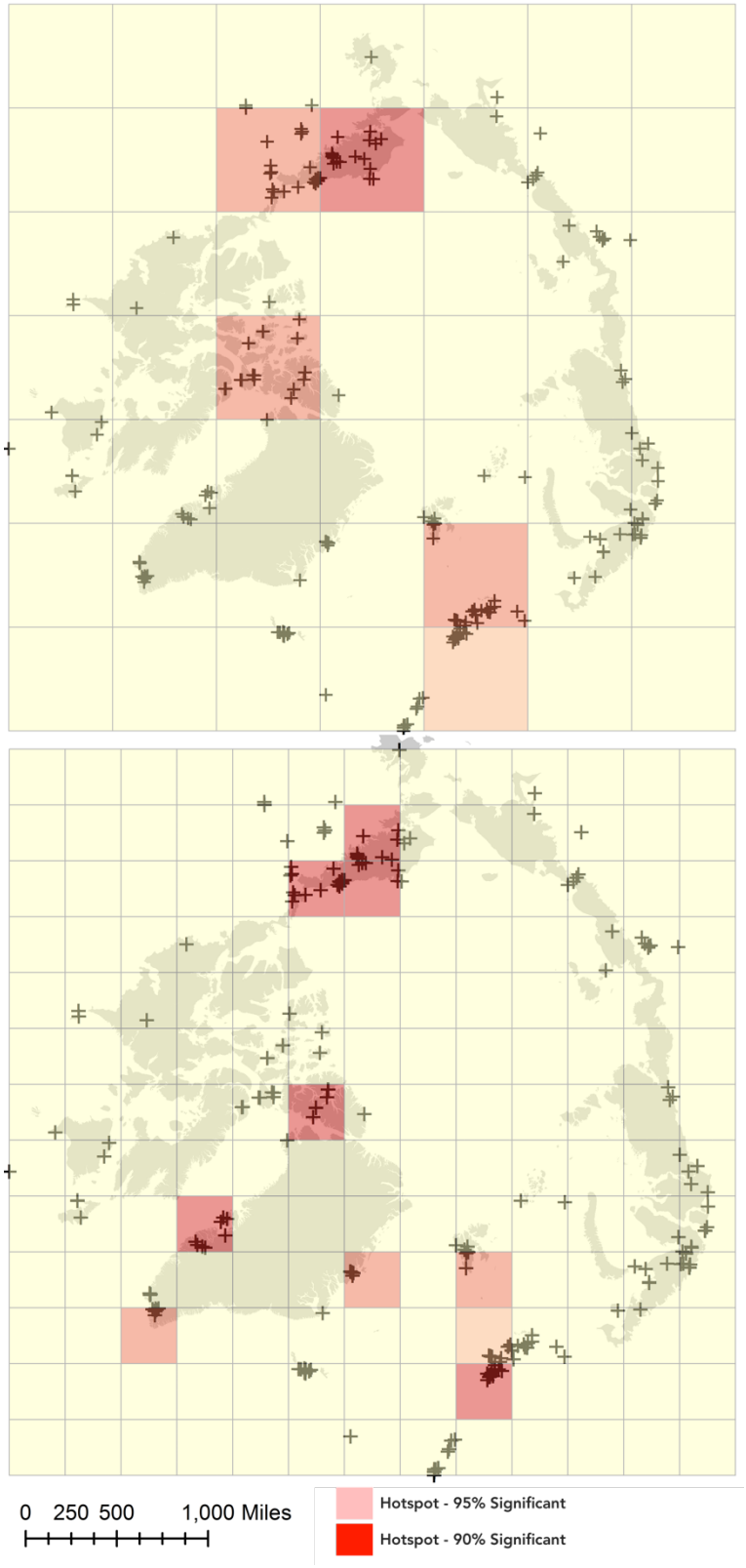

Figure 2–8 Hotspot analysis for all evidence points, at two spatial scales. Top: hotspot analysis conducted on 500km fishnet with 500km neighbourhood; Bottom: hotspot analysis conducted on 1000km fishnet with 1000km neighbourhood.

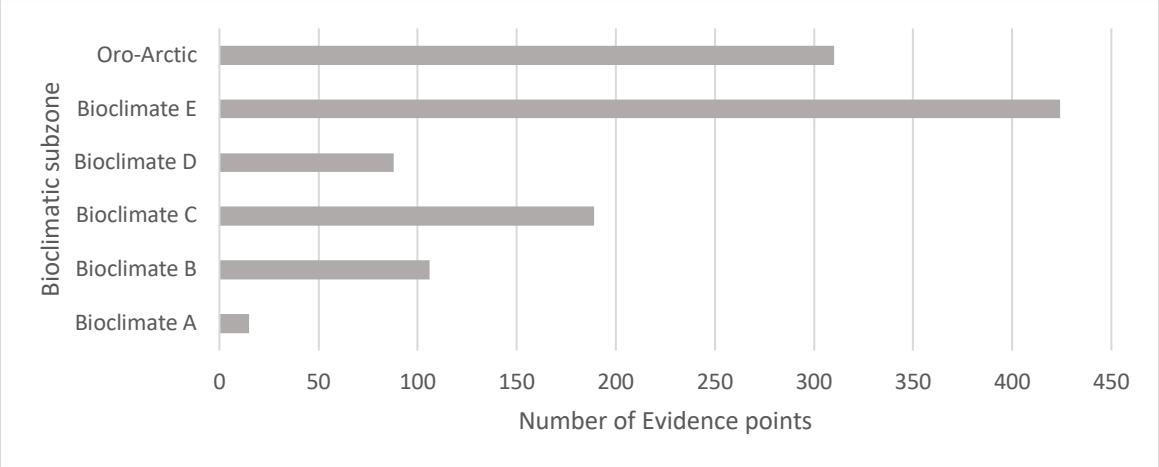

Figure 2–9 Count of evidence points per bioclimate subzone for controls on Arctic shrub growth and expansion (reported in peer-reviewed literature during the period 1 January 2012 – 31 January 2017).

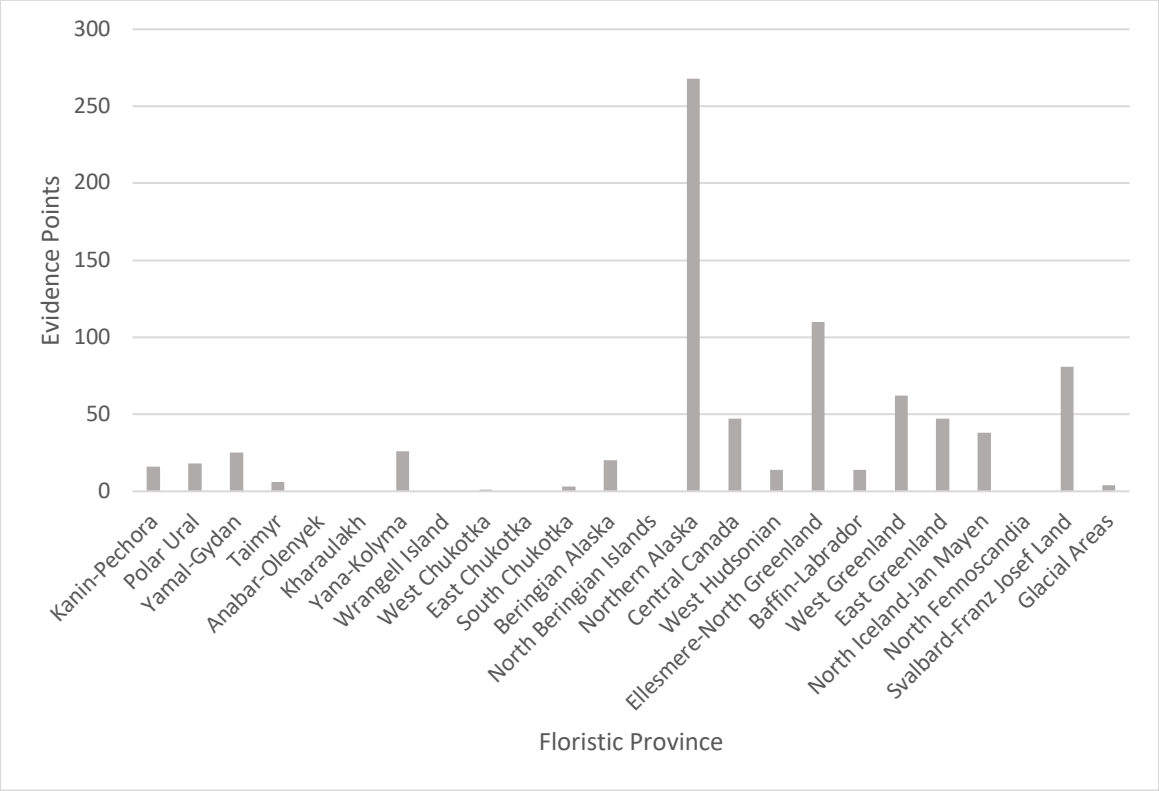

Figure 2–10 Count of evidence points per floristic province for controls on Arctic shrub growth and expansion (reported in peer-reviewed literature during the period 1 January 2012 – 31 January 2017).

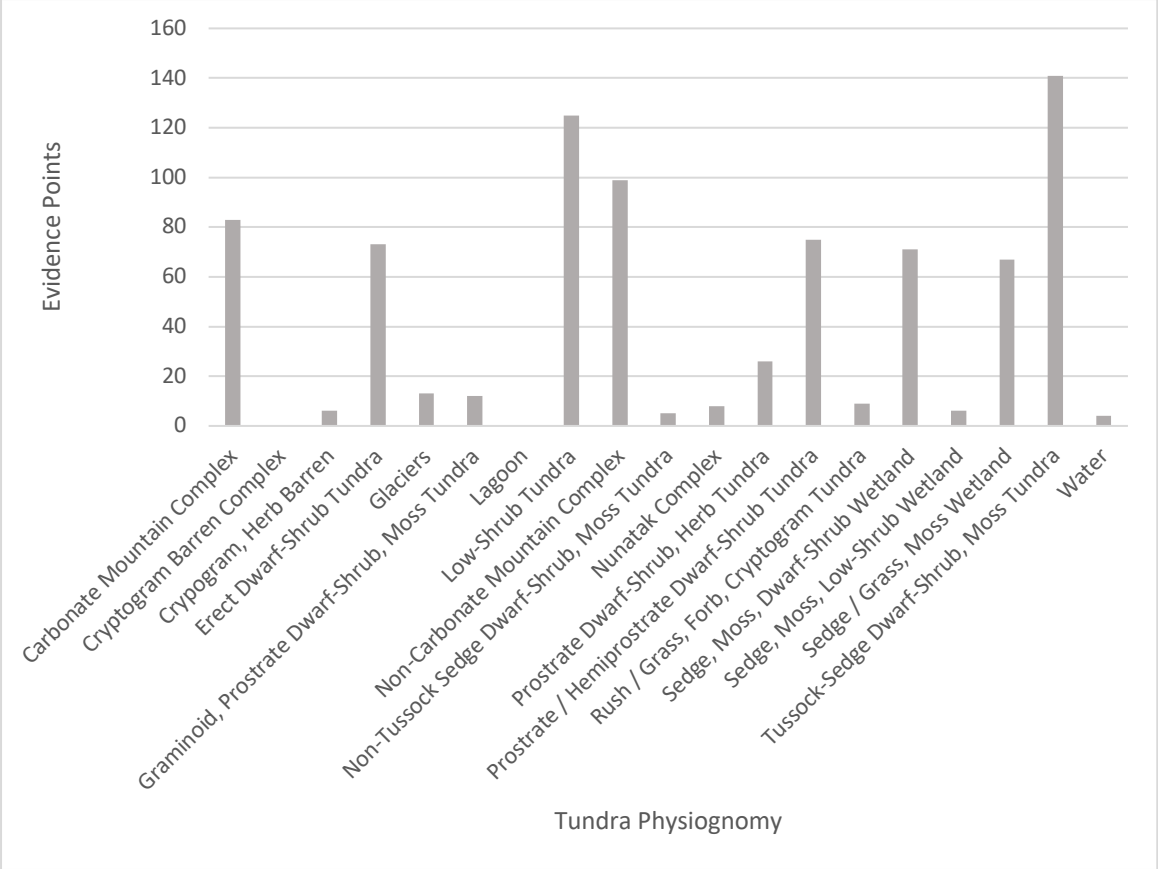

Figure 2–11 Count of evidence points per tundra physiognomy for controls on Arctic shrub growth and expansion (reported in peer-reviewed literature during the period 1 January 2012 – 31 January 2017).

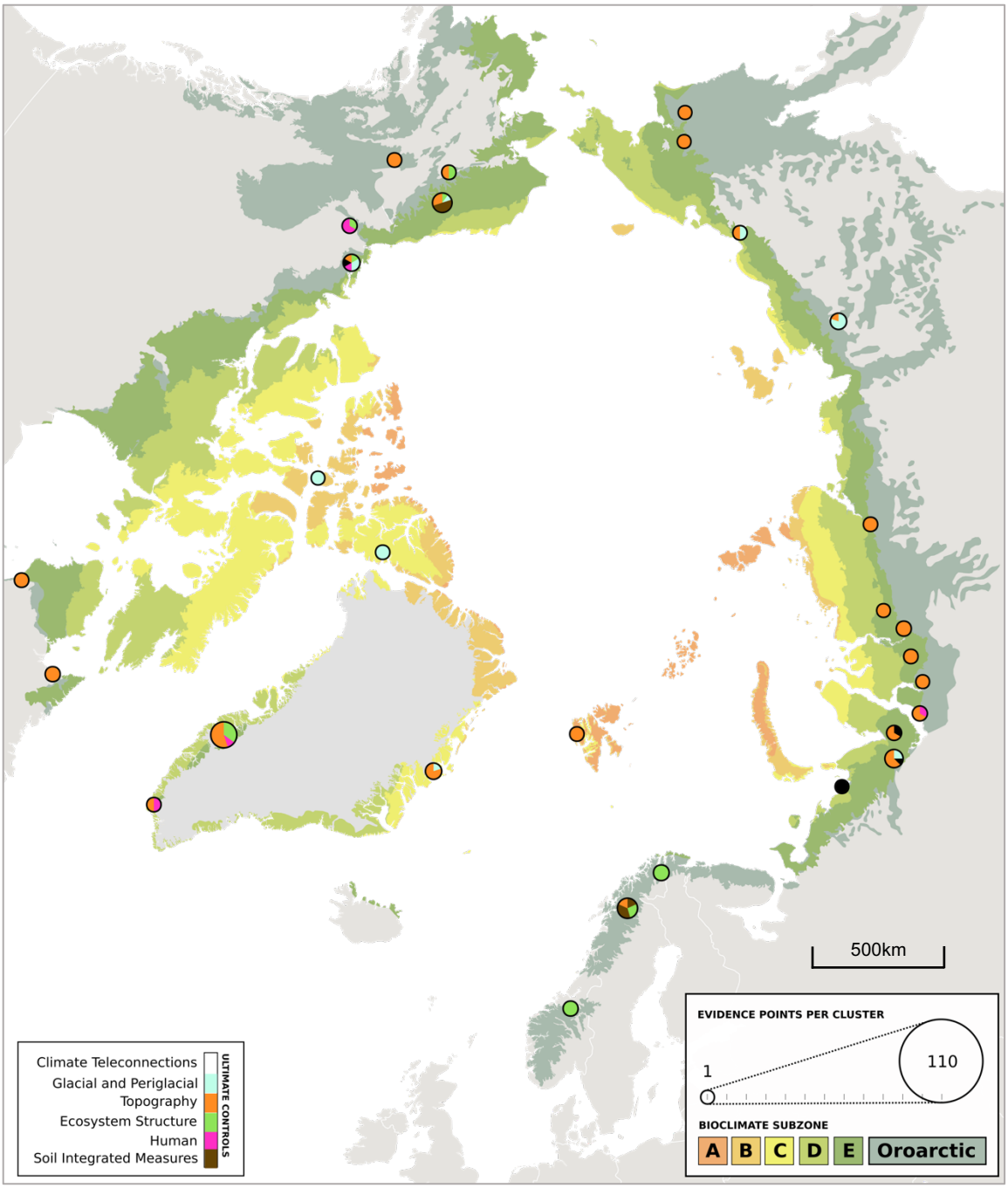

Figure 2–12 Pan-Arctic map showing evidence points generated for ultimate controls on Arctic shrub growth and expansion (reported in peer-reviewed literature during the period 1 January 2012 – 31 January 2017). Each circle represents one location at which an evidence point was generated, or a regional cluster if more than one location occurred within 150km. Circle size represents the count of evidence points that occurred at the location. Pie segments represent a percentage of the evidence points at a location for each control type, represented by colour. Landmass colouring indicates bioclimatic subzone (Walker et al 2005), or Oro-Arctic (defined in ***Section 2a***).

2.8.3.4 *Temporal Intersects*

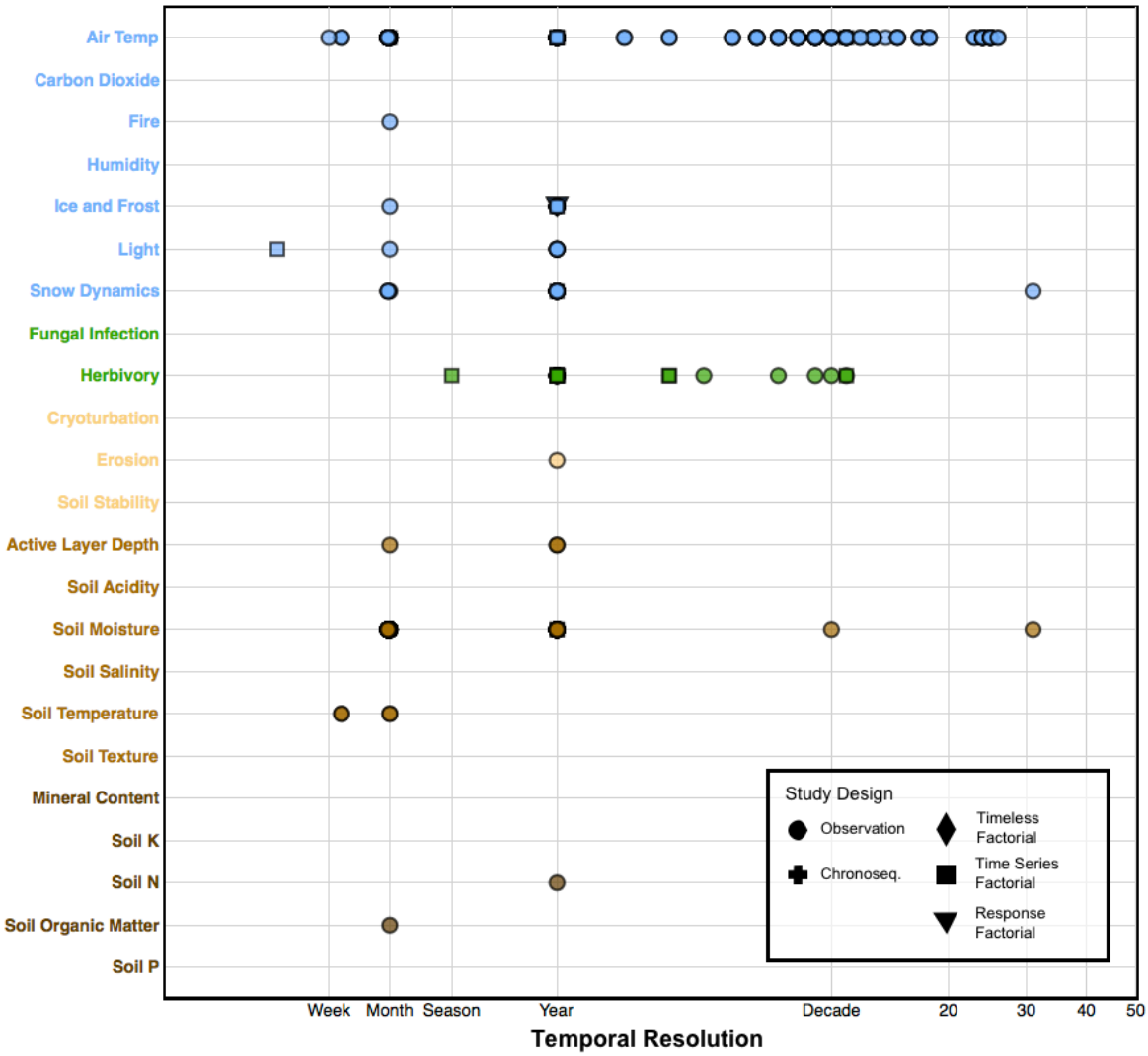

Figure 2–13 Temporal resolution of proximal control–shrub response test pairs (reported in peer-reviewed literature during the period 01 Jan 2012 – 31 Jan-2017).

2.8.4 *References*

Collaboration for Environmental Evidence. (2013). Guidelines for systematic reviews in environmental management. Retrieved from http://environmentalevidence.org/wp-content/uploads/2014/06/Review-guidelines-final-print.pdf.

Myers-Smith, I.H., Forbes, B.C., Wilmking, M., Hallinger, M., Lantz, T., Blok, D., Tape, K.D., Macias-Fauria, M., Sass-Klaassen, U. & Lévesque, E., 2011, Shrub expansion in tundra ecosystems: dynamics, impacts and research priorities, *Environmental Research Letters*, 6(4), p. 045509.

Orshan, G. 1989, Shrub as a Growth Form, in *The Biology and Utilization of Shrubs,* pp. 249-65.

Virtanen, R., Oksanen, L., Oksanen, T., Cohen, J., Forbes, B.C., Johansen, B., Käyhkö, J., Olofsson, J., Pulliainen, J. & Tømmervik, H., 2016, Where do the treeless tundra areas of northern highlands fit in the global biome system: toward an ecologically natural subdivision of the tundra biome, *Ecology and Evolution*, 6(1), pp. 143-58.

1

Chapter 3

Nitrogen limitation of Arctic shrub growth over four decades: inference from mechanistic modelling of dendroecological data, Yamal, Russia

This paper has been prepared for submission to **New Phytologist**.

In the previous chapter I identified evidence gaps for the role of soil nitrogen availability in shrub growth and expansion. Here I create the first time series of wood ring stable nitrogen isotopes for ten shrub individuals at Yuribei; I then develop a modelling approach that may be used to extend evidence for the mechanisms controlling shrub-nutrient relations to a longer temporal extent.

Nitrogen limitation of Arctic shrub growth over four decades: inference from mechanistic modelling of dendroecological data, Yamal, Russia

Andrew C. Martin[1], Marc Macias-Fauria[2], Michael B. Bonsall[3], Bruce Forbes[4], Pentti Zetterberg[5], and Elizabeth S. Jeffers[1]

1. Oxford Long-Term Ecology Laboratory, Department of Zoology, University of Oxford, OX1 3PS, UK
2. School of Geography and the Environment, University of Oxford, OX1 3QY, UK
3. Mathematical Ecology Research Group, Department of Zoology, University of Oxford, OX1 3PS, UK
4. Arctic centre, University of Lapland, Rovaniemi, Finland
5. Department of Forest Sciences Faculty of Science and Forestry, University of Eastern Finland, Joensuu, Finland

3.1 Abstract

1. Over recent decades, there has been widespread biomass increase of deciduous shrubs across the Arctic tundra biome. Shrub sensitivity to climate is heterogeneous across the biome, and remotely sensed indicators suggest that tundra productivity may be recently decoupling from air temperature. There may therefore be an increasingly important role for other environmental controls on shrub growth. Nitrogen (N) is an essential nutrient for plant growth, yet temporal trends in soil N availability remain understudied. With limited information on soil N beyond a decade, information available through space-for-time approaches may mask the rate and importance of such processes. At a northern fringe of tall shrub expansion (Yuribei, Yamal Peninsula, Russia), we sought to: (a) identify trends in plant-available N over recent decades; and (b) determine the role of N in limiting shrub secondary growth.
2. Two methods were employed to understand temporal dynamics of N and shrub growth. First, we analysed stable nitrogen isotope ratios in *Salix lanata* wood rings to reconstruct bioavailable N to individual shrubs at an annual timescale. Second, we implemented a suite

of ecological models that described the role of N in shrub growth. We varied three components within the models: the form of N limitation; plant-soil feedbacks; and geometric limits to growth. We then applied a model-fitting and model-selection approach to the ring width and isotope data to determine the most appropriate model for each shrub individual given the ring width and isotope data.

3. We reconstructed N availability from 1980-2013 from ten shrub individuals, finding a significant declining trend over time for seven shrubs and significantly increasing for two shrubs. Model-fitting and model-selection indicated that N limitation was an important control to shrub growth for all ten shrub individuals studied; this was best represented using a linear rather than saturating form of N limitation in nine of ten shrubs. The addition of a plant-soil feedback mechanism improved model fits to the observed ring width and $\delta^{15}N$ data for eight of the ten individuals. Finally, the importance of geometric limits to maximum shrub size was important for six of the ten shrub individuals; this was unrelated to age or mass of individuals.
4. Our results suggest that: (a) N availability is limiting secondary growth of deciduous shrubs in this Arctic region; (b) *Salix lanata* are actively controlling their environment, with an important role of plant-soil feedbacks for supporting further plant growth; and (c) there are important differences at the individual shrub scale, which may be related to small-scale biotic and abiotic environmental variability or phenotypic plasticity.

Keywords: greening of the Arctic; model-fitting; model-selection; nitrogen limitation; optimisation; plant-resource coupling; *Salix lanata*; time-series.

3.2 Introduction

Ground-based observations indicate that an increase in woody deciduous shrub biomass – 'shrubification' – has occurred in the Arctic tundra over recent decades, through three processes: (1) increasing shrub height, (2) patch infilling, and (3) range expansion (Myers-Smith et al. 2011). Shrubification trends have been related to temperature (Elmendorf et al. 2011): Arctic tundra

environments are experiencing the fastest rates of climate warming on Earth (Post et al. 2009), with declines in sea ice extent causing warming of the largely coastal biome (Screen & Simmonds 2010). In addition, increased shrub growth may enable significant feedbacks to regional climates (Loranty & Goetz 2012). Remotely-sensed 'greenness' – a proxy of vegetation productivity (Normalised Difference Vegetation Index, NDVI) – further suggests Pan-Arctic increases in productivity over the last decades (Epstein et al. 2015). However, 'greenness' has become progressively decoupled from rising air temperatures (Piao et al. 2014), and evidence syntheses demonstrate that shrub sensitivity to climate has been spatially heterogeneous (Elmendorf et al. 2011; Myers-Smith, Elmendorf, et al. 2015). These findings suggest that other environmental controls may be important in controlling shrubification processes.

Nitrogen (N) availability may be an important determinant of observed shrubification trends. N is a key macronutrient for plant growth, and Arctic soils are relatively N-poor with most N used by plants deriving from organic forms (i.e. amino acids, dissolved organic N) rather than inorganic forms (Zamin & Grogan 2012; Epstein et al. 2004). Plot-scale fertilisation experiments indicate that tundra shrubs respond to N addition by increasing above-ground biomass production in at least some contexts (Shaver & Chapin 1980; Henry et al. 2011), suggesting that growth release will occur with elevated N supply. Indeed, many plant species respond to increased nutrient availability by increasing allocation to photosynthetic mass (Poorter et al. 2012). As the availability of soil resources depends on geology, glacial history, and soil conditions, these differences may be reflected in differences of shrub growth responses within and between regions.

Shrub-soil feedbacks may introduce positive feedbacks to shrub performance. Shrubification, through increased height and density of aboveground woody biomass, can influence the local microclimate (Lantz et al. 2012), biotic interactions (Deslippe & Simard 2011), soil conditions (Blok et al. 2010; Aalto et al. 2018), and soil resources (Sturm et al. 2005) (although evidence for this is unclear, see: Myers-Smith & Hik (2013)). Biogeochemical cycling may be enhanced with shrubification for example by increasing litter inputs to soils and increasing decomposition rates (Buckeridge et al. 2009; DeMarco et al. 2014), although belowground responses may be dependent

on relations between shrub species and soil microbial diversity (Shi et al. 2015). Many woody plant species occurring in the Arctic do, however, have traits adapted for resource conservation (Rossi et al. 2014), such as significant translocation before senescence, and very low intrinsic growth rates. Thus, plasticity of shrub species' traits may explain a proportion of the observed spatial-temporal heterogeneity in shrub-climate responses. Species-specific differences in plasticity have been implicated in tall shrub expansion (Heskel et al. 2013). Further, fertilisation studies suggest that certain species are highly plastic in response to nutrients; *Betula nana* L, for example, has been observed to shift allocation to shoot production in eight years following nutrient fertilisation, which was attributed to geometrical advantages over other species, namely switching to the production of many long shoots and thus many meristems (Bret-Harte et al. 2001).

The ecological mechanisms driving shrub-nitrogen relations may operate on varying temporal resolutions, including longer timescales than current observations. In order to predict the future dynamics of deciduous shrubs in the Arctic, we need to understand the potential for N availability to constrain growth over decadal time, which is currently poorly represented in land system models (Bouskill et al. 2014). Space-for-time substitution analyses have been demonstrated to overestimate the rates and order of processes (Elmendorf et al. 2015), owing to each location's varying history. Without observations over decades, it is unclear if short-term processes are masking longer-term N limits to growth (Luo et al. 2004).

Recent research has demonstrated the use of stable N isotopes in tree rings as an integrated indicator of point-based soil N availability (McLauchlan et al. 2007; Gerhart & McLauchlan 2014). Here, we adapt this approach to Arctic shrub wood rings, which can be absolutely dated using dendrochronological techniques (Myers-Smith et al. 2015); their slow growth however poses challenges to the N isotope method due to their low annual wood production. By combining ring width and N isotope data from shrub rings, it becomes possible to reconstruct individual-based time series of local soil N availability and plant secondary growth. This method is useful because we can observe plant-N relations in the past beyond the spatial and temporal constraints of long-term experimental plots.

Here, we sought to demonstrate a method to assess the nature and strength of N limitation to shrub growth covering the period of recent shrubification. To achieve this, we measured time-series of stable N isotopes from shrub wood rings covering a 35-year period that matches the remote sensing record, and is of sufficient length to capture processes of plant-N relations beyond short term physiological responses to variability in soil N. We measured individual time-series from ten individuals of the same species – *Salix lanata* – from a site in central Yamal to establish between-shrub variability in absolute values of the N isotope proxy, taking into account the number of individuals (often five or less) used for oxygen and carbon wood ring isotope proxies (McCarroll & Loader 2004). We used the time-series to address four key questions:

1. What is the direction of change of soil N availability over recent decades, and to what extent are trends in N availability homogeneous within the landscape?
2. Has N limitation played a role in the secondary growth patterns of *Salix lanata* L. shrubs within this landscape? If N limitation is occurring, which functional form best describes the data?
3. To what extent are plant-soil feedbacks important in explaining the rate of *Salix lanata* L. secondary growth?
4. Is there evidence for density-dependent or geometric limits to maximum shrub growth?

3.3 Methods

3.3.1 Site

Our study site was Yuribei, Yamal Peninsula, Russia (68.91 °N, 70.23 °E). Between 1980 and 2019 the mean July temperature was 12.42°C (95% between 8.54°C and 16.16°C), and mean January temperature was -23.42°C (95% between -29.87°C and -15.10°C). Temperatures rise above zero for only four months of the year (June-September), although since 1980 summer temperatures have warmed 1°C to 2°C (Menne et al. 2012). Belowground, the soil is a Histic Cryosol characterised by poor drainage (Mikhajlov 2017). Yuribei is classified as low-shrub tundra in the Circumpolar Arctic Vegetation Atlas (Walker et al. 2009). The plant community consists of deciduous shrubs

and graminoids. *Salix lanata* L is the dominant shrub species in lowland areas: in recent decades this species has increased substantially in height to upwards of two metres (Forbes et al. 2009).

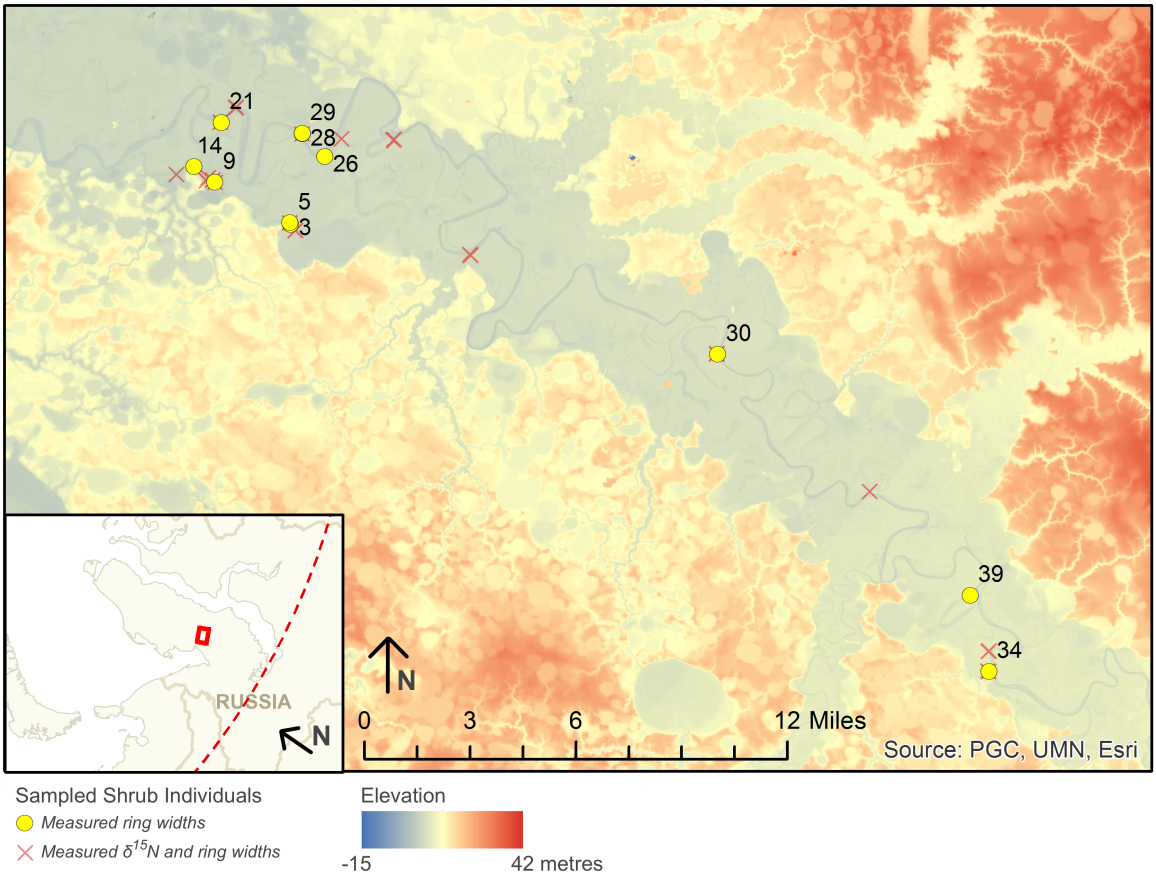

Figure 3–1 Location map of the study area (Yuribei, Russia) marked with locations from which individual shrub wood discs were collected (each shrub code = YUSL## where ## is the numeric label given next to the map point). Ring width and nitrogen isotope time-series were measured from ten wood discs (yellow circle); only ring width time-series were measured from the remaining 42 discs. Base map is ArcticDEM elevation at 2 metre resolution (Porter et al 2018).

During a field campaign in July 2013, 52 shrub discs were collected from the riparian lowland at Yuribei (**Figure 3–1**). Shrub stems were sampled to obtain basal discs at the closest level to the ground. Only larger individuals were sampled for the purposes of ring-width chronology development. Effort was taken to sample from independent genets. We measured ring width increments on wood discs to a precision of 0.01mm. Standard dendrochronological techniques were employed to age and cross-date each individual shrub disc (Fritts 1976). Thus, each ring measurement is dated to a calendar year. We also collected data to calibrate allometric equations (see **Section 3.3.3.4**). Shrub size metrics were measured on 200 *Salix lanata* individuals: these included stem length, stem basal circumference, and stem diameter.

3.3.2 $\delta^{15}N$ Time Series Development

$\delta^{15}N$ in bulk wood has previously been validated as a proxy of point-based soil nitrogen availability (McLauchlan et al. 2017; Gerhart & McLauchlan 2014; McLauchlan et al. 2007). From our 52 shrub samples, we selected ten at random from which we developed time-series of $\delta^{15}N$ using the dated annual wood increments (**Figure 3–1**). Of these 10 randomly sampled individuals, 3 (shrubs *YUSL03*, *YUSL05*, and *YUSL09*) grew on slightly elevated gentle slopes, whereas the rest were sampled from the lowest elevations in the landscape, growing on thickets close to the Yuribei river main and adjacent channels. A major methodological consideration for wood $\delta^{15}N$ chronologies is temporal resolution: as the quantity of bulk wood required is high (between 10 and 30mg depending on mass spectrometry setup) in comparison to other isotope proxies, pooling of annual increments into bins from increment cores is usually required to obtain the necessary wood, either equally or variably along the time series. However, we sought to develop annual time-series by taking advantage of the higher wood quantity available from wood discs versus increment cores.

To obtain $\delta^{15}N$ samples, we: (a) smoothed a rectangular section of the disc; (b) made a cutting-guide by making and digitising a thin-section on which ring boundaries were marked; (c) separated rings under a macroscope; (d) milled each ring to a fine powder; and (e) weighted replicate subsamples for analysis. The shrub discs did not have symmetrical growth forms: for each shrub disc, a 15mm-wide wood block was sectioned following the longest radial from bark to pith. The height of wood blocks varied between 8 and 15mm. To increase visibility of the annual ring boundaries, the surface and reverse of the wood block were wet with de-ionised water for 10 minutes, then smoothed using a GSL1-microtome (Gärtner et al. 2014).

To create a cutting guide, a stained thin section was made from each shrub wood block (**Figure 3–2**). To create each thin section, a 20μm wood thin section was taken using a microtome. We applied only de-ionised water rather than a stabilising (non-Newtonian) fluid to avoid isotopic contamination. Thin sections were stained following standard procedures (Gärtner & Schweingruber 2013); each was washed with water, then stained for five minutes using an evenly-

spread mixture of 0.5% Alcian Blue / 0.5% Safranin. Samples were then washed with water, 70% ethanol, 90% ethanol, dehydrated with xylene, sealed in Canada Balsam, and finally baked for 12 hours in an 80°C oven to harden. Samples were immediately sealed using Canada balsam and glass cover. Slides were scanned at 7200dpi, and rings identified manually using Fiji image analysis software (Schindelin et al. 2012). These measurements were verified against pointer years from existing raw measurements for validation.

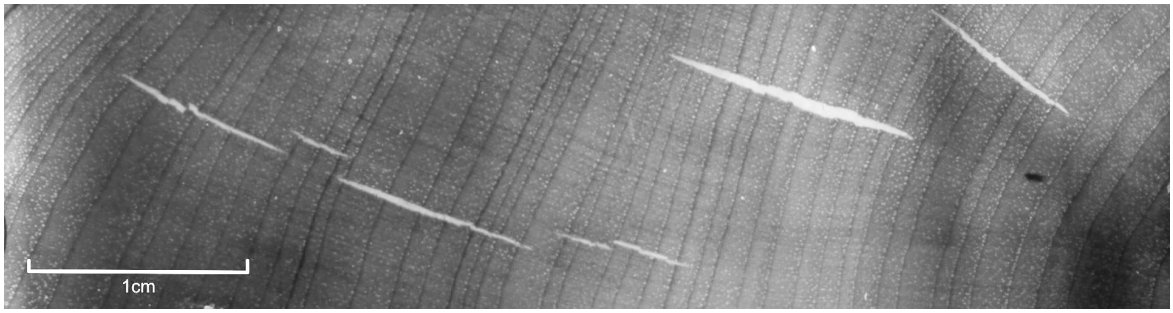

Figure 3–2 Example of a stained wood thin section used to identify and measure shrub wood rings. This example is showing *YUSL30*.

For isotopic analysis, bulk wood was extracted from each ring. Each wood block was separated into annual increments using a Stanley blade on a granite cutting surface under a Leica DSM 300 macroscope. Cuts were made in the direction of the grain and verified against ring boundaries on both surfaces of the wood block to minimise sampling error between adjacent annual increments. Wood from each individual increment was homogenised by: (a) finely chopping the sample using a Stanley blade, and (b) milling the sample into a wood powder using a Spex MixerMill 8000M. Milled samples are more homogenised thus reducing standard deviation of isotope measurements (Riechelmann et al. 2014). Each binned sample was milled in a steel capsule using two ball-bearings for 60 minutes. From each resultant powder, 11.00±0.05mg was weighed into a 5x8mm tin capsule. Replicates were weighed for one in three samples to characterise sample variability. The $\delta^{15}N$ and %N content of each sample was analysed with a Thermo Fisher Delta V+ mass spectrometer coupled to a Carlo Erba NC 2500 Elemental Analyzer at the Central Appalachian Stable Isotope Facility, University of Maryland Centre for Environmental Science. Samples were analysed in random order so that any potential biases from the mass spectrometer were not structured within the time series.

We identified significant trends in $\delta^{15}N$ time-series by fitting linear models based on Theil-Sen single median, as implemented in the *mblm* R package (Komsta 2013). The Theil-Sen statistic is especially suited to short and noisy time-series (Hoaglin et al. 2000).

3.3.3 Modelling of Plant – Nitrogen Interactions

To infer the underlying mechanisms operating on shrub growth and nitrogen availability, we used a Model-Fitting and Model-Selection (MFMS) approach (Bonsall & Hastings 2004). MFMS approaches compete alternative ecological models to determine the most appropriate model structure to explain the observed time-series, while also estimating the strength of the mechanisms involved. We constructed a set of mechanistic top-down models (Poorter et al. 2013) that relate shrub secondary growth to a single limiting resource (**Figure 3–3**). We also addressed specific considerations that enabled the use of dendroecological data: (a) allometric relations between biomass and basal diameter / ring width (**Section 3.3.3.4**); and (b) use of $\delta^{15}N$ as a proxy for N availability (**Section 3.3.3.5**).

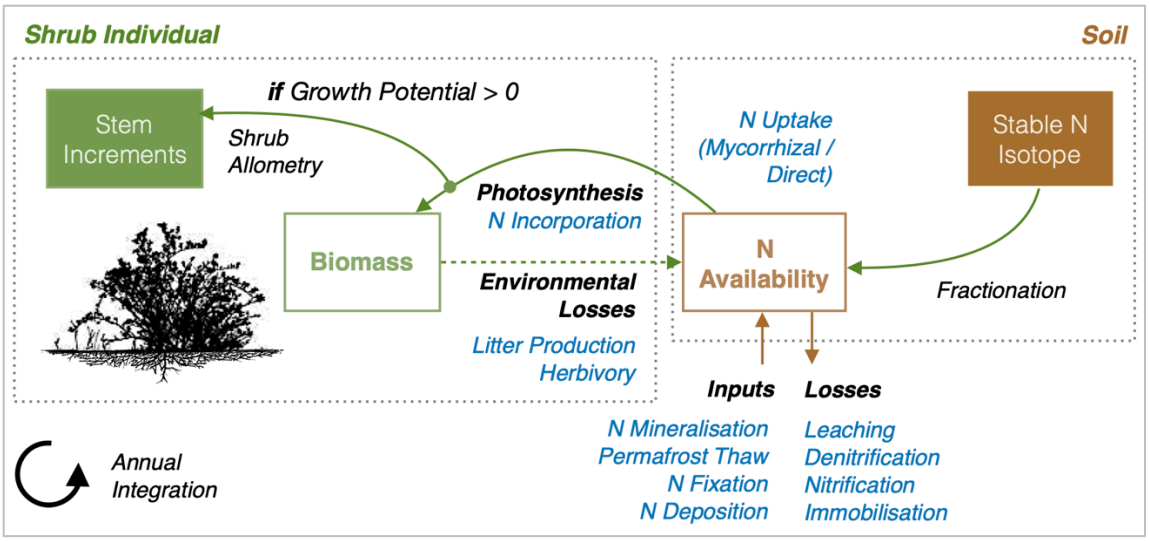

Figure 3–3 Schematic of time-series model structure that combines shrub ring-widths with stable nitrogen isotope data to represent interactions between an individual shrub and soil N resources. This is the base model that is used to test all hypotheses. The filled boxes indicate measured time-series inputs, and hollow boxes the modelled stocks. Arrows and black labels indicate modelled N flows, alongside the processes that may give rise to them (blue text). Environmental losses (dotted line) may or may not be connected to soil N availability depending on the hypothesis under testing.

We adapted Tilman's resource-ratio models (Tilman 1990; Tilman 1988; Huisman 1994; Jabot & Pottier 2012) to capture the main processes in plant-nitrogen dependence through continuous-time ordinary differential equations (ODEs). We assume that a shrub's ability to grow is a function of its photosynthetic capacity, minus respiration costs, and loss of existing material to the environment (e.g. via litter). Given that N is an essential macronutrient (Tilman 1990), we use a nitrogen-economy approach (Garnier 1991) where nitrogen availability may limit the production of new biomass as a single limiting resource. Soil nitrogen availability is assumed to be a function of background nitrogen replenishment in the soil, minus the nutrient requirement of any plant material grown, minus environmental losses relative to the amount of nitrogen present. Here, background N replenishment may include inputs from biotic processes (i.e. decomposition, N mineralisation, N fixation) and abiotic processes (i.e. N becoming available from thawing permafrost, N deposition), which are outlined in **Figure 3–3**. Conceptually, the model equals:

Change in Biomass = Biomass Production – Environmental Loss

Change in Nitrogen = Background Replenishment – Plant Uptake – Environmental Loss [+ Plant Inputs]

The model is defined by a base model, with three substitutable functions representing (a) N limitation, (b) plant-soil feedback, and (c) geometric constraint. In the base model, shrub biomass, *B,* and soil nitrogen dynamics, *N*, are represented by a dual-equation ODE system:

$$\frac{dB}{dt} = r \cdot g(B) \cdot f(N) - \gamma_B B$$

$$\frac{dN}{dt} = \lambda - g(B) \cdot f(N) - \gamma_N N + y(B)$$

Here, $f(N)$ is a resource-constrained net growth function (which accounts for photosynthesis and respiration); $g(B)$ is a geometric effect on the growth rate; r represents an intrinsic growth rate of plant biomass; and γ_B represents the rate of environmental loss of biomass from other factors (e.g. litter). λ is a linear background replenishment rate of soil nitrogen; $y(B)$ is a plant-soil feedback

mechanism that depends on current biomass; and γ_N is a density-dependent loss term for nitrogen from soils. We include two additional key assumptions to extend this approach to wood ring data. First, allometric relations determine the proportionality of basal diameter to total biomass. Second, the basal diameter of the main stem can never decrease once grown, whereas shrub mass may decline. The individual components, the product of which form the model hypotheses, are outlined in

Table 3–1.

Table 3–1 Model components that were combined with the base model in this study.

Component	Case	Function
N Nitrogen Dependency	**N1** Nitrogen-independent growth	$f(N) = 1$
	N2 Nitrogen-dependent growth: linear	$f(N) = aN$
	N3 Nitrogen-dependent growth: saturating	$f(N) = \frac{aN}{1 + arhN}$
F Plant-Soil Feedback	**F1** No Plant-Soil feedback	$y(B) = 0$
	F2 Plant-Soil Feedback	$y(B) = \alpha\gamma_B B$
R Maximum Potential Growth Rate	**R1** Exponential (Non-Asymptotic)	$g(B) = 1$
	R2 Chapman-Richards (Asymptotic)	$g(B) = 1 - \frac{B}{K}$

Parameters: *a* = N-use efficiency; *r* = N-conversion efficiency to biomass; *h* = handling time of N in uptake and incorporation into biomass; *α* = conversion factor of litter into N; γ_B= environmental loss rate of shrub biomass; *K* = asymptotic plant mass owing to mechanical or other constraints.

3.3.3.1 Resource Limitation f(N)

We conceptualised nitrogen limitation as occurring via two mechanisms: (a) limits on photosynthetic rate; and (b) limits to the shrub's ability to scavenge for N. First, low N availability can be linked to reductions in leaf health; it has previously been deduced that, below a saturation point, tissue N concentration relates to photosynthetic productivity with a Monod saturating function $f(N) = N/(K + N)$ (Van Rees 1994), where K is a half-saturating constant. Second, photosynthetic demand for N may be greater than the efficiency of roots to scavenge for and uptake

available N. Root uptake rate is monotonically increasing, and usually also represented by a Monod or Michaelis-Menten function (Jabot & Pottier 2012), requiring a similar constant *K* that represents the half-saturation N required for growth at half of the maximum rate, and a scalar *a* that represents the N-use efficiency:

$$f(N) = aN/(K + N)$$

McNickle and Brown (2014) demonstrate that the Michaelis-Menten equation can be rearranged to a Holling disc foraging model, where the parameters more closely relate to biologically meaningful root traits:

$$f(N) = B_r \frac{aN}{1 + ahN}$$

Here, a represents N-use efficiency, and *h* represents the 'handling' or processing time for each unit of N (McNickle & Brown 2014). Assuming that plant root systems act as a colony of individual 'foragers' for N, the individual forager nitrogen uptake rate is multiplied by the units of root biomass, B_r. Given that both photosynthesis and uptake may be rate-limited by N, and both can share a Holling disc functional form, the operation of both processes is here abstracted to a single function:

$$f(N) = \frac{aN}{1 + arhN}$$

Where total biomass production = $rBf(N)$ and total N uptake = $Bf(N)$. Here, f(N) represents the combined effect of nitrogen uptake and conversion into plant biomass. The parameter *r* represents the efficiency of converting N into biomass, *a* represents the efficiency of root uptake, and *h* represents the rate at which the combined processes of uptake and incorporation occur. This implies that given the similarity in the form of the modelled functions between both processes, a saturating model in our study would not distinguish between photosynthetic rate limitation or rate-limited root uptake, but would clearly indicate the efficiency of each process individually and the levels of N availability able to saturate one (or both) of the two ecological processes. We assessed N limitation

using this model, a linear N model, and a non-limiting model. The linear N model would indicate N availability far from the values in which a saturating function would be expected.

3.3.3.2 Plant-Soil Feedbacks

Salix lanata have ectomycorrhizal associations in Yamal (Akhmetzhanova et al. 2012), which may access organic N forms to overcome in part the microbial bottleneck (Chapman et al. 2006). We represented plant-soil feedback as an addition to the N stock, where the addition is proportional to the current biomass loss rate. Thus, the strength of the feedback depends on current shrub biomass. We assume that the relation is linear, following Jeffers et al. (2011):

$$y(B) = \alpha\gamma_B B$$

Here, α represents a conversion factor of plant biomass into soil N, and γ_B represents environmental loss as a fraction of total plant biomass B.

3.3.3.3 Geometric constraint

In dendrochronological studies of Arctic shrubs, age-related / ontogenetic growth trends are often absent (e.g. Macias-Fauria et al. (2012)). Assuming that the maximum size of woody plants is constrained by mechanical limits, this indicates that either: (a) such shrubs are far from their asymptotic stem diameter and growing slowly, thus appearing to grow linearly over the observed timeframe; or (b) shrubs preferentiate investment in new young stems versus old stems, thus never approaching asymptotic size. To assess the role of geometrical constraints on shrub secondary growth, we included models with and without asymptotic growth. We chose a Richards' model to represent mechanical constraints as it is a non-linear plant growth model that has a mechanistic basis (Paine et al. 2011) (see Supplementary Material for model-fitting of alternative models).

3.3.3.4 Allometry

To gain a mechanistic understanding of the processes driving shrub ring production, it is necessary to apply an allometric model; ring width is a one-dimensional size variable of a plant stem,

compared to two-dimensional cross-sectional area, and three-dimensional volume (Burkhart & Tomé 2012). As the conceptual models used here require information on total biomass, we apply an allometric model to quantify the size-specific three-dimensional stem volume laid down for each millimetre of one-dimensional wood increment. We connected ring width to stem mass using a shrub allometric model that mimics fractal woody structure within a multi-stemming plant individual (Götmark et al. 2016). We used model parameters defined in Götmark et al (2016) that result in a plant of multi-stemmed shrub form. Stem length L, a requirement of the model, was derived from stem radius S_r using a growth-hydraulic model, which is biologically realistic for small shrubby plant forms (Niklas & Spatz 2004):

$$S_r = \frac{100\left(\frac{0.01L+M_1}{M_2}\right)^{\frac{3}{2}}}{2}$$

Where M_1 and M_2 are allometric parameters. We used the non-linear least squares (*nls*) function in R to estimate M_1 and M_2 for the metrics collected from the 200 measured shrub individuals at Yuribei.

3.3.3.5 Nitrogen Availability

We applied an explicit transform of $\delta^{15}N$ to standardised N availability using an existing empirical relationship. As $\delta^{15}N$ is an index relative to air (0‰), values of $\delta^{15}N$ may fall in a positive – negative range. In Arctic and alpine environments, soils and plant tissues exhibit negative $\delta^{15}N$ values (Craine et al. 2018; Körner et al. 2016; Craine et al. 2015). Negative $\delta^{15}N$ values occur in high latitude environments (i.e. relatively low N availability) because: (a) a greater proportion of plant N uptake is organic forms of N via mycorrhizae, a process which discriminates in favour of ^{14}N (Craine et al. 2015); and (b) plant uptake is especially efficient at competing against loss pathways (e.g. denitrification) that deplete the soil pool of ^{14}N, which results in a global pattern of greater losses of ^{15}N-depleted forms of N with increasing mean annual temperature (Amundson et al. 2003). Our models require positive quantities of N to function in a biologically realistic manner, thus transform of the $\delta^{15}N$ index to positive values is necessary. We used two lines of evidence to

represent $\delta^{15}N$ as N availability. First, patterns of $\delta^{15}N$ indicate that intra-plant variability is low: wood and leaf $\delta^{15}N$ have been found as positively related and in a similar range (<0.5‰ fractionation) within regional (Bukata & Kyser 2007) and global (Craine et al. 2009) comparisons; therefore it is reasonable to assume a constant relationship between wood and foliar $\delta^{15}N$. Second, Craine et al. (2009) compiled available datasets that contained global foliar $\delta^{15}N$ alongside in-situ N mineralisation rates and / or resin bag measurements of soil N availability stocks (Craine et al. 2009). After correcting for inter-site differences in mean foliar $\delta^{15}N$ and standardising N measurements between measurement techniques, a linear relation was identified between $\delta^{15}N$ and unitless N availability ($r^2 = 0.25$, $p<0.001$, $n = 102$): $N = (100*\delta^{15}N+309)/359$ (Craine, Brookshire, et al. 2015). Working with the assumption that fractionation between $\delta^{15}N$ in leaves and wood is insignificant, we transformed our $\delta^{15}N$ data with the above model.

3.3.4 Modelling Fitting and Model Selection

A model-fitting and model-selection (MFMS) approach was used to assess the most appropriate model hypothesis for each of the ten coupled growth-nitrogen model systems. First, we conducted maximum likelihood estimation (MLE) for each model. MLE identifies the best set of model parameters given the data via an optimisation routine that maximises the goodness-of-fit, as represented by a likelihood function. To assess goodness-of-fit, the negative log likelihood to be minimised was defined as a bivariate normal distribution:

$$-\log\left(L\left(\sigma_x, \sigma_y, \rho\right)\right) = 2\pi\sigma_x\sigma_y\sqrt{1-\rho^2} + \frac{1}{2}\left(\frac{z}{1-\rho^2}\right)$$

$$z = \left[\left(\frac{x_{obs}-x_{est}}{\sigma_x}\right)^2 - 2\rho\left(\frac{x_{obs}-x_{est}}{\sigma_x}\cdot\frac{y_{obs}-y_{est}}{\sigma_y}\right) + \left(\frac{y_{obs}-y_{est}}{\sigma_y}\right)^2\right]$$

Here, x_{obs} and x_{est} are the observed and estimated cumulative stem radius, y_{obs} and y_{est} are the observed and estimated $\delta^{15}N$. Three parameters are estimated alongside model parameters: σ_x and σ_y indicate the standard deviation of stem radius and $\delta^{15}N$ respectively, and ρ their covariance.

We filled any missing isotope data-points by linear interpolation. Second, we selected the best model for each shrub using a model-selection statistic. We conducted our analysis using an F# modelling library, '*Bristlecone'* (**Chapter 6**). Our *Bristlecone* F# script for this analysis is appended in Supplementary Material.

For model-fitting, an initial point was drawn at random from within given starting bounds (*starting bounds in Supplementary Material*). The ODE models were integrated using a Runge-Kutta 45 solver (Press et al. 1992). We performed parameter estimation using a variant of Fast Simulated Annealing (FSA) (Lee 2015), a stochastic Monte Carlo metaheuristic for global optimisation in continuous parameter space. Simulated annealing is a metaheuristic based on random walk MCMC, which mimics the physical process of annealing metal: the system is elevated to a high energy E, at which particles are likely to accept nearly all uphill ('worse') jumps. The system energy is then gradually lowered, progressively accepting less worse moves (Locatelli 2002). We configured a homogenous-chain simulated annealing heuristic with an energy-dependent Cauchy proposal distribution, a Metropolis-Hastings (Boltzmann) acceptance probability, and a cooling schedule of $\frac{E_0}{k}$, where k = the cooling iteration. At each E, we ran a homogenous Markov Chain for 5,000 improvements, or 15,000 iterations, whichever occurred sooner. We stopped optimisation when $E < 0.50$. For each FSA run, we tuned the per-parameter step size offline to ensure an acceptance rate of 0.25-0.50 for $E = 1$ and tuned E_{max} such that the acceptance rate of worse moves was above 0.60. 68% and 95% confidence intervals were estimated for each model parameter using a likelihood interval approach (Morgan 2000).

For model selection, model comparison was conducted using constrained Akaike Information Criterion (AICc), through which the likelihood is corrected for the number of observations in short time series and penalised for the complexity of mathematical models. We used the AICc to calculate Akaike weights for each model and for each shrub individual (Wagenmakers & Farrell 2004). Akaike weights translate the AICc into a relative measure of evidence in support of each model given the data. In addition, we compared the goodness-of-fit of the shrub-nitrogen models between

individuals by generating one-step-ahead predictions at each models' MLE and then calculated the root mean square error (RMSE) values for both variables.

3.4 Results

3.4.1 Dendroecological Data

Ring Width Time-Series. We successfully cross-dated 52 lowland shrub discs from Yuribei. The date of establishment varied between 1912 – 1987, thus stem ages ranged between 26 and 101 years. The mean date of establishment was 1954, with over half of all of our sampled shrubs established during the 1950s. The complete shrub ring-width data is presented in Supplementary Material.

δ^{15}N Time Series. We successfully created ten annually resolved δ^{15}N time-series for the period 1980-2013 (

Figure 3–4). For the individual measurements of δ^{15}N in all 10 time-series (n = 399), the mean value was -1.15‰ (2dp) with a sample standard deviation of 1.30‰ (2dp). Mean δ^{15}N varied between individual shrub time-series, from -2.83‰ – 0.72‰ (2dp).

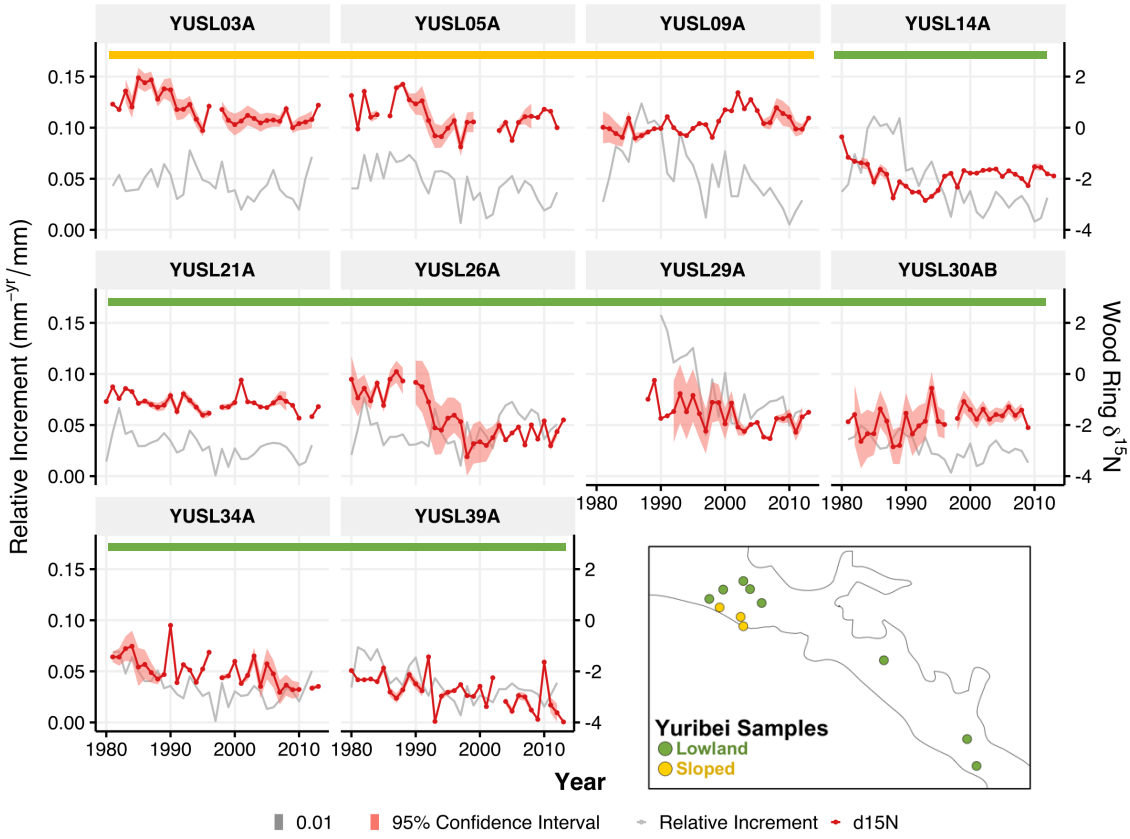

Figure 3–4 Dendroecological data for ten individuals, consisting of annual wood ring $\delta^{15}N$ and annual ring increment relative to current radius. Standard error (red bound) was calculated as the standard deviation of replicate isotope samples (average of 0.303‰ over all $\delta^{15}N$ series). Inset map shows spatial delineation between shrubs on the sloped valley side and lowland areas.

Replicate measurements for one in every three years to determine variability within wood ring $\delta^{15}N$ indicated an overall standard deviation of $\delta^{15}N$ values of 0.303‰ (3dp). The error structure was, however, variable within and between shrub discs (

Figure 3–4). Where a shrub exhibited missing growth rings, we could not measure $\delta^{15}N$; this resulted overall in 11 missing measurements within the ten time-series. To assess variability of $\delta^{15}N$ in space, we conducted an inter-comparison of time-series to ascertain if there were common trends; mean inter-series correlation was 0.207 (3dp) and mean between-shrub correlation $\bar{r}_{bt}$ was 0.055 (3dp), indicating that N availability was heterogeneous between the locations of shrub individuals. It was therefore not appropriate to construct a mean site-level chronology of $\delta^{15}N$. Despite the low overall inter-series correlation, several pairs of series showed high correlations; $\bar{r}_{bt}$ was 0.46 for five of ten individuals.

Nine of the ten N isotope series exhibited significant linear temporal trends. The Theil-Sen summaries are shown in **Table 3–2**:

Table 3–2 Linear fit (Theil-Sen) summary statistics for individual shrub $\delta^{15}N$ series

Shrub ID	Intercept	Slope	Intercept p-value	Slope p-value	Residual SE	DF
YUSL03A	58.78	-0.029	0.000***	0.000***	0.47	30
YUSL05A	34.06	-0.017	0.001***	0.001***	0.59	27
YUSL09A	-55.43	0.028	0.000***	0.000***	0.51	31
YUSL14A	-23.98	0.011	0.151	0.182	0.54	32
YUSL21A	16.55	-0.009	0.001***	0.000***	0.33	30
YUSL26A	155.38	-0.079	0.000***	0.000***	0.66	31
YUSL29A	87.77	-0.045	0.000***	0.000***	0.52	24
YUSL30AB	-51.74	0.025	0.000***	0.001***	0.48	26
YUSL34A	70.47	-0.036	0.000***	0.000***	0.50	29
YUSL39A	75.26	-0.039	0.000***	0.000***	0.58	32

*** = 99% significance; SE = standard error; DF = degrees of freedom

A declining $\delta^{15}N$ trend between 1980-2013 was found for seven time-series while increasing trends were found in two time-series. For the seven declining series, the median decline was -0.036‰ per year – representing a median depetion of $\delta^{15}N$ of 1.188‰ – between 1980 and 2013. When all ten $\delta^{15}N$ were included, the overall median deplention of $\delta^{15}N$ of 0.759‰.

3.4.2 Allometric Relations

To determine the relationship between shrub height and stem diameter, we applied a non-linear least-squares fitting procedure to the Yuribei shrub stem length – basal diameter dataset, using the Niklas and Spatz (2004) allometric form. We estimated m^1 as 19.98237 (SE = 0.65150) and m^2 as 0.42091 (SE = 0.08881), with 99% significance ($p<0.001$). When the empirical stem length – basal diameter function was incorporated into the shrub radius – biomass allometric function, biomass increased exponentially with stem radius (**Figure 3–5**).

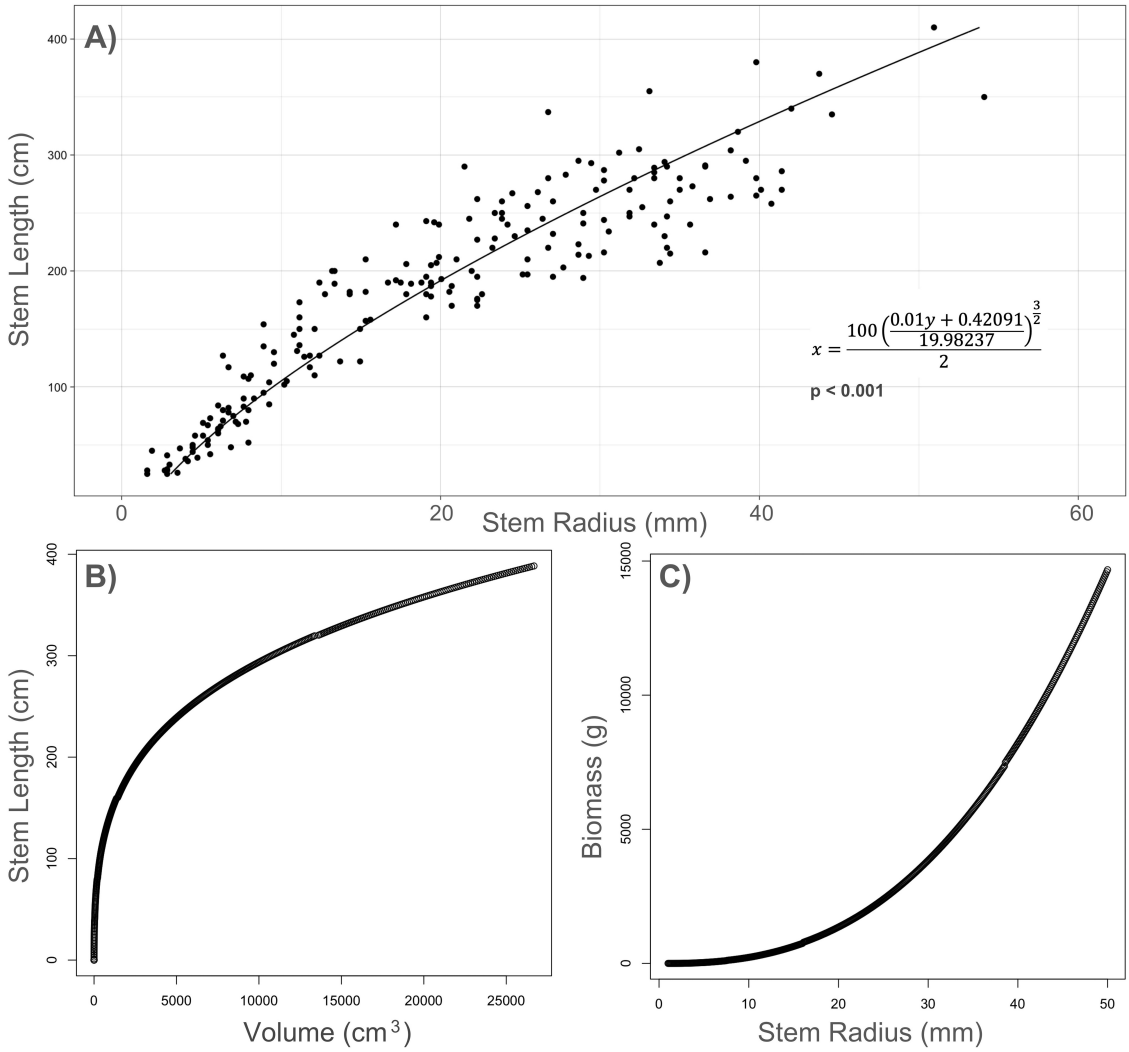

Figure 3–5 Allometric relations: **A)** Stem diameter and stem length (M_1 = 0.421 and M_2 = 19.982 (both 3dp) fit to function in Section 3.3.3.4 using Yuribei field measurements; **B)** stem volume and stem length; and **C)** stem basal radius and stem biomass.

3.4.3 Mechanistic Model Fitting and Selection

We conducted model-fitting and model-selection to identify the best model formulation to explain the observed $\delta^{15}N$ and ring width data for each of N-limitation, plant-soil feedbacks, and geometric effects. Akaike weights – which represent the relative support for each hypothesis - indicated that N-dependent models better represented the data than N-independent ones for all ten shrub individuals assessed. A linear N-limitation effect was most appropriate for nine of ten individuals: only one individual (*YUSL39A*) was best represented by a saturating N-limitation effect. The Akaike weights for all models are shown in **Table 3–3** and likelihood values in **Table 3–4**:

Table 3–3 Akaike weights for model fits (2dp – bold above 10%)

Shrub ID:	**03A**	**05A**	**09A**	**14A**	**21A**	**26A**	**29A**	**30AB**	**34A**	**39A**
Non-Asymptotic										
Saturating	0.00	0.00	0.00	0.00	**15.35**	0.00	0.07	0.00	0.00	0.00
Saturating + Feedback	8.42	0.15	0.22	0.11	8.57	0.03	4.29	0.31	1.43	0.08
Linear	0.06	0.00	0.00	0.19	**15.55**	0.00	0.00	0.00	0.00	0.00
Linear + Feedback	**56.41**	1.18	0.20	1.04	**54.14**	0.29	**93.71**	2.69	**97.72**	0.00
No N Limitation	0.00	0.00	0.00	0.00	0.00	0.00	0.00	0.00	0.00	0.00
Plant-Driven N Cycling	0.00	0.00	0.00	0.00	0.00	0.00	0.00	0.00	0.00	0.00
Asymptotic										
Saturating	0.68	0.00	0.60	0.26	1.41	0.00	0.04	0.00	0.00	**99.92**
Saturating + Feedback	2.87	12.51	0.05	**12.58**	0.71	0.00	0.19	0.07	0.42	0.00
Linear	6.02	0.00	0.00	1.34	1.17	0.00	0.00	**95.96**	0.00	0.00
Linear + Feedback	**25.53**	**86.16**	**57.30**	**84.48**	3.10	**99.67**	1.69	0.98	0.44	0.00
No N Limitation	0.00	0.00	**36.59**	0.00	0.00	0.00	0.00	0.00	0.00	0.00
Plant-Driven N Cycling	0.00	0.00	5.03	0.00	0.00	0.00	0.00	0.00	0.00	0.00

Akaike weights represented as percentages, to two decimal places. Bold = above 10% support; Red = best supported model.

Table 3–4 Minimum -log Likelihood value for model fits

Shrub ID:	**03A**	**05A**	**09A**	**14A**	**21A**	**26A**	**29A**	**30AB**	**34A**	**39A**
Non-Asymptotic:										
Saturating	46.766	85.730	90.627	81.580	52.305	114.884	41.523	86.135	75.977	92.567
Saturating + Feedback	37.026	63.471	79.178	72.890	50.801	108.664	34.483	72.889	65.646	77.850
Linear	46.029	85.728	92.903	76.308	54.206	148.435	48.593	85.492	86.800	101.710
Linear + Feedback	37.270	63.463	81.448	72.694	51.045	108.472	34.258	73.090	63.569	85.623
No N Limitation	130.517	209.118	177.561	184.782	98.494	139.626	147.033	127.110	166.107	201.781
Plant-Driven N Cycling	106.121	209.215	171.700	184.814	95.971	124.019	141.487	122.752	165.946	201.076
Asymptotic:										
Saturating	39.537	69.444	78.194	71.977	52.609	123.749	39.203	83.805	87.023	70.674
Saturating + Feedback	35.740	56.728	78.345	65.826	51.007	108.517	34.286	71.708	64.515	79.174
Linear	39.508	69.333	85.162	72.434	54.877	113.019	54.522	69.513	85.185	108.349
Linear + Feedback	35.916	57.084	73.637	66.207	51.817	100.556	35.414	71.728	66.835	85.801
No N Limitation	58.062	91.518	78.193	86.718	64.073	140.151	104.834	85.472	120.619	142.274
Plant-Driven N Cycling	58.101	91.717	78.217	78.539	64.097	140.029	104.846	82.174	120.656	142.255

All values shown to three decimal places.

The best-fitting models for all shrub individuals were able to replicate the observed trajectories of $\delta^{15}N$. Model performance, however, was relatively poor for *YUSL14*, the only individual for which there was no significant trend in $\delta^{15}N$ over time (**Figure 3–6**). As an additional indicator of goodness-of-fit, we calculated one-step-ahead predictions for the best-fitting model for each shrub individual and calculated the root mean square error (RMSE) for $\delta^{15}N$ and stem predictions. The RMSEs are shown in **Table 3–5**:

Table 3–5 Root mean square error (RMSE) of shrub-nitrogen relations given the most appropriate model for each shrub individual.

Shrub ID	Stem Radius (mm)	$\delta^{15}N$ (‰)
YUSL03A	0.20	0.38
YUSL05A	0.32	0.53
YUSL09A	0.99	0.38
YUSL14A	0.35	0.38
YUSL21A	0.31	0.33
YUSL26A	0.88	0.76
YUSL29A	0.81	1.66
YUSL30AB	1.92	0.53
YUSL34A	1.05	0.65
YUSL39A	0.63	0.73

The RMSE of one-step-ahead predictions indicate predictive accuracy of the model in the original data units and reflecting the differences in variability between each time series. The median RMSE of $\delta^{15}N$ for all ten individuals was 0.53‰. Similarly, the median accuracy for predicting stem radius was 0.72mm. In addition, examination of the squared residuals between observed and expected stem radius indicated that model performance was worse during relatively harsh growing years (i.e. 1988, 1989, and 1997).

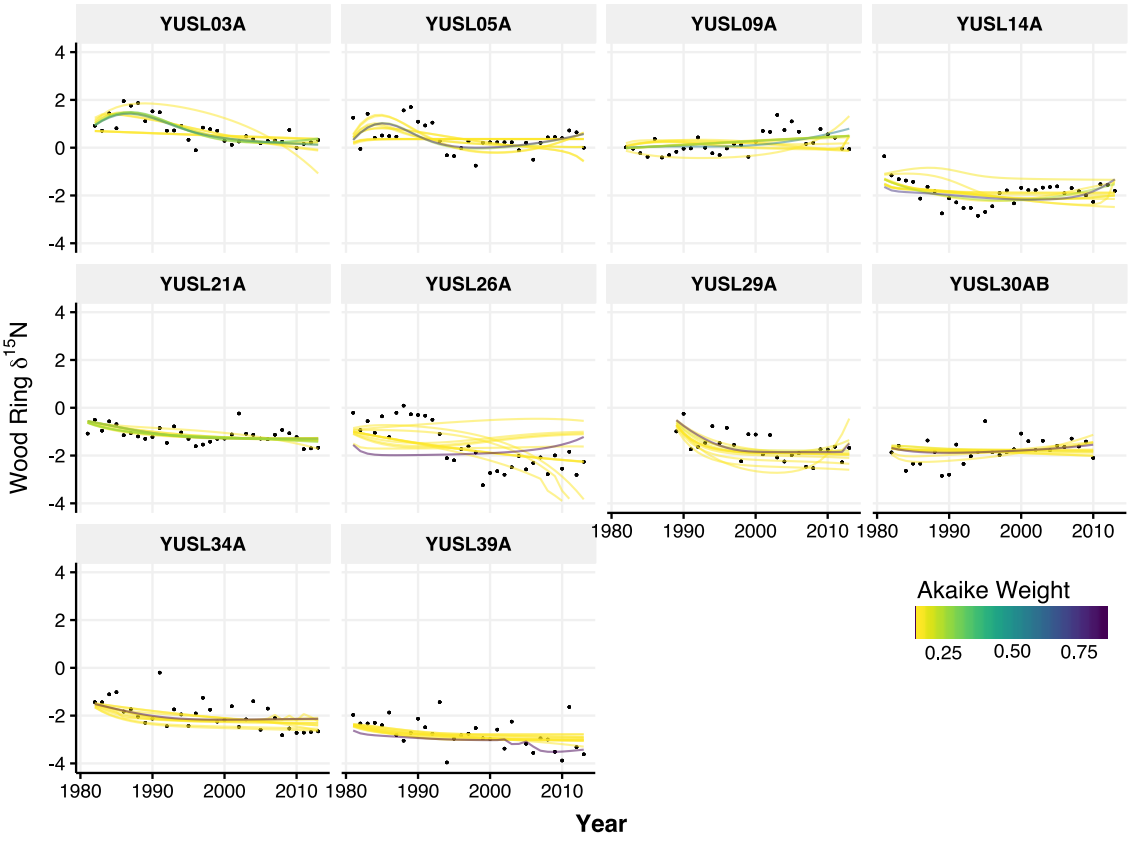

Figure 3–6 Realised $\delta^{15}N$ trajectories for each plant and hypothesis given the best-fitting parameters. Actual measurements are represented by black points. The Akaike weight indicates the probability that a particular model fit is most appropriate to explain the observations, given the complete set of fits.

Form and Strength of N Limitation. The Akaike weights indicated that a linear representation of N-dependent growth (**N2**) best explained the observed time series for nine of ten individuals rather than N-independent growth (**N1**). However, the strength of this mechanism was variable between individuals. Within the model-fitting procedure we estimated the parameter a, which represents the efficiency of N uptake. Given the most likely estimated values of a and their 95% confidence intervals, the variability was greater between individuals with little overlap of the 95% confidence intervals (**Figure 3–7**). For one shrub individual (*YUSL39*), a saturating N-dependent growth function (**N3**) was found to better explain the observed data; the mean observed and predicted $\delta^{15}N$ values were lowest for this individual.

Plant-Soil Feedback. The Akaike weights indiciated that the inclusion of a plant-soil feedback mechanism (**F2**) improved the ability of models to explain the observed data for eight of ten shrub

individuals. Models without a plant-soil feedback (**F1**) were most appropriate for *YUSL30* and *YUSL39*. For the eight shrubs that exhibited important plant-soil feedbacks there was variability in the strength of the feedback as estimated by the litter conversion factor α, which represents the N content derived from each gram of biomass, and the biomass loss rate γ_B. Values of α at the maximum likelihood estimates (MLEs) varied an order of magnitude between 0.001 and 0.018 with little overlap in the 95% confidence intervals. Similarly, the loss rate (γ_B) varied between 0.10 and 0.65 within the eight individuals (**Figure 3–7**).

Non-Nitrogen Asymptotic Limit to Growth. For six of ten shrubs, the most appropriate model included limits to maximum size (**R2**) that were not explained by nitrogen limitation. For four individuals – *YUSL3*, *YUSL21*, *YUSL29*, and *YUSL34* – a linear non-asymptotic functional form (**R1**) was more appropriate. Of the six shrubs for which a limit to maximum size was important, the median asymptotic basal stem diameter was 11.66cm, ranging between 7.36cm – 38.15cm (all 2dp). The equivalent median biomass was 22.03kg: although five shrubs ranged between 6.53kg – 29.53kg asymptotic biomass. An outlier was *YUSL39A*, where the maximum size was estimated as 507.82kg.

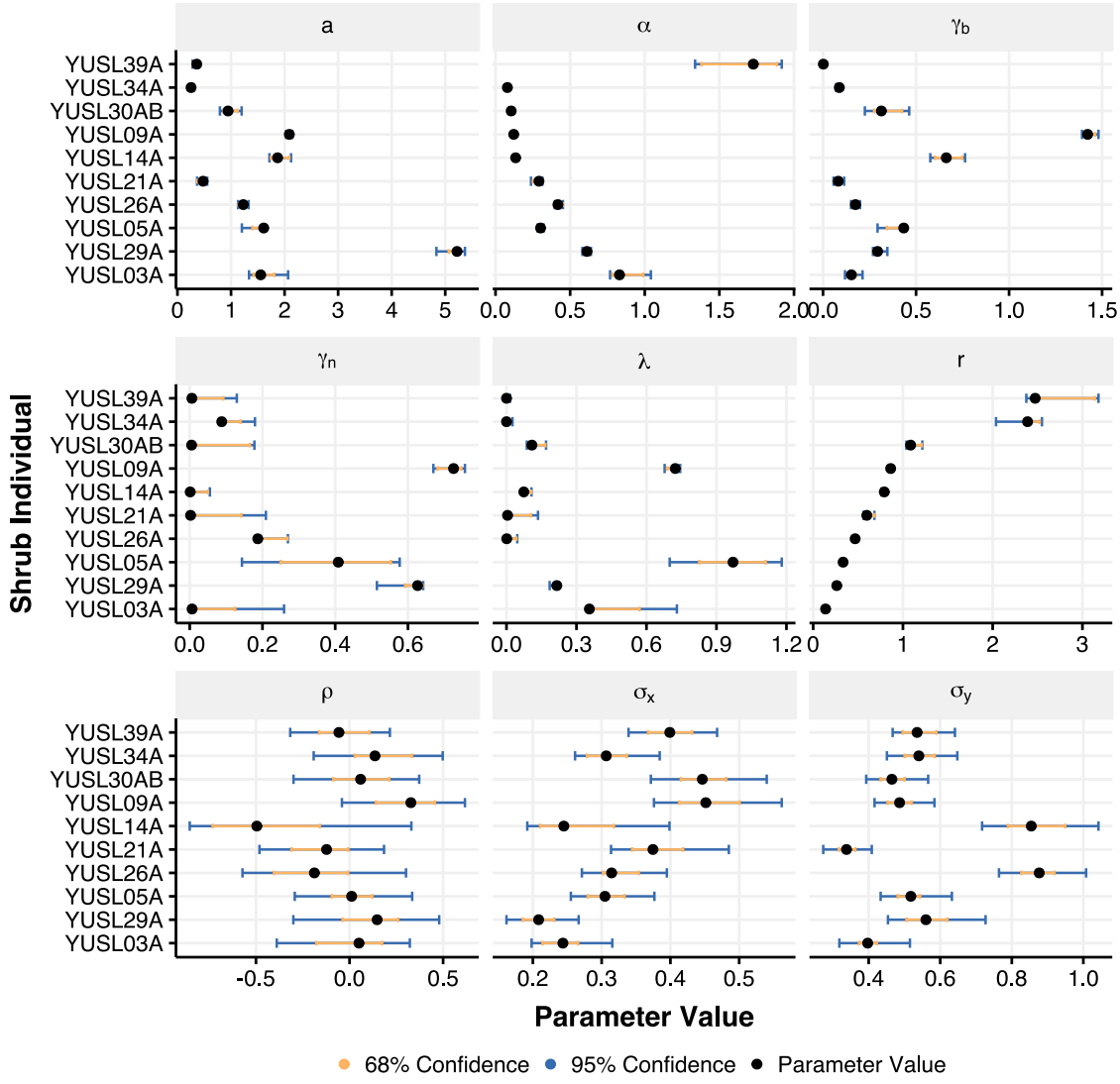

Figure 3–7 Estimated parameter values for the linear N-limitation model (with feedback, without asymptote), ordered by intrinsic growth rate (***r***). 68% and 95% confidence intervals calculated using profile likelihood approach. Parameter are: N-use efficiency (***a***); litter conversion factor ($\boldsymbol{\alpha}$); environmental loss of biomass ($\boldsymbol{\gamma_b}$); environmental loss of nitrogen ($\boldsymbol{\gamma_N}$); background N replenishment rate ($\boldsymbol{\lambda}$); covariance ($\boldsymbol{\rho}$); standard deviation of growth ($\boldsymbol{\sigma_x}$); and standard deviation of N ($\boldsymbol{\sigma_y}$).

3.5 Discussion

3.5.1 Trends in Soil Nitrogen Availability

Our wood $\delta^{15}N$ time-series indicate that soil N availability has declined from 1980 to 2013 at multiple locations within the Yuribei site. However, the presence of positive trends in two sampled individuals indicates increasing N availability at some locations at Yuribei, and highlights the heterogeneity of N availability at the landscape scale. The presence of both declining and increasing

$\delta^{15}N$ trajectories suggests that the observed N availability has derived from local-scale factors (e.g. local plant structure and microtopography) rather than regional climate patterns, from which we would expect a common response.

Given the rapidity of warming that has occurred on the Yamal Peninsula over recent decades, it is surprising that we found declining N signals over decadal time: in experimental plots, warming has – in some cases – increased the efficiency of N-mineralising microbes (Elberling 2007; Rinnan et al. 2007), which could lead to elevated N supply. In addition, Blume-Werry et al. (2019) found that experimental permafrost thaw allowed greater soil exploration and microbial decomposition of deeper soil organic resources, when measured after ten years (Blume-Werry et al. 2019). Soils within the Yamal Peninsula contain major stores of frozen organic matter (Hengl et al. 2017): there is therefore great potential for increasing access to N. However, declining $\delta^{15}N$ in our data suggests that: (a) N supply (i.e. fixation, access to N sources in permafrost) has been constrained; and / or (b) some N has become 'locked up' in long-lived stores such as plant structural material or soil microbial biomass (i.e. via microbial immobilisation). N losses (i.e. nitrification, denitrification, leaching) are likely low as – at low N availability – mineral N is of low concentration thus not a dominant loss pathway.

Differences in the absolute mean $\delta^{15}N$ between individual time-series suggest that the sampled shrubs were split between two landscape patches (in terms of soil N). The two shrub groupings are separated in space (**Figure 3–1**), with higher mean $\delta^{15}N$ values observed in the shrub individuals growing on the slope (*YUSL03*, *YUSL05*, and *YUSL09*) versus lower values in those collected from riparian lowlands. A t-test for difference in the mean $\delta^{15}N$ values confirms that there is a difference between sloped and plain locations ($p=0.00010$). The estimated model parameters (i.e. λ in **Figure 3–7**) suggest that there was a greater background replenishment rate of soil N in the slope patch. An interaction with the soil moisture regime may explain topographic variability in N (Ackerman et al. 2017).

3.5.2 Role of N in shrub growth

Our results demonstrate that N-limitation has played a role in secondary growth patterns of these *Salix lanata* individuals in the recent past. The importance of N-limitation at Yuribei aligns with evidence from tundra fertilisation experiments, which indicate increases in above-ground biomass production following addition of NPK fertilisers (Bouskill et al. 2014). Our time-series modelling approach enabled us to infer the mechanism and rates of N-limitation at annual temporal resolution, with a linear form outcompeting a saturating model that encompassed N-dependent rate limitation to root scavenging or photosynthesis. That a linear function better represents the data than a saturating form suggests that all bioavailable N is utilised during an individual growing season. Thus, any limiting rate on N uptake and N incorporation into biomass occurs at a finer temporal resolution than our data. Indeed, as the *Salix lanata* individuals studied are likely associated with ectomycorrhizal (ECM) fungi (Akhmetzhanova et al. 2012), which enable the use of organic N sources (Chapman et al. 2006), they may have enhanced foraging ability under low N conditions. Although we did not include mycorrhizal interactions explicitly in our models, the linear N-limitation function does suggest that these shrubs are efficient at N uptake under low-N conditions, which could indicate use of organic N sources.

Wild (2018) suggests that N-limitation to Arctic shrubs may be moderated by three major mechanisms: decomposition rate, competition with N-immobilising microbes, and access to resources from thawing permafrost. Here, our model-inferred processes suggest that plant-soil feedbacks have contributed substantially to soil N inputs (**Figure 3–8**) and that this input may even be greater than background N inputs (as estimated within the parameter λ); such background N sources could include increased access to organic deposits within thawing permafrost or biological N_2 fixation. As λ was relatively high within the sloped area, it suggests that such mechanisms are spatially delineated here. In addition, model-inferred rates of soil N loss – which may include gaseous losses, leaching, and N immobilisation by microbes – vary substantially between the individuals studied and may reflect fine spatial variability in loss processes. Indeed, evidence from active layer samples in the Siberian Arctic suggests that plant N limitation did not result from soil

organic matter (SOM) breakdown, but via competition with microbial communities (Wild et al. 2018).

Model-inferred N-uptake rates varied by many orders of magnitude between individuals (**Figure 3–8A**), which may reflect differing local absolute N availability and root competition for N between shrub individuals within *Salix* thickets. The strength of N-limitation, as reflected by the linear N-uptake efficiency parameter a, integrates the role of rooting characteristics and variability in root traits. A process-model of plant-microbe competition by Zhu et al. (2016) suggests that root traits significantly moderate the ability of Arctic vegetation to access any emerging sources of N (Zhu et al. 2016). For the shrubs studied here, the greatest N-uptake rates occurred for shrubs growing on the sloped area, where N-availability was relatively high, but unrelated to the incorporation efficiency of N into biomass (***r***): this suggests that shrubs here may respond to any future increases in N availability by increasing the quantity of biomass production without subsequent increases in litter quality, while also being unconstrained by N-uptake rates.

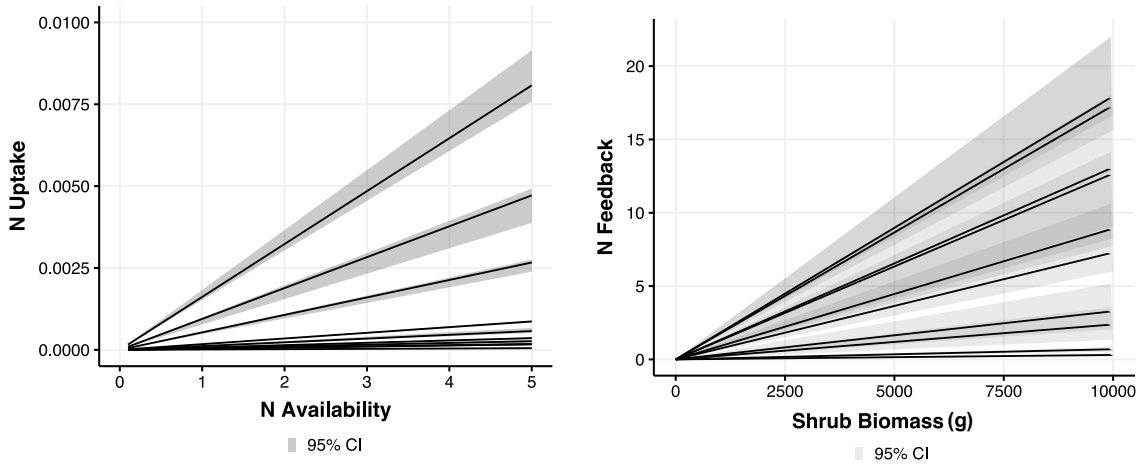

Figure 3–8 Model-inferred shrub N uptake and the strength of the shrub-soil N feedback for all ten shrub individuals given the most appropriate hypothesis for each as determined by model-fitting and model-selection. For each shrub individual, the values of each process were calculated given the parameter values at the maximum likelihood estimate (black lines); 95% confidence intervals (shading) were calculated by calculating the range of function values that occur within the individual parameters' 95% confidence intervals. N Uptake, N Availability and N Feedback are unitless measures of model-inferred N availability. **Left)** shrub N uptake / consumption as a function of soil N availability; **Right)** N feedback from shrub biomass to soil given current shrub biomass.

Model selection also indicated that the maximum size of shrub individuals was constrained by factors other than N-limitation in a number of cases. Given that the modelled asymptotic sizes were highly variable between individuals, we propose that unseen biotic interactions may be causing the

inferred limits to size rather than mechanical limits (beyond which the shrub form cannot support itself); shading and competition for light between individuals provides one plausible explanation.

3.5.3 Shrubs as drivers of N cycling

Our finding of an important shrub-soil feedback mechanism for all of the shrubs tested indicates that *Salix lanata* shrubs drive changes in their abiotic environment over decadal timescales. With the N feedback mechanism included with our models, the quantity of N being cycled between plant and soil increased substantially with significant increases in modelled plant N-uptake (i.e. the median estimated value of N-uptake efficiency (***a)*** increased by an order of magnitude when shrub-soil feedbacks were incorporated into models). Our findings corroborate with other evidence: Buckeridge et al. (2009) found that – in low Arctic tundra – soil N cycling rates were up to three times faster on tall-birch tundra than dwarf shrub tundra due to litter feedbacks (Buckeridge et al. 2009). Our modelling results suggest that shrubs exert significant influence on local N-cycling rates, assuming shrub size is proportional to N litter inputs. We also identified variability in the strength of the plant-soil feedback between individual plants, which is reflected in the parameter values of $\boldsymbol{\gamma}_B$ and $\boldsymbol{\alpha}$ (**Figure 3–7**), which may indicate both the environmental circumstances of the individuals but also phenotypic plasticity in terms of litter quantity and litter quality.

Two lines of evidence - the importance of litter feedbacks, coupled with the linear form of N-limitation – suggest that the *Salix lanata* individuals studied subvert the microbial bottleneck by actively controlling their environment (Chapman et al. 2006). We suggest that *Salix lanata* are able to overcome low-N conditions by accessing organic N forms via their ECM associates, as this would enable fast turnover of shrub litter. Organic N sources can be significant for N nutrition in tundra environments: Hobbie and Hobbie (2006) applied ^{15}N tracers to experimental plots at Toolik Lake, Alaska, identifying that 61 – 86% of N in plant biomass was obtained from mycorrhizal sources (J. E. Hobbie & E. A. Hobbie 2006).

3.5.4 Use of the Mechanistic Approach in Dendroecology

The application of our modelling approach to shrub-nitrogen data indicates that – as an alternative to traditional dendrochronological approaches – it may be useful to identify common mechanisms underlying the structure of 'multi-proxy' time-series data pertaining to a plant individual. Using standard ring width methods, correlative approaches are used to identify a common signal across ring, isotope, or wood anatomy series, from many plants. Here we have constructed an index of common mechanistic structure between individuals, and the associated strength of these mechanisms. Some of the parameters in our models represent abstractions of plastic plant traits, such as the scavenging efficiency of root systems. A stand could therefore be represented as a function of mechanistic limits to growth and the variability of their traits and apply such methods across multiple sites.

3.6 Conclusions

Our findings demonstrate how the combination of stable nitrogen isotope time series from wood rings and mechanistic models yield new insights into shrub-nitrogen interactions in Arctic environments. We successfully created annually resolved stable nitrogen isotope time-series from shrub wood rings at Yuribei. Our ten annually-resolved $\delta^{15}N$ time-series suggest a decline in soil N from 1980 – 2013. In addition, N availability curves were individualistic, reflecting high heterogeneity of soil N through time. Differences in absolute values of $\delta^{15}N$ between the series appear to reflect spatial heterogeneity of N within the landscape (patchiness), where individuals growing on slopes had more access to N than those growing on the flat plains.

We applied a mechanistic modelling approach to infer the role of nitrogen in controlling the stem wood production of Arctic shrubs at the individual scale from the shrub growth and N availability data. When fit to shrub data at Yuribei, our models identified that the growth of all ten individuals was N-limited. We found consistency of the N-limitation mechanism within the landscape, but variability in its relative strength. The most appropriate form of N-limitation was common for nine of these shrubs: linear N-limitation. That a linear mechanism is more appropriate than a saturating

mechanism of limitation suggests that all available N resources were utilised for plant growth within a year, with no evidence that N-limitation is tapering off.

We found an important role for N feedbacks between shrub and soil. The addition of a plant-soil feedback mechanism improved model quality for eight of ten shrub individuals assessed. However, the conversion factor of biomass into soil bioavailable N varied considerably between individuals, suggesting that environmental factors and / or phenotypic plasticity are important determinants of litter production and litter quality. Model selection also indicated that an asymptote to growth was of variable importance between shrub individuals. Without an asymptote, our base models of N-growth interactions allow exponential growth given infinite resources. Common plant growth models assume that the asymptote reflects a combination of mechanical and nutrient limits to growth. We found that the importance of an asymptote was unrelated to the shrub stem size during the modelling timeframe, suggesting that unseen ecological or behavioural mechanisms are driving stem thickening. These may consist of competition for space / shading, or a habit of stem abandonment.

Our modelling approach allows interrogation of the ecological mechanisms that may limit shrub growth, and their rates over the lifetime of individual shrubs. We suggest that our approach may be expanded: (a) to include other Arctic shrub species to assess inter- and intra-species trait variability; (b) to expand to a centennial timescale given the longevity of Arctic shrub stems; and (c) to combine N-limitation with climatology to examine the relative importance of competing limitations on Arctic shrub growth.

3.7 Acknowledgements

The authors thank Robin Paulman for advice on mass spectrometry, Chris Terry for model-fitting advice, Danielle Sinclair for lab assistance, and Kathy Willis for providing lab facilities.

3.8 Author Contributions

ACM developed the nitrogen isotope method, determined mathematical models, implemented, and conducted the mathematical modelling method, and led the writing of the manuscript. ESJ & MMF conceptualised the research. MBB provided guidance on the MFMS approach. BF, and MMF completed field work, and ZP created ring width chronologies. All authors contributed to the writing of the manuscript.

3.9 References

Aalto, J., le Roux, P.C. & Luoto, M., 2018. Vegetation Mediates Soil Temperature and Moisture in Arctic-Alpine Environments. *Arctic, Antarctic, and Alpine Research*, 45(4), pp.429–439.

Ackerman, D. et al., 2017. Arctic shrub growth trajectories differ across soil moisture levels. *Global Change Biol*ogy 23(10), pp.4294–4302.

Akhmetzhanova, A.A. et al., 2012. A rediscovered treasure: mycorrhizal intensity database for 3000 vascular plant species across the former Soviet Union. *Ecology*, 93(3), pp.689–690.

Amundson, R. et al., 2003. Global patterns of the isotopic composition of soil and plant nitrogen. *Global biogeochemical cycles*, 17(1), p.220.

Blok, D. et al., 2010. Shrub expansion may reduce summer permafrost thaw in Siberian tundra. *Global Change Biology*, 16(4), pp.1296–1305.

Blume-Werry, G. et al., 2019. Dwelling in the deep - strongly increased root growth and rooting depth enhance plant interactions with thawing permafrost soil. *The New phytologist*, p.nph.15903.

Bonsall, M.B. & Hastings, A., 2004. Demographic and environmental stochasticity in predator-prey metapopulation dynamics. *Journal of Animal Ecology*, 73(6), pp.1043–1055.

Bouskill, N.J., Riley, W.J. & Tang, J.Y., 2014. Meta-analysis of high-latitude nitrogen-addition and warming studies implies ecological mechanisms overlooked by land models. *Biogeosciences*, 11(23), pp.6969–6983.

Bret-Harte, M.S. et al., 2001. Developmental Plasticity Allows Betula nana to Dominate Tundra Subjected to an Altered Environment. *Ecology*, 82(1), pp.18-32.

Buckeridge, K.M. et al., 2009. Soil nitrogen cycling rates in low arctic shrub tundra are enhanced by litter feedbacks. *Plant and Soil*, 330(1-2), pp.407–421.

Bukata, A.R. & Kyser, T.K., 2007. Carbon and Nitrogen Isotope Variations in Tree-Rings as Records of Perturbations in Regional Carbon and Nitrogen Cycles. *Environ Sci Technol*, 41(4), pp.1331–1338.

Burkhart, H.E. & Tomé, M., 2012. Growth Functions. In *Modeling Forest Trees and Stands*. Dordrecht: Springer Netherlands, pp. 111–130.

Chapman, S.K. et al., 2006. Plants actively control nitrogen cycling: uncorking the microbial bottleneck. *New Phytologist*, 169(1), pp.27–34.

Craine, J.M. et al., 2009. Global patterns of foliar nitrogen isotopes and their relationships with climate, mycorrhizal fungi, foliar nutrient concentrations, and nitrogen availability. *New Phytologist*, 183(4), pp.980–992.

Craine, J.M. et al., 2018. Isotopic evidence for oligotrophication of terrestrial ecosystems. *Nature ecology & evolution*, 2(11), pp.1735–1744.

Craine, J.M., Brookshire, E.N.J., et al., 2015. Ecological interpretations of nitrogen isotope ratios of terrestrial plants and soils. *Plant and Soil*, 396(1-2), pp.1–26.

Craine, J.M., Elmore, A.J., et al., 2015. Convergence of soil nitrogen isotopes across global climate gradients. *Scientific Reports*, 5(1), p.889.

DeMarco, J., Mack, M.C. & Bret-Harte, M.S., 2014. Effects of arctic shrub expansion on biophysical vs. biogeochemical drivers of litter decomposition. *Ecology*, 95(7), pp.1861–1875.

Deslippe, J.R. & Simard, S.W., 2011. Below-ground carbon transfer among Betula nana may increase with warming in Arctic tundra. *The New phytologist*, 192(3), pp.689–698.

Elberling, B., 2007. Annual soil CO2 effluxes in the High Arctic: The role of snow thickness and vegetation type. *Soil Biology and Biochemistry*, 39(2), pp.646–654.

Elmendorf, S.C. et al., 2015. Experiment, monitoring, and gradient methods used to infer climate change effects on plant communities yield consistent patterns. *Proc Natl Acad Sci U S A*, 112(2), pp.448–452.

Elmendorf, S.C. et al., 2011. Global assessment of experimental climate warming on tundra vegetation: heterogeneity over space and time. *Ecology Letters*, 15(2), pp.164–175.

Epstein, H.E. et al., 2004. The nature of spatial transitions in the Arctic. *Journal of Biogeography*, 31(12), pp.1917–1933.

Epstein, H.E. et al., 2015. *Tundra Greenness*, Arctic Report Card.

Forbes, B.C. et al., 2009. High resilience in the Yamal-Nenets social-ecological system, West Siberian Arctic, Russia. *Proc Natl Acad Sci U S A*, 106(52), pp.22041–22048.

Fritts, H.C., 1976. *Tree Rings and Climate*, Academic Press.

Garnier, E., 1991. Resource capture, biomass allocation and growth in herbaceous plants. *Trends in Ecology & Evolution*, 6(4), pp.126–131.

Gärtner, H. & Schweingruber, F.H., 2013. *Microscopic Preparation Techniques for Plant Stem Analysis*,

Gärtner, H., Lucchinetti, S. & Schweingruber, F.H., 2014. New perspectives for wood anatomical analysis in dendrosciences: The GSL1-microtome. *Dendrochronologia*, 32(1), pp.47–51.

Gerhart, L.M. & McLauchlan, K.K., 2014. Reconstructing terrestrial nutrient cycling using stable nitrogen isotopes in wood. *Biogeochemistry*, 120(1-3), pp.1–21.

Götmark, F., Götmark, E. & Jensen, A.M., 2016. Why Be a Shrub? A Basic Model and Hypotheses for the Adaptive Values of a Common Growth Form. *Frontiers in plant science*, 7(654), p.313.

Hengl, T. et al., 2017. SoilGrids250m: Global gridded soil information based on machine learning B. Bond-Lamberty, ed. *PLOS ONE*, 12(2), p.e0169748.

Henry, G.H.R., Freedman, B. & Svoboda, J., 2011. Effects of fertilization on three tundra plant communities of a polar desert oasis. *Canadian Journal of Botany*, 64(11), pp.2502–2507.

Heskel, M. et al., 2013. Differential physiological responses to environmental change promote woody shrub expansion. *Ecology and evolution*, 3(5), pp.1149–1162.

Hoaglin, D.C., Mosteller, F. & Tukey, J.W., 2000. *Understanding robust and exploratory data analysis*, Wiley-Interscience.

Hobbie, J.E. & Hobbie, E.A., 2006. 15N in Symbiotic Fungi and Plants Estimates Nitrogen and Carbon Flux Rates in Arctic Tundra. *Ecology*, 87(4), pp.816–822.

Huisman, J., 1994. The Models of Berendse and Tilman: Two Different Perspectives on Plant Competition? *Functional Ecology*, 8(3), p.282.

Jabot, F. & Pottier, J., 2012. A general modelling framework for resource-ratio and CSR theories of plant community dynamics J. Fridley, ed. *Journal of Ecology*, 100(6), pp.1296–1302.

Jeffers, E.S. et al., 2011. Climate change impacts on ecosystem functioning: evidence from an Empetrum heathland. *New Phytologist*, 193(1), pp.150–164.

Komsta, L., 2013. **mblm: Median-Based Linear Models**. Available at: https://cran.r-project.org/web/packages/mblm/index.html.

Körner, C. et al., 2016. Carbon and nitrogen stable isotope signals for an entire alpine flora, based on herbarium samples. *Alpine Botany*, 126(2), pp.153–166.

Lantz, T.C., Marsh, P. & Kokelj, S.V., 2012. Recent Shrub Proliferation in the Mackenzie Delta Uplands and Microclimatic Implications. *Ecosystems*, 16(1), pp.47–59.

Lee, C.-Y., 2015. Fast simulated annealing with a multivariate Cauchy distribution and the configuration's initial temperature. *Journal of the Korean Physical Society*, 66(10), pp.1457–1466.

Locatelli, M., 2002. *Simulated annealing algorithms for continuous global optimization, Handbook of global optimization*,

Loranty, M.M. & Goetz, S.J., 2012. Shrub expansion and climate feedbacks in Arctic tundra. *Environmental Research Letters*, 7(1), p.011005.

Luo, Y. et al., 2004. Progressive nitrogen limitation of ecosystem responses to rising atmospheric carbon dioxide. *Bioscience*, 54(8), pp.731–739.

Macias-Fauria, M. et al., 2012. Eurasian Arctic greening reveals teleconnections and the potential for structurally novel ecosystems. *Nature Climate Change*, 2(8), pp.613–618.

McCarroll, D. & Loader, N.J., 2004. Stable isotopes in tree rings. *Quaternary Science Reviews*, 23(7-8), pp.771–801.

McLauchlan, K.K. et al., 2017. Centennial-scale reductions in nitrogen availability in temperate forests of the United States. *Scientific Reports*, 7(1), p.7856.

McLauchlan, K.K., Craine, J.M., Oswald, W.W., Leavitt, P.R. & Likens, G.E., 2007b. Changes in nitrogen cycling during the past century in a northern hardwood forest. *Proceedings of the National Academy of Sciences*, 104(18), pp.7466–7470.

McNickle, G.G. & Brown, J.S., 2014. When Michaelis and Menten met Holling: towards a mechanistic theory of plant nutrient foraging behaviour. *AoB PLANTS*, 6, p.7.

Menne, M.J. et al., 2012. An Overview of the Global Historical Climatology Network-Daily Database. *dx.doi.org*, 29(7), pp.897–910.

Mikhajlov, I.S., 2017. The expirience of creation of soil-ecological map of Yamal-Nenets autonomous district. *Bulletin of V.V. Dokuchaev Soil Science Institute*.

Morgan, B.J.T., 2000. *Applied Stochastic Modelling*, Hodder Arnold.

Myers-Smith, I.H. & Hik, D.S., 2013. Shrub canopies influence soil temperatures but not nutrient dynamics: An experimental test of tundra snow-shrub interactions. *Ecology and evolution*, 3(11), pp.3683–3700.

Myers-Smith, I.H. et al., 2011. Shrub expansion in tundra ecosystems: dynamics, impacts and research priorities. *Environmental Research Letters*, 6(4), p.045509.

Myers-Smith, I.H., Elmendorf, S.C., et al., 2015. Climate sensitivity of shrub growth across the tundra biome. *Nature Climate Change*, 5(9), pp.887–891.

Myers-Smith, I.H., Hallinger, M., et al., 2015. Methods for measuring arctic and alpine shrub growth: A review. *Earth-Science Reviews Earth-Science Reviews*, 140(4), pp.1–13.

Niklas, K.J. & Spatz, H.-C., 2004. Growth and hydraulic (not mechanical) constraints govern the scaling of tree height and mass. *Proc Natl Acad Sci U S A*, 101(44), pp.15661–15663.

Paine, C.E.T. et al., 2011. How to fit nonlinear plant growth models and calculate growth rates: an update for ecologists. *Methods in Ecology and Evolution*, 3(2), pp.245–256.

Piao, S. et al., 2014. Evidence for a weakening relationship between interannual temperature variability and northern vegetation activity. *Nature Communications*, 5, p.5018.

Poorter, H. et al., 2012. Biomass allocation to leaves, stems and roots: meta-analyses of interspecific variation and environmental control. *The New phytologist*, 193(1), pp.30–50.

Poorter, H., Anten, N.P.R. & Marcelis, L.F.M., 2013. Physiological mechanisms in plant growth models: do we need a supra-cellular systems biology approach? *Plant, Cell & Environment*, 36(9), pp.1673–1690.

Porter, C et al, 2018, "ArcticDEM", https://doi.org/10.7910/DVN/OHHUKH, Harvard Dataverse, V1, [Accessed 13th September 2019].

Post, E. et al., 2009. Ecological Dynamics Across the Arctic Associated with Recent Climate Change. *Science*, 325(5946), pp.1355–1358.

Press, W.H. et al., 1992. *Numerical Recipes in C*, Cambridge University Press.

Riechelmann, D.F.C. et al., 2014. Sensitivity of whole wood stable carbon and oxygen isotope values to milling procedures. *Rapid Commun Mass Spectrom*, 28(12), pp.1371–1375.

Rinnan, R. et al., 2007. Fifteen years of climate change manipulations alter soil microbial communities in a subarctic heath ecosystem. *Glob Chang Biol*, 13(1), pp.28–39.

Rossi, S. et al., 2014. Control over Growth in Cold Climates. In *Trees in a Changing Environment*. Plant Ecophysiology. Dordrecht: Springer, Dordrecht, pp. 191–219.

Schindelin, J. et al., 2012. Fiji: an open-source platform for biological-image analysis. *Nature methods*, 9(7), pp.676–682.

Screen, J.A. & Simmonds, I., 2010. The central role of diminishing sea ice in recent Arctic temperature amplification. *Nature*, 464(7293), pp.1334–1337.

Shaver, G.R. & Chapin, F.S., 1980. Response to Fertilization by Various Plant Growth Forms in an Alaskan Tundra: Nutrient Accumulation and Growth. *Ecology*, 61(3), pp.662–675.

Shi, Y. et al., 2015. Vegetation-Associated Impacts on Arctic Tundra Bacterial and Microeukaryotic Communities P. D. Schloss, ed. *Applied and Environmental Microbiology*, 81(2), pp.492–501.

Sturm, M. et al., 2005. Winter Biological Processes Could Help Convert Arctic Tundra to Shrubland. *Bioscience*, 55(1), p.17.

Tilman, D., 1990. Mechanisms of Plant Competition for Nutrients: The Elements of a Predictive Theory of Competition. In *Perspectives on Plant Competition*. Elsevier, pp. 117–141.

Tilman, D., 1988. *Plant Strategies and the Dynamics and Structure of Plant Communities*, Princeton University Press.

Van Rees, K., 1994. Michaelis-Menten kinetics: Calculation and use in nutrient uptake models. *New Zealand Journal of Forestry Science*, 24(2).

Wagenmakers, E.-J. & Farrell, S., 2004. AIC model selection using Akaike weights. *Psychonomic Bulletin & Review*, 11(1), pp.192–196.

Walker, D.A. et al., 2009. The Circumpolar Arctic vegetation map. *Journal of Vegetation Science*, 16(3), pp.267–282.

Wild, B. et al., 2018. Amino acid production exceeds plant nitrogen demand in Siberian tundra. *Environmental Research Letters*, 13(3), pp.034002–11.

Zamin, T.J. & Grogan, P., 2012. Birch shrub growth in the low Arctic: the relative importance of experimental warming, enhanced nutrient availability, snow depth and caribou exclusion. *Environmental Research Letters*, 7(3), p.034027.

Zhu, Q. et al., 2016. Root traits explain observed tundra vegetation nitrogen uptake patterns: Implications for trait-based land models. *Journal of Geophysical Research: Biogeosciences*, 121(12), pp.3101–3112.

3.10 Supplementary Material

This supplementary material contains wood %N data; explanatory information for ring width time-series; the starting bounds used within model-fitting; and the F# script used for model fitting and model selection (**at the reverse of this thesis**).

The Simulated Annealing model-fitting process was initialised using a randomised location in parameter space to ensure that the maximum likelihood returned was robust. Starting bounds were selected after exploration of model behaviour given the range and variability of the ring width and $\delta^{15}N$ time-series. The bounds used are in **Table 3–6**.

Table 3–6 Parameter bounds from which starting values were drawn for each model-fitting procedure.

Parameter	Constraint	Lower Bound	Upper Bound
λ	Positive	0.001	0.500
γ_N	Positive	0.001	0.200
γ_B	Positive	0.001	0.200
ρ	None	-0.500	0.500
σ_x	Positive	0.001	0.100
σ_y	Positive	0.001	0.100
K	Positive	3000	5000
α	Positive	0.0001	0.010
a	Positive	1.000×10^{-4}	4.000×10^{-4}
h	Positive	0.100	0.400
r	Positive	0.100	1.000

Starting values were drawn from a uniform distribution between the lower and upper bound. During the model-fitting procedure, it was illegal for parameter estimates to invalidate the constraint.

3.10.1 One-Step-Ahead Predictions

We assessed goodness-of-fit through time by calculating the root mean square error (RMSE) between each observation and a one-step-ahead prediction. RMSE values for all models and shrub individuals are presented in **Table 3–7** and **Table 3–8**.

Table 3–7 Root mean square error (RMSE) values for ring width (mm) given one-step-ahead predictions of shrub-nitrogen relations

Shrub ID:	**03A**	**05A**	**09A**	**14A**	**21A**	**26A**	**29A**	**30AB**	**34A**	**39A**
Non-Asymptotic										
Saturating	0.19	0.31	0.64	0.52	0.35	0.38	1.16	0.47	1.25	13.78
Saturating + Feedback	0.20	0.45	0.96	0.69	0.31	0.80	0.91	0.78	0.94	1.48
Linear	0.18	0.31	0.56	0.51	0.34	1.02	1.21	0.75	1.03	1.57
Linear + Feedback	0.20	0.48	0.87	0.86	0.31	0.92	0.81	0.77	1.05	1.08
No N Limitation	0.28	0.51	0.83	0.74	0.31	0.35	0.83	0.40	0.45	0.50
Plant-Driven N Cycling	0.27	0.51	0.83	0.74	0.31	0.35	0.84	0.40	0.45	0.50
Asymptotic										
Saturating	0.18	0.26	1.11	0.39	0.34	0.38	1.13	0.40	0.66	0.63
Saturating + Feedback	0.18	0.31	0.41	0.50	0.33	0.83	0.74	0.50	0.95	2.19
Linear	0.18	0.26	0.42	0.41	0.29	0.75	1.41	1.92	1.03	1.41
Linear + Feedback	0.18	0.32	0.99	0.35	0.28	0.88	0.91	0.56	0.91	1.07
No N Limitation	0.19	0.27	0.41	0.38	0.27	0.35	0.64	0.34	0.52	0.47
Plant-Driven N Cycling	0.19	0.27	0.41	0.40	0.27	0.35	0.64	0.34	0.52	0.47

All values shown to two decimal places.

Table 3–8 Root mean square error (RMSE) values for d15N (permil) given one-step-ahead predictions of shrub-nitrogen relations

Shrub ID:	**03A**	**05A**	**09A**	**14A**	**21A**	**26A**	**29A**	**30AB**	**34A**	**39A**
Non-Asymptotic										
Saturating	0.36	0.66	0.40	0.41	0.33	0.60	0.58	0.53	0.65	0.92
Saturating + Feedback	0.38	0.71	1.47	0.39	0.33	0.70	0.56	0.52	0.66	0.92
Linear	0.36	0.66	0.41	0.72	0.32	0.59	0.60	0.51	0.65	0.81
Linear + Feedback	0.38	0.63	1.54	0.47	0.33	0.71	1.66	0.56	0.65	0.76
No N Limitation	0.45	0.50	0.39	0.34	0.34	0.58	0.61	0.49	0.67	0.90
Plant-Driven N Cycling	0.42	0.50	0.39	0.34	0.32	0.61	0.64	0.51	0.66	0.91
Asymptotic										
Saturating	0.38	0.54	-	0.36	0.33	0.61	0.58	0.50	0.72	0.73

Saturating + Feedback	0.39	0.53	0.39	0.34	0.34	0.69	0.78	0.50	0.65	0.96
Linear	0.38	0.54	0.36	0.36	0.33	0.78	0.62	0.53	0.65	0.77
Linear + Feedback	0.39	0.53	0.38	0.38	0.32	0.76	0.58	0.50	0.63	0.76
No N Limitation	0.45	0.50	0.39	0.34	0.35	0.58	0.58	0.50	0.72	0.90
Plant-Driven N Cycling	0.45	0.50	0.39	0.36	0.35	0.58	0.58	0.49	0.72	0.90

All values shown to two decimal places.

3.10.2 A. Wood N concentration

Measurements of the nitrogen concentration of wood increments (Wood [N]) were produced alongside $\delta^{15}N$ (**Figure 3–9**). The measurements conform with other evidence that N concentrations in wood decrease from the bark inwards before stabilising, which reflects N nutrition within the plant (Gerhart & McLauchlan 2014). We did not use this data within our modelling approach, as wood [N] has not been found to record any environmental signals.

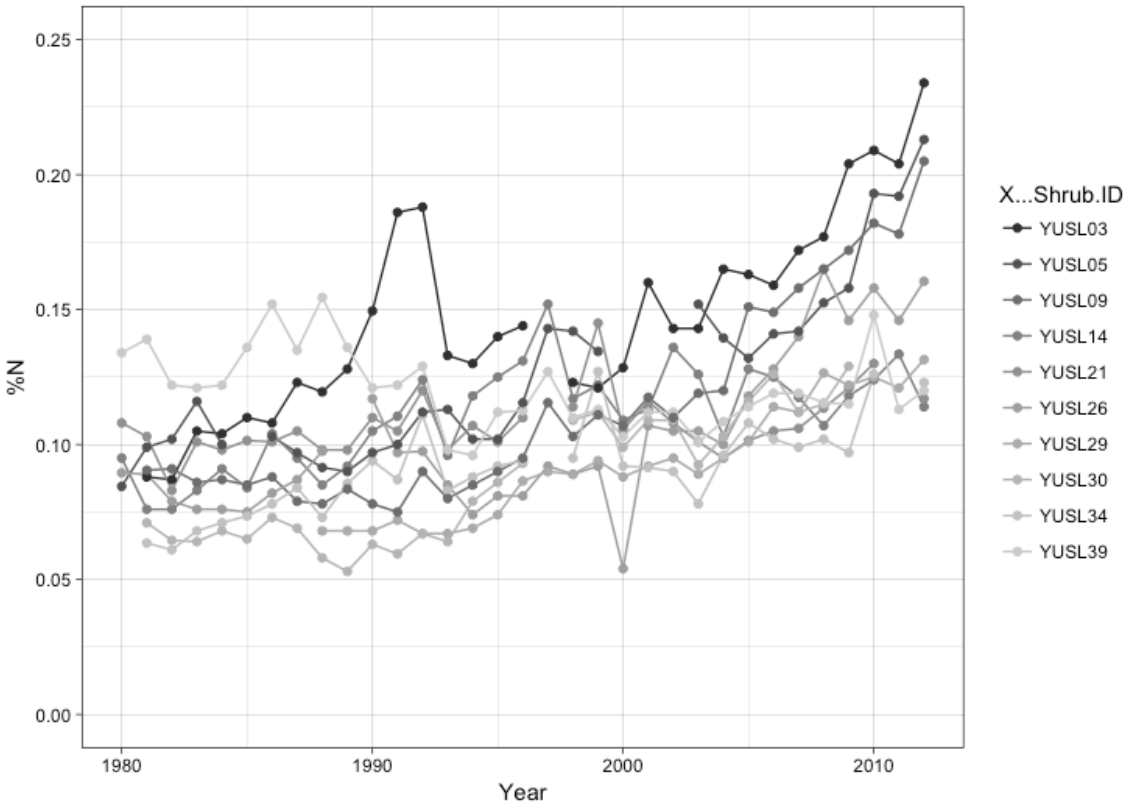

Figure 3–9 Percentage nitrogen concentration (%N) time-series for ten shrub individuals at Yuribei.

3.10.3 Ring Width Data

We did not detrend any of the measured ring width series, as they exhibited no age-related trends. We created a mean ring-width chronology using the Dendrochronology Program Library in R (Bunn 2008). The full ring width data and chronology will be uploaded to the International Tree Ring Database on publication.

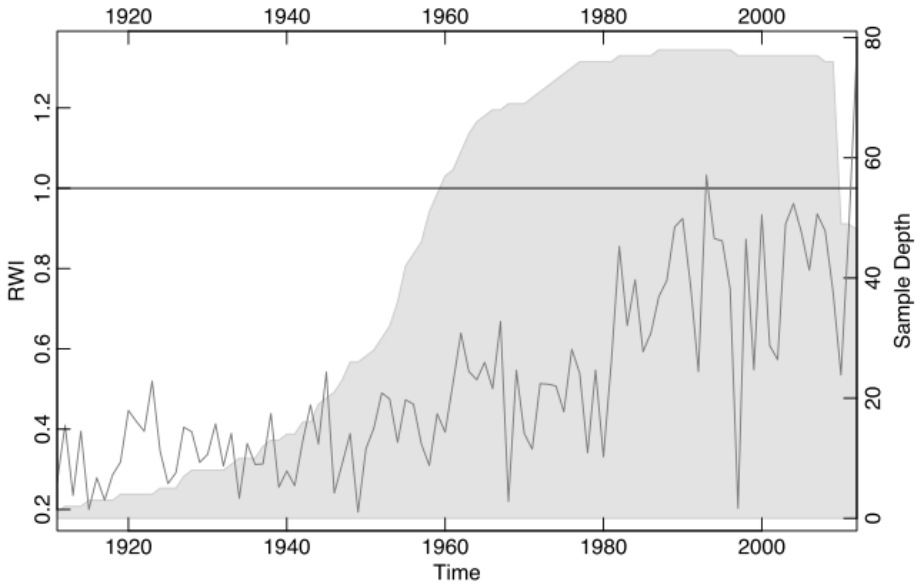

Figure 3–10 Mean ring width chronology for Yuribei developed from 52 shrub disc ring width measurements. RWI = Ring Width Index. Sample Depth is the number of increments contributing to the mean of each year respectively.

We conducted preliminary time-series growth modelling to identify the best-fitting growth models for the ring width series using least-squares. Of five non-linear plant growth models, the Lundqvist-Korf growth model could best explain the observed ring width data (**Figure 3–11**).

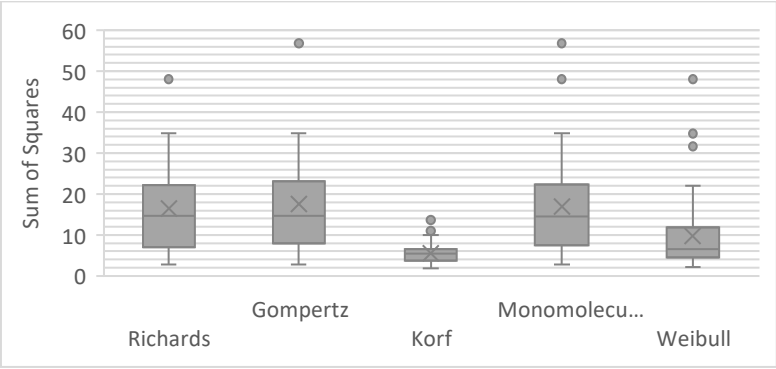

Figure 3–11 Comparison of the sum-of-squared fits between raw ring width time-series and five non-linear plant growth models.

We found that – given the parameter estimates – the Lundqvist-Korf model was collapsing into a linear form, indicating that there are no substantial age-related trends within each ring width series.

3.10.4 Estimated shrub growth trajectories

The one-step-ahead predictions indicate that model fits were good for both nitrogen isotope and ring width time series. The model-predicted absolute and relative increments tracked the observations (**Figure 3–12**).

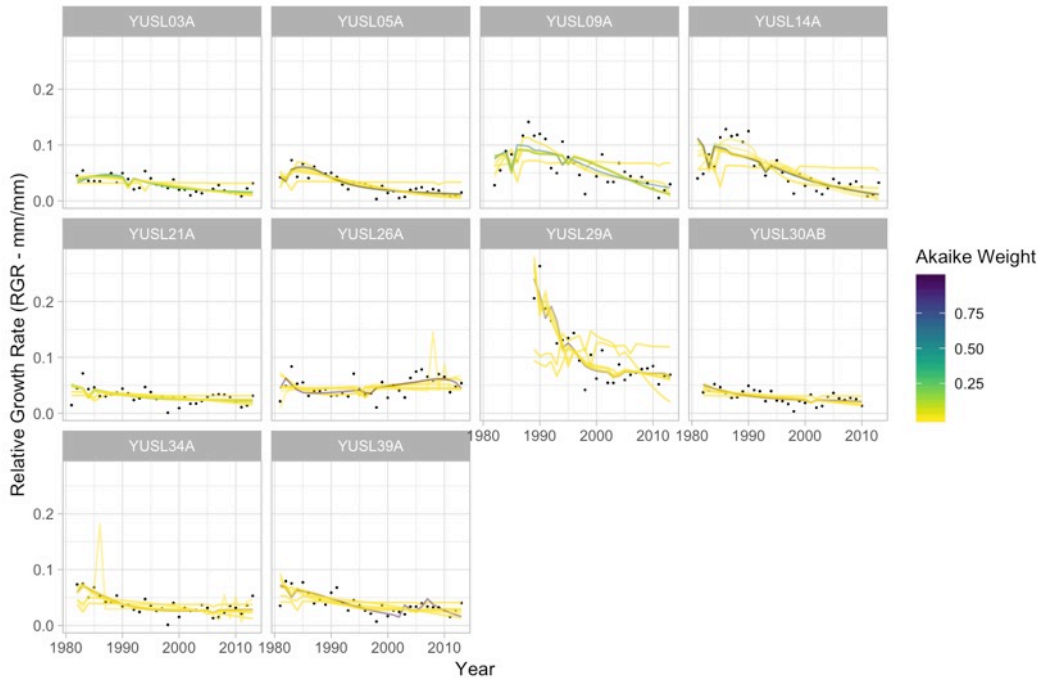

Figure 3–12 Expected growth trajectories for each plant and hypothesis given the best-fitting parameters. Actual measurements are represented by black points.

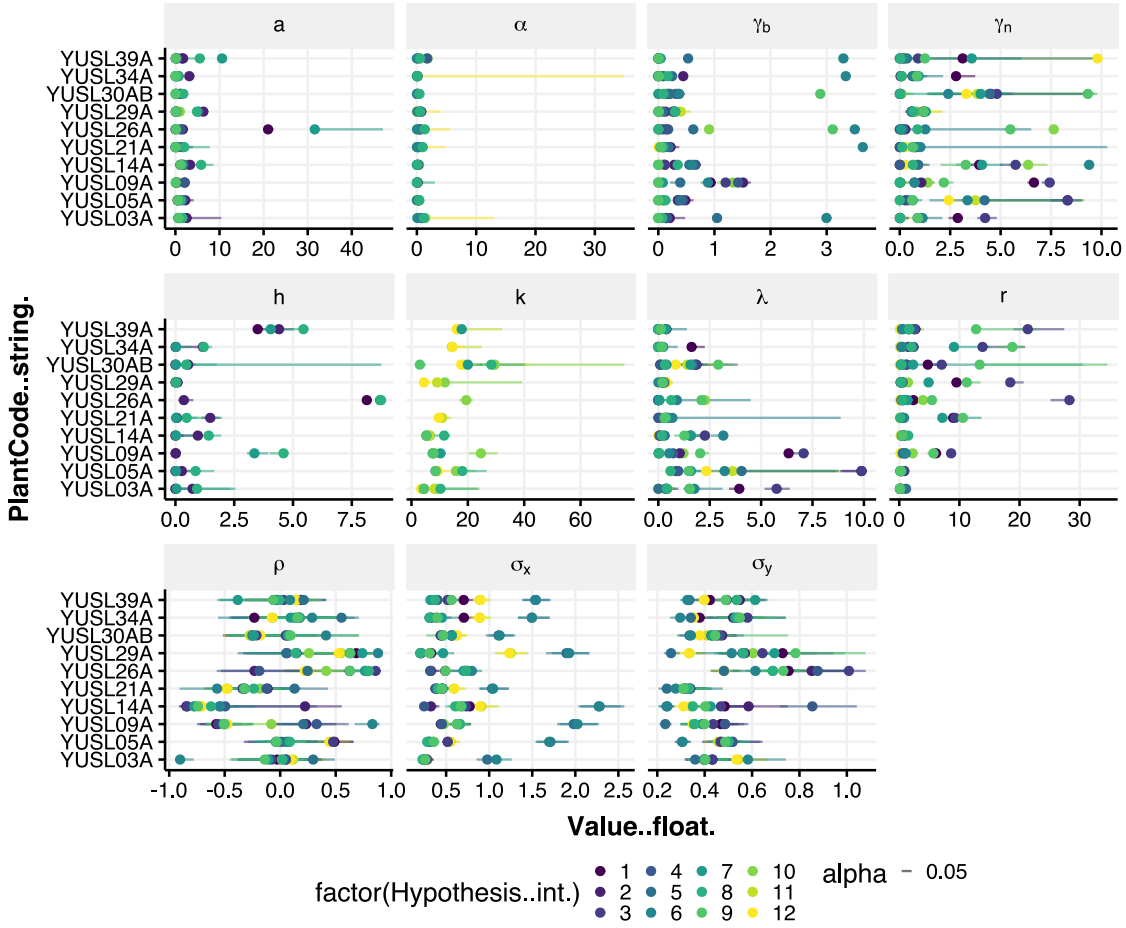

Figure 3–13 Plot showing parameter estimates and their confidence intervals for all shrub individuals and all hypotheses combined.

3.10.5 Wood $\delta^{15}N$ characteristics

Summary statistics for each individual $\delta^{15}N$ time-series are given in **Table 3–9**.

Table 3–9 Summary statistics for individual $\delta^{15}N$ time-series.

Shrub Individual	Mean $\delta^{15}N$	Standard Deviation $\delta^{15}N$
YUSL3	0.719	0.57496399
YUSL5	0.478684211	0.616214121
YUSL9	0.211428571	0.439476248
YUSL21	-1.116666667	0.325853804
YUSL26	-1.623333333	1.002517968
YUSL29	-1.647179487	0.56582473
YUSL30	-1.802	0.559662714

YUSL14	-1.880714286	0.485704883
YUSL34	-1.989	0.602187465
YUSL39	-2.833809524	0.687824256

References

Bunn, A.G., 2008. A dendrochronology program library in R (dplR). *Dendrochronologia*, 26(2), pp.115–124.

Gerhart, L.M. & McLauchlan, K.K., 2014. Reconstructing terrestrial nutrient cycling using stable nitrogen isotopes in wood. *Biogeochemistry*, 120(1-3), pp.1–21.

Chapter 4

Nitrogen limitation of tundra shrub growth associated with decadal-scale declines in soil nitrogen availability in Western Siberia

This paper has been prepared for submission to Journal of Ecology.

In Chapter 3 I identified that there were declining trends in N availability for a single location – Yuribei – on the Yamal Peninsula between 1980 and 2013, although trajectories were variable within the landscape. Here I use the method developed in Chapter 3 to increase the spatial and temporal coverage to three locations in Western Siberia; I generate new N isotope time series at two additional locations and extend time series for Yuribei to the earliest attainable dates.

Nutrient limitation of tundra shrub growth associated with decadal-scale declines in nitrogen availability in Western Siberia

Andrew C. Martin[1], Elizabeth S. Jeffers[1], Bruce Forbes[2], Pentti Zetterberg[3], and Marc Macias-Fauria[4]

1. Oxford Long-Term Ecology Laboratory, Department of Zoology, University of Oxford, OX1 3PS, UK
2. Arctic centre, University of Lapland, Rovaniemi, Finland
3. Department of Forest Sciences Faculty of Science and Forestry, University of Eastern Finland, Joensuu, Finland
4. School of Geography and the Environment, University of Oxford, OX1 3QY, UK

4.1 Abstract

1. Deciduous shrubs have been increasing in biomass across the Arctic tundra biome over recent decades. Although linked to warmer air temperatures, shrub growth trends have been heterogeneous, suggesting that alternative limiting mechanisms may be important. Nitrogen (N) is an important limiting macronutrient for tundra plants that is patchy within landscapes: if N is stationary or declining through time, it may explain observed shrub productivity stagnation in some areas across the Arctic tundra. For tundra ecosystems spanning a climate gradient and up to seven decades, we sought to: (a) determine the directionality and strength of temporal trends in soil N availability; (b) assess the role of N in limiting shrub growth in the long-term; and (c) assess the role of topographic controls in relation to shrub-nitrogen relationships.

2. We reconstructed point-based soil N availability for 24 shrub individuals from three sites in Western Siberia over their lifetime by analysing stable N isotopes ($\delta^{15}N$) in wood ring increments. Temporal trends were assessed for directional changes in N availability. We then applied a model-fitting and model-selection approach using mechanistic models to the

$\delta^{15}N$ time-series and ring width time series to identify: (i) the most likely N-limitation mechanism; (ii) the existence of plant-soil feedbacks; (iii) geometric limits to growth; and (iv) the role of temperature. We tested for significant relationships between estimated model parameters and topographic variables derived from earth observation.

3. Decadal declines in soil N over decades were identified in all three locations although trends were spatially heterogeneous; 13 declined and four increased over time. $\delta^{15}N$ and ring width time-series were best explained by a model of N-limited shrub growth, although the mechanism varied with a more complex root foraging model providing the best fit to the data for six individuals. Plant-soil feedbacks were important determinants of $\delta^{15}N$ and ring width for 17 of 24 individuals as were temperature-dependent photosynthetic rates. Asymptotes to growth explained observations for half of shrub individuals and were not related to size but were related to topographic wetness. Model-inferred dynamics suggested that N uptake was increasing faster than N supply for all individuals overall.

4. Our results strongly suggest that declining N has occurred within multiple bioclimatic subzones of the Arctic tundra, although N trajectories differed at fine spatial resolution reflecting local-scale N dynamics. Strong plant-soil coupling suggests that shrubs are important drivers of soil N availability in Western Siberia through litter feedbacks. A declining role of temperature as well as increased N uptake versus supply suggest that the role of N-limitation has increased in importance during the recent past.

Keywords: *arctic shrubs; dendroecology; mechanistic modelling; soil nitrogen; stable isotope; tundra.*

4.2 Introduction

Across the Arctic tundra biome, shrubs are becoming taller, and expanding to cover a greater proportion of tundra landscapes. Substantial evidence from experimental plots (Elmendorf et al. 2011), ethnographic research (Henry et al. 2012), repeat photography (Lantz et al. 2012), and earth observation (Tape et al. 2012) indicates that recent increases in the performance of deciduous shrubs

has been a pan-Arctic phenomenon. Increasing shrub biomass could have considerable implications for regional climate, biodiversity, and people. Increased tundra shrub biomass has been implicated in hastening the breakdown of soil organic carbon from melting permafrost and increased CO_2 release to the atmosphere (Blume-Werry et al. 2019), and reduced albedo (Chapin et al. 2005), which may accelerate climate warming. Increasing shrub height has had socio-ecological impacts, with nomadic reindeer herding becoming progressively disrupted (Forbes et al. 2009).

Increasing deciduous shrub biomass has coincided with recent rapid warming across the Arctic (Piao et al. 2006). However, recent evidence from ring widths and earth observation suggest an increasing role for alternative limitations to shrub productivity. First, shrub ring width data shows that shrub temperature responses in the recent past have been highly spatially heterogeneous (Myers-Smith, Elmendorf, et al. 2015), suggesting that responses to increasing air temperature have not been universal. Second, remotely sensed 'greenness' – which proxies overall vegetation productivity – has become progressively less sensitive to temperature since 1982 (Piao et al. 2014). In addition, overall trends reversed between 2014 and 2017, resulting in a net 'browning (Bhatt et al. 2013), a trend that has since reversed again (National Academies of Sciences, Engineering, and Medicine 2019). Without identification of progressively important alternative limiting factors to shrub growth and expansion, there remains high uncertainty when predicting future rates and consequences of shrub growth and expansion.

We hypothesised that changes in soil nutrient availability may explain in part the observed heterogeneity in shrub responses to climate. Nitrogen (N) is an essential macronutrient required for plant biomass production and maintenance. Fertilisation experiments across the Arctic tundra indicate N-limited shrub growth (Bouskill, Riley & Tang 2014), as N addition leads to substantial investment in shoots and woody structure (Heskel et al. 2013). However, experimental studies have only considered the effect of elevated soil N on shrub growth, whereas it is currently unclear whether natural N availability has been increasing, stationary, or declining over the last years to decades. In addition, soil N resources are spatially heterogeneous at a local (Jackson & Caldwell 1993; Rodionov et al. 2007) and regional scale owing to topographic wetness (Tape et al. 2012),

soil age (Vitousek & Howarth 1991; Bormann & Sidle 1990) and soil carbon (Craine, Elmore, et al. 2015). It is plausible that variability in soil N availability may correspond with observed variability in shrub growth. Here we aim to infer shrub-N relationships by fitting candidate models to dendroecological time series. We also aim to determine if heterogeneity in growth and N availability correspond with differences in model-inferred shrub-N relationships, and to assess which landscape characteristics correspond with differences in shrub use of N.

Evidence for the strength and variability of N-limitation on shrub growth is limited to space-for-time gradients, and years rather than decades (Martin et al. 2017). Yet multiple processes that affect N availability are known to operate on decadal timescales. Depending on the current rate-limiting processes and rates of environmental change, soil N elevation may occur as: (a) rising air / soil temperatures increase the efficiency of N-mineralising microbes (Aerts 2006; Auffret et al. 2016); (b) permafrost melt (and breakup due to shrub root exploration) enable access to new sources of organic matter (Blume-Werry et al. 2019); and / or (c) shrub capturing of snow to insulate winter soil temperatures, thus elevating winter decomposition rates (Brooks et al. 2011). Alternatively, the progressive N limitation (PNL) hypothesis suggests that scarce N may become progressively locked-up into long-lived biomass (Luo et al. 2004; Norby et al. 2010). PNL hypothesises that an environmental stimulus drives investment in woody structure, thus incorporating N into long-lived biomass. To assess the importance of these mechanisms in shrub-nitrogen relationships, decadal time-series are required.

The Western Siberian floristic group, which incorporates the Yamal peninsula, is a bellwether for ecological responses in Arctic ecosystems (Macias-Fauria et al. 2012). The region contains the full breadth of Arctic bioclimatic subzones from the warmest boreal-tundra ecotone northwards to polar desert (Walker et al. 2009). During recent decades (2000-2015), vegetation sensitivity (inferred from earth observation products) to air temperature, cloudiness, and soil moisture has shown differences over a latitudinal gradient on the Yamal peninsula (Seddon et al. 2016). In addition, dendroecological data indicate that – within the last century – the overall climate sensitivity of woody shrubs has been greatest at the frontier of shrub expansion (bioclimatic subzones C – D), as

opposed to lower latitude shrub tundra, and higher latitude polar desert (Myers-Smith, Elmendorf, et al. 2015). The Yamal peninsula has young soils, which are N-poor within the Arctic tundra biome; therefore, it is a tundra environment where N-limitation is likely to be relatively important. The region is also subject to relatively low anthropogenic N input (Bobbink et al. 2010), making it more likely that we can examine intrinsic processes of N limitation.

We used dendroecological approaches to establish the role of soil N limitation in shrub growth over decades, accounting for variability in climate and landscape characteristics. Here, we combine dendroecological techniques, stable isotope analysis, and ecological modelling. Shrub wood rings are suitable for dendrochronological analysis enabling reconstruction of individual-based stem growth through time (Myers-Smith, Hallinger, et al. 2015). Similarly, stable N isotope measurements from wood rings have been demonstrated as a proxy of soil bioavailable N (McLauchlan et al. 2007; McLauchlan et al. 2017; Gerhart & McLauchlan 2014; Craine, Brookshire, et al. 2015), allowing reconstruction through time. Here we describe shrub ring and N availability data from 1940 to 2013 at three-year resolution; we apply a model-fitting and model-selection (MFMS) approach (Bonsall & Hastings 2004) to infer shrub-nitrogen relationships for each of 30 shrub individuals with hypotheses encoded as mathematical models (**Chapter 3**). We use these techniques to address the following key questions:

1. Is soil N availability increasing or decreasing in Western Siberia and do the trends vary between regions?
2. To what extent is N availability limiting shrub growth?
3. Is there evidence for positive feedbacks between shrub growth and N availability?
4. How does resource limitation vary with landscape characteristics?

We use a two-stage approach to address our four research questions. First, we conduct model-fitting and model-selection independently for each shrub individual (each of which has its own ring width and nitrogen isotope time-series) to infer the nature and strength of ecological processes, where possibilities for each process are expressed as discrete hypotheses. Second, we synthesise the

MFMS results across all individuals to determine the relationship between inferred processes and landscape characteristics (akin to a "meta-analysis" approach).

4.3 Methods

4.3.1 Study Region

Our study region is the Western Siberian Arctic tundra, which includes the Yamal Peninsula (**Figure 4–1**). The region spans nearly all bioclimatic subzones of the Arctic tundra, from bioclimate subzone B (polar desert) to E (tall shrub tundra). In subzones C, D and E, tall shrub areas consist primarily of *Salix lanata* L. and mainly occur in depressions and along watercourses. Soils where tall shrubs are prevalent are dominated by cryic histosols with shallow ice-rich permafrost, moderate fertility, and a pH of 5.3 – 6.2 (Mikhailov 2016).

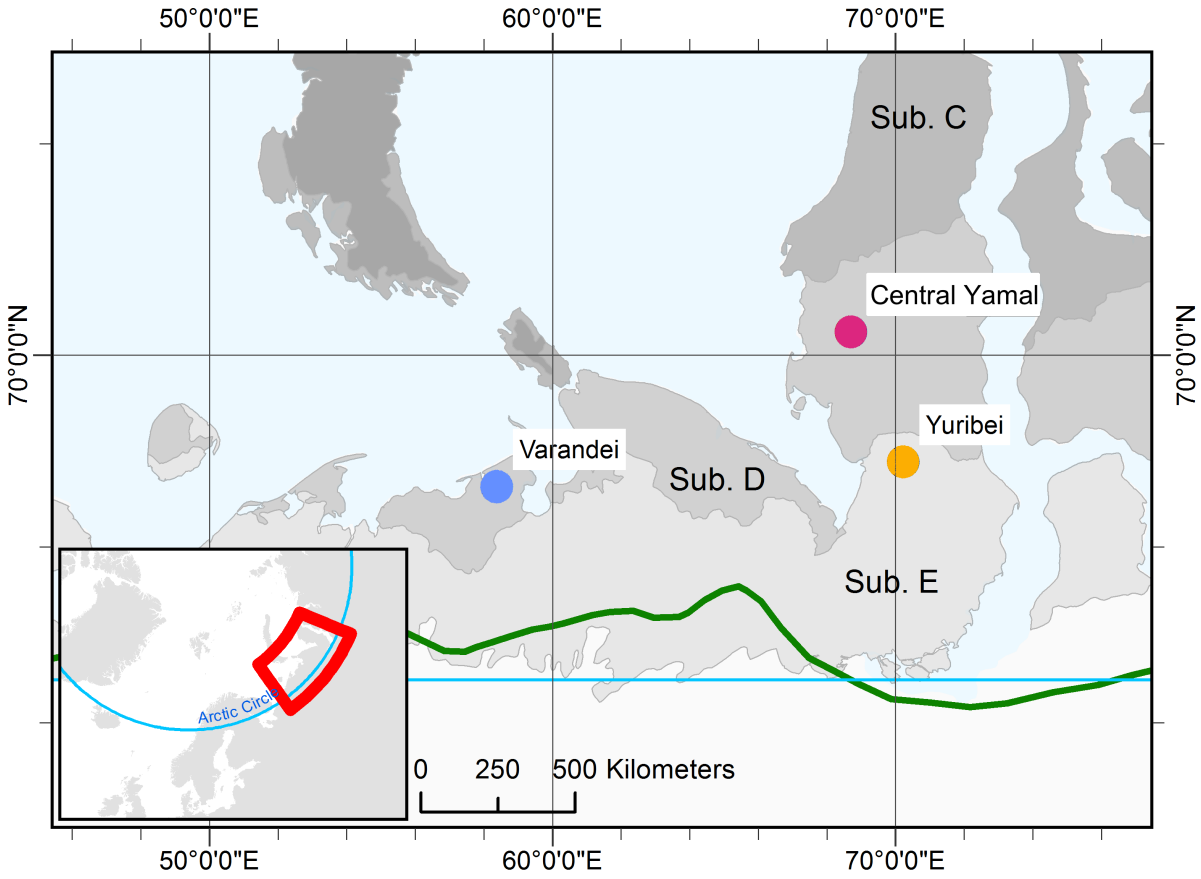

Figure 4–1 Map of the Western Siberian study region, indicating three sampling locations. Shading indicates bioclimatic subzones (Subzones C, D and E) as defined by the Circumpolar Arctic Vegetation Map (Walker et al. 2009). Thick green line indicates the Arctic treeline. Colour coding of sites is consistent with later figures for purposes of comparison.

Shrub wood discs were collected from bioclimatic subzones D and E during three field campaigns to Varandei (2005 – 68.63N, 58.26E), Yuribei (2013 – 68.79N, 70.14E), and Bovanenko / Mordy-Yaha referred to subsequently as 'Central Yamal' (2013 – 70.22N, 68.58E). Ring width time series have been reported elsewhere for Yuribei (**Chapter 3**) but other locations are new for this study. Edaphic conditions are similar within all sampling locations: riparian lowlands of peaty gley soils where thickets of tall shrubs occurred. At all of the sites studied, the dominant deciduous shrub species is *Salix lanata* L, a tall shrub with maximum observed stem lengths of approximately four metres. All shrub wood discs were cut as close to ground level as possible to maximise ring sizes. Collection of shrub discs was biased towards individuals of greater stem diameter, to maximise the likelihood of successful cross-dating and chronology development. Standard dendrochronological techniques were employed to age and cross-date each individual shrub disc (Fritts 1976).

4.3.2 $\delta^{15}N$ Time Series

To determine if soil N availability has been increasing or otherwise, and whether the trends are consistent in space, we measured $\delta^{15}N$ in shrub wood rings. We selected ten shrub discs at random from each of three locations: Varandei, Yuribei, and central Yamal (Bovanenko / Mordy Yaha). For Yuribei, ten annually resolved $\delta^{15}N$ time-series for 1980 – 2013 were reported elsewhere (**Chapter 3**); in this study, we extended the time-series for these ten individuals backwards in time to cover a longer time period. Each measurement of $\delta^{15}N$ required 12mg of bulk wood. As the rings of most individuals were small (<0.5mm) during a juvenile phase exhibited by most individuals, we chose to combine rings in an optimum strategy to achieve the highest resolution over the longest period. To optimise the sampling resolution given the minimum wood constraint, we created a computer model that estimated the wood content of the wood discs (**Figure 4–2**). For all 30 ring width series, the model indicated a three-year fixed resolution as the highest resolution achievable where all time bins would have at least 15mg of wood available. We used a common three-year period, rather than variable temporal resolution, to avoid complexity in measuring goodness-of-fit of our mathematical models (Towers 2014) (as defined in **Section 4.3.4**).

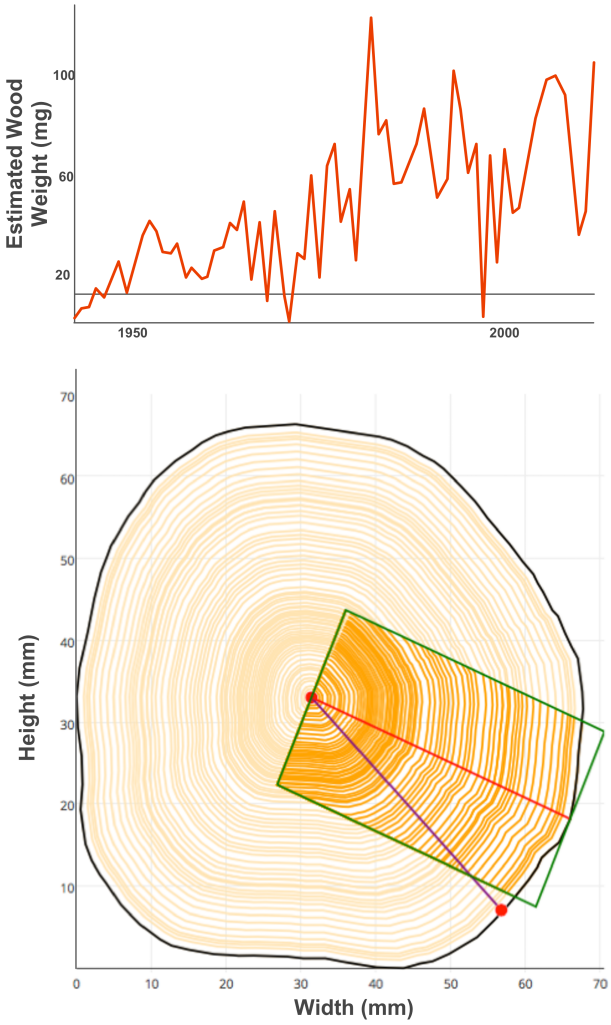

Figure 4–2 Example wood disc simulation used to compute wood weights. **Top:** modelled wood weights within each ring sample showing required weight of 12mg for a single un-replicated nitrogen isotope analysis as grey horizontal line. **Bottom:** a wood disc simulation showing the computer-recommended wood block to use for isotope sampling (green box), as it contains the longest radius available (red) to maximise wood yield per ring. The purple line indicates the radius from which ring width measurements were originally taken.

Arctic willow stems are prone to damage and disease. If wood coinciding with the maximum radius showed signs of disease, the maximum radius that minimised wood imperfection was selected. When sectioning wood, any knots or imperfect wood material, for example with wood decay or infection (identified by discolouration within thin sections) was not processed for isotope analysis, as this may affect the structure and chemical properties of the wood.

For each shrub, we extracted material for stable N isotope analysis as follows: (1) we sectioned the disc to obtain a 1cm-wide section along the widest radius and microtomed both sides (to make smooth surfaces); (2) we made a 30μm-thick thin-section of this section, digitised it, and identified

ring boundaries using previously-measured raw increment measurements; (3) we separated the same section into common three-year increments using a Stanley blade, following the ring boundary on the top along the grain direction, then from the reverse, to minimise cross-bin contamination; (4) milled each sample into a fine powder using a Spex Micromill with one stainless steel ball bearing per stainless steel capsule (splitting any large samples across multiple capsules if necessary), to ensure a homogenous material (mill time of 60 minutes); and (5) weighed 12±0.05mg per sample into tin capsules using a micro-balance. The $\delta^{15}N$ and %N content of each sample was analysed with a Thermo Fisher Delta V+ mass spectrometer coupled to a Carlo Erba NC 2500 Elemental Analyzer at the Central Appalachian Stable Isotope Facility, University of Maryland Centre for Environmental Science. Samples were analysed in random order so that any biases from the mass spectrometer are not structured within time series. We analysed a replicate for one in three samples within each time-series.

We identified significant trends in $\delta^{15}N$ time-series by fitting linear models based on Theil-Sen single median to individual $\delta^{15}N$ time-series and the pooled data as a whole, as implemented in the *mblm* R package (Komsta 2013). The Theil-Sen statistic is especially suited to short and noisy time-series (Hoaglin et al. 2000).

4.3.3 Climate Data

We obtained mean daily temperature time-series for the nearest weather station to each sample area from the GHCN-D v2 database (Menne et al. 2012). The weather station at *Marre Sale* (69.72ºN, 66.82ºE) was the closest weather station to our sites on the Yamal Peninsula that had data for our study period (87km to Central Yamal; 167km to Yuribei). Similarly, *Khoseda-Khardsky* (67.08ºN, 59.38ºE) was the closest station to *Varandei* (179km) with data spanning the study period.

4.3.4 Modelling of Shrub-Nitrogen Dynamics

To identify the extent that N availability limits shrub growth (Q2) and the role of positive feedbacks between shrub growth and N availability (Q3), we modelled shrub-nitrogen dynamics. To understand the form and strength of N limitation in wood ring production, we used a model-fitting

and model-selection (MFMS) approach to identify ecological models that could most appropriately represent the ring width and $\delta^{15}N$ data. The MFMS approach interrogates the observed data with theoretical models to calculate a goodness-of-fit for each model in question; the most appropriate model is then selected using model-selection criteria (Burnham & Anderson 2007). We used this approach to determine the role of four processes in shrub-nitrogen relationships: (1) nitrogen limitation; (2) plant-soil feedbacks; (3) geometric limitations on growth; and (4) temperature limitation to plant growth. We conducted MFMS for each shrub individually. All MFMS analysis was completed using *Bristlecone*, an F# library for MFMS of long-term ecological time series (**Chapter 6**). The script used for analysis is attached in **Supplementary Material**.

4.3.4.1 Model Definition

We represented shrub-nitrogen relationships using a resource-economy approach (Tilman 1990; Garnier 1991) where nitrogen availability may limit shrub biomass production acting as a single limiting resource. To achieve this, we applied a previously defined model for Arctic shrubs at Yuribei that connects $\delta^{15}N$ and ring width data (**Chapter 3**): this model integrates an ecological model of biomass-nitrogen dynamics with an empirically calibrated geometric model of shrub growth (Götmark et al. 2016) and explicit transformation of $\delta^{15}N$ to soil N availability. For this study we represented biomass-nitrogen dynamics as a nested bivariate ordinary differential equation (ODE) system of shrub biomass B, and nitrogen availability N, with four structural components that may be varied:

$$\frac{dB}{dt} = r \cdot \left[f(N) \cdot g(B) \cdot t\left(B, T_{jja}\right)\right] - \gamma_B B$$

$$\frac{dN}{dt} = \lambda - \left[f(N) \cdot g(B) \cdot t\left(B, T_{jja}\right)\right] - \gamma_N N + y(B)$$

Here, $f(N)$ is a nitrogen-constrained net growth function (which accounts for photosynthesis and respiration); $g(B)$ represents geometric or hydraulic limitations to maximum shrub size; $t\left(B, T_{jja}\right)$ represents the limiting effect of temperature on biomass production independent of N; r represents

an intrinsic growth rate of plant biomass; and γ_B represents the background loss rate of biomass. λ is a linear background input of available nitrogen that may arise from a number of biotic and abiotic processes (i.e. N fixation, N deposition, N mineralization); $y(B)$ is a plant-soil feedback mechanism that depends on current biomass; and γ_N is a density-dependent loss term for nitrogen from soils.

We varied model structure by including three functional forms for $f(N)$ and two functional forms for $g(B)$, $y(B)$, and $t(B, T_{jja})$. All combinations of models were assessed for each shrub individual resulting in 24 hypotheses per individual. The functional forms used for each model component are shown in **Table 4–1**:

Table 4–1 Functional forms for each of the four structural components varied within our representation of shrub-nitrogen dynamics.

Component	Case	Function
T Temperature-Dependent Photosynthesis	**T0** Temperature-independent growth rate	$t(B, T_{jja}) = 1$
	T1 Temperature-limited growth: Arrhenius	$t(B, T_{jja}) = e^{\left(-\frac{1000E_a \cdot (T_{jja} - 298)}{8.314 \cdot 298 T_{jja}}\right)}$
F Nitrogen-Dependent Photosynthesis	**F0** Nitrogen-independent growth	$f(N) = 1$
	F1 Nitrogen-dependent growth: linear	$f(N) = aN$
	F2 Nitrogen-dependent growth: saturating	$f(N) = \frac{aN}{1 + arhN}$
U Plant-Soil Feedback	**U0** No Plant-Soil feedback	$u(B) = 0$
	U1 Plant-Soil Feedback	$u(B) = \alpha \gamma_B B$
G Maximum Potential Growth Rate	**G0** Exponential (Non-Asymptotic)	$g(B) = 1$
	G1 Chapman-Richards (Asymptotic)	$g(B) = 1 - \frac{B}{K}$

Parameters: E_a = activation energy of temperature-limited photosynthesis; a = N-use efficiency; r = N-conversion efficiency to biomass; h = handling time of N in uptake and incorporation into biomass; α = conversion factor of litter into N; γ_B = environmental loss rate of shrub biomass; K = asymptotic plant mass owing to mechanical or other constraints. The time-varying parameter T_{jja} is mean July – August air temperature in Kelvin.

We accounted for Nitrogen-, temperature-, and geometric-limitations to shrub growth. First, we represented N-limited growth using two alternative forms that distinguish between root foraging characteristics: the saturating form of N limitation (**F2**) assumes that root foraging is dependent on

the N-uptake efficiency and N-uptake rate of roots (Van Rees 1994; McNickle & Brown 2014); the linear form (**F1**) alternatively suggests that the rate of N uptake is not an important factor in N-limitation to growth. Second, to determine the role of temperature in shrub growth over time we included models for temperature-independent growth (**T0**) and temperature-dependent growth (**T1**). Temperature-dependence of biomass production was represented as an Arrhenius response to air temperature (Kim et al. 2007), as this recognises that enzymes involved in photosynthesis and respiration respond non-linearly to temperature. Third, we included a geometric term to represent limits on plant growth. Biomass growth as represented in our base model is exponential (**G0**), whereas in reality plants cannot grow indefinitely large owing to hydraulic (or geometric) and resource constraints (Paine et al. 2011; Zhao-gang & Feng-ri 2003; Enquist & Bentley 2012). Here we included an asymptotic growth model (**G1**) to assess if other factors aside from N-limitation have controlled maximum shrub size.

Plants can influence their environment through plant-soil feedbacks, which here may influence the role and strength of N-limitation on shrub growth (Chapman et al. 2006). We represented this possibility with a feedback effect of shrub biomass loss on soil N availability (**U1**), where we assume that additional N inputs to soil occur in proportion to the biomass loss rate of the individual shrub under study; the feedback effect is scaled by a conversion factor (α) following Jeffers et al. (2011).

4.3.4.2 Model-Fitting and Model-Selection

We measured goodness-of-fit for all models using a bivariate gaussian negative log likelihood function:

$$-\log\Big(L\big(\sigma_x,\sigma_y,\rho\big)\Big) = 2\pi\sigma_x\sigma_y\sqrt{1-\rho^2} + \frac{1}{2}\left(\frac{z}{1-\rho^2}\right)$$

$$z = \left[\left(\frac{x_{obs}-x_{est}}{\sigma_x}\right)^2 - 2\rho\left(\frac{x_{obs}-x_{est}}{\sigma_x}\cdot\frac{y_{obs}-y_{est}}{\sigma_y}\right) + \left(\frac{y_{obs}-y_{est}}{\sigma_y}\right)^2\right]$$

Here, x_{obs} and x_{est} are the observed and estimated cumulative stem radius, y_{obs} and y_{est} are the observed and estimated $\delta^{15}N$. Three parameters are estimated alongside model parameters: σ_x and σ_y indicate the standard deviation of stem radius and $\delta^{15}N$ respectively, and ρ their covariance. Negative log likelihood was calculated for each timepoint in time-series and summed to calculate an overall value for each shrub and hypothesis.

To avoid losing the annual variability captured within ring width data, we ran models at an annual resolution. Each point in the $\delta^{15}N$ time-series represents a homogenised mean value for a three-year time interval; we therefore replicated the mean $\delta^{15}N$ value for each year within the time interval. To find the set of parameters that minimised the negative log likelihood value for a given model, we used a variant of Fast Simulated Annealing (FSA), using a Cauchy proposal distribution (Lee 2015). Simulated annealing is a metaheuristic based on random walk MCMC, which mimics the physical process of annealing metal: the system is elevated to a high energy *E*, at which particles are likely to accept nearly all uphill ('worse') jumps. The system energy is then gradually lowered, progressively accepting less worse moves (Locatelli 2002). Our implementation (in *Bristlecone*) computed the initial energy by heating until the acceptance rate of bad moves was >0.85, then ran a homogenous Markov chain at each energy level with an end condition of 5000 improvements, and lowering energy on a cooling schedule of $E_{t+1} = \frac{E_0}{k}$, stopping when the energy fell below 0.5. We ran each analysis from a random start point five times, to ensure that a common local optimum was reached. We further verified results by ensuring that more complex models fit at least as well as less complex models.

Model selection was conducted by calculating constrained Akaike Information Criterion (AICc) in which the likelihood is corrected for the number of observations in short time series and penalised for the complexity of mathematical models. The AIC_c was used to calculate Akaike weights, which indicate the weight of evidence for the model given the data (Wagenmakers & Farrell 2004). In addition, we compared the goodness-of-fit of the shrub-nitrogen models between individuals by

generating one-step-ahead predictions at each models' MLE and then calculated the root mean square error (RMSE) values for both variables.

To examine the behaviour of the models given the best-fitting structure and estimated parameters, we calculated the rates of modelled processes through time at the Maximum Likelihood Estimates and within 95% confidence intervals to examine variability in the rates of model-inferred processes. This resulted in time series for each model component; from these, we calculated the ratio of soil N supply (background N input and plant-soil feedback) versus N uptake by the plant individual.

4.3.5 Landscape Characteristics and their Relation to Model-Inferred Processes

To understand how resource limitation varied with landscape characteristics, we collected each individual shrubs' estimated parameter values and tested these for relationships with three landscape characteristics: hillslope, topographic wetness, and distance to water. We used earth observation data to calculate hillslope, topographic wetness, and distance to water for each sampled shrub location. For a 100km bounding box around each sample location, we calculated per-pixel local slope and upslope contributing area (Quinn et al. 1991) at 30 metre resolution by combining the ASTER digital elevation model and GlobeLand30-2010 landcover products. We then calculated the topographic wetness index (TWI) as:

$$TWI = \ln\left(\frac{A}{\tan S}\right)$$

Where S = slope, and A = upslope contributing area (Sörensen et al. 2006). We calculated distance to water using the GlobeLand30-2010 global land cover product, by reclassifying to water versus non-water and measuring the distance from each shrub to the nearest water body. To assess the relationship of each landscape variable (topographic wetness index, distance to water, and slope) in nitrogen-shrub relations, we computed linear regressions between each landscape variable and parameter estimates at the maximum likelihood estimate (MLE) using the *lm* function in R. Parameter values were weighted in the linear regressions by the Akaike weight of the MLE; we excluded models with Akaike weights below 5% to remove models that may have fit poorly to data.

4.4 Results

4.4.1 $\delta^{15}N$ Time Series

We successfully reconstructed $\delta^{15}N$ time-series for 24 shrub individuals with the earliest start date at 1942 and latest start date at 1988. Reconstructions were not possible for six of the targeted individuals at Central Yamal, as these shrub individuals contained rot and infiltration by fungal hyphae throughout most of the stem wood disc. Replicate measurements to determine variability within wood ring $\delta^{15}N$ (n = 82 pairs) indicated an overall mean standard deviation of $\delta^{15}N$ values of 0.237‰ (SD = 0.197‰) (3dp).

We determined trends in $\delta^{15}N$ using the Thiel-Sen statistic. 17 of 24 $\delta^{15}N$ series were non-stationary indicating significant linear temporal trends. At 95% confidence, 13 $\delta^{15}N$ time-series declined significantly over time, while 4 increased significantly. Full statistics are described in **Supplementary Table 4–4**. When all $\delta^{15}N$ measurements were combined (n = 580), a linear model indicated that $\delta^{15}N$ declined significantly over the period 1940 – 2013 (**Figure 4–5**). When partitioned by location: five series were declining and one increasing at Varandei; seven were declining and two increasing in Yuribei; and one was declining and one increasing at Central Yamal. Significant slope coefficients ranged between 0.028 and -0.074, with a median of -0.033.

We assessed heterogeneity in $\delta^{15}N$ signals by calculating mean inter-series correlation using two methods: a stepwise procedure and the mean of inter-series correlations ($\bar{r}_{bt}$). Overall correlations within study locations were negligible: for the shrubs at Varandei $\bar{r}_{bt}$ was 0.06, at Yuribei -0.07 and Northern Yamal 0.00 (all 2dp). It was therefore not appropriate to construct mean site-level chronologies of $\delta^{15}N$. Despite the low overall inter-series correlation, within each site several pairs of series showed high correlations; for example, $\bar{r}_{bt}$ for six of ten individuals at Varandei was 0.40 (2dp).

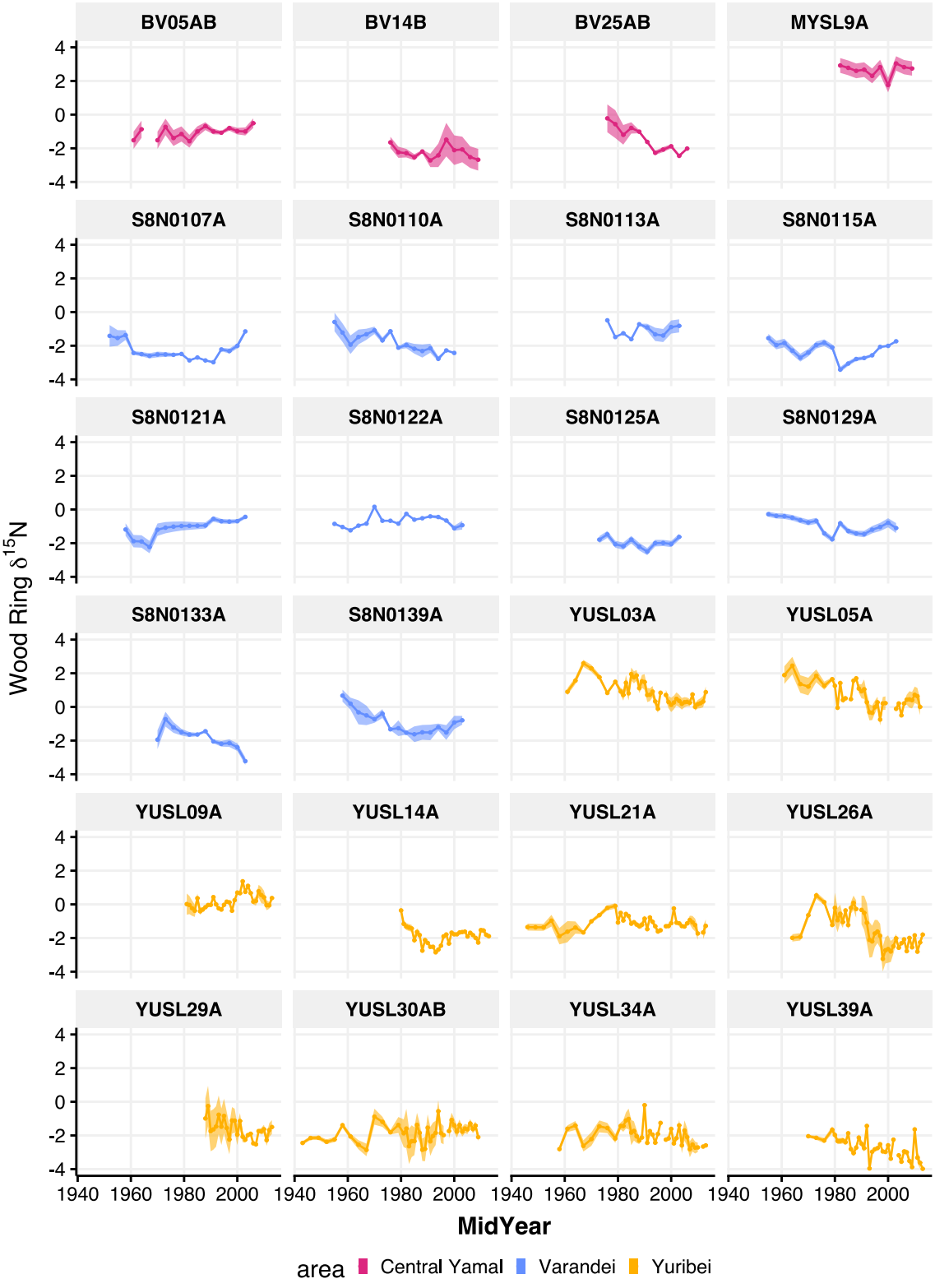

Figure 4–3 Individual measured $\delta^{15}N$ (‰) time series for each of 24 shrub individuals. Colouring indicates the site from which wood discs were originally collected. Standard error (shaded area) was calculated as the standard deviation of replicate isotope samples. Overall, the mean standard deviation was 0.237‰ as calculated from replicate samples from all $\delta^{15}N$ series).

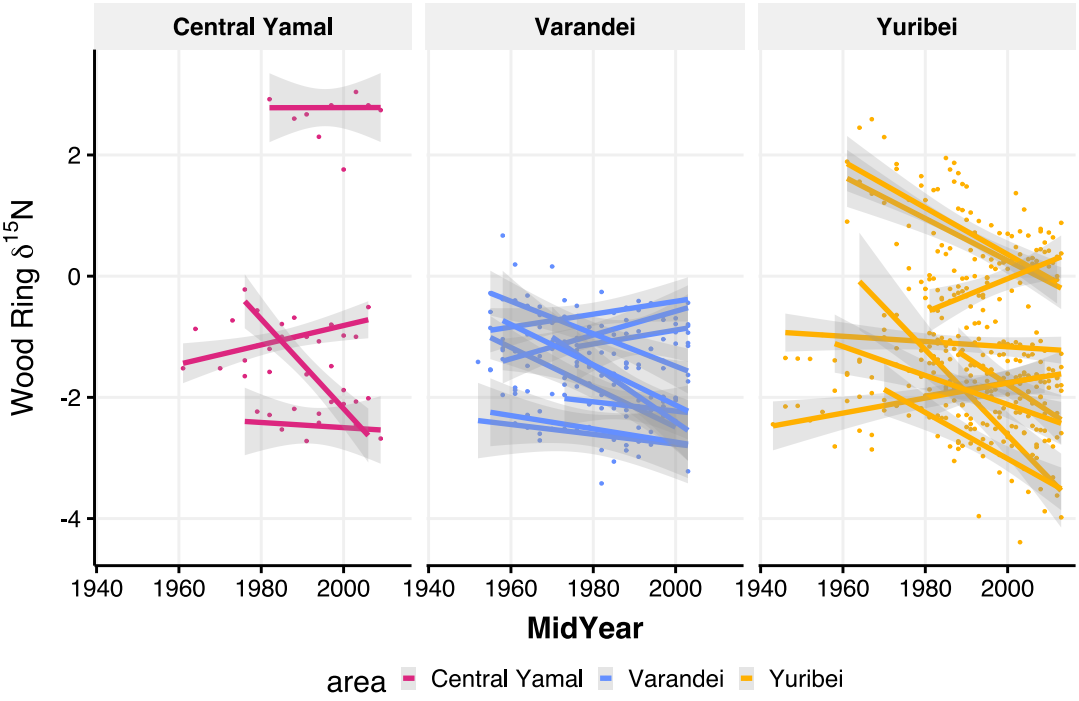

Figure 4–4 Theil-Sen linear fits to 24 individual shrub wood ring δ^{15}N (‰) time-series. Shaded areas indicate 95% confidence interval for each Theil-Sen fit to the measured δ^{15}N data. Points indicate δ^{15}N measurements. δ^{15}N measurements and fits delineated by area from which the original wood discs were collected.

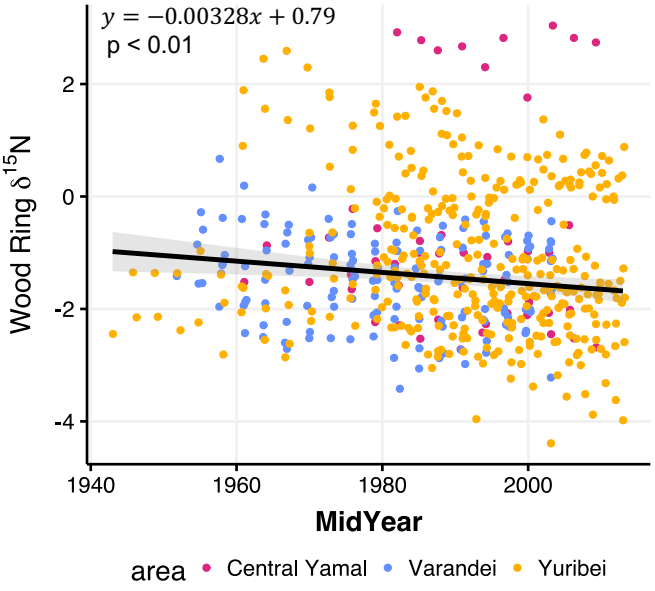

Figure 4–5 Overall trend of δ^{15}N (‰) data (*n* = 580). A Theil-Sen fit was conducted to determine if there was any significant trend in the timestamped δ^{15}N measurements; there was a significant slope in the resultant fit of -0.00328 (*p=0.01779*) with intercept of 0.79 (*p=0.00334*). Standard error was 0.2762 with 578 degrees of freedom.

4.4.2 Role of nitrogen limitation for shrub growth

We conducted a model-fitting and model-selection approach to determine the most appropriate model of shrub-nitrogen dynamics for each shrub individual. The Akaike weights indicate that N-limitation best explained the observed $\delta^{15}N$ and wood increment time-series for all 24 shrub individuals. However, the functional form of N-limitation differed between the individuals: linear N-limitation (**F1**) was most appropriate for 18 individuals while saturating N-limitation (**F2**) best described the dynamics of six individuals (**Figure 4–8**, **Figure 4–9**).

As an additional measure of goodness-of-fit we calculated the RMSE using one-step-ahead predictions for each of the best models. For all 24 models the median RMSE for stem radius was 0.72mm and for $\delta^{15}N$ was 0.38‰. The best model for YUSL03A was a relatively poor fit for both time-series; for all other individuals RMSE for $\delta^{15}N$ was below 1‰. The best model for every shrub individual and the RMSE for stem radius and $\delta^{15}N$ is illustrated in **Table 4–2**:

Table 4–2 The best fitting model of the 24 fit for each shrub individual and root mean square error for each time-series.

Shrub Individual	Pith Year	Temporal Extent of $\delta^{15}N$ Series	$\delta^{15}N$ Trajectory	Best Model					Stem Radius RMSE (mm)	$\delta^{15}N$ RMSE (‰)	Alternative models above 5% Akaike weight (weight, %)
				Akaike (%)	F	U	G	T			
BV05AB	1954	1960-2007	↑	100	1	•	•		3.04	0.43	-
BV14B	1949	1975-2010	-	80	1			•	0.51	0.62	F1UT (11)
BV25AB	1951	1975-2007	↓	51	1	•			0.31	0.44	F1 (22), F1UT (6)
MYSL9A	1950	1981-2010	-	53	1	•		•	0.71	0.55	F1GT (25), F1T (13)
S8N0107A	1931	1951-2004	-	40	1	•		•	1.46	0.52	F2U (28), F1GT (13), F1UGT (11)
S8N0110A	1942	1954-2005	↓	100	2	•	•	•	0.66	0.47	-
S8N0113A	1937	1975-2005	-	32	1			•	1.22	0.36	F2UGT (21), F1UT (17), F1 (8), F1GT (6)
S8N0115A	1952	1954-2005	↓	55	1	•	•	•	5.45	0.55	F2UGT (25), F1U (15)
S8N0121A	1954	1957-2005	↑	100	2		•	•	0.72	0.31	-
S8N0122A	1953	1954-2005	-	100	1	•	•	•	4.82	0.28	-
S8N0125A	1945	1972-2005	-	27	1			•	1.54	0.41	F1GT (22), F1UGT (14), F0GT (13)
S8N0129A	1952	1954-2005	↓	66	1	•	•	•	2.27	0.64	F1UT (31)
S8N0133A	1953	1969-2005	↓	50	1				0.66	0.44	F2G (27), F1G (9)
S8N0139A	1933	1960-2005	↓	89	2				0.29	0.08	F0UGT (6)
YUSL03A	1959	1960-2013	↓	100	2	•		•	15.08	2.00	-

YUSL05A	1954	1960-2013	↓	100	1	•		•	0.72	0.49	-
YUSL09A	1972	1981-2013	↑	99	1			•	0.43	0.40	-
YUSL14A	1952	1980-2013	-	92	2	•	•	•	0.80	0.35	-
YUSL21A	1942	1945-2013	↓	38	1	•	•	•	0.31	0.39	F1UG (33), F2UG (21), F2UGT (8)
YUSL26A	1958	1963-2013	↓	100	1	•	•	•	3.55	0.55	-
YUSL29A	1982	1988-2013	↓	48	1	•			1.18	0.55	F2U (40), F1UT (7)
YUSL30AB	1919	1942-2013	↑	100	1	•	•	•	0.60	0.51	-
YUSL34A	1953	1957-2013	↓	78	1	•	•		0.57	0.98	F2UG (11), F1UGT (10)
YUSL39A	1964	1966-2013	↓	93	2	•		•	4.29	1.01	-

Only models with greater than 5% Akaike weight are included in this table. Akaike weights rounded to nearest percentage point. RMSE figures to two decimal places. F, U, G and T indicate the presence of mechanisms as coded in **Table 4–1**. $\delta^{15}N$ Trajectories show directionality when Thiel-Sen fit was significant to 95% confidence. Shrub codes BV and MY are from Central Yamal, S8N from Varandei, and YUSL from Yuribei.

There did not appear to be a clear relationship between the model-estimated form of N-limitation and the linear temporal trend in $\delta^{15}N$; shrub individuals with a saturating form of N-limitation (**F2**) were evenly split in $\delta^{15}N$ trend with two stationary, two increasing, and three declining through time.

Constraints on a shrub's maximum size did not always occur alongside N-limitation. A geometric limitation was only present in the best-fitting model for half of the shrub individuals investigated. Parameter estimates and confidence bounds, however, indicated high inter-plant variability in the model-inferred asymptotic biomass: the median was 14.4kg with standard deviation of 8.22kg.

4.4.3 Plant-Soil Feedback Effects

We assessed the role of a plant-soil feedback effect within the model-fitting and model-selection procedure. The Akaike weights indicated that plant-soil feedbacks better explained the observed time-series for 17 of the 24 shrub individuals. The litter conversion factor (α) varied by orders of magnitude between individuals between 0.00916 and 2.54.

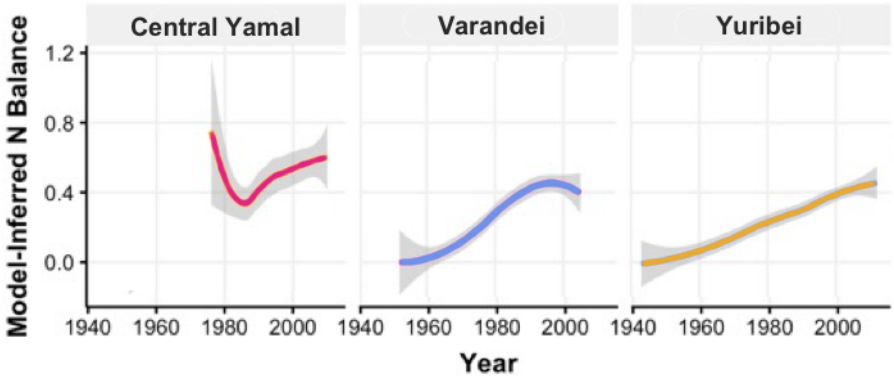

Figure 4–6 Model-inferred ratio of plant N uptake to N supply summarised across all individuals on a per-site basis using a loess fit. N supply is defined as background N replenishment plus shrub litter N feedback. In all three sites, values were below 1.0, which indicates that N uptake was less than N supply but increasing over the time period of analysis.

We calculated the rates of modelled processes through time at the Maximum Likelihood Estimates and within 95% confidence intervals to examine variability in the rates of model-inferred processes. In particular, we examined the ratio of plant N uptake to N supply where N supply is the sum of background N replenishment (λ) and soil N inputs from the plant-soil feedback (if applicable). The

model-inferred dynamics indicated that – even with shrub inputs of N to soil – the ratio of N uptake to N supply increased over the temporal extent all best-fitting models (**Figure 4–6**).

4.4.4 Role of temperature and local conditions in shrub-N relations

To understand the role of climatology in individual shrub-nitrogen relationships we tested the inclusion of a temperature-limiting effect within shrub-nitrogen models. The inclusion of the temperature-limitation effect improved the best model for 17 of 24 shrub individuals with high variability in their temperature-sensitivity.

In order to explain variability in the inferred parameter values for the best-fitting models, we assessed the relationship between each parameter and three topographic variables: TWI, slope, and distance to water. Significant relations were identified between certain combinations of landscape position and parameter estimates (**Figure 4–7**). Each linear regression conducted is illustrated in **Table 4–3**.

Table 4–3 Weighted linear regression models of estimated parameter values as predicted by environmental covariates.

Par.	Ecological Interpretation	Topographic Wetness Index (TWI)	Topographic Slope (degrees)	Distance to Water (metres)
a	N-use efficiency	$-0.38x + 3.94$	$0.08x + 2.50$	$0.001x + 4.08$
α	Litter conversion factor	$-3.36x + 16.00$	$1.58x - 2.49$ **	$0.001x + 4.24$
E_a	Photosynthetic activation energy	$-0.42x + 29.6$	$0.07x + 27.80$	$0.001x + 26.6$
γ_B	Biomass loss	$0.14x + 0.123$ **	$-0.01x + 0.56$	$0.01x + 0.60$
γ_N	Nitrogen loss	$-0.14x + 2.74$	$-0.01x + 2.35$	$0.001x + 2.25$
h	N handling time	$-0.39x + 2.34$ *	$-0.38x - 2.24$ **	$0.001x + 1.64$
K	Asymptotic Size	$2.33x + 9.14$ *	$-0.52x + 17.8$	$-0.02x + 20.8$ *
λ	N background replenishment	$-0.29x + 2.27$	$0.18x + 0.73$ *	$0.001x + 0.74$
r	N incorporation factor	$-7.92x + 38.8$ **	$-1.67x + 21.6$	$-0.01x + 18.1$
ρ	-	$0.11x - 0.368$ **	$-0.02x + 0.04$	$0.001x - 0.09$
σ_x	-	$0.01x + 0.482$	$0.01x + 0.47$	$0.001x + 0.57$

σ_y	-	$0.08x + 0.392$	$0.61x + 0.00$	$0.001x + 0.70$

Models with Akaike weights below 5% were removed. * = p < 0.05; ** = p < 0.01; *** = p < 0.001.

Relationships between model-inferred parameter values and topographic indicators suggest that – in cases where N-limitation was of saturating form – foraging rates (h) are greater in relatively wet locations. Similarly, model-inferred litter feedbacks are greater in relatively wet locations (as evidenced by the relation of γ_B to TWI). Inferred maximum asymptotic shrub size appears related to water availability, as it is positively related to both the closeness to water sources and TWI. The positive relationship between σ_y and TWI suggests that our theoretical models of shrub-nitrogen dynamics could better explain variability in $\delta^{15}N$ time-series at relatively dry locations.

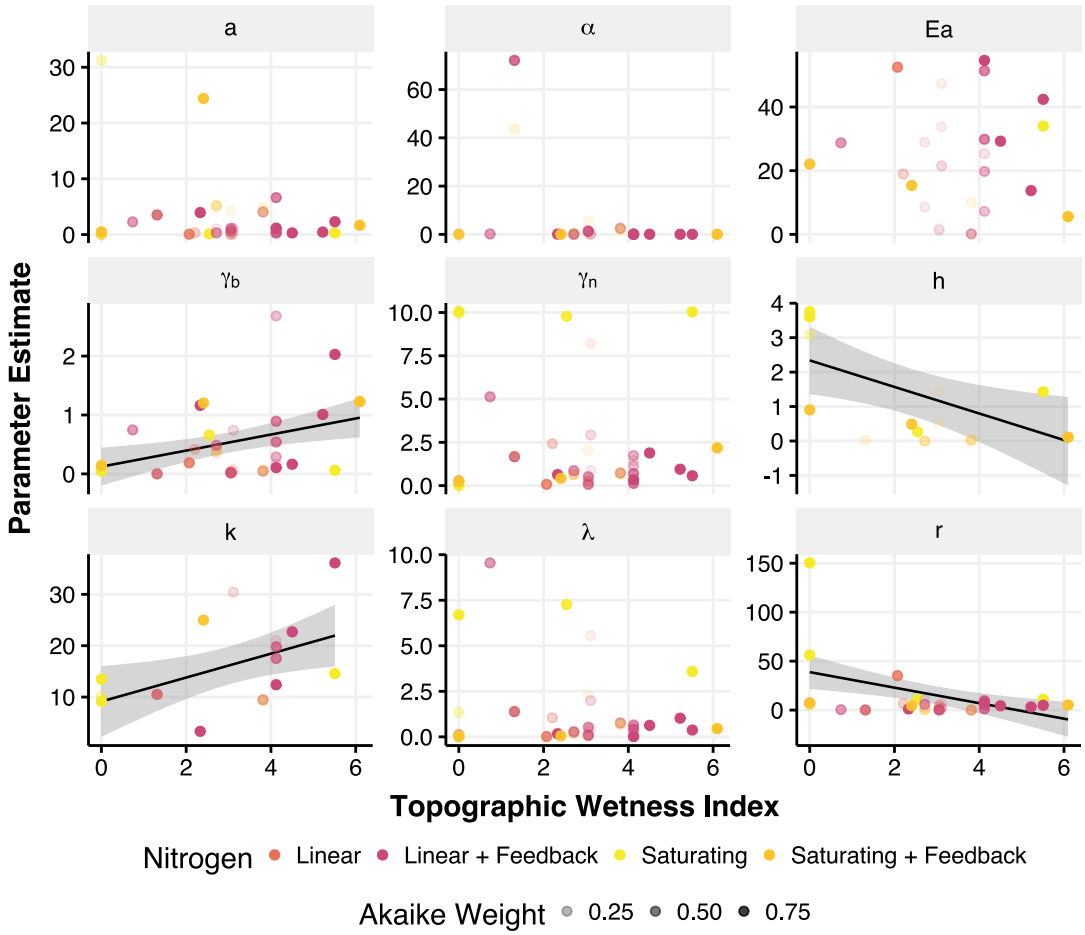

Figure 4–7 Estimated parameters for every shrub individual and model hypothesis versus topographic wetness. Only significant linear regressions are shown (p<0.05). Relation between Topographic Wetness Index (TWI) and parameter maximum likelihood estimates as found for each shrub individual and each hypothesis where the Akaike weight was greater than 5%. Linear regressions were conducted by weighting parameter values for all shrubs and models by their Akaike weights.

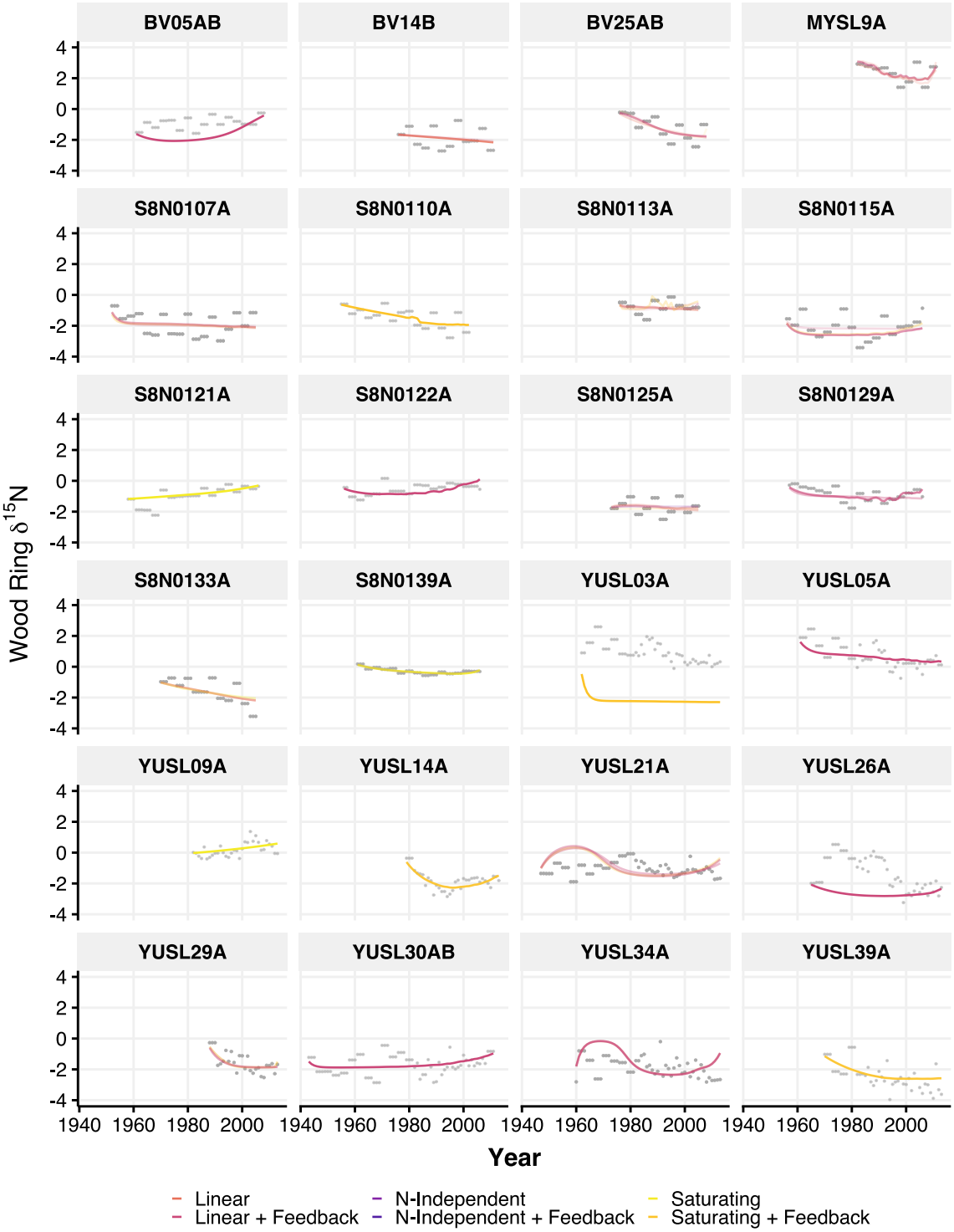

Figure 4–8 Predicted $\delta^{15}N$ time-series for every shrub individual and their best-fitting hypothesis. Hypotheses have been grouped by the form of N-limitation and N-feedbacks to emphasise these two structural components. Shrub codes BV and MY are from Central Yamal, S8N from Varandei, and YUSL from Yuribei.

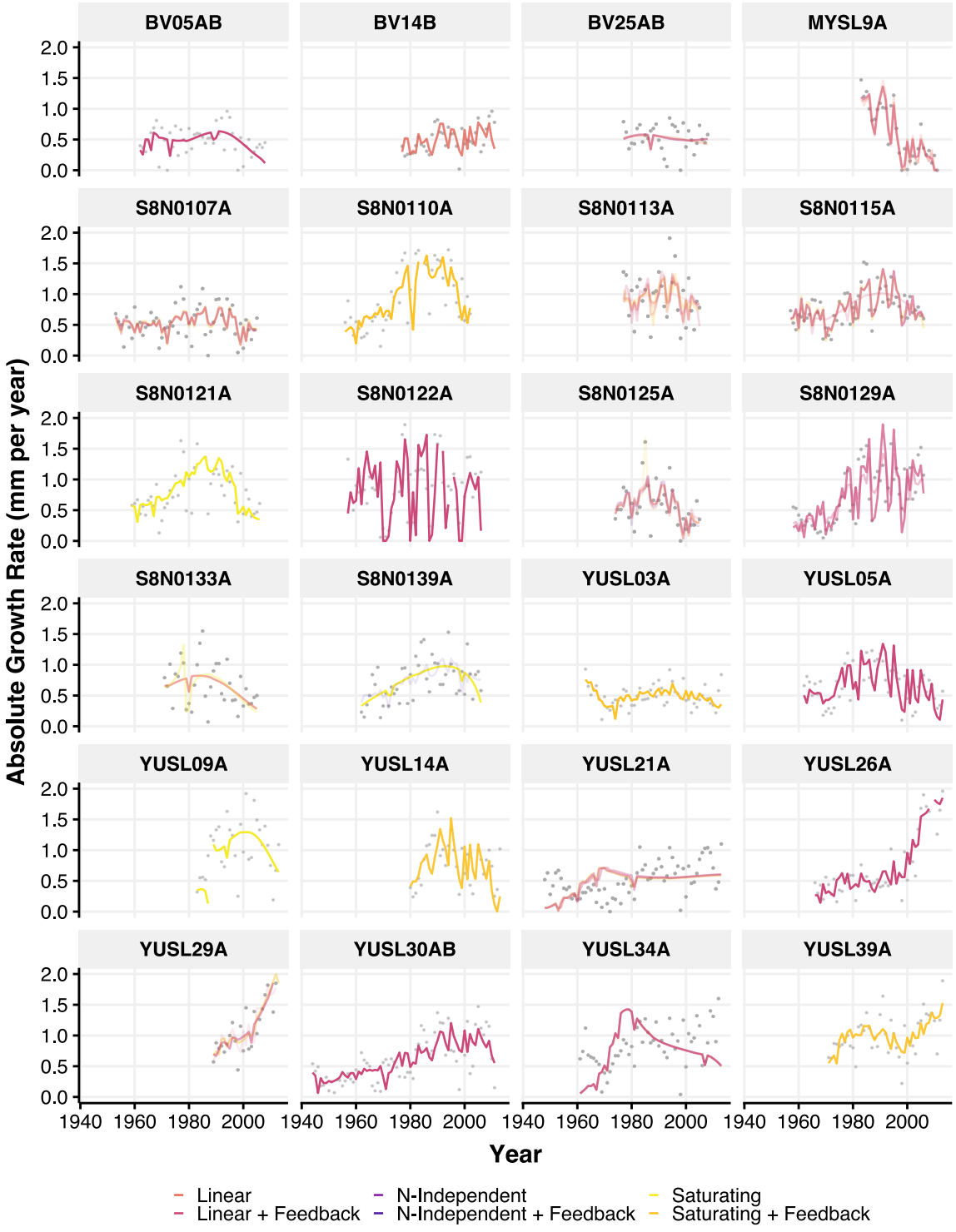

Figure 4–9 Predicted annual wood increment time-series for every shrub individual and their best-fitting hypothesis. Opacity is proportional to Akaike weight. Hypotheses have been grouped by the form of N-limitation and N-feedbacks to emphasise these two structural components. Shrub codes BV and MY are from Central Yamal, S8N from Varandei, and YUSL from Yuribei.

4.5 Discussion

4.5.1 Divergent trends in N availability

Our results demonstrate that N availability has been declining in multiple bioclimatic subzones of the Western Siberian tundra, although soil N has also increased in some locations. Increasing summer and winter air temperatures are expected to increase the efficiency of N-mineralising microbes and therefore increase N availability to tall shrubs. However, trends in the $\delta^{15}N$ data suggest that this effect may be of lesser importance compared to decreased N inputs, increased N demand by shrubs or otherwise, or increased N loss. Here, shrub N demand is defined as annual biomass growth multiplied by the N content of biomass under conditions where N is not limiting (Ma, Ahuja and Bruulsema 2008); alternatively, shrub N uptake is defined as the realised annual N use given the present N supply. The most important N input to Arctic tundra ecosystems is through biological N fixation by moss-associated microbes (Rousk et al. 2018). One explanation for the results is therefore that shrubification has driven compositional changes in our locations whereby mosses have been progressively replaced by deciduous shrubs, reducing N fixation rates in tall shrub dominated landscape patches. It is also possible that N losses by leaching, gaseous pathways (i.e. nitrification, denitrification) or N immobilisation by microbes may have increased. For example, reduced moisture content in soils may have enabled greater volatilisation of available N. Finally, increased N demand driven by woody shrub growth release may have increased N uptake thus locking up N into long-term plant biomass stores. The large experimental N addition at Daring Lake indicates a substantial capacity for immobilisation by soil microbes in some low Arctic environments (Churchland et al. 2010); this suggests that progressively increasing N inputs arising from temperature-induced elevated efficiency of N mineralising microbes can be matched by increased non-plant N demand.

Alternatively, the temperature profile of tundra soils at our locations may be mismatched to the temperature optima of soil processes. ITEX warming experiments indicate increased litter decomposition and N-mineralisation in response to warming (Bjorkman et al. 2019). Calibrated

response functions of tundra N-mineralisation to increasing air temperature suggest a non-linear response with an upward inflection at approximately 5°C, but declining performance above 15°C (Mikan et al. 2002).

Our results demonstrate that declining N has occurred within different bioclimatic subzones. The data also, however, indicate heterogeneity in N trajectories, indicating that N availability to shrub individuals is a function of local-scale N dynamics. We did not however observe direct relationships between trends in $\delta^{15}N$ and the topographic variables under study (TWI, Slope, Water Distance), which suggests that processes driving change of $\delta^{15}N$ may be relatively insensitive to variability in topography-driven soil moisture compared to other factors such as biotic interactions. That declining N availability occurred within all study locations (within both bioclimatic subzones D and E) suggests that overriding regional-scale increases in air temperature are not of greater importance than local-scale factors across an envelope of climatology.

The envelope of variability in $\delta^{15}N$ was shared between all three sampling locations, suggesting that tall shrubs have established within similar N niches across landscapes. Aerial photography indicates that *Salix lanata* shrubs have established on thaw slumps and drying lake beds, which may be indicative of newly exposed soils of relatively greater nutrient availability (Bruce Forbes, *personal communication*).

4.5.2 Importance of N limitation to shrub growth

The model-fitting and model-selection of N-dependent versus N-independent growth models confirmed that *Salix lanata* tall shrubs are strongly N-limited. Model selection indicated that the ring width and $\delta^{15}N$ time-series for all *Salix lanata* individuals studied were better explained by models containing N-dependent growth than N-independent growth. This finding corroborates with increased shrub biomass after N fertilisation in ITEX plots (Bouskill, Riley & Tang 2014).

The functional form of N-limitation, however, varied between the shrubs under study between linear and saturating form. Preference for the saturating form over the linear form in some cases

indicates that there was a temporal constraint to N uptake, which may be interpreted as the handling time for a given quantity of nutrient (McNickle & Brown 2014). As our inference is on an annual temporal resolution a saturating functional form suggests that N uptake is constrained independent of the soil N levels. This may be explained by the role of organic N uptake. The dominance of linear N-limitation mechanism within our sampled shrubs suggests that N uptake is directly proportional to its availability for a proportion of *Salix lanata* individuals. The presence of linear N uptake suggests that handling time is insignificant. Lines of evidence suggest that higher-latitude tundra environments may be more sensitive to N addition. Small increases in N availability in the Greenlandic high Arctic dwarf-shrub tundra were found to substantially increase shrub cover (Arens et al. 2008).

Our MFMS results identified an important role for geometric constraints, despite the general lack of an age-related trend in individual wood ring time series. The presence of a geometric constraint appears unrelated to the initial or final size of shrub stems, indicating that the geometric constraint likely arises due to competitive effects. It has been suggested that tall Arctic shrubs may gradually abandon old stems as their locality becomes progressively nutrient-depleted. The dominant form of reproduction for Arctic *Salix* is clonal (Douhovnikoff et al. 2018), allowing for abandonment of old stems and creation of new 'main' stems from lateral root systems, and suggesting that the asymptotic growth observed may be a reflection of nutrient conditions.

The performance of theoretical models for predicting ring width was generally high but dropped for some individuals: this appears to be related to unexplained limiting mechanisms during the start of growth time-series (**Supplementary Table 4–7**). A threshold of growth release was visible within ring time-series, but not synchronous between individuals in age or year, suggests that shading (competitive effects) may be responsible for the lower overall performance of models for certain individuals. This interpretation is supported by the residuals of the best model fits, where residuals are greater earlier during the earlier time period.

4.5.3 Plant-soil feedback mechanisms

The $\delta^{15}N$ and ring width time-series were best explained by theoretical models that incorporated a plant-soil feedback effect for 17 of 24 shrub individuals, which suggests that shrub biomass exerts increasing control on soil N availability. A progressively increasing role of litter feedbacks here corroborates with evidence from the Canadian Arctic, where environments dominated by the tall form of *Betula glandulosa* shrubs were found to have litter feedbacks over three times greater than in dwarf form-dominated environments (Buckeridge et al. 2009). Our best-fitting models suggest relatively high biomass loss rates linked to litter feedback, which suggests that decomposition rates have kept up with increased shrub litter inputs. It has been suggested that shrub canopies exert a positive feedback on winter soil temperature by capturing snow (Sturm et al. 2005). The model-inferred dynamics here support this hypothesis, as the model-inferred quantity of soil N derived from litter feedbacks increases substantially through time (**Figure 4–10**). In addition, the model-inferred dynamics may illustrate an important role for ectomycorrhizal (ECM) fungi: given relatively low N availability in Arctic soils, *Salix lanata* shrubs in Western Siberia have formed mycorrhizal associations with ectomycorrhiza species capable of utilising organic forms of N, such as amino acids (Akhmetzhanova et al. 2012), which likely contribute to strong litter feedbacks; use of organic forms of N 'shortcuts' complete decomposition of organic matter, which would act to shorten the time between litterfall and uptake of the derived nutrients.

The model-inferred parameters, however, suggest that there is an envelope of variability in the strength of plant-soil feedbacks within areas that have experienced tall shrub expansion. Although a biome-wide study of litter decomposition suggested that there is a greater role in litter feedbacks for changes in species composition rather than within-species variation in litter quality (Cornelissen et al. 2007), our data illustrates that within-stand variability may be significant at high spatial resolution. Variability in plant-soil feedbacks arises predominantly from the model-inferred litter conversion factor (α). As the litter conversion ('quality') factor varied by orders of magnitude within the best-fitting models and this occurred alongside high environmental loss rates for plant

biomass, our mechanism may be capturing the role of stand dynamics in soil-litter feedbacks. This may arise if there has been a synchronous rise in shrub biomass within neighbouring individuals.

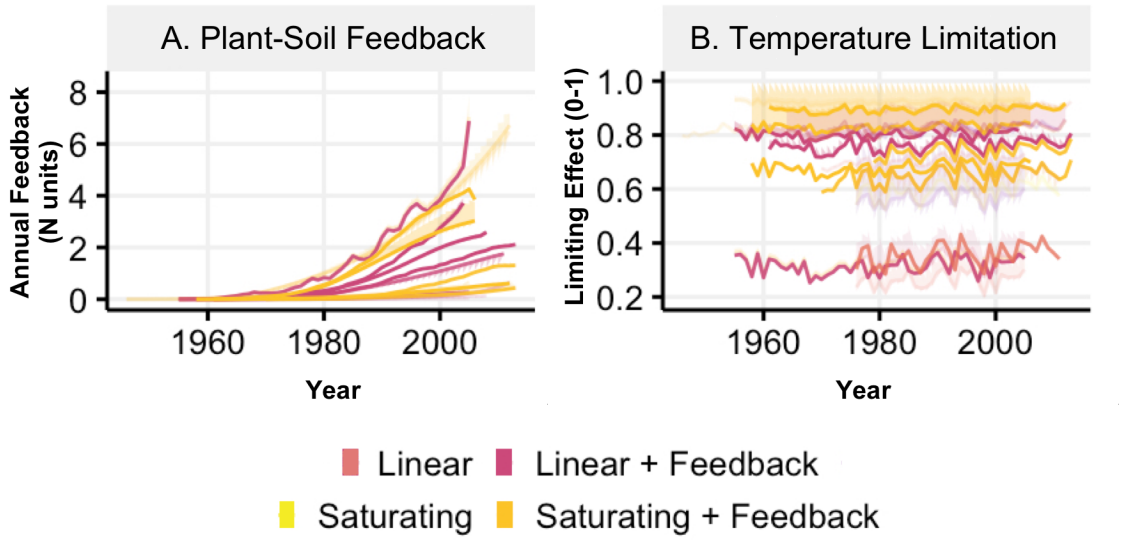

Figure 4–10 Model-inferred rates of ecological processes through time for the best-fitting hypothesis for each shrub individual; colours indicate mechanism as in **Figure 4–9**; shaded areas indicate 95% confidence intervals. **A)** plant-soil feedbacks. **B)** temperature-limiting effect on shrub growth rate (1 = no effect, 0 = perfect effect).

The simple functional form of plant-soil feedback used here may mask more complex processes. One limitation of the functional form of shrub-soil feedback applied here is that we have assumed constant litter quality (i.e. the litter conversion factor between biomass and N, α, is fixed through time). A second process that we did not model here is nutrient retention and storage. The prevalence of plant-soil feedbacks inferred from our data may be reflective of N-conserving traits of *Salix lanata* shrubs, including resource conservation and storage.

4.5.4 Model-Inferred N Uptake versus N Supply

Taking the best model of shrub-nutrient dynamics for each shrub individual, model-inferred processes suggest that increasing shrub N uptake may be outpacing increases in soil N supply (background N replenishment and litter feedbacks) at our study locations. However, although we were able to calculate model-inferred soil N supply and N uptake by plants, we could not use model-inferred processes to estimate shrub N demand (defined as the N required under optimal conditions where N is not limiting to biomass growth). As the dominant mechanism of N-limitation inferred

was of a linear form, shrub growth is sufficiently far from any saturating asymptote that we cannot determine the level of N where growth would no longer be N limited (i.e. N demand).

The rates of model-inferred processes over decades indicate that the ratio of N uptake to N supply has been increasing (**Figure 4–11**), which may reflect biomass dynamics; there may be increasing competitive ability of shrub individuals at obtaining N sources as they increase in size. As shrub growth consumes a greater proportion of N supply through time, this is indicative of increasing N storage in shrub biomass over decades. In addition, the overall decline in soil N availability over decades was matched by declines in the model-inferred absolute environmental N loss from soil, suggesting that the importance of alternative loss pathways (i.e. nitrification, denitrification, N immobilisation) versus shrub uptake declined. Taken together, these lines of evidence – declining overall absolute N availability, model-inferred increases in N uptake versus N supply; an increasing role of shrub litter feedbacks in N supply; and overall declines in model-inferred alternative soil N loss pathways – support the interpretation that N may be increasingly 'locked up' into long-lived shrub biomass, which may work to constrain N supply in line with the progressive N limitation (PNL) hypothesis. Model-inferred increases in N uptake and N supply partly reflect stand development and associated biomass dynamics, as the sampled sites have become progressively shrub-covered over the last 100 years. However, our individuals do not represent a single cohort but are of variable establishment date and basal diameters through time, which reduces the role of individual age-related effects. PNL is thought to occur on a timescale of decades to centuries, depending on the size of N pools in the environment (Luo et al. 2004) so may be observed over the timeframe here. The model-inferred processes conform to PNL, which is characterised by increased N demand relative to N supply. However, as our models represent N loss as a density-dependent process and N availability has been declining for many shrub individuals, our model inference suggests that N losses have been declining; the dominant process governing the N balance is therefore increased plant N uptake. In PNL N supply is thought to be constrained by one or many sinks including N-immobilisation by microbes, environmental loss, or plant lock-up of N into long-lived stores. Observed changes in the environments under study here indicate substantial increases

in woody material and tall shrub forms: the model-inference therefore supports the hypothesis that plant growth release has contributed to declines in N and increased the ratio of N uptake to N supply.

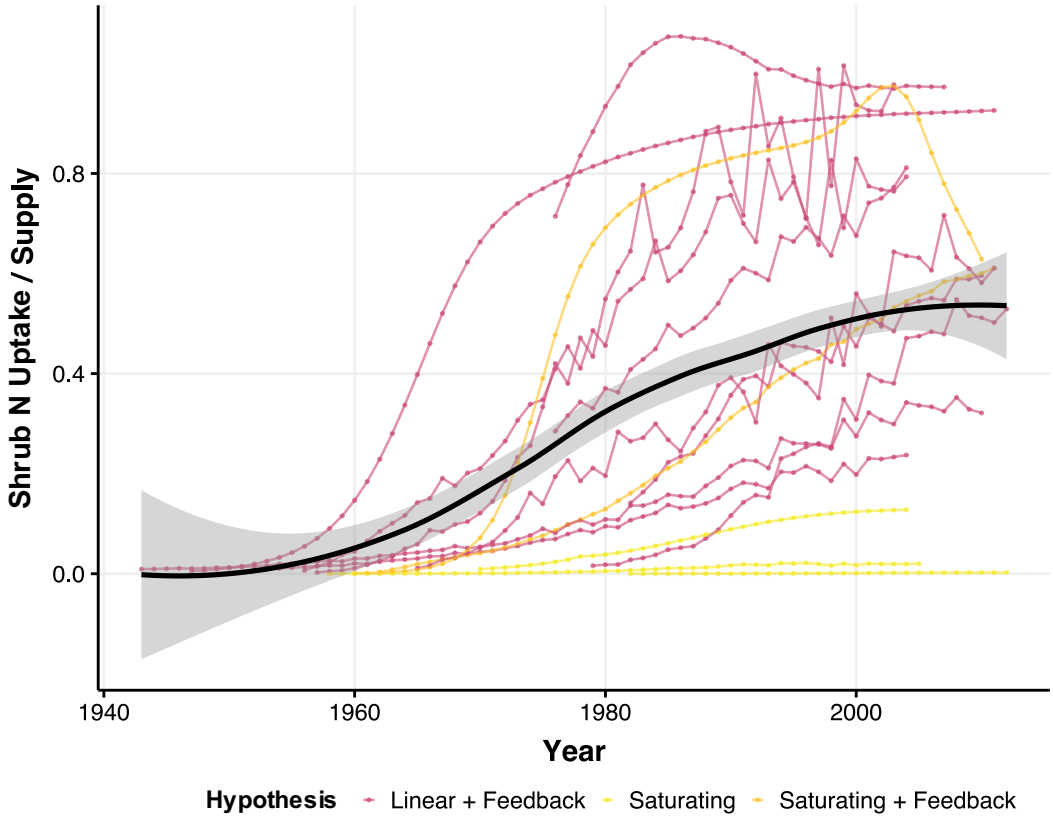

Figure 4–11 Model-inferred nitrogen uptake versus nitrogen supply for each of the best-fitting models to observed shrub $\delta^{15}N$ and ring width time series. N uptake represents the model-inferred plant N use within the year whereas N supply consists of the background N replenishment rate plus litter inputs to the soil N pool.

The model-inferred processes also elude to an increasing role of N limitation relative to temperature limitation in the growth of the *Salix lanata* shrub individuals. We applied the best-fitting models and parameters to generate the expected contributions of temperature limitation and asymptotic effects on the expected growth rate through time for each shrub individual (**Figure 4–12**). Overall trends indicate that the contribution of temperature limitation on growth has declined in line with increasing air temperature. Increased summer air temperatures enabled 'growth release' to occur relative to earlier decades. However, the role of asymptotic limitations to growth may be an important factor over the coming years, as the model-inferred limitation effects suggest that asymptotic constraints have become increasingly important since the late 1990s; this may reflect

maturation of tall shrub stands. We did not include a summary statistic for N limitation in **Figure 4–12** as the N-limiting effect – represented by per-unit biomass N uptake – is sensitive to per-shrub absolute N availability.

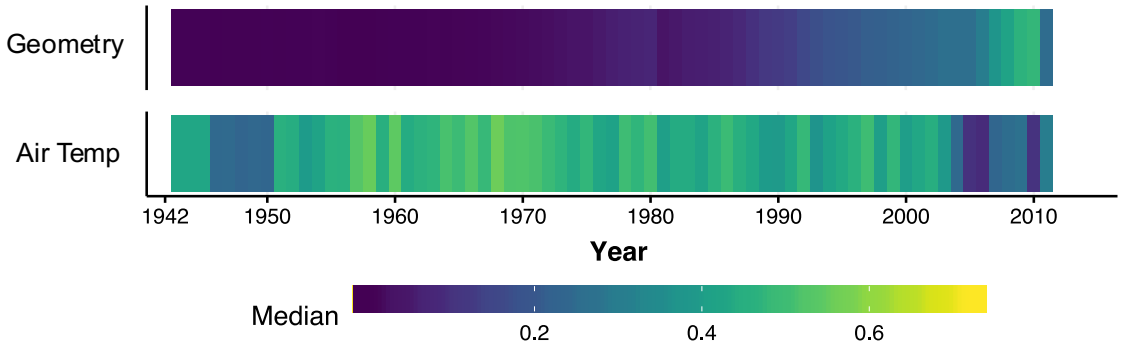

Figure 4–12 Median of model-inferred variability through time of two limiting processes to shrub growth: temperature and geometric limitation. Geometry and air temperature limitation effects are standardised on a zero – one scale. Median limiting effects were calculated from the best-fitting models for all 24 shrubs. Where geometry or temperature effects were not included in the best model these the respective limiting effects were marked as zero.

Our modelling approach did not account for a fertilisation effect from increasing atmospheric CO_2, which has been suggested as the environmental stimulus to cause PNL in natural environments by increasing water-use efficiency (Luo et al. 2004). There are indications that vegetation productivity in the Arctic tundra may be more responsive to CO_2 fertilisation than previously thought (Winkler et al. 2019).

4.5.5 Environmental considerations

We found that topography could explain some of the variability in the processes governing plant-nitrogen relations; this suggests that moisture and microclimate play a role in shrub-nitrogen interactions:

Asymptotic Growth. A positive connection between asymptotic size (***k***) and the topographic wetness index suggests that shrub individuals can achieve greater size in relatively wet landscape positions. TWI represents potential wetness within landscapes, but these areas likely occur in hollows and sheltered microclimates. There are therefore coincident factors that may plausibly

explain greater maximum size, which include herbivory, active layer depth, and protective effects. First, herbivory is lower in depressions and sheltered locations as reindeer seek to avoid midges. Second, there is a deeper active layer, through which deeper rooting may incur mechanical advantages in terms of stem stability. Third, there may be a greater protective effect in these locations from storm damage; snow accumulation is also greater, which may provide a protective effect to aboveground biomass (Bokhorst, Bjerke, Davey, et al. 2010).

Soil N Input and Loss. Soil N inputs were greater on valley sides than in the valley bottom, whereas soil loss rates did not appear dependent on topography. Greater absolute values of $\delta^{15}N$ on valley sides as well as greater N replenishment (λ) supports the hypothesis that N inputs are a function of N-fixing mosses, as moss presence in the flat lowland areas is effectively zero compared to valley slopes where some mosses may be present. Topography has previously been identified as a driver of N losses from Arctic soils (Stewart et al. 2014). We did not, however, find a significant relation between environmental N loss (γ_N) and the topographic factors assessed.

Plant-Soil Feedbacks. The inferred model parameters suggest that the environmental loss rate of shrubs is greater in relatively wetter or sheltered positions. Soil moisture is an important determinant of decomposition rates (Aerts 2006), which may enable greater plant-soil feedbacks to occur in relatively wet landscape positions and explain this result. Alternatively, these areas may have deeper active layers, which may lead to increased decomposer biomass thus greater decomposition rates.

4.6 Conclusions

We identified that *Salix lanata* shrub growth in Western Siberia has been N-limited over recent decades. To achieve this, we created long-term $\delta^{15}N$ time series from 24 individual shrubs in Western Siberia to infer local soil N availability; we then combined the $\delta^{15}N$ time series with ring width data within theoretical ecological models that represented plant-nitrogen dynamics over decades. A model-fitting and model-selection approach enabled us to identify the N-dependent growth better explained the time-series data for all 24 individuals than N-independent growth.

The $\delta^{15}N$ time-series demonstrate that there are locations in the Arctic in which N availability has been declining during recent decades. In addition, declining N has occurred within different bioclimatic subzones of the Arctic tundra. Different soil N trajectories also occurred at fine spatial resolution indicating that N availability to shrub individuals is a function of local-scale N dynamics. Model inference suggested that declines in N availability and strong N-limitation to shrub growth was coincident with an increase of shrub N uptake relative to N supply. In addition, model-inferred temperature-limiting effects on shrub growth suggest that the role of temperature has progressively declined as summer temperatures have been increasing; this has increased the role of N limitation relative to temperature limitation. These findings together suggest that declines in N availability may have been driven by increased plant N uptake rather than N loss pathways. However, model-inferred rates of N uptake versus N supply reflect increasing dominance of shrub biomass from individual growing shrubs; it is therefore plausible that a progressively increasing role of competitive effects and geometric constraints (as inferred within the shrub individuals here) may limit biomass production and lead to lower shrub N requirements.

We found that litter feedbacks between shrubs and soil was an important component to explain shrub-nutrient dynamics. Shrub-soil nitrogen feedbacks were important determinants for growth and N availability for the sampled shrubs. This finding suggests that shrubs are important drivers of soil N availability in Western Siberia. Topography explained variability in the inferred processes governing plant-nitrogen relations. Greater asymptotic size of shrub individuals was related to depressions and lowlands, which may arise from biotic interactions or mechanical advantages. Increased soil N inputs in sloped environments may reflect a greater role of N-fixation on the fringes of tall shrub areas. Our research cannot prove or disprove regional-scale trends in N availability, but only indicate the existence of high spatial heterogeneity. Further research is required to expand the spatial coverage of $\delta^{15}N$ time-series.

4.7 Acknowledgements

The authors thank Peter Long for guidance on remote sensing; Gillian Petrokofsky; Mike Bonsall for advice on modelling techniques; Danielle Sinclair for lab assistance; Robin Paulman for advice and assistance with nitrogen isotope analysis; and Kathy Willis for providing lab facilities.

4.8 Author Contributions

ACM developed the nitrogen isotope method, determined mathematical models, implemented, and conducted the mathematical modelling method, and led the writing of the manuscript. ESJ and MMF conceptualised the research. BF, and MMF completed field work, and ZP measured and cross-dated ring widths. All authors contributed to the writing of the manuscript.

4.9 References

Aerts, R., 2006. The freezer defrosting: global warming and litter decomposition rates in cold biomes. *Journal of Ecology*, 94(4), pp.713–724.

Arens, S.J.T., Sullivan, P.F. & Welker, J.M., 2008. Nonlinear responses to nitrogen and strong interactions with nitrogen and phosphorus additions drastically alter the structure and function of a high arctic ecosystem. *J. Geophys. Res.*, 113(G3), p.664.

Auffret, M.D. et al., 2016. The Role of Microbial Community Composition in Controlling Soil Respiration Responses to Temperature R. Grosch, ed. *PLOS ONE*, 11(10), p.e0165448.

Bhatt, U.S. et al., 2013. Recent Declines in Warming and Vegetation Greening Trends over Pan-Arctic Tundra. *Remote Sensing*, 5(9), pp.4229–4254.

Bjorkman, A.D. et al., 2019. Status and trends in Arctic vegetation: Evidence from experimental warming and long-term monitoring. *Ambio*, 23, pp.4294–15.

Blume-Werry, G. et al., 2019. Dwelling in the deep - strongly increased root growth and rooting depth enhance plant interactions with thawing permafrost soil. *The New phytologist*, p.nph.15903.

Bobbink, R. et al., 2010. Global assessment of nitrogen deposition effects on terrestrial plant diversity: a synthesis. *Ecol Appl*, 20(1), pp.30–59.

Bonsall, M.B. & Hastings, A., 2004. Demographic and environmental stochasticity in predator-prey metapopulation dynamics. *Journal of Animal Ecology*, 73(6), pp.1043–1055.

Bormann, B.T. & Sidle, R.C., 1990. Changes in Productivity and Distribution of Nutrients in a Chronosequence at Glacier Bay National Park, Alaska. *The Journal of Ecology*, 78(3), p.561.

Bouskill, N.J., Riley, W.J. & Tang, J.Y., 2014. Meta-analysis of high-latitude nitrogen-addition and warming studies implies ecological mechanisms overlooked by land models. *Biogeosciences*, 11(23), pp.6969–6983.

Brooks, P.D. et al., 2011. Carbon and Nitrogen Cycling in Snow-Covered Environments. *Geography Compass*, 5(9), pp.682–699.

Buckeridge, K.M. et al., 2009. Soil nitrogen cycling rates in low arctic shrub tundra are enhanced by litter feedbacks. *Plant and Soil*, 330(1-2), pp.407–421.

Burnham, K.P. & Anderson, D.R., 2007. *Model Selection and Multimodel Inference*, Springer Science & Business Media.

Chapin, F.S. et al., 2005. Role of land-surface changes in arctic summer warming. *Science*, 310(5748), pp.657–660.

Chapman, S.K. et al., 2006. Plants actively control nitrogen cycling: uncorking the microbial bottleneck. *New Phytologist*, 169(1), pp.27–34.

Churchland, C. et al., 2010. Soil microbial and plant community responses to single large carbon and nitrogen additions in low arctic tundra. *Plant and Soil*, 334(1-2), pp.409–421.

Cornelissen, J.H.C. et al., 2007. Global negative vegetation feedback to climate warming responses of leaf litter decomposition rates in cold biomes. *Ecol Letters*, 10(7), pp.619–627.

Craine, J.M., Brookshire, E.N.J., et al., 2015. Ecological interpretations of nitrogen isotope ratios of terrestrial plants and soils. *Plant and Soil*, 396(1-2), pp.1–26.

Craine, J.M., Elmore, A.J., et al., 2015. Convergence of soil nitrogen isotopes across global climate gradients. *Scientific Reports*, 5, p.8280.

Douhovnikoff, V. et al., 2018. Clonal Diversity in an Expanding Community of Arctic Salix spp. and a Model for Recruitment Modes of Arctic Plants. *Arctic, Antarctic, and Alpine Research*, 42(4), pp.406–411.

Elmendorf, S.C. et al., 2011. Global assessment of experimental climate warming on tundra vegetation: heterogeneity over space and time. *Ecology Letters*, 15(2), pp.164–175.

Enquist, B.J. & Bentley, L.P., 2012. Land Plants: New Theoretical Directions and Empirical Prospects. In *Metabolic Ecology*. A Scaling Approach. Chichester, UK: John Wiley & Sons, Ltd, pp. 164–187.

Forbes, B.C. et al., 2009. High resilience in the Yamal-Nenets social-ecological system, West Siberian Arctic, Russia. *Proc Natl Acad Sci U S A*, 106(52), pp.22041–22048.

Fritts, H.C., 1976. *Tree Rings and Climate*, Academic Press.

Garnier, E., 1991. Resource capture, biomass allocation and growth in herbaceous plants. *Trends in Ecology & Evolution*, 6(4), pp.126–131.

Gerhart, L.M. & McLauchlan, K.K., 2014. Reconstructing terrestrial nutrient cycling using stable nitrogen isotopes in wood. *Biogeochemistry*, 120(1-3), pp.1–21.

Götmark, F., Götmark, E. & Jensen, A.M., 2016. Why Be a Shrub? A Basic Model and Hypotheses for the Adaptive Values of a Common Growth Form. *Frontiers in plant science*, 7(654), p.1095.

Henry, G.H.R. et al., 2012. Effects of observed and experimental climate change on terrestrial ecosystems in northern Canada: results from the Canadian IPY program. *Climatic Change*, 115(1), pp.207–234.

Heskel, M. et al., 2013. Differential physiological responses to environmental change promote woody shrub expansion. *Ecology and evolution*, 3(5), pp.1149–1162.

Hoaglin, D.C., Mosteller, F. & Tukey, J.W., 2000. *Understanding robust and exploratory data analysis*, Wiley-Interscience.

Jackson, R.B. & Caldwell, M.M., 1993. The Scale of Nutrient Heterogeneity Around Individual Plants and Its Quantification with Geostatistics. *Ecology*, 74(2), pp.612–614.

Jeffers, E.S., Bonsall, M.B. & Willis, K.J., 2011. Stability in ecosystem functioning across a climatic threshold and contrasting forest regimes. *PLOS ONE*, 6(1), p.e16134.

Kim, S. et al., 2007. Temperature dependence of growth, development, and photosynthesis in maize under elevated CO2. *Environmental and Experimental Botany*, 61(3), pp.224–236.

Komsta, L., 2013. **mblm: Median-Based Linear Models**. Available at: https://cran.r-project.org/web/packages/mblm/index.html.

Lantz, T.C., Marsh, P. & Kokelj, S.V., 2012. Recent Shrub Proliferation in the Mackenzie Delta Uplands and Microclimatic Implications. *Ecosystems*, 16(1), pp.47–59.

Lee, C.-Y., 2015. Fast simulated annealing with a multivariate Cauchy distribution and the configuration's initial temperature. *Journal of the Korean Physical Society*, 66(10), pp.1457–1466.

Locatelli, M., 2002. *Simulated annealing algorithms for continuous global optimization, Handbook of global optimization*,

Luo, Y. et al., 2004. Progressive nitrogen limitation of ecosystem responses to rising atmospheric carbon dioxide. *Bioscience*, 54(8), pp.731–739.

Ma, L., Ahuja, L.R. & Bruulsema, T., 2008. *Quantifying and Understanding Plant Nitrogen Uptake for Systems Modeling*, CRC Press.

Macias-Fauria, M. et al., 2012. Eurasian Arctic greening reveals teleconnections and the potential for structurally novel ecosystems. *Nature Climate Change*, 2(8), pp.613–618.

Martin, A.C. et al., 2017. Shrub growth and expansion in the Arctic tundra: an assessment of controlling factors using an evidence-based approach. *Environmental Research Letters*, 12(8), p.085007.

McLauchlan, K.K. et al., 2017. Centennial-scale reductions in nitrogen availability in temperate forests of the United States. *Scientific Reports*, 7(1), p.7856.

McLauchlan, K.K. et al., 2007. Changes in nitrogen cycling during the past century in a northern hardwood forest. *Proc Natl Acad Sci U S A*, 104(18), pp.7466–7470.

McNickle, G.G. & Brown, J.S., 2014. When Michaelis and Menten met Holling: towards a mechanistic theory of plant nutrient foraging behaviour. *AoB PLANTS*, 6, p.7.

Menne, M.J. et al., 2012. An Overview of the Global Historical Climatology Network-Daily Database. *dx.doi.org*, 29(7), pp.897–910.

Mikhailov, I.S., 2016. Soil map of the Russian Arctic on a 1 : 1 M scale: Contents and compilation methods. *Eurasian Soil Science*, 49(4), pp.377–385.

Myers-Smith, I.H., Elmendorf, S.C., et al., 2015. Climate sensitivity of shrub growth across the tundra biome. *Nature Climate Change*, 5(9), pp.887–891.

Myers-Smith, I.H., Hallinger, M., et al., 2015. Methods for measuring arctic and alpine shrub growth: A review. *Earth-Science Reviews*, 140, pp.1–13.

National Academies of Sciences, Engineering, and Medicine, 2019. *Understanding Northern Latitude Vegetation Greening and Browning: Proceedings of a Workshop*, Washington, DC: National Academies Press.

Norby, R.J. et al., 2010. CO2 enhancement of forest productivity constrained by limited nitrogen availability. *Proc Natl Acad Sci U S A*, 107(45), pp.19368–19373.

Paine, C.E.T. et al., 2011. How to fit nonlinear plant growth models and calculate growth rates: an update for ecologists. *Methods in Ecology and Evolution*, 3(2), pp.245–256.

Piao, S. et al., 2006. Effect of climate and CO2 changes on the greening of the Northern Hemisphere over the past two decades. *Geophysical Research Letters*, 33(23).

Piao, S. et al., 2014. Evidence for a weakening relationship between interannual temperature variability and northern vegetation activity. *Nature Communications*, 5, p.5018.

Quinn, P. et al., 1991. The prediction of hillslope flow paths for distributed hydrological modelling using digital terrain models. *Hydrological Processes*, 5(1), pp.59–79.

Rodionov, A. et al., 2007. Organic carbon and total nitrogen variability in permafrost-affected soils in a forest tundra ecotone. *European Journal of Soil Science*, 58(6), pp.1260–1272.

Rousk, K., Sorensen, P.L. & Michelsen, A., 2018. What drives biological nitrogen fixation in high arctic tundra: Moisture or temperature? *Ecosphere*, 9(2), p.e02117.

Seddon, A.W.R. et al., 2016. Sensitivity of global terrestrial ecosystems to climate variability. *Nature*, 531(7593), pp.229–232.

Sörensen, R., Zinko, U. & Seibert, J., 2006. On the calculation of the topographic wetness index: evaluation of different methods based on field observations. *Hydrology and Earth System Sciences Discussions*, 10(1), pp.101–112.

Stewart, K.J. et al., 2014. Topography as a key factor driving atmospheric nitrogen exchanges in arctic terrestrial ecosystems. *Soil Biology and Biochemistry*, 70, pp.96–112.

Sturm, M. et al., 2005. Winter Biological Processes Could Help Convert Arctic Tundra to Shrubland. *Bioscience*, 55(1), p.17.

Tape, K.D. et al., 2012. Landscape Heterogeneity of Shrub Expansion in Arctic Alaska. *Ecosystems*, 15(5), pp.711–724.

Tilman, D., 1990. Mechanisms of Plant Competition for Nutrients: The Elements of a Predictive Theory of Competition. In *Perspectives on Plant Competition*. Elsevier, pp. 117–141.

Towers, S., 2014. Potential fitting biases resulting from grouping data into variable width bins. *Physics Letters B*, 735, pp.146–148.

Van Rees, K., 1994. Michaelis-Menten kinetics: Calculation and use in nutrient uptake models. *New Zealand Journal of Forestry Science*, 24(2).

Vitousek, P.M. & Howarth, R.W., 1991. Nitrogen limitation on land and in the sea: How can it occur? *Biogeochemistry*, 13(2), pp.87–115.

Wagenmakers, E.-J. & Farrell, S., 2004. AIC model selection using Akaike weights. *Psychonomic Bulletin & Review*, 11(1), pp.192–196.

Walker, D.A. et al., 2009. The Circumpolar Arctic vegetation map. *Journal of Vegetation Science*, 16(3), pp.267–282.

Winkler, A.J. et al., 2019. Earth system models underestimate carbon fixation by plants in the high latitudes. *Nature Communications*, 10(1), p.885.

Zhao-gang, L. & Feng-ri, L., 2003. The generalized Chapman-Richards function and applications to tree and stand growth. *Journal of Forestry Research*, 14(1), pp.19–26.

4.10 Supplementary Material

4.10.1 Linear Fits to Nitrogen Isotope Time-Series

17 of 24 N isotope series exhibited significant linear temporal trends. A declining $\delta^{15}N$ trend was found for 13 time-series. The Theil-Sen summaries are shown in **Table 4–4**:

Table 4–4 Theil-Sen linear fit summary statistics for each individual shrub $\delta^{15}N$ series.

Shrub ID	Intercept	Slope	Intercept p-value	Slope p-value	Residual SE	DF
BV05AB	-32.76	0.016	0.001	0.002	0.29	13
BV14B	6.01	-0.004	0.470	0.339	0.46	10
BV25AB	145.48	-0.074	0.001	0.001	0.35	9
MYSL9A	2.54	0.000	0.375	0.625	0.42	8
S8N0107A	13.42	-0.008	0.151	0.117	0.65	16
S8N0110A	63.20	-0.033	0.000	0.000	0.35	14
S8N0113A	-23.67	0.011	0.415	0.415	0.41	8
S8N0115A	19.17	-0.011	0.064	0.035	0.57	15
S8N0121A	-39.81	0.020	0.000	0.000	0.36	14
S8N0122A	-21.63	0.011	0.057	0.064	0.37	15
S8N0125A	13.17	-0.008	0.206	0.175	0.35	9
S8N0129A	52.10	-0.027	0.000	0.000	0.37	15
S8N0133A	90.93	-0.047	0.003	0.003	0.41	10
S8N0139A	64.35	-0.033	0.004	0.004	0.80	14
YUSL03A	69.92	-0.035	0.000	0.000	0.59	37
YUSL05A	77.22	-0.038	0.000	0.000	0.56	34
YUSL09A	-55.43	0.028	0.000	0.000	0.51	31
YUSL14A	-23.98	0.011	0.151	0.182	0.54	32
YUSL21A	7.51	-0.004	0.009	0.006	0.41	42
YUSL26A	138.21	-0.070	0.000	0.000	1.02	37
YUSL29A	87.77	-0.045	0.000	0.000	0.52	24

YUSL30AB	-26.59	0.012	0.000	0.000	0.52	39
YUSL34A	45.72	-0.024	0.000	0.000	0.60	37
YUSL39A	73.35	-0.038	0.000	0.000	0.56	36

SE = standard error; DF = degrees of freedom. Shrub codes BV and MY are from Central Yamal, S8N from Varandei, and YUSL from Yuribei.

4.10.2 Full Model-Fitting and Model-Selection Results

Complete negative log likelihood and Akaike weight tables are shown in **Table 4–5** and

Table 4–6:

Table 4–5 Akaike weights (%) indicating support for each of 24 model hypotheses (vertical) per each of 24 shrub individuals (horizontal). Akaike weights sum to 100% for the 24 model hypotheses on a per-shrub basis.

Model Code	Northern Yamal								Varandei										Yuribei								
	BV05	BV14	BV25	M9	S107	S110	S113	S115	S121	S122	S125	S129	S133	S139	Y03	Y05	Y09	Y14	Y21	Y26	Y29	Y30	Y34	Y39
N1	0.0	0.0	4.4	0.0	0.0	0.0	0.3	0.0	0.0	0.0	0.2	0.0	3.1	89.1	0.0	0.0	0.0	0.0	0.0	0.0	0.0	0.0	0.0	0.0
N1-U1	0.0	0.1	**5.8**	0.0	0.0	0.0	0.0	0.0	0.0	0.0	0.0	0.0	0.8	0.0	0.0	0.0	0.0	0.0	0.0	0.0	**39.8**	0.0	0.0	**5.0**
N2	0.0	0.1	**22.1**	0.0	0.1	0.0	**8.0**	0.0	0.0	0.0	2.0	0.0	50.3	0.0	0.0	0.0	0.0	0.0	0.0	0.0	0.1	0.0	0.0	0.0
N2-U1	0.0	0.6	51.3	0.0	0.0	0.0	0.6	**15.5**	0.0	0.0	0.2	0.0	2.4	0.0	0.0	0.0	0.0	0.0	0.0	0.0	48.2	0.0	0.0	0.3
N0	0.0	0.0	0.0	0.0	0.0	0.0	0.0	0.0	0.0	0.0	0.0	0.0	0.0	0.0	0.0	0.0	0.0	0.0	0.0	0.0	0.0	0.0	0.0	0.0
N0-U1	0.0	0.0	0.0	0.0	0.0	0.0	0.0	0.0	0.0	0.0	0.0	0.0	0.0	0.0	0.0	0.0	0.0	0.0	0.0	0.0	0.0	0.0	0.0	0.0
N1-G1	0.0	0.0	0.5	0.0	0.0	0.0	0.1	0.0	0.0	0.0	0.0	0.0	**26.6**	0.0	0.0	0.0	99.3	0.0	0.0	0.0	0.0	0.0	0.0	0.0
N1-U1-G1	0.0	0.0	0.9	0.0	0.1	0.0	0.0	0.1	0.0	0.0	0.0	0.0	0.0	0.1	0.0	0.0	0.0	1.4	**21.2**	0.0	0.2	0.0	**10.7**	0.8
N2-G1	0.0	0.0	3.5	0.0	0.0	0.0	0.8	0.0	0.0	0.0	1.3	0.0	**8.7**	0.0	0.0	0.0	0.0	0.0	0.0	0.0	0.0	0.0	0.0	0.0
N2-U1-G1	100.0	0.1	1.6	0.0	0.6	0.0	0.4	1.2	0.0	0.0	0.0	0.0	0.7	0.0	0.0	0.0	0.0	0.0	**32.5**	0.0	3.5	0.0	78.4	0.1
N0-G1	0.0	0.0	0.0	0.0	0.0	0.0	3.1	0.0	0.0	0.0	0.0	0.0	0.3	1.3	0.0	0.0	0.0	0.0	0.0	0.0	0.0	0.0	0.0	0.0
N0-U1-G1	0.0	0.0	0.0	0.0	0.0	0.0	1.0	0.0	0.0	0.0	0.0	0.0	0.0	2.2	0.0	0.0	0.3	3.6	0.0	0.0	0.0	0.0	0.0	0.0
N1-T1	0.0	1.0	0.3	0.5	3.9	0.0	1.1	0.0	0.0	0.0	3.8	0.0	1.2	0.0	0.0	0.0	0.0	0.0	0.0	0.0	0.0	0.0	0.0	0.0

N1-U1-T1	0.0	0.1	0.4	4.5	**28.1**	0.0	0.0	1.6	0.0	0.0	0.3	0.0	0.1	0.0	**100.0**	0.0	0.0	0.1	0.0	0.0	0.2	0.0	0.0	**92.5**
N2-T1	0.0	**79.8**	2.2	**12.9**	0.8	0.0	**32.4**	0.0	0.0	0.0	**27.1**	0.0	3.0	0.0	0.0	0.0	0.0	0.0	0.0	0.0	0.0	0.0	0.0	0.0
N2-U1-T1	0.0	**10.7**	**6.4**	**53.0**	**39.6**	0.0	**16.7**	1.2	0.0	0.0	4.3	**30.8**	1.3	0.0	0.0	**100.0**	0.0	0.0	0.0	0.0	**7.4**	0.0	0.0	0.9
N0-T1	0.0	0.0	0.0	0.0	0.0	0.0	0.0	0.0	0.0	0.0	0.0	0.0	0.0	0.0	0.0	0.0	0.0	0.0	0.0	0.0	0.0	0.0	0.0	0.0
N0-U1-T1	0.0	0.0	0.0	0.0	0.0	0.0	0.0	0.0	0.0	0.0	0.0	0.0	0.0	0.0	0.0	0.0	0.0	0.0	0.0	0.0	0.0	0.0	0.0	0.0
N1-G1-T1	0.0	0.2	0.0	1.1	1.4	0.0	0.4	0.0	**100.0**	0.0	2.1	0.0	0.1	0.0	0.0	0.0	0.0	0.0	0.0	0.0	0.0	0.0	0.0	0.0
N1-U1-G1-T1	0.0	0.1	0.0	0.0	1.2	**99.7**	**21.5**	**25.4**	0.0	0.0	**8.9**	3.0	0.0	0.1	0.0	0.0	0.0	**91.6**	**7.8**	0.0	0.0	0.0	0.8	0.2
N2-G1-T1	0.0	1.7	0.4	**24.8**	**13.3**	0.0	**5.9**	0.0	0.0	0.0	**22.4**	0.0	1.1	0.0	0.0	0.0	0.0	2.3	0.0	0.0	0.0	0.0	0.0	0.0
N2-U1-G1-T1	0.0	2.9	0.3	3.0	**10.6**	0.0	**5.4**	**55.0**	0.0	**100.0**	**13.9**	**66.2**	0.1	0.0	0.0	0.0	0.0	0.1	**38.4**	**100.0**	0.6	**99.5**	**10.1**	0.3
N0-G1-T1	0.0	2.3	0.0	0.2	0.0	0.2	1.9	0.0	0.0	0.0	**12.8**	0.0	0.0	1.2	0.0	0.0	0.2	0.0	0.0	0.0	0.0	0.3	0.0	0.0
N0-U1-G1-T1	0.0	0.2	0.0	0.0	0.0	0.0	0.4	0.0	0.0	0.0	0.7	0.0	0.0	**5.9**	0.0	0.0	0.2	0.8	0.0	0.0	0.0	0.1	0.0	0.0

Akaike weights represented as percentages, to one decimal place. Bold = above 5% support; Red = best supported model. Model codes indicate model components as specified in **Table 4–1**. Shrub codes BV and MY are from Central Yamal, S8N from Varandei, and YUSL from Yuribei.

Table 4–6 Minimum negative log likelihoods as estimated during the model-fitting procedure for every shrub individual (horizontal) and model (vertical).

Model Code	**Northern Yamal**				**Varandei**										**Yuribei**									
	BV05	**BV14**	**BV25**	**M9**	**S107**	**S110**	**S113**	**S115**	**S121**	**S122**	**S125**	**S129**	**S133**	**S139**	**Y03**	**Y05**	**Y09**	**Y14**	**Y21**	**Y26**	**Y29**	**Y30**	**Y34**	**Y39**
N1	138.0	81.5	52.9	72.4	114.4	121.5	61.4	135.9	215.5	300.0	65.2	223.2	75.2	42.3	306.2	184.3	91.8	94.3	356.5	302.5	49.7	218.3	338.7	133.1
N1-U1	125.3	78.3	50.5	61.0	116.3	121.6	62.0	147.5	142.5	181.3	65.2	125.2	74.6	68.7	276.5	149.0	93.7	94.2	286.7	281.9	35.6	220.0	338.6	115.3
N2	201.6	82.5	53.2	70.5	114.9	137.1	60.3	130.3	175.2	299.8	64.8	245.9	74.3	63.9	306.2	177.0	97.0	97.7	354.7	302.4	47.5	217.8	338.6	136.9
N2-U1	187.5	78.7	50.4	60.7	115.5	137.8	60.7	112.8	156.8	273.6	65.0	135.5	75.5	65.3	276.5	143.0	86.3	94.0	285.3	282.2	38.2	218.5	338.5	119.8
N0	322.8	128.6	137.0	207.5	383.1	316.1	117.6	616.4	482.7	481.8	155.3	360.3	199.1	83.5	540.2	491.6	175.4	199.3	491.5	458.7	164.2	323.8	647.2	429.5

N0-U1	318.1	128.6	136.0	203.7	383.1	315.4	111.0	616.4	438.7	439.6	155.3	360.3	199.0	83.2	514.6	490.1	171.7	199.4	491.5	406.3	161.2	323.6	647.3	425.8
N1-G1	148.8	82.2	53.0	64.1	114.3	122.3	60.6	135.2	210.6	288.0	69.4	219.2	71.1	49.4	310.6	188.7	65.0	88.8	317.0	302.5	50.6	220.8	302.9	133.2
N1-U1-G1	152.1	79.0	50.0	61.0	110.1	123.4	59.1	114.2	178.6	190.0	64.9	144.2	75.2	46.0	310.7	149.9	78.3	80.9	269.6	197.5	37.3	206.9	287.2	115.4
N2-G1	174.6	82.7	53.1	64.1	114.9	137.1	60.4	130.9	214.7	278.6	63.3	145.0	74.2	57.3	270.5	163.1	84.6	92.6	316.8	302.4	49.9	218.0	302.8	136.9
N2-U1-G1	110.0	79.0	51.8	60.8	110.3	136.4	58.7	113.7	145.4	183.6	64.4	129.7	74.7	56.8	246.1	149.2	77.3	91.4	270.6	199.4	38.0	208.2	286.8	119.8
N0-G1	196.0	83.8	64.8	77.0	229.3	126.4	61.2	403.6	240.3	302.3	71.0	231.2	79.5	48.1	337.1	242.5	78.2	92.4	372.5	353.3	118.9	226.7	433.5	275.0
N0-U1-G1	192.1	83.8	64.8	76.8	221.2	126.5	60.2	395.6	240.4	292.1	71.1	219.2	79.6	46.0	413.4	242.5	73.1	84.2	372.6	353.3	118.9	224.1	433.6	275.3
N1-T1	135.2	76.2	53.4	51.3	108.4	118.4	57.8	128.1	206.3	165.2	60.0	193.7	74.2	60.8	231.2	157.0	88.8	88.8	346.4	302.5	56.2	209.2	338.9	134.2
N1-U1-T1	137.6	76.0	50.8	46.4	104.8	117.4	58.5	111.8	167.2	165.7	60.1	126.3	74.2	62.2	211.7	145.8	78.8	83.4	285.5	281.6	37.5	210.8	313.0	110.6
N2-T1	201.7	73.8	53.6	50.4	111.5	137.4	56.7	127.2	251.4	168.0	60.2	220.0	75.2	61.1	229.5	150.6	89.0	94.7	353.5	302.5	49.7	219.2	338.9	147.4
N2-U1-T1	189.3	73.9	50.4	46.6	106.1	136.1	55.0	113.7	176.5	202.3	59.9	114.5	74.1	62.1	270.9	128.5	78.5	91.8	289.1	193.4	37.2	215.5	339.1	117.1
N0-T1	203.4	102.5	137.1	155.6	383.1	316.1	101.3	480.7	286.8	360.9	119.4	253.0	122.8	66.2	339.5	257.8	138.1	128.8	385.2	459.7	137.2	324.0	414.0	267.3
N0-U1-T1	203.4	102.5	136.3	160.2	362.5	316.3	101.3	616.4	438.7	439.6	121.0	254.9	123.8	66.3	331.3	490.2	171.7	129.0	359.3	406.5	144.9	323.7	647.3	263.6
N1-G1-T1	134.2	76.0	53.2	47.8	107.8	119.9	56.1	130.1	112.0	211.9	58.3	192.2	74.2	47.2	263.2	150.0	74.0	84.7	316.3	302.5	56.2	207.8	303.3	150.2
N1-U1-G1-T1	146.4	74.2	50.8	48.1	106.3	107.1	49.1	107.3	128.9	139.7	54.2	113.4	74.3	44.0	247.3	140.5	75.8	74.3	269.1	195.9	37.1	218.7	288.1	114.6
N2-G1-T1	134.2	75.7	53.1	47.3	107.2	122.5	56.1	127.9	209.7	221.8	58.3	191.7	74.2	53.3	262.8	144.1	80.4	82.7	316.4	302.5	52.5	216.2	303.3	132.7
N2-U1-G1-T1	148.0	73.0	51.2	46.8	105.8	123.4	53.5	108.3	133.9	132.6	56.4	112.1	74.7	51.7	235.3	137.5	71.6	83.9	269.0	170.3	36.5	199.0	287.3	116.4
N0-G1-T1	160.3	77.4	64.9	54.8	174.4	118.7	59.6	291.0	216.9	218.9	61.0	211.9	79.6	46.6	286.1	237.6	73.6	92.3	337.0	353.4	119.0	207.8	392.0	275.2
N0-U1-G1-T1	156.7	77.6	64.9	56.1	168.6	119.1	58.8	283.6	210.3	205.2	61.8	211.4	79.6	43.4	283.6	239.0	71.4	83.7	365.1	353.8	119.0	207.1	402.3	275.3

Model codes indicate model components as specified in **Table 4–1**. Shrub codes BV and MY are from Central Yamal, S8N from Varandei, and YUSL from Yuribei.

We calculated the goodness-of-fit for each of the 24 best-fitting models in comparison to shrub ages and sizes. The Root Mean Square Error (RMSE) of one-step-ahead predictions was recalculated from stem radius to absolute (AI) and relative (RI) increments. Comparisons of AI and RI with shrub size characteristics are shown in **Table 4–7**.

Table 4–7 Stem characteristics and Root Mean Square Error for each of the best-fitting models for each shrub individual.

		Root Mean Square Error (RMSE)			Stem Radius (cm)		
Shrub	**Years**	**Radius (mm)**	**AI (mm/year)**	**RI (mm/mm/year)**	**Start**	**End**	**Change**
BV05AB	47	3.04	1.25	0.008962	2.68	24.78	22.10
BV14B	35	0.51	0.29	0.000977	8.22	25.65	17.43
BV25AB	32	0.31	0.15	0.000381	10.98	27.11	16.13
MYSL9A	29	0.71	0.09	0.000174	16.09	32.21	16.12
S8N0107A	53	1.46	1.42	0.002787	7.19	34.69	27.50
S8N0110A	47	0.66	0.50	0.001374	6.52	51.79	45.27
S8N0113A	29	1.22	1.28	0.000982	23.42	49.40	25.98
S8N0115A	50	5.45	8.45	0.035186	2.94	41.12	38.18
S8N0121A	48	0.72	0.24	0.001121	3.59	43.04	39.45
S8N0122A	50	4.82	6.94	0.022423	4.82	47.42	42.60
S8N0125A	32	1.54	1.91	0.002961	12.62	30.80	18.18
S8N0129A	49	2.27	2.94	0.021104	2.75	38.19	35.44
S8N0133A	35	0.66	0.49	0.001129	9.82	32.44	22.62
S8N0139A	45	0.29	0.16	0.000305	11.27	44.31	33.04
YUSL03A	51	15.08	3.64	0.012330	3.27	27.35	24.08
YUSL05A	52	0.72	0.60	0.003468	4.2	38.62	34.42
YUSL09A	31	0.43	0.29	0.000870	6.16	37.63	31.47
YUSL14A	34	0.8	0.17	0.000914	5.97	32.21	26.24
YUSL21A	66	0.31	0.07	0.000543	3.12	36.29	33.17
YUSL26A	48	3.55	4.20	0.017206	2.72	38.48	35.76
YUSL29A	25	1.18	2.54	0.017692	3.34	31.89	28.55
YUSL30AB	68	0.6	0.09	0.000213	7.21	47.35	40.14

YUSL34A	53	0.57	0.19	0.001841	2.89	47.81	44.92
YUSL39A	43	4.29	38.71	0.018780	6.32	48.71	42.39

Shrub codes BV and MY are from Central Yamal, S8N from Varandei, and YUSL from Yuribei. AI = Absolute Increment; RI = relative increment.

Chapter 5

Snow dynamics affect shrub growth but not shrub-nitrogen relations on the Yamal Peninsula, Western Siberia

This paper is in preparation for submission to Biogeosciences.

Given previous findings in Chapter 4 – that model-inferred shrub N uptake is outpacing N supply – I sought to investigate how the seasonality of snow dynamics may be moderating nitrogen-shrub dynamics. Here I generate a new dataset of stable oxygen and carbon isotopes for five shrubs at Yuribei; I integrate these new time series with earth observation data, the nitrogen isotope time series from Chapter 3, and an extension of the previous modelling techniques to examine mechanisms through which snow may control shrub-nitrogen relations, both directly and indirectly.

Snow dynamics affect shrub growth but not shrub-nitrogen relations on the Yamal Peninsula, Western Siberia

Andrew C. Martin[1], Marc Macias-Fauria[2], and Elizabeth S. Jeffers[1]

1. Oxford Long-Term Ecology Laboratory, Department of Zoology, University of Oxford, OX1 3PS
2. School of Geography and the Environment, University of Oxford, OX1 3QY

5.1 Abstract

Rationale. Recent rapid warming in the Arctic tundra biome has driven the proliferation of woody deciduous shrubs at the expense of lichens, graminoids, and mosses. However, spatial heterogeneity in the growth response of shrubs to warming is poorly understood. In particular, snow dynamics – the depth and seasonality of accumulation – may cause complex and non-linear growth responses to a changing climate. Snow accumulation may have direct effects on the growth of shrub individuals through protective effects, or indirect effects by influencing soil nutrient availability and microclimate. The snow-shrub hypothesis suggests that there may be a positive feedback to increased shrub biomass; taller shrubs capture more snow, which insulates soils during winter, ultimately driving nitrogen (N) mineralisation and increased available N for plant growth. The magnitude and role of these processes relative to change in natural environments remains unquantified. We sought to assess the long-term role of these processes over decades within a moist shrub tundra environment on the Yamal Peninsula.

Method. To identify the presence and magnitude of the indirect processes governing shrub-nutrient relations, we interrogated existing time series of $\delta^{15}N$ (a proxy for N availability) and ring widths for five *Salix lanata* shrub individuals at Yuribei using mechanistic models. At annual temporal resolution, we obtained $\delta^{15}N$ (as a proxy for localised soil nitrogen availability), $\delta^{18}O$ (a localised proxy of water sources used for growth) and $\delta^{13}C$ isotope time-series for 1980-2013; this resulted

in 140 individual measurements per shrub. We assessed the relation between $\delta^{18}O$ versus regional indicators of snow dynamics. We applied time-series models of shrub-nutrient dynamics using a model-fitting and model-selection approach to identify the most appropriate mechanisms to explain snow effects on shrub-nutrient relations at: (a) annual and monthly temporal resolutions; and (b) regional and localised spatial scale.

Results. The length of the snow free season has doubled at Yuribei as the timing of spring snowmelt has advanced. $\delta^{13}C$ was related to these dynamics, in particular with the day of snowmelt and snow-free period length. Model-fitting and model-selection indicated temperature-independent soil N replenishment rates best explained observed $\delta^{15}N$ and ring width data for all five shrubs, while snow protective effects better explained the growth of a single shrub; these findings were insensitive to the spatial and temporal scale of analysis. Incorporation of seasonal dynamics did not improve model fits. $\delta^{18}O$ series appeared spatially partitioned between sloped and flat terrain.

Synthesis. Our findings together suggest that snow cover duration has exerted a far greater control on the growth of these shrub individuals than variability in snow depth over the last 35 years. The $\delta^{13}C$ time-series – taken as a proxy for photosynthetic capacity – indicate that earlier spring melt has been highly beneficial for shrub performance. In addition, the insensitivity of background soil N inputs and coupled shrub-nitrogen dynamics to snow depth suggests that depth effects have been relatively invariant over the period studied.

Keywords: *model-fitting; model-selection; optimisation; plant-resource coupling; shrub allometry; snow dynamics; snow-shrub hypothesis; time-series.*

5.2 Introduction

There have been rapid increases in shrub biomass and tall shrub cover in Arctic tundra environments, commonly termed 'shrubification' (Myers-Smith et al. 2011). The incursion of tall shrub species into tundra environments previously dominated by creeping dwarf shrubs and graminoids has consequences for regional climate: decreased albedo (Juszak et al. 2014) and root

interactions with melting permafrost (Blume-Werry et al. 2019) may both lead to additional climate warming, and this may warm soils thus further melting permafrost. Shrubification may therefore provide a positive feedback to climate warning, as recent increases in shrub biomass have been observed to occur alongside rising air temperatures (Post & Hoye 2013). However, evidence from long-term in-situ warming experiments indicate significant heterogeneity in shrub growth responses to rising temperatures, thought to derive from ecological and landscape mechanisms operating at a local scale (Bjorkman et al. 2019). Variability in shrub responses may arise from climate, ecological interactions, soil conditions, and soil resources (Martin et al. 2017). Without a more holistic understanding of the limitation mechanisms at a local scale, future trajectories of shrub expansion and climate feedbacks are uncertain.

Changes in snow dynamics – including the period of snow cover, timing of snowfall, and snow depth – may directly control shrub growth and spatial expansion while contributing to perceived heterogeneity in shrub-temperature responses. Snow dynamics are variable at a high spatial resolution: topography (Kemppinen et al. 2018) and vegetation structure (i.e. tall shrubs) controls snow depth, as snow is blown and captured in both sheltered areas (Ménard et al. 2014) and by tall and complex woody plants (McCartney et al. 2006), although tall shrubs may also cause faster melt (Pomeroy et al. 2006). Winter snow accumulation may provide a direct mechanical advantage to Arctic plants by reducing exposure to storms and wind while also insulating plant tissues during winter (Rapacz et al. 2014). Temporal variability in snow dynamics may also be significant: the timing and rate of snowmelt are both controlled by air temperature and snow accumulation during winter months (Wipf & Rixen 2016). The growing season can be shortened further than the already-constrained photoperiod by prolonged spring snow cover (Templer 2011). Alternatively, there are disadvantages to reduced winter snow cover and earlier spring snowmelt, as plant tissues can become exposed to early frosts (Bjerke et al. 2015), ice encasement (Milner et al. 2016), or subject to damage deriving from winter warming events (Bokhorst, Bjerke, Davey, et al. 2010). Declines in the snow cover period in the Arctic have even been linked to biodiversity loss through changes in vegetation composition (Niittynen et al. 2018).

Snow dynamics may limit shrub growth through indirect mechanisms. In particular, the presence or absence of snow could have implications for soil nitrogen, shrub growth, and shrub-nitrogen relations. Arctic vegetation can be strongly limited by nitrogen availability, an essential macronutrient for photosynthesis and wood formation (Rossi et al. 2014). Soil nitrogen (N) availability can, however, vary considerably between landscape patches as microtopography influences soil conditions including temperature and moisture (Tape et al. 2012). Snow provides an insulating layer between air and soil temperatures, an effect that is moderated by the timing of snowfall and resultant density of layers within the snowpack (Cook et al. 2007). Snow can also elevate soil temperatures leading to increased N mineralisation (Schimel et al. 2004). The snow-shrub hypothesis was proposed as a positive feedback mechanism whereby increasing shrub aboveground biomass leads to snow insulation of soils, which leads to elevated soil temperatures and greater efficiency of N-mineralising microbes, and increased shrub growth rates as N becomes less limiting (Sturm et al. 2005). A two-year experimental test of the snow-shrub hypothesis in moist tussock identified that increased N uptake was species-specific and occurred in relatively fertile soils (Vankoughnett & Grogan 2013). Snow-induced increases in soil N did not cause increased N uptake for deciduous shrubs in relatively infertile environments (Vankoughnett & Grogan 2013), which may reflect differences in root morphology influenced by previous levels of N availability. In addition, at Toolik Lake experimental snow addition around tall shrubs was met by increased winter soil temperatures but without any increase in decomposition rates over three years (DeMarco et al. 2014). These lines of evidence suggest that a longer temporal extent than a few years may be required to observe medium- to long-term effects of elevated N on root N uptake.

It is plausible that snow dynamics control plant growth both directly and indirectly by affecting soil nitrogen availability. To assess the role of snow in plant growth and plant-nitrogen relations, we sought to integrate long-term datasets that co-occur with recent shrubification trends observed by remote sensing and rising winter air temperatures in the Arctic. Shrub wood ring increments provide an annual indicator of individual shrub growth (Myers-Smith et al. 2015). Wood rings are useful not only for measuring growth: stable isotopes in wood can provide time-series evidence for

growing-season plant water source use ($\delta^{18}O$) (McCarroll & Loader 2004), soil nitrogen availability ($\delta^{15}N$) (McLauchlan et al. 2007; Gerhart & McLauchlan 2014; McLauchlan et al. 2017), and stomatal conductance / stress ($\delta^{13}C$) (Farquhar et al. 1982).

In an Arctic environment where shrub growth has been N-dependent over recent decades (**Chapter 3**), we sought to examine the presence and importance of snow dynamics in plant-nutrient interactions. To achieve this, we aimed to quantify the response of soil N availability – and its relationship with shrub growth at the individual scale – to variability in snow dynamics by investigating these dynamics on a varying spatial-temporal frame of reference (**Figure 5–1**). For spatial scale, we compared highly localised indicators of snow dynamics (stable isotopes) to regional indicators (obtained from earth observation products). For temporal scale, we looked to identify if the mechanisms driving N availability and shrub-N relations could be better explained by fine-grained seasonality. We applied a multi-proxy dendro-isotope and modelling approach to address the following research questions:

1. How important is the snow insulation effect on soil processes for: (a) determining soil nitrogen supply; and (b) determining the growth rate of plant individuals?
2. Does accumulated snow provide a protection effect to shrub individuals, and if so, how does this influence plant-driven N cycling rates?
3. How related are annual, plant-scale proxies of water sources to regional snow dynamics, and are these differences reflected in the mechanisms underlying plant-nitrogen relations?

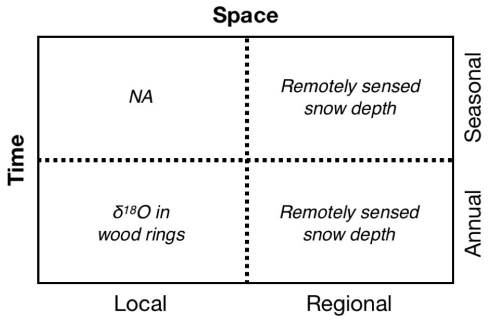

Figure 5–1 Schematic indicating environmental proxy measurements that may capture snow dynamics, and their spatial and temporal scales of reference. Note that seasonal extraction of $\delta^{18}O$ is possible (using earlywood versus latewood) but this can be challenging for slow growing and ring-diffuse deciduous species such as *Salix* spp. in the Arctic.

5.3 Methods

5.3.1 Study Region

The study site is Yuribei, in the central Yamal Peninsula, Russia (68.91°N, 70.23°E). The region is within bioclimatic subzone D of the Arctic tundra biome (Walker et al. 2009), where the temperature regime is characterised by a short growing season where air temperatures rise above zero degrees Celsius between May and September. Growing Degree Days (GDD), however vary substantially between years: weather station data from the nearest weather station (Marre Sale - 69.72°N, 66.82°E) indicates that in recent decades GDD has varied between 133.3°C (1980) and 506.9°C (1994) (Menne et al. 2012). Mean annual air temperatures have increased by 2°C between 1980 and 2013. Recent change has occurred in both climate and vegetation: azonal expansion of tall woody shrubs has occurred primarily within riparian corridors and thaw slumps (Bruce Forbes, *pers. comm.*). The dominant deciduous shrub species is *Salix lanata* L, which grows up to two metres in height in tall shrub patches (Forbes et al. 2009). During a field campaign in July 2013, wood discs were taken from the base of the main stem of 52 Salix *lanata* individuals within a 15km^2 area. Wood discs were collected as close to the soil as possible. Effort was taken to sample from independent genets. Standard dendrochronological techniques were employed to age and cross-date each individual shrub disc. Raw ring widths and the master chronology have been published previously (**Chapter 3**).

5.3.2 Climate and Weather Data

We obtained mean daily air temperature data from the nearest weather station at Marre Sale (69.72°N, 66.82°E), which is 161km from the study region, which is largely flat (Menne et al. 2012). We calculated monthly mean air temperatures from daily time-series. We also obtained monthly and seasonal mean temperature interpolated time-series from the CRU-TS 4.02 data product (Harris et al. 2013) (**Figure 5–2**).

To establish variability in snow dynamics over the study period (1980-2013), we calculated indices of snow depth from earth observation data. The available snow depth data at nearby weather stations

was incomplete, while also representing a local signal. The earth observation data have low spatial resolution (50km) and provides a more regional signal. We obtained daily passive microwave brightness temperature data for the Yamal Peninsula from 1980 – 2013 (SSMI/S). We calculated the Chang and Aschbacher indices for daily snow depth, both of which are modelled on the empirical relationship between brightness temperature and snow depth (Tedesco et al. 2014). We calculated the mean of the indices and used their standard deviation as a measure of uncertainty. The Chang index is based on the direct relationship between snow depth and temperature spectra (Chang et al. 1987):

$$SD = R_c(Tb_{19} + Tb_{37})$$

Here, SD = snow depth, R_c = 1.59cm/K and Tb_{19} and Tb_{37} are brightness temperatures at two frequencies. We also computed snow depth using the Spectral and Polarisation Difference (SPD) algorithm (Aschbacher 1993):

$$SPD = A_0([Tb_{19V} - Tb_{37V}] + [Tb_{19V} - Tb_{19H}]) - A_1$$

Here, A_0 = 0.68 or 0.72 for temperatures below 0°C, and A_1 = -0.67 or -1.24 for temperatures below 0°C (Tedesco et al. 2014). We truncated both indices such that any negative values represented zero snow depth.

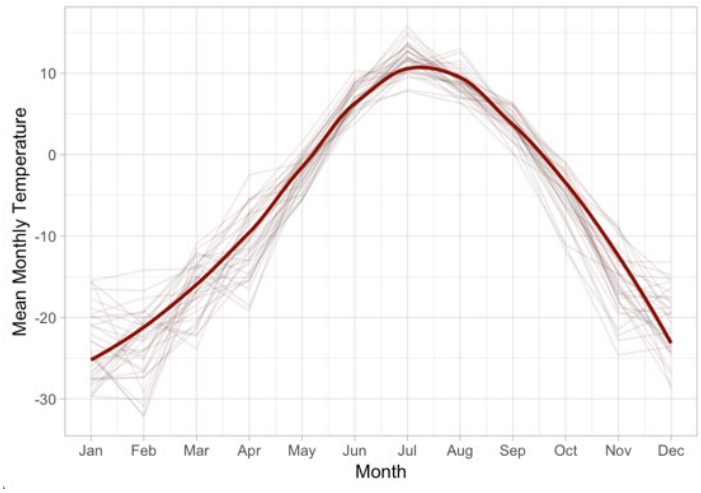

Figure 5–2 Mean monthly temperature profile (bold red) and individual yearly temperature profiles (faint grey) for Yuribei (68.91°N, 70.23°E) derived from the CRU-TS 4.02 dataset (Harris et al. 2013).

5.3.3 Wood $\delta^{15}N$, $\delta^{18}O$ and $\delta^{13}C$ Time-Series

We analysed wood discs to reconstruct annual stable isotope time-series for a subset of the individuals that were used to make the ring width chronology. We selected five shrub discs at random to capture the presence of mechanisms. In addition, dendro-isotope studies of wood $\delta^{18}O$ and $\delta^{13}C$ indicate less noise and greater correlation between individuals than ring width data, thus requiring fewer individuals to produce an absolute mean isotope chronology (Robertson et al. 1997), for example requiring five individuals to capture a common winter precipitation signal in the Russian boreal forest (Holzkämper et al. 2008). Of the five randomly sampled individuals, 2 (shrubs *YUSL03* and *YUSL05*) grew on slightly elevated gentle slopes, whereas the rest were sampled from the lowest elevations in the landscape, growing on thickets close to the Yuribei river main and adjacent channels.

For each of the five shrub discs, we sectioned a one-centimetre wide wood block along the longest radius. We took 30nm thin sections from both the front and reverse of each wood block using a GSL-1 microtome (Gärtner et al. 2014), which was stained and mounted (Gärtner & Schweingruber 2013). We marked the previously cross-dated ring measurements onto digital scans of the thin sections using ImageJ software. Under a macroscope, we used a Stanley blade to separate each annual wood ring: care was taken to minimise cross-contamination by slicing along the grain and referring to the ring lines on both sides of the wood block. The separated wood increments were homogenised to a fine powder using a micro-mill: each sample was milled for 60 minutes in a steel capsule with a single steel ball bearing.

The most appropriate wood components from which to measure stable isotopes differ by element. Plant carbon and oxygen is fixed into wood α-cellulose during the growing season (McCarroll & Loader 2004); nitrogen however is not fixed into any particular component making the analysis of bulk wood appropriate (Gerhart & McLauchlan 2014). For $\delta^{18}O$ and $\delta^{13}C$ analysis, we separated a 20mg subsample from each homogenised shrub wood increment and for each subsample isolated α-cellulose by conducting a fast Brendel extraction as follows (Brendel et al. 2000; Anchukaitis et

al. 2008). First, samples were heated at 120°C with a mixture of 80% acetic acid and 69% nitric acid for 30 minutes. Second, samples were washed with deionised water then 60%, 80% and 100% ethanol, centrifuging before and removing the supernatant after each wash stage. Finally, samples were dried in a 70°C oven. Before final weighing of the samples, these were freeze-dried overnight to remove any remaining moisture. For each required measurement, 0.0325±0.0025mg was weighed into an aluminium capsule. $\delta^{18}O$ and $\delta^{13}C$ were measured using a SerCon Callisto CF-IRMS mass spectrometer at the University of Swansea. We used two standards, an internal α-cellulose and benzoic acid (IAEA-601), to measure analytical error and correct for drift. We ran replicate samples for one in three years of each time-series to quantify standard error for α-cellulose $\delta^{18}O$ and $\delta^{13}C$. From the remaining bulk wood powder for each year and shrub, we weighted 11±0.05mg into a tin capsule. $\delta^{15}N$ and %N content of each sample was analysed with a Thermo Fisher Delta V+ mass spectrometer coupled to a Carlo Erba NC 2500 Elemental Analyzer at the Central Appalachian Stable Isotope Facility, University of Maryland Centre for Environmental Science. Replicate samples were run for one in three years in each time-series. Samples were analysed in random order so that any biases from the mass spectrometer are not structured within time series.

$\delta^{18}O$ was calibrated to delta Standard Mean Ocean Water (SMOW) and $\delta^{13}C$ to delta Pee Dee Belemnite (PDB). In addition, $\delta^{13}C$ values were corrected for each shrub individually to account for changing $\delta^{13}C$ of atmospheric carbon dioxide from anthropogenic CO_2 emissions to the atmosphere (McCarroll et al. 2009).

5.3.4 Individual Modelling of Shrub-Nitrogen Relations

To determine the role of snow and temperature in shrub-nitrogen dynamics, we modelled the relations between shrub individuals and soil nitrogen as simultaneous ordinary differential equations (ODEs). Previous research at Yuribei combined allometric relations with $\delta^{15}N$ and ring width data to assess the nature and strength of N-limitation to *Salix lanata* shrub individuals (**Chapter 3**). In this paper we expand the earlier modelling approach in three key areas: (1) we

increased the temporal resolution from annual to monthly to reflect seasonal variability in climate, light availability and growing conditions and assess the role of seasonality in N-limitation; (2) we included model hypotheses to capture the role of snow in soil N replenishment rates; and (3) we included model hypotheses to represent snow protection on plant material (**Figure 5–3**). We assessed the performance of models for every shrub and hypothesis by measuring goodness-of-fit of each model using a maximum-likelihood approach and a model selection technique (‘*model fitting and model selection’*) (Burnham & Anderson 2007).

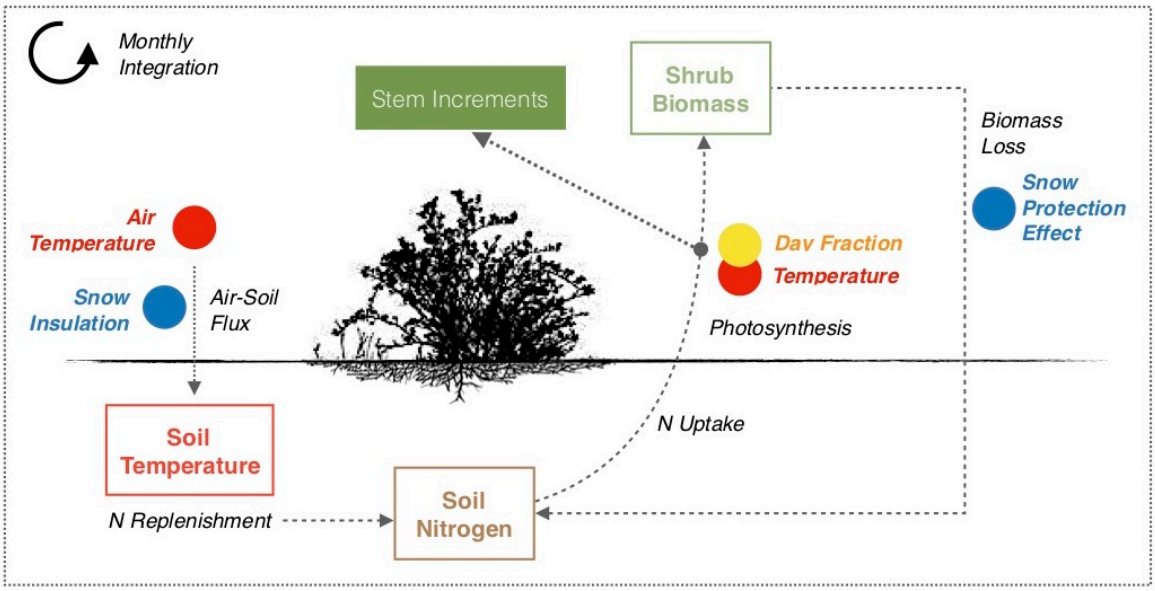

Figure 5–3 Schematic of components within the high-resolution (monthly) shrub-nutrient model. Circles indicate environmental forcing mechanisms on model processes for air temperature (red), light availability (yellow), and snow depth (blue).

5.3.4.1 Nested Model and Components

To assess the mechanisms through which snow may interact with shrub-nitrogen dynamics, we varied mechanistic representations of four key processes within a base model formulation of shrub-nitrogen dynamics. The base shrub-nitrogen model applied in all model hypotheses included: (1) a plant-soil feedback mechanism; and (2) limits to exponential growth that may arise for example from competition or mechanical limits. First, we included a feedback in the base model because N-dependent growth of shrub individuals at this location was found to occur alongside strong litter feedback (**Chapter 3**); the instantaneous plant-soil feedback rate was defined as $\alpha\gamma_B B$, where α = a conversion factor of biomass into nutrient (Jeffers et al. 2012). Second, we applied a Chapman-

Richards asymptotic model (Paine et al. 2011) to add a non-linear constraint to maximum shrub biomass: $g(B) = 1 - \frac{B}{K}$. Here, K = maximum shrub biomass. The coupled ordinary differential equation base model of soil nitrogen (N) and shrub biomass (B) dynamics was:

$$\frac{dB}{dt} = r\left[f(N) \cdot t(B,T) \cdot L_f \cdot \left(1 - \frac{B}{K}\right)\right] - u(B,S)$$

$$\frac{dN}{dt} = y(N,T_{soil}) - \left[f(N) \cdot t(B,T) \cdot L_f \cdot \left(1 - \frac{B}{K}\right)\right] + \alpha u(B,S) - \gamma_N N$$

In the above model formulation are four interchangeable functions: $f(N)$ indicates the functional form of root uptake; $t(B,T)$ is a temperature-dependent effect applied to net photosynthetic rate, $u(B,S)$ is a biomass loss function that may depend on snow depth, $y(N,T_{soil})$ is a monotonically-increasing function that represents a background replenishment rate for soil nitrogen (Huisman 1994) and may be dependent on soil temperature; and $\cdot L_f$ is the light fraction (see **Section 5.3.4.4** below). The choice of model hypotheses for each of these four key processes is discussed below; the components that vary within the base model are listed in full in **Table 5–1**:

Table 5–1 Four model components and their varying hypotheses that were substituted into the shrub-nitrogen base model to form a suite of 24 model hypotheses.

Component	Case	Function
N Nitrogen Uptake	**N1** Continuous uptake	$f(N) = aN$
	N2 Rate-limited root-foraging	$f(N) = \frac{aN}{1 + ahrN}$
T Photosynthetic Rate	**T0** Temperature-independent	$t(B,T) = 1$
	T1 Temperature-dependent: Arrhenius	$t(B,T) = e^{\left(\frac{1000 \cdot E_a (T-298)}{298 \cdot 8.314 \mathrm{T}}\right)}$
R Background Replenishment Rate of Soil Nitrogen	**R0** Temperature-independent	$y(N, T_{soil}) = \lambda$ $c = 1$
	R1 Temperature-dependent microbial activity	$y(N, T_{soil}) = \lambda e^{\left(\frac{1000 \cdot \mathrm{E_a}_{soil} (T_{soil}-298)}{298 \cdot 8.314 \cdot T_{soil}}\right)}$ $c = 1$
	R2 Temperature-dependent microbial activity, with a snow-insulation effect on soil temperature	$y(N, T_{soil}) = \lambda e^{\left(\frac{1000 \cdot \mathrm{E_a}_{soil} (T_{soil}-298)}{298 \cdot 8.314 \cdot T_{soil}}\right)}$ $c = e^{-\rho S}$
L Biomass Loss Rate	**L0** Density-dependent loss rate	$u(B,S) = 1$
	L1 Height-dependent snow protection effect	$u(B,S) = \frac{SpH}{1 + SpH}$

Parameters: E_a = activation energy of temperature-limited photosynthesis; *a* = N-use efficiency; *r* = N-conversion efficiency to biomass; *h* = handling time of N in uptake and incorporation into biomass; *α* = conversion factor of litter into N; γ_B= environmental loss rate of shrub biomass; *K* = asymptotic plant mass owing to mechanical or other constraints; p = snow protection effect; H = shrub height. Time-varying parameters are: *T* =mean air temperature (Kelvin); and S = mean snow depth (cm).

We represented the N-limitation mechanism as two alternative forms to detect if N availability influenced the performance of root scavenging in a non-linear way. N-limited shrub growth was thus represented by two alternative mechanistic representations of root uptake: a simpler linear form ($f(N) = aN$) (**N1**), and a saturating form that represents functional root-foraging (McNickle & Brown 2014): $f(N) = \frac{aN}{1+arhN}$ (**N2**). Here, *a* = N-use efficiency, *r* = N-conversion efficiency to biomass, and *h* = handling time of N in uptake and incorporation into biomass.

To determine the role of temperature in shrub growth over time we included models for temperature-independent growth (**T0**) and temperature-dependent growth (**T1**). Temperature-dependence of biomass production was represented as an Arrhenius response to air temperature (Kim et al. 2007), as this recognises that enzymes involved in photosynthesis respond non-linearly to temperature.

5.3.4.2 Snow and Temperature Effects on Soil-Nitrogen Relations

To assess the effect of snowpack on soil processes, we created three variations of soil background N replenishment $y(N, T_{soil})$. First, we identified a null hypothesis **R0** where N-replenishment is temperature- and snow-independent; we represented this as a linear monotonically increasing function. Second, we proposed that N-replenishment rate may be related directly to soil temperature, as the rate of N-mineralising microbes is dependent on temperature (**R1**). We represented this hypothesis with an Arrhenius function, which reflects the rates of enzyme activity:

$$y(N, T_{soil}) = \lambda e^{\left(\frac{1000 \cdot \mathrm{E_a}_{soil}(T_{soil}-298)}{298 \cdot 8.314 \cdot T_{soil}}\right)}$$

Here, λ is a replenishment constant, $\mathrm{E_a}_{soil}$represents the activation energy for enzyme activity in N-mineralising soil microbes; and T_{soil} is the soil temperature in Kelvin. Third, we proposed the same temperature-dependency of soil processes, but where soil temperature itself is dependent on snow depth (**R2**). The thermodynamic response of soil temperatures to snowpack depth has been demonstrated to have a substantial, asymptotically nonlinear form (Ge & Gong 2010). We use an approach similar to Huang et al. (2017) where the effect of snow is represented through a snow depth insulation regulator *I*:

$$I(S) = 1 - e^{\left(-a\left(\frac{S}{\rho}\right)\right)}$$

Here, *a* represents an insulation effect of snow, *S* is snow water equivalent, and *rho* is the density of the snowpack (Huang et al. 2017). As we are using snow depth directly, we collapsed $-a\frac{S}{\rho}$ into a single estimable parameter for snow insulation, $-pS$.

5.3.4.3 The Mechanical Advantage of Snow Depth

To test for a protective effect of snow on shrub biomass, we modified the environmental loss rate of biomass to account for snow depth. Our null hypothesis (**L0)** represents plant-driven N cycling where the loss rate of plant biomass is determined directly by a density-dependent effect on plant biomass. To represent a snow-sheltering effect on biomass loss rate, we assumed that increasing snow depth increases protection to plant biomass from environmental damage (e.g. exposure to storms, wind, and frost damage) until snow depth is greater than plant height, after which there is no additional protection effect. In addition, we assumed that snow accumulation at lower levels would have a greater protective effect relative to shrub height, as shrubs are structured with increasing biomass towards ground level. We represented our assumptions with a saturating functional form (**L1**):

$$f(B,S) = \frac{SpH}{1 + SpH}$$

Here, H = shrub height as computed using allometric relations, S = snow depth (cm), and p = snow protection factor.

5.3.4.4 Seasonal versus Annual dynamics

We interrogated the $\delta^{15}N$ and ring width data at two temporal resolutions by computing the internal dynamics of biomass and N availability at two different resolutions: annual and monthly resolution. The time-varying forcing parameters – temperature and snow accumulation – were incorporated differently at each of the resolutions. At annual resolution, growing season temperatures were summarised as the mean June – August air temperature. For assessments of the role of winter insulation processes at annual resolution, we represented winter soil temperature as the difference

between growing season air temperature (T_{jja}) and the mean December – February air temperature (T_{djf}), where the difference was derived using Fourier conductivity (c):

$$T_{soil} = T_{jja} - c(T_{jja} - T_{djf})$$

Alternatively, in the monthly resolution formulation we included all individual mean monthly air temperatures. Soil temperature was inferred by extending the base model to acknowledge the role of soil temperature on soil processes:

$$\frac{dT_{soil}}{dt} = -c(T_{soil} - T_{air})$$

Here, *c* represents a conductivity factor between the external air temperature and soil temperature as stated by Newton's law of cooling. Additional considerations were required for the monthly resolution model formulation. To fully capture environmental variability, we computed the models at a monthly temporal resolution, and aggregated rates of change at annual timesteps. Wood increments and nitrogen stocks were calculated on the last day of September in every year, as this represents the last end-of-month in the year that occurs after the growing season. An important additional consideration was light seasonality: in the Arctic the annual cycle from midnight sun to permanent winter darkness provide hard limits to plant photosynthetic activity regardless of snow cover, weather, and climate. We incorporated daylength-related light limitation into our monthly models through an implementation of the Sunrise Equation (Meeus 1998): for a given longitude, latitude, time-zone, and time, a day-length fraction (L_f – between zero and one) is returned. A lookup table is autogenerated to ensure efficiency in model calculation. Growth performance was multiplied by the day length fraction for any given month represented by L_f. For annual resolution models, this was simply set to $L_f = 1$.

5.3.4.5 Representation of Snow Accumulation

To assess the role of winter snow in nitrogen-shrub relations, we ran analyses with three different indicators of snow accumulation: (1) annual resolution remotely sensed October – March mean

snow depth; (2) monthly resolution remotely sensed snow depth; and (3) annual resolution and plant-specific $\delta^{18}O$.

The oxygen isotope composition ($\delta^{18}O$) of wood rings have been demonstrated to proxy local environmental conditions. $\delta^{18}O$ in wood α-cellulose retains a fixed annual signal of the isotopic signature of water sources used by the plant and relative humidity during the growing season (McCarroll & Loader 2004). The oxygen isotopic composition of wood rings ($\delta^{18}O$) is expressed as deviation from the primary reference standard, Vienna Standard Mean Ocean Water (V-SMOW):

$$\delta^{18}O = ([\ (^{18}O/^{16}O)_{\text{sample}} / (^{18}O/^{16}O)_{\text{V-SMOW}}] - 1) \times 1000\ ‰.$$

Although $\delta^{18}O$ in wood derives from the signature of source water, within-plant isotopic fractionation may distort this signal. Transpiration at the leaf surface preferentially removes lighter ^{16}O, isotopically *enriching* leaf water; there may also be an incorporated signal, therefore, of relative humidity as a control on transpiration. For source water, the ability for $\delta^{18}O$ in annual wood increments to proxy winter snow accumulation owing to two fractionating effects acting on water sources in the environment: (1) the temperature effect; and (2) the seasonality of precipitation. The isotopic composition of local precipitation is related to local mean air temperature across mid and high latitudes (the '*temperature effect*'). The temperature effect arises because the processes of evaporation and condensation fractionate the $\delta^{18}O$ of atmospheric water vapour. Evaporation preferentially moves the lighter ^{16}O isotope (i.e. air masses become *isotopically depleted* and water sources *enriched*), as less energy is required than to evaporate ^{18}O. In comparison, atmospheric water vapour is further depleted of ^{18}O during rainout, as the heavier ^{18}O isotope is preferentially condensed. As water progresses from its original source Rayleigh distillation occurs, precipitation becomes isotopically depleted further from its source. Subsequently, as greater condensation occurs in cooler air masses, precipitation in high latitudes is isotopically depleted. Importantly, the *temperature effect* occurs temporally as well as spatially (Kendall & McDonnell 1998). In high latitudes, the $\delta^{18}O$ of precipitation is strongly seasonal with winter snowfall isotopically strongly depleted compared to summer rainfall. A spatial model of precipitation $\delta^{18}O$ parameterised with

the 'Global Network of Isotopes in Precipitation' dataset estimates that winter precipitation at Yuribei is substantially depleted (October–March = -25.33±1.58‰) versus precipitation that falls during the growing season (June–August = -12.15±1.26‰) (Terzer et al. 2013). The seasonal curve of Yuribei precipitation $\delta^{18}O$ is shown in **Supplementary Figure 5–12**.

The use of $\delta^{18}O$ as a potential proxy for snow accumulation here was based on the key assumptions that wood $\delta^{18}O$ records an integrated signal of water sources utilised by the shrub during the growing season; that the relative proportion of water deriving from snowmelt used by shrubs increases in years with greater winter snowfall; and that the $\delta^{18}O$ of melting winter snow is substantially isotopically depleted compared to summer rainfall. Increasing (*enriched*) $\delta^{18}O$ is taken therefore to indicate lower snowfall in the preceding winter to the growing season.

5.3.4.6 Model Fitting and Model Selection

We computed a maximum likelihood estimate (MLE) for each hypothesis and each shrub using a Monte Carlo Markov Chain (MCMC) technique as implemented in the *Bristlecone* MFMS library (**Chapter 6**). Goodness-of-fit for shrub-nitrogen models was measured by applying a bivariate gaussian negative log-likelihood function:

$$-\log\Big(L\big(\sigma_x,\sigma_y,\rho\big)\Big) = 2\pi\sigma_x\sigma_y\sqrt{1-\rho^2} + \frac{1}{2}\left(\frac{z}{1-\rho^2}\right)$$

$$z = \left[\left(\frac{x_{obs}-x_{est}}{\sigma_x}\right)^2 - 2\rho\left(\frac{x_{obs}-x_{est}}{\sigma_x}\cdot\frac{y_{obs}-y_{est}}{\sigma_y}\right) + \left(\frac{y_{obs}-y_{est}}{\sigma_y}\right)^2\right]$$

Here, x_{obs} and x_{est} are the observed and estimated cumulative stem radius, y_{obs} and y_{est} are the observed and estimated $\delta^{15}N$. Three parameters are estimated alongside model parameters: σ_x and σ_y indicate the standard deviation of stem radius and $\delta^{15}N$ respectively, and ρ their covariance.

We used weakly informative Gaussian priors for all parameters (see **Supplementary Information**), which allow efficient exploration of parameter space. We applied the Filzbach MCMC metaheuristic that has been previously used for problems involving complex and heterogeneous

ecological data (e.g. García-Valdés et al. 2015; Rosa et al. 2015). For each MCMC chain, we ran a burn-in phase of 100,000 iterations during which time the scale of the proposal distribution could adapt, followed by a "clean" sampling phase of 200,000 iterations. We ensured that three independent chains with random starting parameter sets converged by calculating the Gelman-Rubin statistic ($\hat{R}$) (Gelman et al. 1992) for every estimated parameter as ensuring that all $\hat{R}$ values were less than 1.1. Uncertainty for each estimated parameter was quantified by the 95% credible interval from the posterior distribution of the combined sampling phases from MCMC chains. To determine the most appropriate model for each shrub, we calculated the Akaike Information Criterion (AICc), which penalises models for their complexity based on the number of estimated parameters and corrects for short time-series (Wagenmakers & Farrell 2004).

5.3.5 Statistical Analysis of Isotope Time Series

To assess how local-scale indicators related to regional climate, we assessed correlations between remotely sensed and weather station environmental covariates and isotope time series. Alongside $\delta^{18}O$, we measured $\delta^{13}C$ to obtain a multi-proxy perspective on plant performance. The carbon isotopic composition of wood rings is expressed as deviation from PDB:

$$\delta^{13}C = ([\ (^{13}C/^{12}C)_{sample} / (^{13}C/^{12}C)_{PDB}] - 1) \times 1000\ ‰.$$

The carbon isotope ratio ($\delta^{13}C$) of wood rings derives from two key fractionating effects: (1) carbon dioxide containing lighter isotopes preferentially pass through stomata into the plant, which causes internal CO_2 to be become isotopically depleted (i.e. lower $\delta^{13}C$); and (2) when internal CO_2 is used for photosynthesis CO_2 containing the lighter isotope is preferentially utilised, leaving the remaining internal CO_2 isotopically enriched (i.e. higher $\delta^{13}C$) (McCarroll & Loader 2004). Taken together, these two fractionation effects indicate that the $\delta^{13}C$ of wood derives from and is a proxy for the ratio of stomatal conductance to photosynthetic rate (McCarroll et al. 2009). In turn, wood $\delta^{13}C$ therefore is likely to reflect environmental variables that control moisture in relatively dry environments, versus variables controlling photosynthetic rates in moist environments.

We used the *dendrochronological program library in R* (Bunn 2008) to calculate mean chronologies for $\delta^{18}O$ and $\delta^{13}C$: we chose to use an arithmetic mean rather than Tukey's biweight robust mean as our data has small sample size. To identify significant relationships between climate and mean isotope time-series, we calculated cross-correlation coefficients directly and with ±2-year lag effects. For $\delta^{18}O$ and $\delta^{13}C$, we calculated cross-correlation with seasonal and monthly subsets of 'total precipitation' and 'mean air temperature' CRU data, including 6-monthly and 3-monthly segments and individual months. We also calculated cross-correlation with remotely sensed snow depth data using four subsets: maximum and mean winter snow depths, cumulative winter snow depth, and the first day of the spring snow-free period (defined as the start day of the first five days where snow depth is zero).

5.4 Results

5.4.1 Regional Snow Dynamics

We reconstructed regional-scale snow dynamics – snow depth and cover – from 1980 to 2018 using earth observation data. The snow cover time-series indicated that the average length of the snow-free season has doubled: season length was 64 – 76 days from 1980 to 1985, but was 128 – 158 days in 2008 – 2013 (**Supplementary Figure 5–9**). Winter (October – March) mean and maximum snow depth summaries indicate that, although there has been an increase from 1980 – 2013, mean inter-annual variability was greater than the temporal trends (**Supplementary Figure 5–10**). Inter-year variability of snow depth was greatest between April and June (**Figure 5–4**). The maximum June snow depth has declined: in the 1980s and 1990s snow was always present in July, but from 2000 to 2013 there were five years of zero June maximum snow depth.

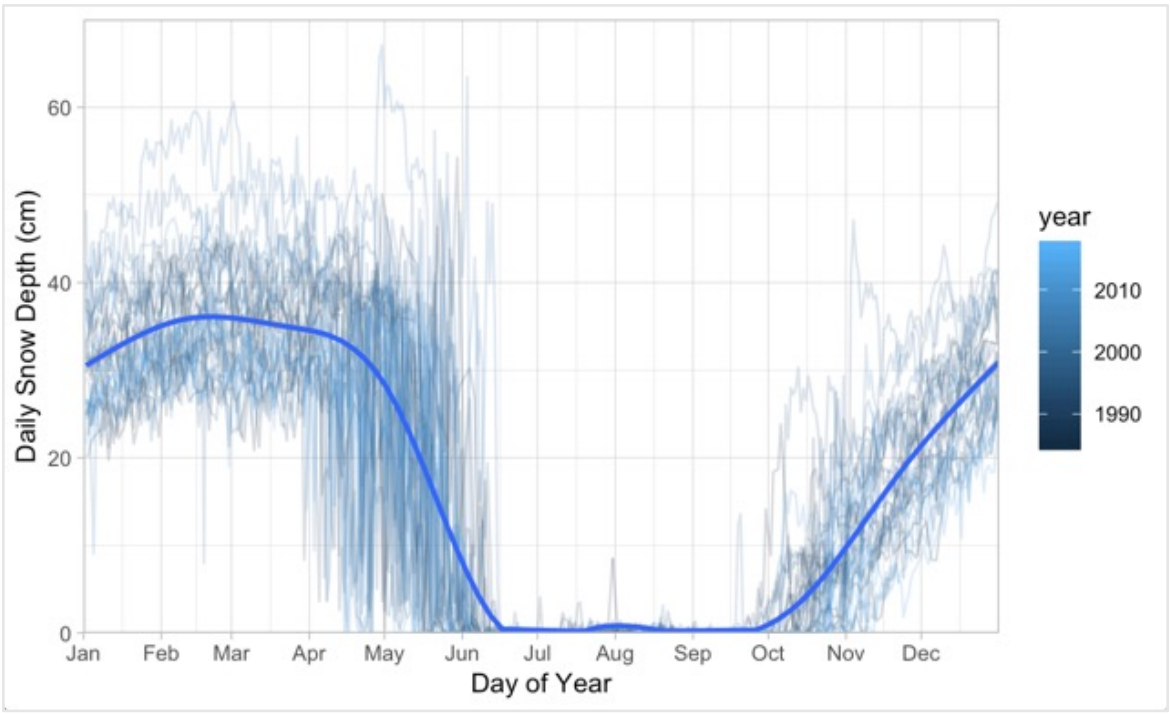

Figure 5–4 Aschbacher snow depth index as calculated for Yuribei showing inter-year variability (1980-2013).

5.4.2 $\delta^{3}C$ and $\delta^{8}O$, and their Relationship with Climate and Snow Dynamics

$\delta^{18}O$ and $\delta^{13}C$ time-series were created for five shrub individuals. Replicate measurements indicated mean standard error of 0.39‰ for $\delta^{13}C$ and 0.28‰ for $\delta^{18}O$ (2dp). The Expressed Population Signal (EPS) for the mean standard chronologies were 0.764 and 0.410 respectively (3dp). We identified significant relationships between climatic indicators and the mean $\delta^{18}O$ and $\delta^{13}C$ chronologies at 95% confidence (**Figure 5–5**). Pearson's product-moment correlation coefficients indicated significant relationships between $\delta^{18}O$ and $\delta^{13}C$ and growing season temperatures. For $\delta^{13}C$, the only significant relation to mean air temperature was for May (*R=0.394, p=0.021*); no monthly combinations were significant. For $\delta^{18}O$ and mean air temperature, significant positive monthly combinations occurred for April – September (*R=0.53, p=0.0013*) and June – August (*R=0.454, p=0.0071*). For both $\delta^{18}O$ and $\delta^{13}C$, we found no significant correlations with precipitation sum for either individual months or month combinations.

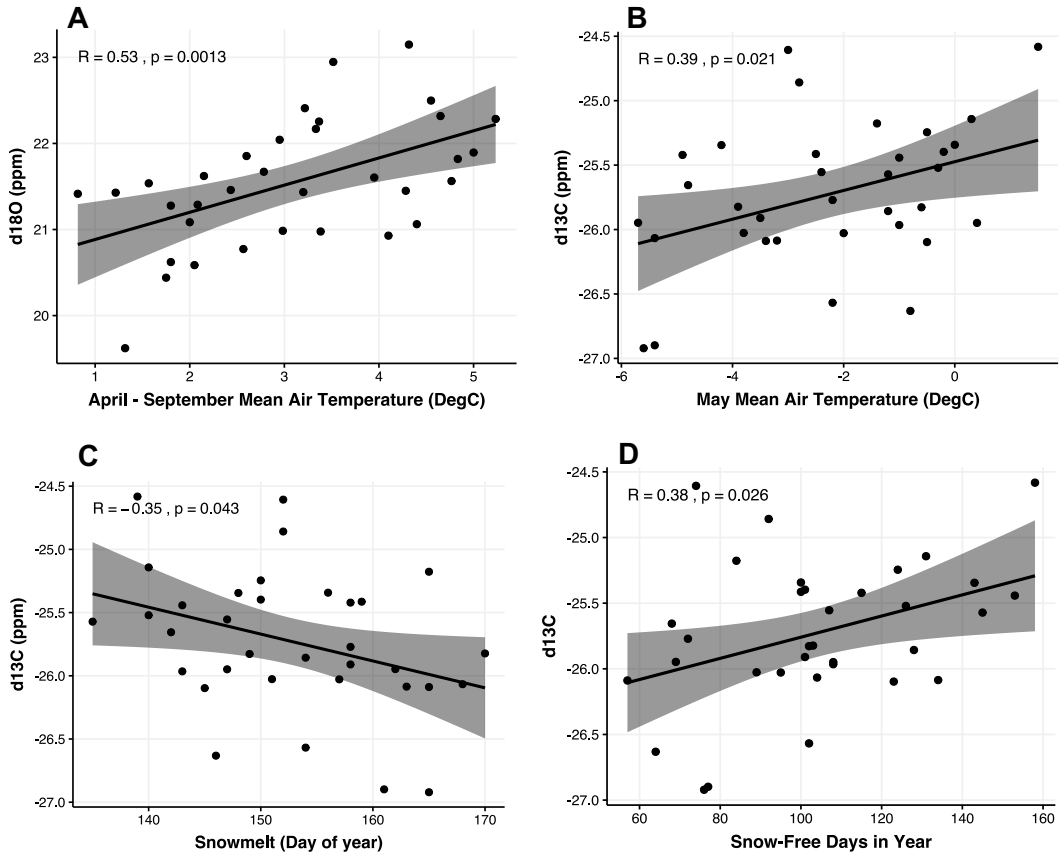

Figure 5–5 Significant correlations between mean $\delta^{18}O$ and $\delta^{13}C$ time series and air temperature and snow characteristics. **A)** $\delta^{18}O$ versus April - September air temperature. **B)** $\delta^{13}C$ versus May air temperature. **C)** $\delta^{13}C$ versus the date of snowmelt. **D)** $\delta^{13}C$ versus snow-free period length.

We identified significant relationships between isotope time-series and regional snow cover duration, but not snow depth. We measured snow cover through two properties: the start day and duration of the snow-free period. $\delta^{13}C$ – but not $\delta^{18}O$ – correlated with snow cover: significant correlations were found between $\delta^{13}C$ and the start of the snow-free period (*R=0.378, p=0.027*), and $\delta^{13}C$ and the duration of the snow-free period (*R=-0.668, p<0.0001*). We did not find any significant correlations between $\delta^{18}O$ and $\delta^{13}C$ and snow depths within the previous winter (October – March mean / October – March maximum).

5.4.3 Snow and Temperature interactions with Growth-Nitrogen Relations

We conducted model-fitting and model-selection of growth-nitrogen dynamics for five shrub individuals to determine the role of regional snow dynamics in the processes governing shrub-nitrogen dynamics. Model-fitting and model-selection indicated that – when representing processes

annually – the $\delta^{15}N$ and ring width time series were best explained by models that did not incorporate snow effects for four of five individuals. Model-selection indicated that a temperature-limiting effect on growth potential did sufficiently improve goodness-of-fit to be included in the best model for two of five individuals. The characteristics for the most appropriate models as selected by Akaike weights are shown in **Table 5–2**:

Table 5–2 Mechanisms selected in the most appropriate models using remotely sensed snow depth and annual resolution for each of five shrub individuals.

Shrub ID	**Mechanisms selected within best model**				**Consistent with Monthly Resolution?**	**Consistent with $\delta^{18}O$ proxy?**
	N Replenishment	Snow Protection	N-Dependent	T-Limit		
YUSL03A	Independent		Linear		Saturating N-dependent	Protection Effect
YUSL05A	Independent		Linear		Yes	Yes
YUSL26A	Independent		Linear	•	Saturating N-dependent	Yes
YUSL29A	Independent		Linear		Yes	Yes
YUSL39A	Independent	•	Linear	•	Saturating N-dependent	No Protection Effect

Consistency metrics identifies differences in the most appropriate mechanisms when assessed using $\delta^{18}O$ as a proxy for localised snow conditions (local scale) and when assessed at monthly temporal resolution using regional, remotely sensed snow indicator.

Using an annual representation of seasonal dynamics and regional indicators of snow accumulation, the Akaike weights indicated that the N replenishment rate in soils was insensitive to variability in soil temperature through the time-series and was therefore also insensitive to snow insulation effects on soil temperature (**Figure 5–6**). Snow insulation of soils did not exert a substantial-enough improvement on goodness-of-fit to be included in any of the most appropriate models for any individual. In addition, model selection indicated an important snow protection effect for one of the five individuals studied. For this shrub individual, the addition of the snow protection effect improved the explanatory power for ring width more-so than for $\delta^{15}N$.

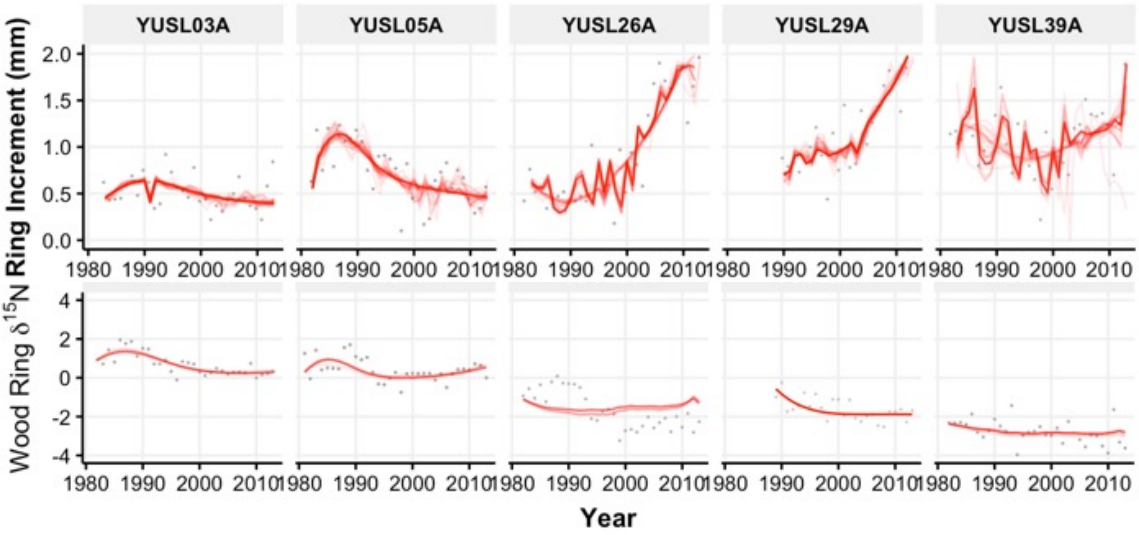

Figure 5–6 Annual model estimated time-series of ring increments using regional (top) and wood ring $\delta^{15}N$ (bottom) at the maximum likelihood estimate for each model hypothesis and each shrub individual. The transparency of each predicted time series is equal to the Akaike Weight.

To determine if higher-resolution seasonality could better explain shrub-nitrogen dynamics – and therefore the role of snow dynamics – we represented shrub-nitrogen dynamics as a monthly process that was responsive to photoperiod and monthly variability in remotely sensed snow depth (**Figure 5–7**). The Akaike weights indicated that the selection of snow and temperature effects was identical given air temperature and mean snow depth observations for each individual month. However, the most appropriate functional form to represent N-dependent shrub growth changed from linear (**N1**) to saturating (**N2**) form for three shrub individuals. Comparison of the likelihoods of the selected models indicated that model fits were better for the annual resolution than monthly resolution models: there was a mean increase in the negative log likelihood values for monthly versus annual models of 2.5 when comparing the model of saturating N-limitation with no temperature or snow effects.

We assessed sensitivity of the most appropriate hypotheses to the spatial representation of snow accumulation (regional versus local). To achieve this, we conducted a separate model-fitting and model-selection assessment of annual models that incorporated the $\delta^{18}O$ time series specific to each shrub as the indicator of snow accumulation (replacing the remotely sensed data). The Akaike weights indicated that the most appropriate model for each shrub did not include temperature or

snow dependent soil processes; this conformed to the findings using the regional snow indicator at both annual and monthly resolution. However, there was variability in the snow protection effect; this was found to be important for one shrub on the slope (*YUSL03*) and not important for *YUSL39*, both results contrary to the results for the regional snow indicator.

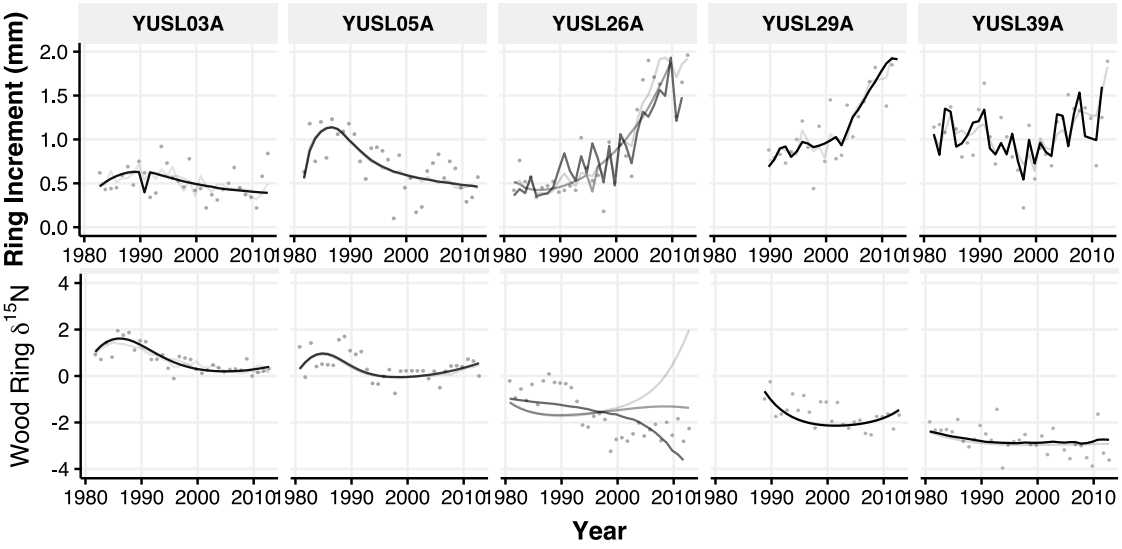

Figure 5–7 Monthly model estimated time-series of ring increments (top) and wood ring $\delta^{15}N$ (bottom) at the maximum likelihood estimate for each model hypothesis and each shrub individual. The transparency of each predicted time series is equal to the Akaike Weight.

5.5 Discussion

5.5.1 Local and Regional Snow Dynamics

Our $\delta^{13}C$ and $\delta^{18}O$ isotope results taken together suggest that snow dynamics may dictate the annual rate of photosynthesis of the shrubs studied primarily by controlling growing-season length. Previous dendrochronological research at this site identified that shrub ring widths at Yuribei are most sensitive to summer temperature rather than precipitation (*see Chapter 3 Appendix*). That ring production is insensitive to moisture is to be expected, as these shrubs have established on poorly drained mesic to wet soils in lowland positions. The $\delta^{13}C$ ratio of wood in plants represents changes in the concentration of CO_2 within plant cells, reflecting the balance between stomatal conductance and photosynthetic rate (McCarroll et al. 2009). We suggest that – given the poorly drained ground here – our $\delta^{13}C$ time-series are more indicative of limiting factors to photosynthetic rate than

variability in moisture stress (that would drive variability in stomatal conductance). We found an inverse relationship between $\delta^{13}C$ and the first day of the first five-day snow free period of the year, a relation between $\delta^{13}C$ and snow-free growing season length, and a relation between $\delta^{13}C$ and May mean air temperature. As the $\delta^{13}C$ correlates with snow and temperature data from independent sources, our results suggest that the annual photosynthetic rate for the five shrub individuals studied has been most responsive to the extension of the growing season due to earlier snowmelt and early season warming, rather than air temperatures during the growing season.

The individual shrub $\delta^{18}O$ time-series exhibited higher inter-shrub variability than the $\delta^{13}C$ time-series, which may indicate that the processes driving variability in $\delta^{18}O$ are more localised to each individual. The mechanisms driving $\delta^{18}O$ are: (1) the isotopic signature of source water uptake, and (2) enrichment by transpiration as moderated by xylem water exchange (see Section 5.3.4.5). As transpiration is primarily moderated by relative humidity, here we suggest that spatial variability between $\delta^{18}O$ of our five individual shrubs may be explained by local-scale partitioning of water sources used within the landscape. Our interpretation would therefore support the use of $\delta^{18}O$ as a mixed local water source signal. In addition, we identified a potential separation in water source access between shrub individuals on the sloped valley sides and those on the flat lowland: inter-series correlations of $\delta^{18}O$ for shrubs on sloped terrain (*YUSL03* and *05*) was 0.40, and for shrubs on flat lowland (*YUSL26*, *29*, and *39*) inter-series correlation was 0.36. The difference suggests that different water sources are accessed during growth between shrubs on the sloping valley sides and the valley plain.

Significant correlations between $\delta^{18}O$ and summer air temperature but not precipitation of the previous winter suggest that inter-annual variability in winter snow accumulation is of lesser importance than variability in the $\delta^{18}O$ of summer rainfall (caused by the *temperature effect* – see Section 5.3.4.5) within water sources accessed by the five shrub individuals. We did not identify a link between the individual scale water source indicator ($\delta^{18}O$) and regional snow cover and snow depth metrics; this suggests that winter snow accumulation at Yuribei has a different or suppressed

variability compared to whole-landscape variability. Tall shrub thickets – including those studied here – occur in lowlands and concave – topographically sheltered – areas within the landscape, which are more likely to capture and accumulate snow. There may therefore have been relatively lower variability in snow depths at the locations of our five shrubs than across the regional landscape as a whole; this may explain the low sensitivity of $\delta^{18}O$ to regional indicators of snow depth, snow cover, and precipitation, as there may have been relatively consistent access to water sources derived from snowmelt. It is plausible that our five shrub individuals may be subject to deep snow in almost every winter. Melting permafrost does not appear a significant component of plant water use here: an application of eco-physiological models of tree ring $\delta^{18}O$ and $\delta^{13}C$ in northern Yakutia indicated that *Larix cajanderi* Major. accesses melting permafrost water during very dry summers (Sidorova et al. 2016). This does not however appear to be the case for the five shrub individuals assessed here, as permafrost water is heavily depleted and would therefore be reflected in an inverse relationship between summer temperature and $\delta^{18}O$.

5.5.2 Snow Sheltering Effects on Shrub Biomass

We only identified a significant snow protection effect on shrub biomass for one of five shrub individuals through interrogation of the ring width and $\delta^{15}N$ time-series with mechanistic models. This finding corroborates with the interpretation of isotope values (**Section 5.5.1**) that there has been low variability in localised snow depths between 1980 – 2013, and the lack of a significant temporal trend in the remotely sensed snow depth (1980 – 2013). The shrub that exhibited an important snow protection effect (*YUSL39*) was the largest shrub studied (in terms of stem radius in 2013) and also exhibited a relatively strong asymptotic effect; it is plausible therefore that snow protective effects only become relevant in the largest individuals as they are able to escape the snow protective layer, and/or that asymptotic growth is a function of snow protection. In addition, a weak snow protection effect was selected for one shrub on the slope (*YUSL03*) when using $\delta^{18}O$ as a proxy for snow; this shrub is taller and more exposed.

5.5.3 The Indirect Role of Snow in Nitrogen-Shrub Dynamics

We expected that soil temperatures would exert an important control on N mineralisation primarily by moderating winter N-mineralisation rates. However, interrogation of the ring width and $\delta^{15}N$ time series for the five shrub individuals indicated that soil microbial processes were insensitive to variability in soil temperature and thus also to variability in winter snow accumulation. The snow-shrub hypothesis suggests that as above-ground shrub biomass increases their fractal form captures snow, which leads to elevated soil temperatures and greater N mineralisation rates (Sturm et al. 2005). Our isotope series and mechanistic modelling from Yuribei suggest that these temperature-dependent effects may be less pronounced in established shrub thickets where snow capture is already occurring; the mechanisms may thus be a more important factor in shrub expansion rather than individual shrub performance.

Lack of sensitivity of decomposition and N mineralisation rates to warming temperatures have been identified in other Arctic tundra environments, although with significant variability in the response coincident with seasonality. This may be due in part to variable seasonality of microbial activity between microbial species (McMahon et al. 2011). At Abisko, Sweden, winter-warming events did not influence winter decomposition rates (Bokhorst, Bjerke, Melillo, et al. 2010); in addition, lab experiments indicated that decomposition primarily occurs within the fall with negligible function during winter (Bokhorst, Bjerke, Melillo, et al. 2010). In Alaskan moist acidic tundra at Toolik Lake, decomposition rates after two decades of warming responded more strongly to warmer winter soil temperatures caused by shrub snow capture than the summer temperature effects (Sistla & Schimel 2013), which was attributed to microbial N-limitation during summer (Sistla et al. 2012). In addition, negative biotic feedbacks were suggested whereby declines in late growing season extracellular enzyme activity (EEA) were related to a seasonal reversal of nutrient stoichiometry (Sistla & Schimel 2013).

We did not find a role for snow depth in predicting annual N availability and shrub growth, as soil processes did not respond to natural variability in air temperatures and model-inferred soil temperature. Winter soil respiration is highly variable across landscapes and has been related to the

direct and indirect effects of snow: directly by insulating soils and indirectly by co-occurring with shrub growth (Elberling 2007). For *Eriophorum vaginatum*-dominated moist tussock, experimentally increased snow depth has led to substantially increased N mineralisation during winter (Schimel et al. 2004). Insensitivity however has been identified within both natural and manipulated shrub-dominated settings. A short-term experimental test of the snow-shrub hypothesis in *Salix*-dominated tall shrub tundra found no link between shrub canopy height and decomposition or N uptake, even though the snowpack did elevate winter soil temperatures (Myers-Smith & Hik 2013). Similarly, for a Scandinavian arctic-alpine space-for-time substitution, winter microbial activity in shrub tundra was found to be the same in snow and snow-free situations (Löffler et al. 2008). Winter snow accumulation at Toolik Lake also did not have a noticeable effect on N mineralisation during winter months, although there was an associated effect on summer N mineralisation rates (DeMarco et al. 2011).

The captured shrub-nitrogen dynamics over 35 years here, and the selection of temperature-independent soil process models – supports the assertation that it may take decades for the impact of nutrient and warming changes to become apparent (Lamb et al. 2011). Microbial biomass has been observed to increase only slowly in response to environmental manipulations with lag-effects of a decade (Rinnan et al. 2007), indicating that indirect mechanisms over the longer-term may be important. Snow may also moderate soil moisture as well as soil temperature such that a simple increase in temperature does not necessarily increase decomposition rates (Aerts 2006). However, this is unlikely for our Yuribei shrubs, as they occur on poorly drained soils and there has been no coincident decline in winter snow accumulation.

5.5.4 Model-Inferred Seasonal Nitrogen Dynamics

We interrogated the $\delta^{15}N$ and ring width data at annual and seasonal (monthly) resolution to examine how seasonality influences shrub-nitrogen dynamics and their relation to snow. There was no difference in the selection of temperature- and snow-dependent hypotheses, which suggests that the role of snow depth was captured by October - March mean depth. In addition, we found that the mechanism of N-limitation varied between the best annual and seasonal models selected by Akaike

weights. For two shrubs, N-dependent growth was best represented as a linear process year-to-year (**N1**) but through a mechanistic *root foraging model* (**N2**) on seasonal time (*YUSL03* and *YUSL26*). The root foraging model represents temporal limits to either photosynthetic rate or uptake such that N foraging by roots takes longer at lower N availability; that the rate-limited model was a more appropriate representation at seasonal resolution suggests that there may be switching between organic and inorganic sources of N during the growing season. Continuous N uptake would be expected when the shrub individual is exchanging carbon with ectomycorrhizal fungi for organic-derived N; this pathway is significant for Arctic tundra shrubs (Hobbie & Högberg 2012). Model-inferred N availability and N uptake at monthly resolution suggest that N availability is greatest at the start of the growing season and declines shortly thereafter. This concurs with observed nutrient pulses coincident with snowmelt, as winter microbial activity can cause accumulation of nutrients under snow insulation (Sistla & Schimel 2013), although seasonal variability in amino acids in arctic soils reflects periods of plant N demand (Weintraub & Schimel 2005).

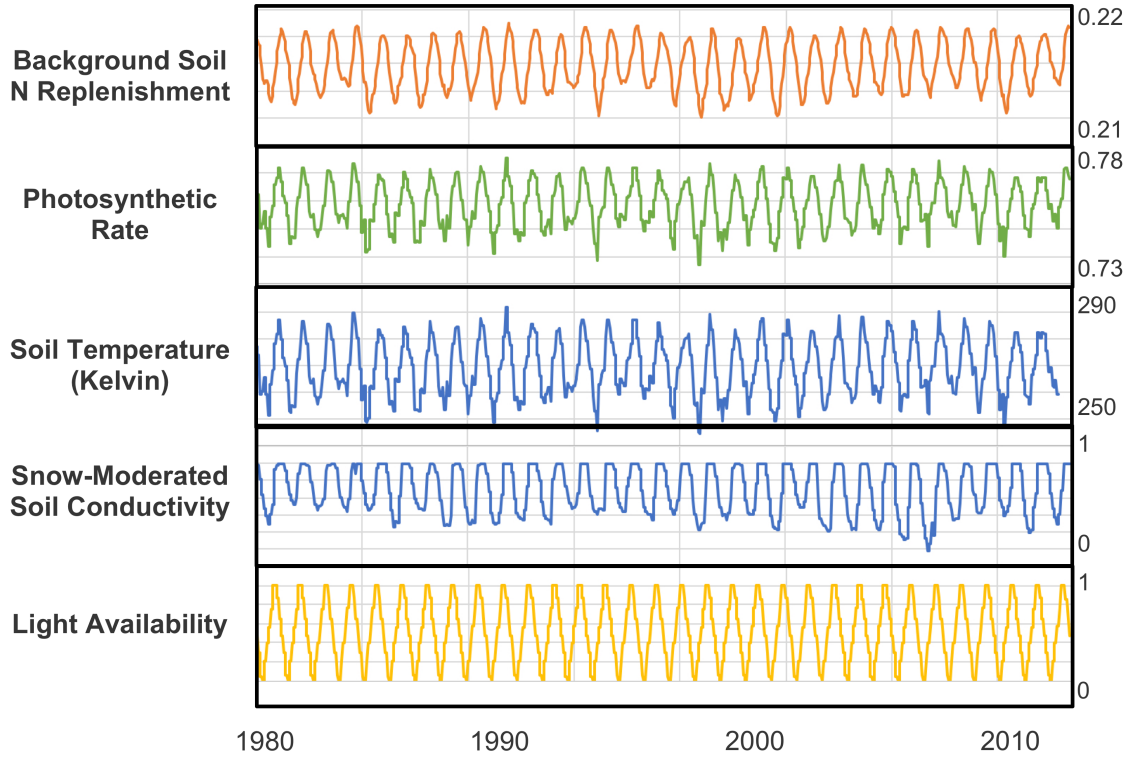

Figure 5–8 Example of model-inferred monthly dynamics by year (x axis) for a monthly-resolution model fit to $\delta^{15}N$ and ring width data that represents N-dependent and temperature-dependent biomass production with temperature-dependent soil N replenishment.

The seasonal dynamics of model-inferred processes reflected expectations of the seasonal cycling of plant growth and N availability within the models when run at monthly resolution (**Figure 5–8**). Shrub growth occurred during the light-dependent growing season with temperature-dependent growth for two of five shrub individuals. The model-inferred N dynamics concurred with observed seasonal patterns of N availability, as N economy is reflected in seasonal cycles: amino acid concentrations are highest at the start of the growing season and lowest at its peak, reflecting temporal variability in plant N demand (Weintraub & Schimel 2005). However, interrogation of the ring width and $\delta^{15}N$ data for the five shrub individuals indicated that there was no improvement in the goodness-of-fit when modelling shrub-nitrogen dynamics as monthly rather than annual processes, contrary to expectations. As the seasonal (monthly) model dynamics account for full seasonality in air temperature and snow depth, we expected these models to predict observed ring width and $\delta^{15}N$ better than annually resolved models. The finding suggests therefore that mechanisms important at monthly but not annual resolution have been overlooked. These could include lag effects of temperature-limitation on shrub photosynthetic rates (Buermann et al. 2018), the timing of xylem formation, and plant nitrogen storage (Millard & Grelet 2010). The timing of xylogenesis in cold-adapted woody plants often responds to particular environmental cues and may only occur as an event during part of the growing season (Rossi et al. 2014). In addition, short-term N-dependent growth may exhibit temporal lags, as Arctic plants that rely on organic N sources may make greater use of internal N storage during the early part of the growing season and root growth is limited by frozen soils (Weintraub & Schimel 2005).

5.5.5 Role of Growing Season Length

The combination of our modelling results and $\delta^{13}C$ and $\delta^{18}O$ time-series suggest the growth of the shrub individuals studied was enhanced by earlier onset of snowmelt and a longer snow-free growing season. Later snowmelt inhibits growth by constraining light availability, although there are positive microclimatic effects on soil moisture and temperature (Kemppinen et al. 2018) and evergreen shrubs have been observed to photosynthesise under snow (Starr & Oberbauer 2003). Given that N availability ($\delta^{15}N$) for all of these shrubs has declined and growing season length has

doubled over the last 35 years, these data may indicate '*terrestrial oligotrophication*' (Craine et al. 2018). In North America, the earlier onset of spring has been associated with increased total N demand for the growing season (Elmore et al. 2016). Craine et al. (2018) suggest that longer growing seasons may have driven Progressive Nitrogen Limitation (PNL); the best-fitting nitrogen-shrub dynamics models here suggest that N uptake for the individual shrubs has increased over time whereas N replenishment has been insensitive to warming summer and winter air temperatures, which would support this hypothesis. The earlier onset of the snow-free growing season may also act negatively on N replenishment, as earlier snowmelt has been noted to cause freezing soil temperatures thus reducing decomposition rates, for example in an alpine shrub-dominated landscape (Baptist et al. 2009). Such mechanisms may be important in the boreal forest, where remotely sensed productivity (NDVI) has been related to later snowmelt and deeper winter snow (Grippa et al. 2005).

5.6 Conclusions

We combined ring width and wood isotope data to determine the role of snow in shrub-nutrient relations over three decades for five *Salix lanata* individuals at Yuribei, Yamal Peninsula. We generated $\delta^{13}C$ and $\delta^{18}O$ time series from wood rings, then interrogated wood $\delta^{15}N$, $\delta^{18}O$ and ring width time series using a mechanistic shrub-nutrient model of nitrogen-dependent growth to assess two key model hypotheses: (1) that soil nitrogen replenishment increases under snow insulation; and (2) that snow protects shrub biomass. We found that temporal variability in individual-scale soil nitrogen and shrub growth could not be better explained by the incorporation of snow insulation effects on soil microbial processes. In fact, soil N replenishment rates were insensitive to increases in air temperature between 1980 and 2013; this suggests that the role of soil warming on soil N mineralisation under natural conditions and over decades may be weaker than previously thought within mature shrub thickets. Variability in snow depth for the period was not sufficient to yield a temperature response that outweighed alternative drivers of variability acting on soil N availability. We also found that snow protection effects were only important for one of five shrub individuals;

this individual was the largest of those studied and therefore was most likely to be subject to snow damage.

The direct and indirect effects of snow on shrub-nutrient relations were identical when assessed using annual versus monthly representations of the dynamics. However, we identified that seasonal versus annual nitrogen-shrub dynamics are best represented by different models of N uptake, which could be related to switching between organic and inorganic N sources. The regional versus local proxies for snow accumulation were not related; individual shrub $\delta^{18}O$ time-series exhibited higher inter-shrub variability than $\delta^{13}C$, which may reflect local-scale partitioning of water source use within the landscape.

Our findings suggest that the length of the snow-free growing season, rather than year-to-year variability in winter snow accumulation, has been the dominant method through which snow dynamics have influenced shrub growth. The $\delta^{18}O$ time series suggest that snow accumulation in this *Salix lanata* thicket was less variable over time than regional-scale snow depth observations indicate, which may either be a reflection of shrub snow capture or topography, or both. The $\delta^{13}C$ time series suggest that the annual photosynthetic rate is increased in years with earlier snowmelt and longer snow-free periods. The lengthening of the growing season may be related to observed declines in N availability as plant uptake of N has increased.

1.1 Acknowledgements

The authors thank Iain Robertson for advice and assistance with $\delta^{18}O$ and $\delta^{13}C$ mass spectrometry and access to University of Swansea facilities, Danielle Sinclair for help with isotope lab procedures.

1.2 Author Contributions

ACM, MMF and ESJ conceptualised the research, conducted analysis and led writing of the manuscript. All authors contributed to the writing of the manuscript.

1.3 References

Aerts, R., 2006. The freezer defrosting: global warming and litter decomposition rates in cold biomes. *Journal of Ecology*, 94(4), pp.713–724.

Anchukaitis, K.J. et al., 2008. Consequences of a Rapid Cellulose Extraction Technique for Oxygen Isotope and Radiocarbon Analyses. *Analytical Chemistry*, 80(6), pp.2035–2041.

Aschbacher, J., 1993. Land surface studies and atmospheric effects by satellite microwave radiometry.

Baptist, F., Yoccoz, N.G. & Choler, P., 2009. Direct and indirect control by snow cover over decomposition in alpine tundra along a snowmelt gradient. *Plant and Soil*, 328(1-2), pp.397–410.

Bjerke, J.W. et al., 2015. Impacts of snow season on ground-ice accumulation, soil frost and primary productivity in a grassland of sub-Arctic Norway. *Environmental Research Letters*, 10(9), p.095007.

Bjorkman, A.D. et al., 2019. Status and trends in Arctic vegetation: Evidence from experimental warming and long-term monitoring. *Ambio*, 23, pp.4294–15.

Blume-Werry, G. et al., 2019. Dwelling in the deep - strongly increased root growth and rooting depth enhance plant interactions with thawing permafrost soil. *The New phytologist*, p.nph.15903.

Bokhorst, S., Bjerke, J.W., Davey, M.P., et al., 2010. Impacts of extreme winter warming events on plant physiology in a sub-Arctic heath community. *Physiologia plantarum*, 140(2), pp.128–140.

Bokhorst, S., Bjerke, J.W., Melillo, J., et al., 2010. Impacts of extreme winter warming events on litter decomposition in a sub-Arctic heathland. *Soil Biology and Biochemistry*, 42(4), pp.611–617.

Brendel, O., Iannetta, P.P.M. & Stewart, D., 2000. A rapid and simple method to isolate pure alpha-cellulose. *Phytochemical Analysis*, 11(1), pp.7–10.

Buermann, W. et al., 2018. Widespread seasonal compensation effects of spring warming on northern plant productivity. *Nature*, 562(7725), pp.110–114.

Bunn, A.G., 2008. A dendrochronology program library in R (dplR). *Dendrochronologia*, 26(2), pp.115–124.

Burnham, K.P. & Anderson, D.R., 2007. *Model Selection and Multimodel Inference*, Springer Science & Business Media.

Chang, A.T.C., Foster, J.L. & Hall, D.K., 1987. Nimbus-7 SMMR Derived Global Snow Cover Parameters. *Annals of Glaciology*, 9, pp.39–44.

Cook, B.I. et al., 2007. The thermoinsulation effect of snow cover within a climate model. *Climate Dynamics*, 31(1), pp.107–124.

Craine, J.M. et al., 2018. Isotopic evidence for oligotrophication of terrestrial ecosystems. *Nature ecology & evolution*, 2(11), pp.1735–1744.

DeMarco, J., Mack, M.C. & Bret-Harte, M.S., 2011. The Effects of Snow, Soil Microenvironment, and Soil Organic Matter Quality on N Availability in Three Alaskan Arctic Plant Communities. *Ecosystems*, 14(5), pp.804–817.

DeMarco, J., Mack, M.C. & Bret-Harte, M.S., 2014. Effects of arctic shrub expansion on biophysical vs. biogeochemical drivers of litter decomposition. *Ecology*, 95(7), pp.1861–1875.

Elberling, B., 2007. Annual soil CO2 effluxes in the High Arctic: The role of snow thickness and vegetation type. *Soil Biology and Biochemistry*, 39(2), pp.646–654.

Elmore, A.J., Nelson, D.M. & Craine, J.M., 2016. Earlier springs are causing reduced nitrogen availability in North American eastern deciduous forests. *Nature plants*, 2(10), p.16133.

Farquhar, G.D., O'Leary, M.H. & Berry, J.A., 1982. On the Relationship Between Carbon Isotope Discrimination and the Intercellular Carbon Dioxide Concentration in Leaves. *Functional Plant Biology*, 9(2), pp.121–137.

Forbes, B.C. et al., 2009. High resilience in the Yamal-Nenets social-ecological system, West Siberian Arctic, Russia. *Proc Natl Acad Sci U S A*, 106(52), pp.22041–22048.

García-Valdés, R. et al., 2015. Effects of climate, species interactions, and dispersal on decadal colonization and extinction rates of Iberian tree species. *Ecological Modelling*, 309-310, pp.118–127.

Gärtner, H. & Schweingruber, F.H., 2013. *Microscopic Preparation Techniques for Plant Stem Analysis*,

Gärtner, H., Lucchinetti, S. & Schweingruber, F.H., 2014. New perspectives for wood anatomical analysis in dendrosciences: The GSL1-microtome. *Dendrochronologia*, 32(1), pp.47–51.

Ge, Y. & Gong, G., 2010. Land surface insulation response to snow depth variability. *Journal of Geophysical Research: Atmospheres*, 115(D8), p.247.

Gelman, A., Science, D.R.S.1992, lnference from iterative simulation using multiple sequences. *Citeseer*.

Gerhart, L.M. & McLauchlan, K.K., 2014. Reconstructing terrestrial nutrient cycling using stable nitrogen isotopes in wood. *Biogeochemistry*, 120(1-3), pp.1–21.

Grippa, M. et al., 2005. The impact of snow depth and snowmelt on the vegetation variability over central Siberia. *Geophysical Research Letters*, 32(21), p.678.

Harris, I. et al., 2013. Updated high-resolution grids of monthly climatic observations - the CRU TS3.10 Dataset. *International Journal of Climatology*, 34(3), pp.623–642.

Hobbie, E.A. & Högberg, P., 2012. Nitrogen isotopes link mycorrhizal fungi and plants to nitrogen dynamics. *New Phytologist*, 196(2), pp.367–382.

Holzkämper, S. et al., Stable Isotopes in Tree Rings as Proxies for Winter Precipitation Changes in the Russian Arctic over the Past 150 Years. *Geochronometria*, 32(-1), pp.37–46.

Huang, Y. et al., 2017. Soil thermal dynamics, snow cover, and frozen depth under five temperature treatments in an ombrotrophic bog: Constrained forecast with data assimilation. *Journal of Geophysical Research: Biogeosciences*, 122(8), pp.2046–2063.

Huisman, J., 1994. The Models of Berendse and Tilman: Two Different Perspectives on Plant Competition? *Functional Ecology*, 8(3), p.282.

Jeffers, E.S. et al., 2012. Climate change impacts on ecosystem functioning: evidence from an Empetrum heathland. *The New phytologist*, 193(1), pp.150–164.

Juszak, I. et al., 2014. Arctic shrub effects on NDVI, summer albedo and soil shading. *Remote Sensing of Environment*, 153, pp.79–89.

Kemppinen, J. et al., 2018. Modelling soil moisture in a high-latitude landscape using LiDAR and soil data. *Earth Surface Processes and Landforms*, 43(5), pp.1019–1031.

Kendall, C. & McDonnell, J.J., 1998. *Isotope Tracers in Catchment Hydrology*, Elsevier Science Limited.

Kim, S. et al., 2007. Temperature dependence of growth, development, and photosynthesis in maize under elevated CO2. *Environmental and Experimental Botany*, 61(3), pp.224–236.

Lamb, E.G. et al., 2011. A High Arctic soil ecosystem resists long-term environmental manipulations. *Global Change Biology*, 17(10), pp.3187–3194.

Löffler, U.C.M., Cypionka, H. & Löffler, J., 2008. Soil microbial activity along an arctic-alpine altitudinal gradient from a seasonal perspective. *European Journal of Soil Science*, 59(5), pp.842–854.

Martin, A.C. et al., 2017. Shrub growth and expansion in the Arctic tundra: an assessment of controlling factors using an evidence-based approach. *Environmental Research Letters*, 12(8), p.085007.

McCarroll, D. & Loader, N.J., 2004. Stable isotopes in tree rings. *Quaternary Science Reviews*, 23(7-8), pp.771–801.

McCarroll, D. et al., 2009. Correction of tree ring stable carbon isotope chronologies for changes in the carbon dioxide content of the atmosphere. *Geochimica et Cosmochimica Acta*, 73(6), pp.1539–1547.

McCartney, S.E., Carey, S.K. & Pomeroy, J.W., 2006. Intra-basin variability of snowmelt water balance calculations in a subarctic catchment. *Hydrological Processes*, 20(4), pp.1001–1016.

McMahon, S.K., Wallenstein, M.D. & Schimel, J.P., 2011. A cross-seasonal comparison of active and total bacterial community composition in Arctic tundra soil using bromodeoxyuridine labeling. *Soil Biology and Biochemistry*, 43(2), pp.287–295.

McNickle, G.G. & Brown, J.S., 2014. When Michaelis and Menten met Holling: towards a mechanistic theory of plant nutrient foraging behaviour. *AoB PLANTS*, 6, p.7.

Meeus, J., 1998. *Astronomical Algorithms*,

Menne, M.J. et al., 2012. An Overview of the Global Historical Climatology Network-Daily Database. *dx.doi.org*, 29(7), pp.897–910.

Ménard, C.B., Essery, R. & Pomeroy, J., 2014. Modelled sensitivity of the snow regime to topography, shrub fraction and shrub height. *Hydrology and Earth System Sciences*, 18(6), pp.2375–2392.

Millard, P. & Grelet, G.-A., 2010. Nitrogen storage and remobilization by trees: ecophysiological relevance in a changing world. *Tree Physiology*, 30(9), pp.1083–1095.

Milner, J.M. et al., 2016. Experimental icing affects growth, mortality, and flowering in a high Arctic dwarf shrub. *Ecology and evolution*, 6(7), pp.2139–2148.

Myers-Smith, I.H. & Hik, D.S., 2013. Shrub canopies influence soil temperatures but not nutrient dynamics: An experimental test of tundra snow-shrub interactions. *Ecology and evolution*, 3(11), pp.3683–3700.

Myers-Smith, I.H. et al., 2015. Methods for measuring arctic and alpine shrub growth: A review. *Earth-Science Reviews*, 140, pp.1–13.

Myers-Smith, I.H. et al., 2011. Shrub expansion in tundra ecosystems: dynamics, impacts and research priorities. *Environmental Research Letters*, 6(4), p.045509.

Niittynen, P., Heikkinen, R.K. & Luoto, M., 2018. Snow cover is a neglected driver of Arctic biodiversity loss. *Nature Climate Change*, 8(11), pp.997–1001.

Paine, C.E.T. et al., 2011. How to fit nonlinear plant growth models and calculate growth rates: an update for ecologists. *Methods in Ecology and Evolution*, 3(2), pp.245–256.

Pomeroy, J.W. et al., 2006. Shrub tundra snowmelt. *Hydrological Processes*, 20(4), pp.923–941.

Post, E. & Hoye, T.T., 2013. Advancing the long view of ecological change in tundra systems. *Philosophical Transactions of the Royal Society B: Biological Sciences*, 368(1624), pp.20120477–20120477.

Rapacz, M. et al., 2014. Overwintering of herbaceous plants in a changing climate. Still more questions than answers. *Plant Science*, 225, pp.34–44.

Rinnan, R. et al., 2007. Fifteen years of climate change manipulations alter soil microbial communities in a subarctic heath ecosystem. *Glob Chang Biol*, 13(1), pp.28–39.

Robertson, I. et al., 1997. Signal strength and climate relationships in 13C/12C ratios of tree ring cellulose from oak in east England. *Journal of Geophysical Research: Atmospheres*, 102(D16), pp.19507–19516.

Rosa, I.M.D. et al., 2015. Modelling land cover change in the Brazilian Amazon: temporal changes in drivers and calibration issues. *Regional environmental change*, 15(1), pp.123–137.

Rossi, S. et al., 2014. Control over Growth in Cold Climates. In *Trees in a Changing Environment*. Plant Ecophysiology. Dordrecht: Springer, Dordrecht, pp. 191–219.

Schimel, J.P., Bilbrough, C. & Welker, J.M., 2004. Increased snow depth affects microbial activity and nitrogen mineralization in two Arctic tundra communities. *Soil Biology and Biochemistry*, 36(2), pp.217–227.

Sidorova, O.V. et al., 2016. Application of eco-physiological models to the climatic interpretation of δ13C and δ18O measured in Siberian larch tree-rings. *Dendrochronologia*, 39, pp.51–59.

Sistla, S.A. & Schimel, J.P., 2013. Seasonal patterns of microbial extracellular enzyme activities in an arctic tundra soil: Identifying direct and indirect effects of long-term summer warming. *Soil Biology and Biochemistry*, 66, pp.119–129.

Sistla, S.A., Asao, S. & Schimel, J.P., 2012. Detecting microbial N-limitation in tussock tundra soil: Implications for Arctic soil organic carbon cycling. *Soil Biology and Biochemistry*, 55, pp.78–84.

Starr, G. & Oberbauer, S.F., 2003. Photosynthesis of Arctic Evergreens Under Snow: Implications for Tundra Ecosystem Carbon Balance. *Ecology*, 84(6), pp.1415–1420.

Sturm, M. et al., 2005. Winter Biological Processes Could Help Convert Arctic Tundra to Shrubland. *Bioscience*, 55(1), p.17.

Tape, K.D. et al., 2012. Landscape Heterogeneity of Shrub Expansion in Arctic Alaska. *Ecosystems*, 15(5), pp.711–724.

Tedesco, M. et al., 2014. Remote sensing of snow depth and snow water equivalent. In *Remote Sensing of the Cryosphere*. Tedesco/Remote Sensing of the Cryosphere. Chichester, UK: John Wiley & Sons, Ltd, pp. 73–98.

Templer, P.H., 2011. Changes in winter climate: soil frost, root injury, and fungal communities. *Plant and Soil*, 353(1-2), pp.15–17.

Terzer, S. et al., 2013. Global isoscapes for d18O and d2H in precipitation: improved prediction using regionalized climatic regression models. *Hydrology and Earth System Sciences*, 17(11), pp.4713–4728.

Vankoughnett, M.R. & Grogan, P., 2013. Nitrogen isotope tracer acquisition in low and tall birch tundra plant communities: a 2 year test of the snow–shrub hypothesis. *Biogeochemistry*, 118(1-3), pp.291–306.

Wagenmakers, E.-J. & Farrell, S., 2004. AIC model selection using Akaike weights. *Psychonomic Bulletin & Review*, 11(1), pp.192–196.

Walker, D.A. et al., 2009. The Circumpolar Arctic vegetation map. *Journal of Vegetation Science*, 16(3), pp.267–282.

Weintraub, M.N. & Schimel, J.P., 2005. The seasonal dynamics of amino acids and other nutrients in Alaskan Arctic tundra soils. *Biogeochemistry*, 73(2), pp.359–380.

Wipf, S. & Rixen, C., 2016. A review of snow manipulation experiments in Arctic and alpine tundra ecosystems. *Polar Research*, 29(1), pp.95–109.

5.7 Supplementary Material

5.7.1 Snow Dynamics from Earth Observation

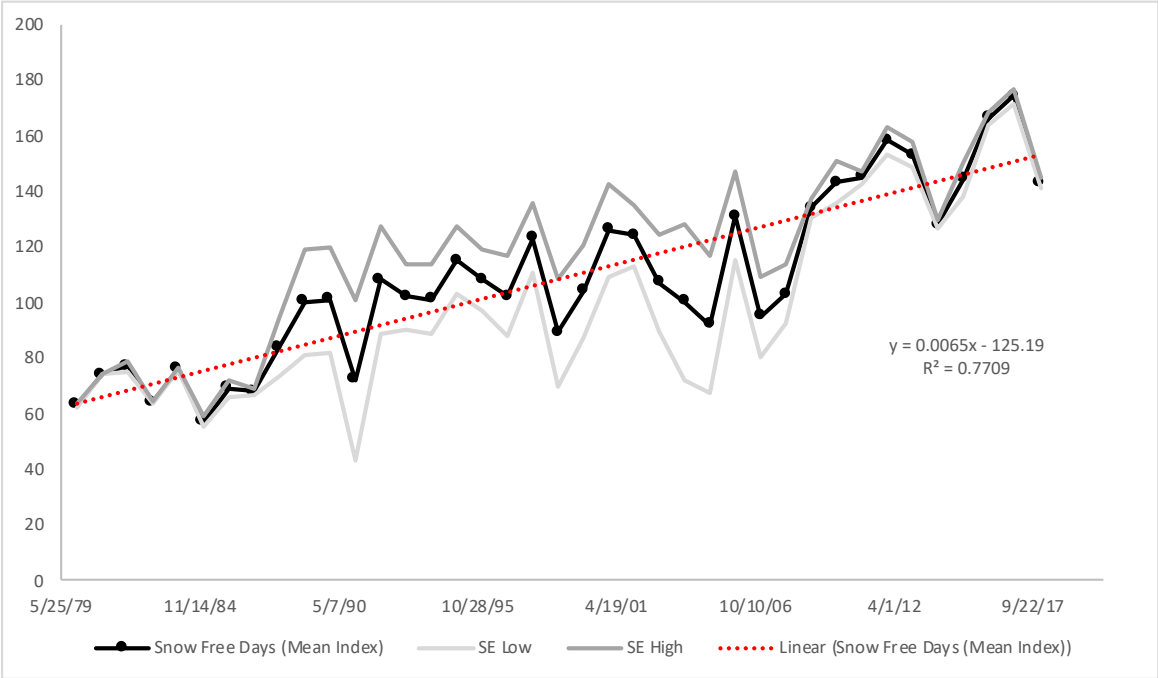

Figure 5–9 Annual snow-free days as a mean of Chang, Aschbacher, and Foster indices. Standard error represented by the standard deviation between the three indices.

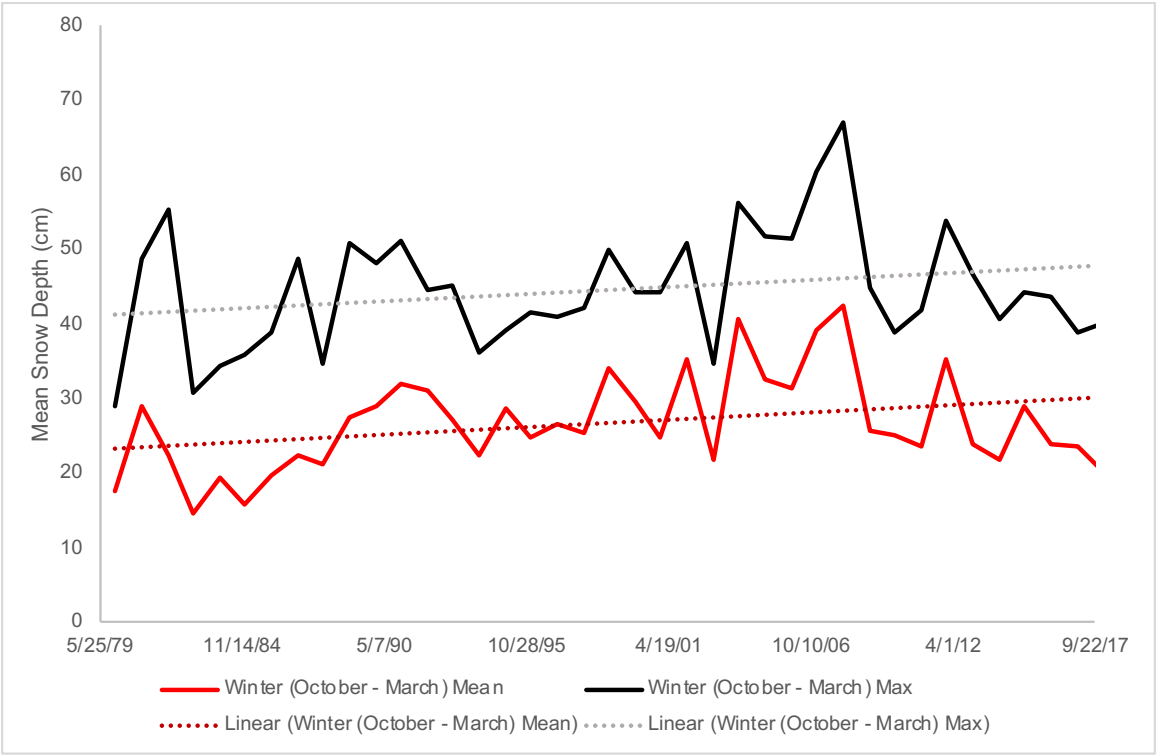

Figure 5–10 Annual winter mean and maximum snow depth derived from the mean of Chang, Aschbacher and Foster daily snow depth indices.

5.7.2 Isotope characteristics for $\delta^{18}O$ and $\delta^{13}C$

In this study we used $\delta^{18}O$ and $\delta^{13}C$ isotopes from individual wood rings. We found a significant relationship between the individual values of $\delta^{18}O$ and $\delta^{13}C$ (**Figure 5–11**).

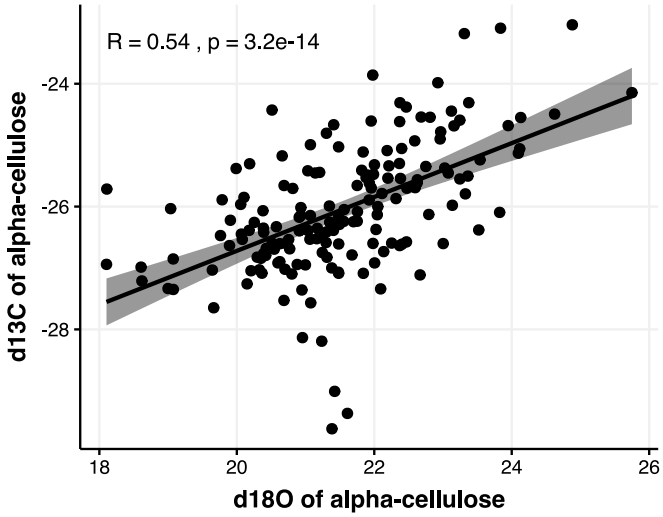

Figure 5–11 Relationship between oxygen and carbon stable isotopes of wood rings for five *Salix lanata* shrubs at Yuribei.

The interpretation of $\delta^{18}O$ as a water source signal relies on the seasonal variability of $\delta^{18}O$ in precipitation. We intersected a global isoscapes product to obtain monthly precipitation $\delta^{18}O$ for Yuribei (**Figure 5–12**); the product was derived from *Global Isotopes in Precipitation* network data (Terzer et al. 2013).

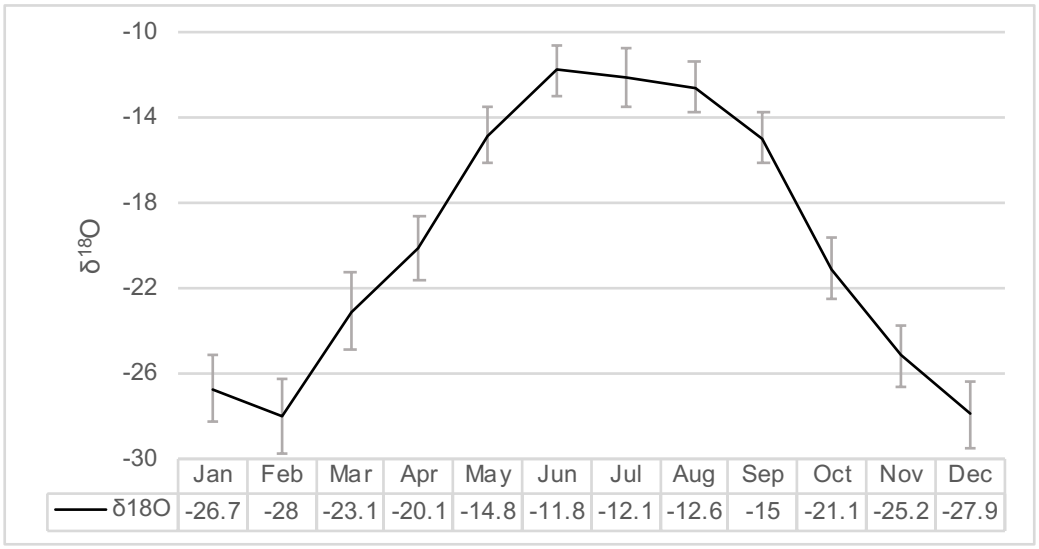

Figure 5–12 Monthly precipitation mean $\delta^{18}O$ at Yuribei. *From Terzer et al. 2013.*

5.7.3 Model Selection

We examined the influence of snow and temperature on the growth of five shrub individuals by interrogating $\delta^{15}N$ and ring width time-series with model hypotheses for the period 1980 – 2013. The best-fitting model was identified for each individual by converting likelihood values to Akaike weights. The full Akaike weights are displayed in **Table 5–3**:

Table 5–3 Akaike weights and negative log likelihoods for high-resolution (monthly) model fits

Snow	N	T	R	L	YUSL03A	YUSL05A	YUSL26A	YUSL29A	YUSL39A
	N2	T0	R0	L0	**80.2** (37.41)	**15.3** (57.79)	0 (111.78)	0 (41.28)	0 (78.66)
	N2	T1	R0	L0	**6.9** (37.14)	3.6 (56.63)	**50.2** (100.86)	0 (40.8)	**11.9** (70.05)
RS	N2	T0	R0	L1	0.5 (39.69)	0.3 (59.03)	0 (121.36)	0 (40.13)	0 (90.22)
RS	N2	T1	R0	L1	0.3 (37.3)	0 (60.27)	0.1 (104.56)	0 (40.23)	**86** (65.17)
	N2	T0	R1	L0	**8.5** (36.94)	0.4 (58.83)	0 (121.63)	0 (43.52)	0 (88.05)
	N2	T1	R1	L0	1.3 (35.77)	0.6 (55.56)	0 (108.43)	0 (36.81)	0.1 (72.6)
RS	N2	T0	R1	L1	0.4 (37.03)	0 (58.35)	0 (117.07)	0 (42.58)	0 (83.29)
RS	N2	T1	R1	L1	0 (50.77)	0 (54.9)	0 (106.4)	0 (38.66)	0.4 (67.29)
RS	N2	T0	R2	L0	0 (45.77)	0.3 (56.36)	0 (123.79)	0 (36.7)	0 (79.37)
RS	N2	T1	R2	L0	0 (35.79)	0 (58.17)	0 (103.87)	0 (38.2)	0.5 (67.1)
RS	N2	T0	R2	L1	0 (36.48)	0 (56.72)	0 (123.55)	0 (36.24)	0 (87.83)
RS	N2	T1	R2	L1	0 (37.47)	0 (53.83)	0 (128.87)	0 (36.59)	0 (65.79)
	N1	T0	R0	L0	0 (48.92)	**61.8** (58.76)	**31.4** (106.3)	**87.1** (36.57)	0 (85.14)
	N1	T1	R0	L0	0 (47.49)	0 (67.58)	0 (113.09)	**9.3** (35.27)	0 (78.62)
RS	N1	T0	R0	L1	0.1 (44.2)	**10.8** (58.14)	0.8 (107.65)	1.2 (37.29)	0 (86.59)
RS	N1	T1	R0	L1	0 (49.85)	3.4 (56.69)	0 (110.5)	0 (36.32)	1 (72.52)
	N1	T0	R1	L0	0 (46.08)	0 (70.16)	4.3 (105.93)	2.3 (36.68)	0 (87.7)
	N1	T1	R1	L0	0 (47.51)	0 (67.47)	**13.1** (102.2)	0 (36.79)	0 (75.96)
RS	N1	T0	R1	L1	1.7 (38.52)	0.1 (60.75)	0 (123.09)	0 (37.05)	0 (90.47)
RS	N1	T1	R1	L1	0 (47.85)	0.5 (55.76)	0 (105.14)	0 (37.09)	0 (79.1)
RS	N1	T0	R2	L0	0 (51.45)	2.7 (56.92)	0 (108.42)	0 (36.92)	0 (84.94)

RS	N1	T1	R2	L0	0 (47.05)	0.2 (56.64)	0 (113.03)	0 (36.95)	0 (75.78)
RS	N1	T0	R2	L1	0 (43.41)	0.1 (56.92)	0 (111.45)	0 (36.78)	0 (85.26)
RS	N1	T1	R2	L1	0 (47.98)	0 (66.6)	0 (105.56)	0 (36.54)	0 (72.29)

Akaike weights expressed as percentages to one decimal place; negative log likelihood values in brackets.

The same 24 model hypotheses were also assessed using an annual temporal resolution. In addition, we assessed if the representation of snow accumulation changed the best model as predicted by Akaike weights; Akaike weights were thus calculated separately within each representation. The Akaike weights are shown in **Table 5–4**:

Table 5–4 Akaike weights for all model hypotheses using (a) earth observation and (b) local indicators for snow accumulation

Hypothesis				Earth Observation					Local Indicator ($\delta^{18}O$)				
N	**T**	**R**	**L**	**03A**	**05A**	**26A**	**29A**	**39A**	**03A**	**05A**	**26A**	**29A**	**39A**
Sat	No	R0	No	**16.8**	**7.3**	0	3.8	0	2.9	1.8	0	9.2	0
Sat	Yes	R0	No	1.5	1.2	**38.8**	0	**17.5**	0	0.5	0	18	0
Sat	No	R0	Yes	0.1	0.7	0	0	0	0	0.7	0	0	0
Sat	Yes	R0	Yes	0	0.1	1.1	0	0	0	0	0	0	0
Sat	No	R1	No	0.1	4.1	0	0	0	0	0.6	0	0	0
Sat	Yes	R1	No	0	0.3	0	0	0	0	0.1	0	0	0
Sat	No	R1	Yes	0	0.1	0	0	0	0	0	0	0	0
Sat	Yes	R1	Yes	0	0.3	0	0	0	0	0	0	0	0
Sat	No	R2	No	0	0	0	0	0	0	0	0	0	0
Sat	Yes	R2	No	0	0	0	0	0	0	0	0	0	0
Sat	No	R2	Yes	0	0	0	0	0	0	0	0	0	0
Sat	Yes	R2	Yes	0	0	0.3	0	0	0	0	0	0	0
Lin	No	R0	No	**62.3**	**58.6**	0	**91.3**	0.2	0.7	**85.5**	0	**70.9**	3.8
Lin	Yes	R0	No	**11.9**	**8.3**	**59**	2.9	**13.3**	1.6	6.4	**99.5**	0.8	**96.1**
Lin	No	R0	Yes	1.5	**7.6**	0	1.9	0	**77.4**	4.1	0	0	0
Lin	Yes	R0	Yes	0.3	0.8	0.8	0	**67.3**	0.1	0	0.4	0	0
Lin	No	R1	No	4.5	0.4	0	0	0	8.3	0.2	0	0.1	0
Lin	Yes	R1	No	0.1	**9.2**	0	0	1.1	0.3	0	0	0	0

Lin	No	R1	Yes	0.1	0.5	0	0	0	1.1	0	0	0	0
Lin	Yes	R1	Yes	0	0	0	0	0	0	0	0	0	0
Lin	No	R2	No	0.6	0.4	0	0.1	0	7.1	0	0	0.4	0
Lin	Yes	R2	No	0	0	0.1	0	0.4	0.2	0	0	0.4	0
Lin	No	R2	Yes	0	0	0	0	0	0.1	0	0	0	0
Lin	Yes	R2	Yes	0	0	0	0	0.1	0	0	0	0	0

Akaike weights expressed as percentages to one decimal place.

For model-fitting and model-selection, we used weakly informative priors set as 1/6 of the width of the maximum parameter bounds as specified in **Table 5–5**.

Table 5–5 Parameter starting bounds used in analysis

Parameter	Starting Minimum	Starting Maximum	Constraints
Base Model			
λ	0.050	0.500	Only positive
γ_B	0.001	0.010	Only positive
γ_N	0.001	0.010	Only positive
ρ	-0.500	0.500	Unconstrained
σ_x	0.001	0.500	Only positive
σ_y	0.001	0.500	Only positive
N Replenishment			
$E_{a_{soil}}$	5.000	30.00	Only positive
c	0.001	0.200	Between 0 and 1
Snow Protection			
p	0.001	1.000	Only positive
Temperature Effect on Photosynthesis			
E_a	30.00	40.00	Only positive

Chapter 6

Bristlecone: An F# library for model-fitting and model-selection of ecological time-series models

This paper has been made available as a preprint and feedback is being taken into account in preparation of the final manuscript.

Martin, Andrew C. 2019. “Bristlecone: An F# Library for Model-fitting and Model-selection of Ecological Time-series Data.” OSF Preprints. September 6. doi:10.31219/osf.io/zt2wn.

Bristlecone: An F# library for model-fitting and model-selection of ecological time-series models

6.1 Abstract

Environmental archives such as sediment cores and tree rings provide important insights on the timing and rates of change in biodiversity and ecosystem function over the long-term. Such datasets are often analysed using empirical methods, which limits their ability to address ecological questions that seek to understand underlying ecological mechanisms and processes. Top down modelling approaches – where data is confronted with simple ecological models – can be used to infer the presence, form, and strength of mechanisms of interest. To aid adoption of time-series mechanistic modelling for long-term ecology, we created a F# library, *Bristlecone*, that can be used to apply this approach using a Model-Fitting and Model-Selection workflow. Our objective with *Bristlecone* was to create a library that could be used to efficiency and effectively conduct a full MFMS analysis for long-term ecological problems. We incorporated techniques to address specific challenges with environmental archives, including uneven time steps from age-depth models (for sediment cores), and allometry and seasonality (for tree rings). We include an example analysis to demonstrate functionality of *Bristlecone*. Our solution presents a straightforward, repeatable, and highly parallel method for conducting inference for long-term ecological problems.

Keywords: *ecological models; dendroecology; dendrochronology; long-term ecology; palaeoecology; mechanistic modelling; model-fitting and model-selection.*

6.2 Introduction

Time-series observations of ecological phenomena and the environment provide essential insights into rates of change, the order of processes, and the resilience or otherwise of ecological systems (Willis et al. 2010). Common sources of long-term environmental time-series are sediment cores, tree rings, and historical records. Analyses that utilise time-series overcome limitations in space-for-time and chronosequence approaches, where the order and relative magnitudes of processes cannot necessarily be determined (Johnson & Miyanishi 2008).

Time-series data of long-term environmental processes are often interrogated using empirical methods. For example, tree rings provide direct and annually resolved observations of plant growth through time. Standard dendrochronological techniques involve correlation to assess the sensitivity of ring-width series to environmental variables such as air temperature and precipitation (Fritts 1976). Similar correlative approaches may also be applied to time-series of direct and indirect proxies measured in sedimentary sequences; for example, pollen counts may be correlated with paleoclimate reconstructions to determine which plant taxa occur with which climate conditions (Binney et al. 2017). Alternatively, palaeoenvironment may be reconstructed by applying modern analogues to sedimentary time-series such as charcoal or geochemistry; statistical analysis is then performed to identify the relationship between biodiversity and the environment (Blaauw et al. 2019; Birks et al. 2014).

There is an increasing importance for rich sedimentary and tree-ring datasets to be able to contribute towards understanding the underlying ecological processes that give rise to observed patterns and trends. Top-down modelling approaches – where simple theoretical models are applied to complex systems (Poorter et al. 2013) – can provide insights into the mechanisms operating within a study system, and their rates. This approach is unlike forward- or projection-modelling where current knowledge is projected forward in time; rather here we aim to infer the structure and parameters of processes that drive previous observations (Peng et al. 2011). Model-fitting and model-selection (MFMS) strategies may be implemented to identify the most appropriate model structure and model

parameters to best explain observed time-series data (Bonsall & Hastings 2004; Archontoulis & Miguez 2015). MFMS approaches have been previously applied to proxy information from sediment cores to assess the underlying causes of the rise and decline of key plant taxa (Jeffers et al. 2011); and to wood rings to identify the strength of limitations on plant growth (Martin et al. n.d.).

Here we describe a library called ***Bristlecone*** that enables the full model-fitting and model-selection workflow, and has been previously used to infer the nature and strength of plant growth processes in dendroecology (Martin et al. n.d.). It is implemented in F#, a strongly typed functional programming language, which is being increasingly used within data-science and machine learning domains. Our objective with *Bristlecone* was to create a library that could be used to efficiency and effectively conduct a full MFMS analysis for long-term ecological problems. To achieve this, we implemented a software library to enable three fundamental concerns:

1. Definition of models, data, and MFMS method using a clear domain-specific language;
2. Minimisation of error in model definition and data before any MFMS analysis is started; and
3. Application of a pre-built workflow for problems that use wood ring time-series.

The full source code for *Bristlecone* is available at https://github.com/AndrewIOM/bristlecone. The paper is structured as follows: in Section 6.3 we outline the MFMS method, in 6.4 we discuss the *Bristlecone* framework; in Section 6.5 we provide an example use-case; and in Section 6.6 we discuss extensibility.

6.3 Method Overview

In *Bristlecone* we provide tools to infer the structure and magnitude of processes from long-term ecological data using an information-theoretic approach of model-fitting and models-selection (Burnham & Anderson 2007). The confrontation of data with models was demonstrated for broad ecological questions in 'The Ecological Detective' (Hilborn & Mangel 1997). There are four key

stages to the model-fitting and model-selection process. First, the hypotheses under interrogation must be represented as mathematical models. An appropriate measure for goodness-of-fit must also be identified at this stage. Second, verification is required that it is possible to infer parameter values successfully for any given mathematical model and method of inference. If this is not the case, there may be problems with the model or the appropriateness of the selected inference method. Third, the real observations must be organised, and the parameter set optimised for each model hypothesis to gain a maximum likelihood estimate. Finally, the most appropriate model must be determined using model-selection criteria.

There are specific challenges when applying this approach to long-term ecological data. Ecological time-series – such as data from sedimentary archives – are often short and noisy posing challenges for model inference. In addition, theoretical models in ecology can be highly non-linear (Bolker 2007), requiring the application of robust model-fitting algorithms and diagnostics. We include suitable model-fitting heuristics in *Bristlecone*. In addition, theoretical models are often described as time-dependent ordinary differential equations (ODEs): these require integration in continuous time, which adds complexity to model-fitting. *Bristlecone* handles both continuous-time and discrete-time model formulations.

Bristlecone includes methods adapted specifically for long-term ecological data: additional considerations exist for tree ring and sedimentary data. Sediment cores rely on an age-depth model where the resultant time-series does not have common timesteps; we therefore included the ability to run models in uneven time intervals. Models of tree ring growth rely on allometric relations that dictate the relationship between different size variables of the plant (e.g. height and stem width). We have included a customisable workflow for analysing ring increment time-series with ecological models.

6.4 Bristlecone Framework

Bristlecone is a .NET Standard 2.0 library, which can be used in cross-platform F# scripting or embedded within cross-platform web or desktop applications. We chose to implement our solution

in the F# language. F# is a functional, strongly typed language that is being increasingly used for data-science, machine learning and web applications. We chose F# to make use of particular language features. First, *type providers* enable data-driven programming by inferring the structure of datasets as F# types (Petricek et al. 2016). Second, the expressive F# type system allows meta-programming of custom domain-specific languages. Third, F# can be scripted and is cross-platform. In addition, the *RProvider* type provider enables interoperability with R, for uses such as the creation of *ggplot* graphics.

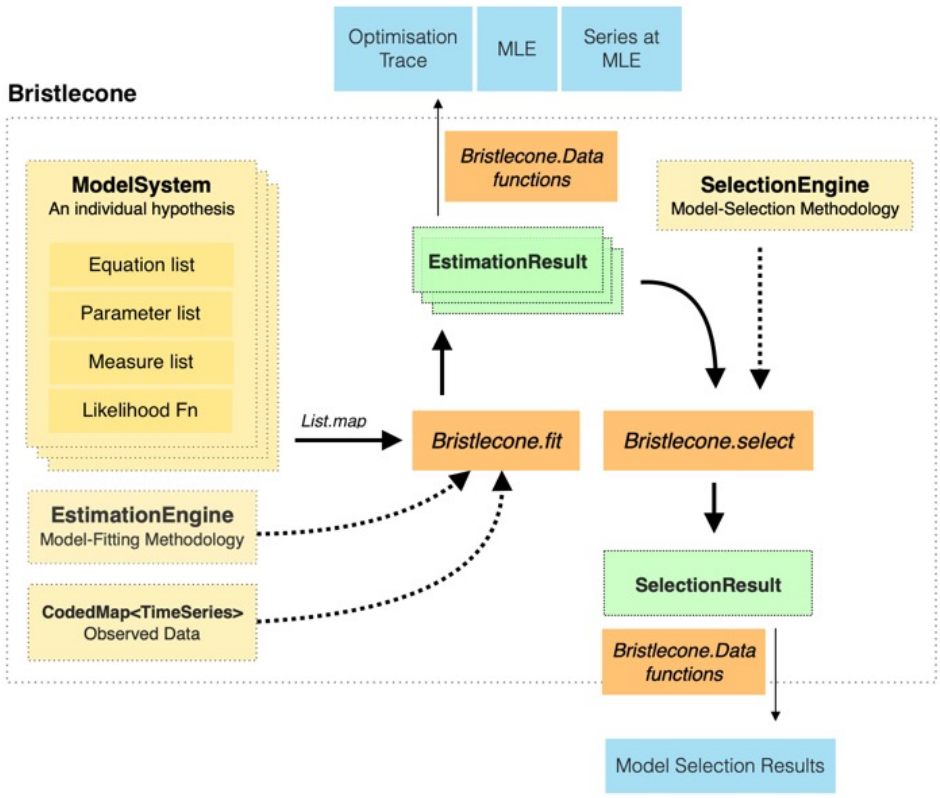

Figure 6–1 Types involved in the model-fitting and model-selection process in Bristlecone. Input types (yellow) represent the observation data, model hypotheses, and methodologies to be used. Bristlecone functions (orange) yield results (green) that can be exported to files on disk (blue) using the *Bristlecone.Data* namespace.

Bristlecone was primarily designed for time-series models, which can be defined in continuous or discrete time. Bristlecone contains functions for data access, time series manipulation, optimisation, integration of ordinary differential equations (ODEs), and diagnostic measures. We represented the flow of a MFMS analysis via core types (**Figure 6–1**). A standard MFMS procedure shares a common abstraction: (1) a series of [nested or non-nested] mechanistic models are developed to

represent the hypotheses under study; (2) likelihood functions are chosen that represent the error structure of the time-series being analysed; (3) observational time-series data are imported and arranged to a format suitable for model-fitting step; (4) model-fitting is conducted for every hypothesis independently; and (5) the maximum likelihood estimates for every model are competed using a model-selection criterion. If there are multiple subjects in a study (e.g. individual trees), then steps 1 – 5 are repeated for each. Bristlecone enables definition and execution of the above pipeline using a domain specific language (DSL). The full definition of steps 1 – 5 is described in the rest of this section.

6.4.1 Inputs

There are four required inputs for a full MFMS analysis: `Bristlecone.fit` requires hypotheses to test, input time-series, and a model-fitting protocol; and `Bristlecone.select` requires a model-selection protocol.

Each hypothesis is encapsulated by a `ModelSystem` type ('model system'). A model system comprises a list of equations to be computed (either ordinary differential equations or discrete-time equations), model parameters, and a likelihood function. When the model hypotheses are nested, partial application can be used to define a base model and pluggable model components. Within the model system, the components are as follows:

- `Equation<'State> = Time -> 'State -> Environment -> 'State`

  An equation in *Bristlecone* has access to the current `Environment`, `ParameterPool`, and time *t*. The environment contains the current value of all model variables, as well as any environmental forcing variables that have been included.

- `ParameterPool = CodedMap<Parameter>`

  The parameter pool contains all of the parameters to be estimated for the model system. Parameters of a model system are created as a map, where each `Parameter` requires a short code (for reference), bounds, and an optional constraint. The bounds for a parameter

may be used differently between different estimation engines. Constraints are required when certain parameter values are not biologically meaningful.

- `LikelihoodFn`

  A likelihood function represents the goodness-of-fit of a model hypothesis to data. A function of `LikelihoodFn` type has access to the observed and estimated dataset. *Bristlecone* will minimise this function; therefore, a negative log likelihood or sum-of-squares measure are appropriate.

- `Measure<'State> = 'State -> Environment -> Environment -> 'State`

  Measures are optional outputs of the model equations that transform the computed time-series into an additional form. Measures are computed before goodness-of-fit.

Input data sources are represented by the `TimeSeries` type. *Bristlecone*'s time-series representation ensures that observations are always correctly ordered. It also ensures that data adheres to any temporal resolution constraints in modelling approach, such as requiring a fixed time increment. The module contains functions for manipulating the temporal extent and resolution of time-series where, for example, there is a mismatch in the resolution of input datasets.

We represent protocols for MFMS through an `EstimationEngine` type, which can be re-used across many analyses. The engine allows configuration of outputs, time mode, optimisation method, and start value conditioning. Model selection is configured in a similar approach with a `SelectionEngine`.

6.4.2 Orchestration and Workflow

For a single research question there can often be many competing model hypotheses (and in some cases more than one subject). We included orchestration tools to run many analyses at once and in parallel. An `OrchestrationAgent` is available in the `Bristlecone.Workflow` namespace. The agent is queue-based: it enqueues `WorkParcel` items and only runs a set number simultaneously. The agent manages shared concerns such as real-time graphing and logging across threads and analyses. We provide simple work parcel functions that iterate hypotheses and subjects,

saving results once complete to disk. In addition, advanced scenarios are supported such as the co-ordination of co-dependent workloads: for example, it allows multiple Monte Carlo chains to end when converged according to a convergence statistic.

6.4.3 Specialist Methods for Long-Term Ecology

We developed *Bristlecone* to address specific needs for tree ring and sediment data. To address the requirement for uneven timesteps derived from sediment age-depth models, *Bristlecone's* estimation functions are aware of temporal-resolution and will solve continuous-time problems accordingly. If optional environmental forcing data is provided on a different timeline, interpolation or another specified method can be used to align time-series.

We included a number of adaptations suitable for tree ring research. The *Bristlecone.Dendro* library contains pre-defined workflows for ring width data. In particular, we have included a model template that fits to ring width data by modelling whole-plant biomass dynamics; translating between biomass and stem width using customisable allometric relations; setting the starting biomass using the allometric relation between stem radius and biomass; and outputting wood ring increments.

Seasonality of environmental conditions is an important consideration within tree ring research. At an annual resolution, time-series of environmental conditions must be sliced and generalised to a lower resolution for use as an input variable, for example by constructing a mean June – August air temperature. This approach is appropriate when models are representative of annual processes but may not fully capture the influence of seasonality through time. We include a method for modelling annual wood production but taking account of higher-resolution variability in the environment, which uses a greater proportion of the underlying data to infer model parameters. Internal high-resolution time-stepping is applied whereas external low-resolution wood increment and other variable data is provided to the likelihood function. Bristlecone also includes functions to compute day length given latitude, longitude, and time zone (Meeus 1998), which can be directly accessed within tree ring models to capture the role of seasonal light availability.

6.5 Example

Here we outline a standard *Bristlecone* procedure for a classic ecological problem: predator-prey dynamics. The example code can be placed an F# script file or run directly using F# interactive. Scripting with *Bristlecone* requires .NET Core 3.0 or greater. Install the *Bristlecone* package into the working directory:

```
$ dotnet tool install -g paket
$ paket init
$ paket add bristlecone
```

After installing .NET Core F# interactive can be run with the **`dotnet fsi`** command in your working directory. You can either run the below code directly or add it to a script file such as ***analysis.fsx*** and pass that file to the previous command. First, import and load *Bristlecone*:

```
#load "packages/Bristlecone/bristlecone.fsx"
open Bristlecone
open Bristlecone.ModelSystem
```

Next define a hypothesis (**`ModelSystem`**). Here we simply define predator-prey dynamics:

```
let ``predator-prey`` =

    /// Number of snowshoe hares
    let dhdt' hare lynx alpha beta =
        alpha * hare - beta * hare * lynx

    /// Number of lynx
    let dldt' lynx hare delta gamma =
        - gamma * lynx + delta * hare * lynx

    let dhdt p t hares env =
        dhdt' hares (lookup env "lynx") (lookup p "alpha") (lookup p "beta")

    let dldt p t lynx env =
        dldt' lynx (lookup env "hare") (lookup p "delta") (lookup p "gamma")

    { Equations =  [ code "hare", dhdt
                     code "lynx", dldt ] |> Map.ofList
      Measures =   [ ] |> Map.ofList
      Parameters = [ code "alpha",  parameter PositiveOnly 0.10 0.60
                     code "beta",   parameter PositiveOnly 0.001 0.0135
                     code "delta",  parameter PositiveOnly 0.001 0.0135
                     code "gamma",  parameter PositiveOnly 0.10 0.60
                     code "sigmax", parameter Unconstrained -0.2 0.2
                     code "sigmay", parameter Unconstrained -0.2 0.2
                     code "rho",    parameter Unconstrained -0.2 0.2
                   ] |> Map.ofList
      Likelihood = ModelLibrary.Likelihood.sumOfSquares ["hare"; "lynx"] }
```

Here predator-prey dynamics are defined as a system of two ODEs. The functions `dhdt` and `dldt` connect the respective pure mathematical functions into *Bristlecone* by specifying which parameter or variable to use for each input to the ODEs. The next step is to define an **`EstimationEngine`** with which to fit our model.

```
let engine =
    Bristlecone.mkContinuous
    |> Bristlecone.withGradientDescent
    |> Bristlecone.withConditioning RepeatFirstDataPoint
```

Engines are specified through chained builder functions. Here we have started with *Bristlecone*'s basic continuous-time engine and further specified that gradient-descent (an Amoeba algorithm) should be used for optimisation, and the variables at time-zero should be repeats of the first

observation. To assess the performance of this engine with our model, we use *Bristlecone*'s test function:

```
open Bristlecone.Test

let endCondition = Optimisation.EndConditions.afterIteration 100000
let testSettings = {
    TimeSeriesLength = 50
    StartValues = [ code "lynx", 30.09
                    code "hare", 19.58 ] |> Map.ofList
    EndCondition = endCondition
    GenerationRules = []
    NoiseGeneration = fun p ts -> ts
    EnvironmentalData = [] |> Map.ofList
    Resolution = 1 |> Years
    Random = System.Random()
    StartDate = System.DateTime.Create 01 01 2012
    Attempts = 10000 }

let testResult = ``predator-prey`` |> Bristlecone.testModel engine testSettings
```

As we used sum-of-squares to assess goodness of fit here, `testResult` should have a likelihood of zero and minimal difference in the parameter estimates. The test function is flexible allowing noise to be generated on individual expected time-series of variable length. After a successful test, a real model-fitting step can be run as follows:

```
// Here, we use the FSharp.Data CSV type provider to read in a CSV file.
type PopulationData = FSharp.Data.CsvProvider<"data/lynx-hare.csv">
let data =
    let csv = PopulationData.Load "data/lynx-hare.csv"
    [ code "hare", TimeSeries.fromObservations
           (csv.Rows |> Seq.map(fun r -> float r.Hare, r.Year))
      code "lynx", TimeSeries.fromObservations
           (csv.Rows |> Seq.map(fun r -> float r.Lynx, r.Year))
     ] |> Map.ofList

let result = ``predator-prey`` |> Bristlecone.fit engine endCondition data
```

The resultant **`EstimationResult`** contains the maximum likelihood estimate (MLE), estimated parameters, and a full trace of the optimisation process. The results can be saved to a file using the **`Data.EstimationResult.saveAll`** function.

When multiple hypotheses are present, model-selection methods can identify the most appropriate model structure for the observed data. In *Bristlecone* we have included Akaike Information Criterion (AIC) model selection using Akaike Weights (Wagenmakers & Farrell 2004), although other model-selection statistics can be substituted such as the Bayesian Information Criterion (BIC) depending on specific research objectives (Burnham & Anderson 2007).

6.6 Interchangeable Components

Bristlecone was designed as a generic workflow, where custom components that match the type signatures in *Bristlecone* can be readily substituted. These include integration and optimisation methods, graphics and real-time logging, and end conditions. We have provided built-in components that have worked well for our research in long-term ecology, but others may substitute their own.

6.6.1 Optimisation

An optimisation technique is responsible for minimising the negative log likelihood to identify the maximum likelihood. The procedure ends in conformance with an **`EndCondition`**: a function depending on the procedure's history that returns true if the condition is met. Any optimisation technique can be used within a *Bristlecone* analysis, so long as it matches the appropriate type signature:

```
type Optimise<'d> = WriteOut -> EndCondition<'d> -> Domain -> Objective ->
Solution<'d> list

and WriteOut = LogEvent -> unit
and EndCondition<'d> = Solution<'d> list -> bool
```

The most appropriate optimisation technique depends on the nature of the problem with extensive reviews available elsewhere (Reali et al. 2017; Rios & Sahinidis 2012). We focus on stochastic gradient descent algorithms that may be applied to any simple or complex function to minimise. Algorithms included in Bristlecone are shown in **Table 6–1**:

Table 6–1 Summary of included optimisation techniques with reference implementation

Family	Technique	Description	Reference
Amoeba	Single	A single Nelder-Mead simplex	(Press et al. 1992)
	Swarm	Many layers of *n* Nelder-Mead simplexes	None
Monte Carlo	Classical Simulated Annealing	Proposal jumps randomly drawn from normal distribution. Exponential cooling.	(Corana et al. 1987; Tsallis & Stariolo 1996; Sharman 1988)
	Fast Simulated Annealing	Proposal jumps randomly drawn from Cauchy distribution with a faster cooling schedule than classical simulated annealing.	(Szu & Hartley 1987; Lee 2015)
	Random Walk	Proposal jumps randomly drawn from multivariate normal distribution. *Suitable as a final MCMC algorithm.*	(Reali et al. 2017)
	Adaptive Metropolis	Weights covariance structure of proposal distribution towards recent chain history. Tunes scale of distribution based on acceptance rate.	(Haario et al. 2001)
	Generalised MCMC	A metaheuristic that conducts rough and fine tuning, before running a 'clean' random walk MCMC.	(Yang & Rosenthal 2016)
	Filzbach	An implementation of the 'Filzbach' algorithm from Microsoft Research.	(Microsoft Corporation 2011)
	Metropolis-within-Gibbs	Proposes jumps for each parameter sequentially.	(Yang & Rosenthal 2016)
	Adaptive Metropolis-within-Gibbs	Tunes the scale of each parameter separately, based on acceptance rates.	(Yang & Rosenthal 2016)

6.6.1.1 Amoeba Algorithms

Amoeba methods provide a local search. The Nelder-Mead simplex expands and contracts an n-dimensional geometry within an unconstrained parameter space, following a 'downhill' gradient (Press et al. 1992). Our implementation draws a random point from a normal distribution, informed by the starting bounds for each parameter. Although simple and relatively fast, as a local search it may be inappropriate for more complex likelihood surfaces that have more than one local minima. To address concerns of local minima, we included a swarm mode. The swarm mode creates an ensemble of 20 amoeba, which all crawl the likelihood surface. After *n* iterations, we discard all

amoeba that have values above the 80th percentile of the negative log likelihood values returned. We run this procedure for five levels but end early if all values returned are identical.

6.6.1.2 Monte Carlo Algorithms

Monte Carlo Markov Chain (MCMC) methods have two key advantages over amoeba solvers: first, given infinite time, a homogenous MCMC chain is guaranteed to identify the lowest likelihood region of parameter space (Chib & Greenberg 2012). Second, the sampled posterior distribution provides an indication of uncertainty for each parameter without the need for additional calculations. Of the included methods, simulated annealing methods are designed specifically for minimisation whereas other methods are distribution-sampling methods and thus relatively inefficient for identifying the minimum.

Monte Carlo approaches may be combined using tuning and sampling periods to tackle the trade-offs of convergence guarantees, generalisability, and speed of convergence. Random walk MCMC is a Metropolis-Hastings algorithm that draws from a Gaussian proposal distribution generating a homogenous MCMC chain, but its efficiency is reliant on the starting parameter bounds (which form the multivariate Gaussian prior distribution).

Simulated annealing (SA) models a minimisation problem in terms of particle entropy, where the function value is analogous to energy (Du & Swamy 2016). At high temperatures, particles are in a high-energy state, thus can move readily. As temperature gradually decreases, particles are less able to move to high energy states, with particles eventually arranging into the 'ground state' of a solid material. When Temperature (T) = 1, the simulated annealing algorithm is identical to a Metropolis-Hastings MCMC algorithm. We have provided two of the most common SA algorithms for continuous systems: Gaussian (GSA) and Cauchy (CSA). In GSA, candidates are drawn from a temperature-dependent normal distribution, with an exponential cooling schedule (Corana et al. 1987). In CSA, a semi-local search is enabled by drawing candidates form a Cauchy distribution, which enables a faster cooling schedule. In these schemes, the distributions 'tighten' as the temperature is lowered, allowing the search to become more focused on the identified minimum

(Szu & Hartley 1987). Our implementation roughly tunes the temperature-dependent scale (Cauchy) or standard deviation (Gaussian) for each individual parameter using a Metropolis-within-Gibbs function to improve sampling efficiency. The acceptance rate for each parameter is tuned to between 0.2 and 0.4.

6.6.2 Real-Time Diagnostics

Bristlecone includes tools for monitoring and diagnosing the model-fitting process. Each `EstimationEngine` has a connector for a `WriteOut` function, which consumes `LogEvents`. *Bristlecone* includes threading-aware console logging by default, and this may be extended or replaced. For instance, we have implemented a multi-chain parallel and real-time graph of each parameter trace within the fitting process. This is implemented through interoperability with the R programming language: plots are rendered by passing real-time data to the *ggplot* R package (**Figure 6–1**).

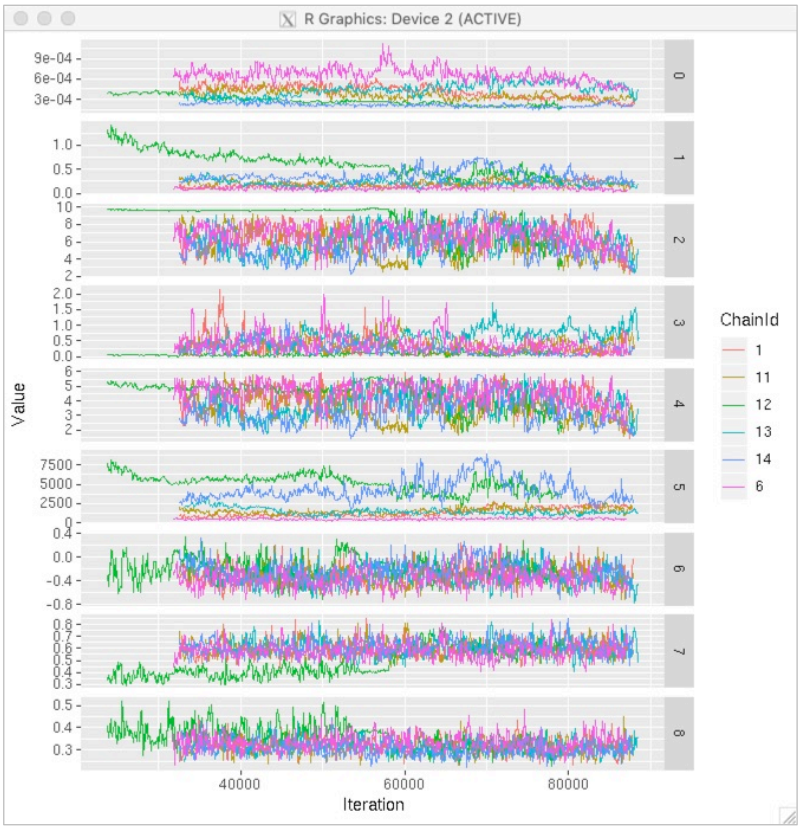

Figure 6–1 Real-time traces of parameter estimates output by the *Bristlecone* library. These charting capabilities demonstrate Bristlecone interoperability with the R programming language using the F# R type provider. Here we use the *ggplot2* R package to generate graphics.

6.7 Discussion

We have described a library called *Bristlecone* that may be used to understand and interrogate ecological mechanism from long-term ecological datasets. It can, however, be used within other fields such as econometrics if desired. The library yields information on the most appropriate model structure and parameters with uncertainty estimates to explain observed data.

We sought to create a straightforward and reproducible workflow to define and conduct the interrogation of ecological time-series using competing theoretical models. Our objective was not to design the most efficient and generalisable global optimisation algorithm. Although other libraries such as Stan (Gelman et al. 2015) may be used to conduct interrogation of ecological time-series with mathematical models, *Bristlecone* handles all considerations to conduct a full model-fitting and model-selection analysis including domain-specific requirements for long-term ecology: handling of time-series data; and complex non-linear models written as ordinary differential equations.

For long-term ecological research we provide tools specifically geared towards interrogating tree ring and sediment core data. Similar top-down modelling approaches exist such as the VS-lite model, which incorporates climate-limitations to wood growth using the principle of limiting factors (Tolwinski-Ward et al. 2010). Various models have included allometric relations (Pommerening & Muszta 2016) and day length (Tolwinski-Ward et al. 2013) into tree ring modelling approaches. We wish to encourage the further interrogation of tree ring datasets using top-down modelling approaches with *Bristlecone*.

6.8 Funding

This work was completed with funding from the Natural Environment Research Council of the United Kingdom (grant number NE/L002612/1).

6.9 References

Archontoulis, S.V. & Miguez, F.E., 2015. Nonlinear Regression Models and Applications in Agricultural Research. *Agronomy Journal*, 107(2), pp.786–798.

Binney, H. et al., 2017. Vegetation of Eurasia from the last glacial maximum to present: Key biogeographic patterns. *Quaternary Science Reviews*, 157, pp.80–97.

Birks, J. et al., 2014. Quantitative Palaeoenvironmental Reconstructions from Holocene Biological Data. In *Global Change in the Holocene*. Routledge, pp. 123–139.

Blaauw, M., Christen, J.A. & Aquino-López, M.A., 2019. A Review of Statistics in Palaeoenvironmental Research. *Journal of Agricultural, Biological and Environmental Statistics*, pp.1–15.

Bolker, B., 2007. *Deterministic Functions for ecological modeling*,

Bonsall, M.B. & Hastings, A., 2004. Demographic and environmental stochasticity in predator-prey metapopulation dynamics. *Journal of Animal Ecology*, 73(6), pp.1043–1055.

Burnham, K.P. & Anderson, D.R., 2007. *Model Selection and Multimodel Inference*, Springer Science & Business Media.

Chib, S. & Greenberg, E., 2012. Understanding the Metropolis-Hastings Algorithm. *The American Statistician*, 49(4), pp.327–335.

Corana, A. et al., 1987. Minimizing multimodal functions of continuous variables with the "simulated annealing" algorithm—Corrigenda for this article is available here. *ACM Transactions on Mathematical Software (TOMS)*, 13(3), pp.262–280.

Du, K.-L. & Swamy, M.N.S., 2016. Simulated Annealing. In *Search and Optimization by Metaheuristics*. Cham: Springer International Publishing, pp. 29–36.

Fritts, H.C., 1976. *Tree Rings and Climate*, Academic Press.

Gelman, A., Lee, D. & Guo, J., 2015. Stan: A Probabilistic Programming Language for Bayesian Inference and Optimization. *Journal of Educational and Behavioral Statistics*, 40(5), pp.530–543.

Haario, H., Saksman, E. & Tamminen, J., 2001. An adaptive Metropolis algorithm. *Bernoulli*, 7(2), pp.223–242.

Hilborn, R. & Mangel, M., 1997. *The Ecological Detective*, Princeton University Press.

Jeffers, E.S. et al., 2011. Climate change impacts on ecosystem functioning: evidence from an Empetrum heathland. *New Phytologist*, 193(1), pp.150–164.

Johnson, E.A. & Miyanishi, K., 2008. Testing the assumptions of chronosequences in succession. *Ecol Letters*, 11(5), pp.419–431.

Lee, C.-Y., 2015. Fast simulated annealing with a multivariate Cauchy distribution and the configuration's initial temperature. *Journal of the Korean Physical Society*, 66(10), pp.1457–1466.

Martin, A.C. et al., **Nitrogen limitation of Arctic shrub growth over three decades: inference from mechanistic modelling of dendroecological data, Yamal, Russia**.

Meeus, J., 1998. *Astronomical Algorithms*,

Microsoft Corporation, 2011. *Filzbach User Gude*.

Paine, C.E.T. et al., 2011. How to fit nonlinear plant growth models and calculate growth rates: an update for ecologists. *Methods in Ecology and Evolution*, 3(2), pp.245–256.

Peng, C. et al., 2011. Integrating models with data in ecology and palaeoecology: advances towards a model-data fusion approach. *Ecology Letters*, 14(5), pp.522–536.

Petricek, T., Guerra, G. & Syme, D., 2016. Types from data: making structured data first-class citizens in F#. In the 37th ACM SIGPLAN Conference. New York, New York, USA: ACM Press, pp. 477–490.

Pommerening, A. & Muszta, A., 2016. Relative plant growth revisited: Towards a mathematical standardisation of separate approaches. *Ecological Modelling*, 320, pp.383–392.

Poorter, H., Anten, N.P.R. & Marcelis, L.F.M., 2013. Physiological mechanisms in plant growth models: do we need a supra-cellular systems biology approach? *Plant, Cell & Environment*, 36(9), pp.1673–1690.

Press, W.H. et al., 1992. *Numerical Recipes in C*, Cambridge University Press.

Reali, F., Priami, C. & Marchetti, L., 2017. Optimization Algorithms for Computational Systems Biology. *Frontiers in Applied Mathematics and Statistics*, 3, p.80.

Rios, L.M. & Sahinidis, N.V., 2012. Derivative-free optimization: a review of algorithms and comparison of software implementations. *Journal of Global Optimization*, 56(3), pp.1247–1293.

Sharman, K.C., 1988. Maximum likelihood parameter estimation by simulated annealing. In ICASSP-88., International Conference on Acoustics, Speech, and Signal Processing. IEEE, pp. 2741–2744.

Szu, H. & Hartley, R., 1987. Fast simulated annealing. *Physics Letters A*, 122(3-4), pp.157–162.

Tolwinski-Ward, S.E. et al., 2010. An efficient forward model of the climate controls on interannual variation in tree-ring width. *Climate Dynamics*, 36(11-12), pp.2419–2439.

Tolwinski-Ward, S.E., Anchukaitis, K.J. & Evans, M.N., 2013. Bayesian parameter estimation and interpretation for an intermediate model of tree-ring width. *Climate of the Past*, 9(4), pp.1481–1493.

Tsallis, C. & Stariolo, D.A., 1996. Generalized simulated annealing. *Physics A*.

Wagenmakers, E.-J. & Farrell, S., 2004. AIC model selection using Akaike weights. *Psychonomic Bulletin & Review*, 11(1), pp.192–196.

Willis, K.J. et al., 2010. Biodiversity baselines, thresholds and resilience: testing predictions and assumptions using palaeoecological data. *Trends in Ecology & Evolution*, 25(10), pp.583–591.

Yang, J. & Rosenthal, J.S., 2016. Automatically tuned general-purpose MCMC via new adaptive diagnostics. *Computational Statistics*, 32(1), pp.315–348.

Chapter 7

Synthesis and Conclusion

Synthesis and Conclusion

The overarching aim of this DPhil thesis was to investigate the extent to which soil nitrogen (N) availability may have limited Arctic shrub growth over the recent past and may explain recent heterogeneity in shrub sensitivity to climate. To achieve this aim, I identified four key research objectives for this DPhil thesis:

1. Identify recent evidence for alternative controls on shrub growth.
2. Determine decadal trends in soil N availability in Western Siberian tundra.
3. Establish the mechanism, strength, and variability of N limitation on shrub growth.
4. Assess the importance of N limitation versus climate (i.e. temperature, snow dynamics).

I addressed all four aims by employing a broad suite of methods including a systematic-evidence based review to synthesise existing studies, dendroecology, stable isotope analysis, time-series modelling and software development. My research focused on a single deciduous shrub species, *Salix lanata*, the dominant tall shrub species in the region.

7.1 Main Findings

7.1.1 Spatial-Temporal Limitations within Recent Evidence for Controls on Shrubification

I sought to identify recent evidence for alternative controls on shrub growth. To achieve this aim, I designed an evidence-mapping protocol (**Chapter 2**) to capture the spatial and temporal characteristics of recent evidence for controls on shrub growth and expansion. The protocol was designed in line with best practices in evidence synthesis (Pullin & Stewart 2006) to ensure objectivity and completeness and providing a new dataset from which a meta-analysis may be conducted in future.

Using the developed approach, I mapped and codified the recent literature. I found that the recent evidence base and method of knowledge production is not sufficiently robust or comprehensive to answer key questions of Pan-Arctic shrub change because: (a) spatial coverage of the evidence is poor (with over half of evidence from the warmest areas of the tundra); (b) there is also poor coverage of studies that extend beyond 10 years of shrub growth; (c) floristic regions are poorly represented, with 43% of evidence from one floristic region; and (d) temporal dynamics are poorly represented due to the use of space-for-time substitution and time-series of low resolution. The resulting evidence map indicated that plot-scale evidence for N-limitation effects on shrub growth and expansion was also temporally constrained, suggesting that the recent evidence is of too-short timescale to examine mechanisms that are thought to occur on decadal time.

7.1.2 Declines in N availability have occurred in Western Siberian tundra

I sought to determine how N availability to Arctic shrubs has changed over the recent past and if trends were common within and between locations in Western Siberian tundra. To achieve this, I developed high-resolution time-series of the stable N isotope ratio ($\delta^{15}N$) of shrub wood rings. Wood $\delta^{15}N$ is a proxy for plant-based N availability (McLauchlan et al. 2017). My reconstructed $\delta^{15}N$ time-series are the first application of this method on Arctic shrub wood. I developed the method for extracting and analysing shrub $\delta^{15}N$ from individuals at Yuribei, a location on the Yamal Peninsula where wood rings are relatively large (**Chapter 3**), although much smaller than tree rings. I was able to achieve annual resolution $\delta^{15}N$ time-series for this site, from which I characterised variability within and between series over time. I then expanded the approach to increase the spatial coverage to other sites where wood rings are even smaller; at these sites, I extended the $\delta^{15}N$ further back in time (**Chapter 4**).

Using the reconstructed $\delta^{15}N$ time-series, I showed that declines in N availability to Arctic shrubs have occurred over recent decades. Declines were observed within locations in bioclimatic subzones D and E between 1940 and 2013. However, different soil N trajectories also occurred at fine spatial resolution including increasing N availability in some individuals that did not appear to

be directly related to topographic variables. The finding of overall decreasing N availability challenges the key assumption that rising air temperatures lead to increased N availability universally within Arctic shrub tundra environments (Mikan et al. 2002). The time-series data indicate that N availability to shrub individuals is largely a function of local-scale N dynamics, and suggest that soil microbial responses to warming temperatures, which result in additional availability of N, are not a universal phenomenon.

7.1.3 Strong N-limitation to shrub growth and important litter feedbacks

Another objective of my research was to establish the mechanism, strength, and variability of N limitation on shrub growth given decadal changes in N availability. To achieve this, I developed a method to infer the processes underlying observed changes in dendrochronological (ring width) and soil nutrient time-series. In **Chapter 3**, I focused on establishing a model to demonstrate the most appropriate theoretical representation of shrub-nitrogen relationships, which could be used to test hypotheses. I assessed a number of approaches to model-fitting and model-selection for the short and noisy isotope time-series, which led to their formalisation within the development of the *Bristlecone* software library (**Chapter 6**). After demonstrating the successful application of the inference methods using annually resolved series for ten individuals covering the period 1980-2013 (**Chapter 3**), I applied the approach to longer datasets and a diversity of tundra woolly willow-dominates sites (**Chapter 4**).

Model-fitting and model-selection of the $\delta^{15}N$ and ring width time-series indicated that the growth of all shrub individuals assessed was N-limited; for a majority of these, plant-soil litter feedback was a significant determinant of shrub-nitrogen dynamics. Within the last four decades, at a typical poorly drained low shrub tundra location (Yuribei), the functional form of inter-annual N limitation was found to be best represented by a simple linear process rather than a root foraging model for most shrub individuals studied, suggesting that available N is readily scavenged and not subject to rate limits. However, I also identified that root foraging models may be more applicable when interrogating data on a monthly temporal resolution (**Chapter 5**). When assessing growth-N dynamics over a longer timespan (with the earliest dates in the 1940s), we found a greater mixture

within the best representations of N-limitation (**Chapter 4**), which may reflect greater variability in N availability over the longer time period. Our results suggest that: (a) N availability is limiting secondary growth of deciduous shrubs in this Arctic region; (b) *Salix lanata* are actively controlling their environment, with an important role of plant-soil feedbacks for supporting further plant growth; and (c) there are important differences at individual shrub scale, which may be related to plant functional traits and/or micro-environmental characteristics.

7.1.4 Importance of N-limitation versus Temperature and Snow Dynamics

I sought to assess the relative importance of N-limitation to growth in relation to other environmental factors. To address this, I examined proximal and key indirect effects of air temperature and snow dynamics on the relationship between individual growth and soil nitrogen availability. First, I included model hypotheses that extended growth-nitrogen models with temperature-dependent photosynthesis (**Chapter 4**). Second, I sought to examine the role of snow dynamics (snow depth and cover) on nitrogen availability and shrub growth through proximal effects (i.e. biomass protection) and indirect effects (i.e. soil insulation). As snow dynamics may be localised depending on topography, and the timing of snowmelt in the Arctic can vary substantially, I chose to examine snow effects using spatial and temporal axes by: (a) applying local and regional proxies for snow conditions; and (b) applying monthly-resolution forcing data within a shrub-nitrogen model adapted for monthly temporal resolution (**Chapter 5**). To provide a proxy for regional snow conditions, I computed daily snow depth indices from remotely sensed data products. For local snow dynamics, I completed additional laboratory analysis to generate time-series of $\delta^{18}O$ and $\delta^{13}C$ from wood rings; the stable oxygen isotope ratio can reflect water sources used by the plant during the growing season and was previously identified to winter precipitation in the boreal forest of Yamal (Holzkamper et al. 2008).

I identified that summer air temperature is an important control on individual shrub growth rates in Western Siberia: model-inferred dynamics, however, indicated that the overall temperature-limiting effect has declined during recent decades (**Chapter 4**). Model-inferred dynamics also suggest that the ratio of N demand to N supply has increased overall, indicating that plant demand is increasing

relative to N supply (even before accounting for environmental N losses). These model-based inferences together support the conclusion that N-limitation is of increasing importance as 'temperature release' (greater photosynthetic rates as summer temperatures have been increasing) of shrub growth occurs. In addition, I identified nuanced shrub growth responses to snow dynamics. The $\delta^{18}O$ and $\delta^{13}C$ time-series suggest that individual shrub growth at Yuribei is more responsive to changes in the timing and seasonality of snow cover rather than winter snow accumulation (**Chapter 5**). As $\delta^{13}C$ was related through time to the start of the snow-free growing season, it suggests that the annual photosynthetic rate is most sensitive to changing seasonality. I also tested snow protection and snow insulation hypotheses using the expanded model-fitting and model-selection approach; this however did not indicate an important role for either of these processes for five shrubs analysed at Yuribei. In addition, this result appeared insensitive to the spatial and temporal scale of analysis. Together, these findings suggest that warming air temperatures have provided a 'growth release' to *Salix lanata* shrubs over the last seven decades, but – contrary to expectation - this has not been coincident with increases in N availability. Both warmer summer temperatures and lengthening of the growing season from earlier snowmelt have contributed to increased photosynthetic activity and therefore increased N demand, which has not been matched by increases in N supply. These findings mirror observations for temperate forest trees in North America where the earlier onset of spring has been associated with declining N availability and increased total N demand for the growing season (Elmore et al. 2016); they also conform with global observations of 'terrestrial *oligotrophication'*(Craine et al. 2018).

7.2 Contribution to understanding of mechanisms driving Arctic shrubification

My work represents a unique contribution to the evidence base for the factors that may explain recent shrubification and greening trends in the Arctic tundra. Piao et al. (2014) identified a biome-wide progressive decline in the correlation between greenness and air temperatures, indicating that the role of temperature has progressively decoupled from vegetation productivity since 1982. My combination of new and novel time-series with model-based hypothesis testing conforms with this finding at the individual shrub scale: for a number of shrub individuals within two bioclimatic

subzones of Western Siberian tundra. I identified a declining role of summer temperatures in predicting shrub growth when assessed using a mechanistic modelling approach. The findings indicate that Arctic shrubs have been and continue to be strongly N-limited. In addition, a combination of model-inferred soil N dynamics and model-based tests of the snow-shrub hypothesis suggested that – in the study region – expected increases in soil N supply with a warming climate may not have been realised to date.

My time-series approaches were able to identify biologically plausible explanations for some of the observed spatial heterogeneity in shrub responses to climate (Myers-Smith et al. 2015). By conducting an annually-resolved study of the mechanisms contributing to the observed trends in N availability and shrub wood production at a typical tall shrub landscape (Yuribei), I was able to establish that there were common inter-annual mechanisms operating at decadal timescales, but their strength varied by individual (**Chapter 3**). The dominant mechanisms included N-dependent shrub growth and strong litter feedbacks. I also identified connections with local-scale topography (**Chapter 4**), which partially explained variability in the inferred processes governing plant-nitrogen relationships. The ability for shrub individuals to grow to larger maximum sizes was related to depressions and lowlands, which may arise from biotic interactions or mechanical advantages. Increased soil N inputs in sloped environments may reflect a greater role of N-fixation on the fringes of tall shrub areas.

7.3 Contributions to computational techniques within long-term ecology

During this thesis I have explored the development of computational methods that enable the application of long-term ecological methods to broader research questions. A primary contribution is *Bristlecone*, a library that I developed specifically to streamline and formalise the process of applying model-fitting and model-selection techniques to dendroecological and palaeoecological data (**Chapter 6**). An additional contribution was the development of an evidence synthesis protocol to code the spatial and temporal properties of research to link study designs to long-term ecological hypotheses (**Chapter 2 – Supplementary Material**). It also led to the creation of

Thalloo, a spatial-temporal map visualisation tool for dissemination and engagement with stakeholders (**Appendices**), which has been used to produce interactive maps for five additional systematic reviews from forestry to palaeoecology.

An additional contribution that stemmed from the research conducted here also seeks to increase the value of long-term ecological data. I developed the *Global Pollen Project*, a web application and platform for the crowdsourcing of pollen identification (**Appendices**). The project aims to establish an uncertainty-based global taxonomy of pollen morphology, which will enable more transparent and robust inferences of the composition of past vegetation.

7.4 Future Directions

Anthropogenic climate change has been responsible for rapid warming at a Pan-Arctic scale, and this is set to continue for the rest of this century. At our study locations in Western Siberia we identified that N-availability is declining in some locations over decadal time, a trend not observed in previous fertilisation experiments that rarely capture temporal dynamics. My findings suggest that the role of N limitation has been relatively stable over recent decades, although it may be emerging as the primary constraint on shrub growth relative to other limiting factors such as summer temperature and the snow-free season length. Here therefore I argue that variability in shrub responses to climate could be representative of mechanisms of progressive N limitation, albeit the results are spatially heterogeneous.

Key questions have arisen from my research. First, we do not know the extent to which the mechanisms and their envelopes of variability found here are common between floristic regions and other tall shrub species. A systematic sampling strategy for collecting shrub wood N isotope time series for the most common tall shrub species would help generate the observations required for determining the strength and variability of mechanisms driving N-limited growth, and how these vary within and between physiographic units of the Arctic in natural conditions. Second, we identified connections between topography and certain mechanisms operating over the long-term, which may be a starting point for further investigation into the drivers of shrub growth and

expansion. My modelling approach has generated several possibilities for the role of nutrient and environmental controls on tundra shrub growth that can be further tested with the collection of site-based field data on soil biota, plant allocation, and physical variables.

The methods developed here present a new approach for integrating nutrient dynamics with dendroecological data that extend far beyond existing approaches (Guiot et al. 2014) applied at lower latitudes. Despite the possibilities arising from the application of machine learning in the environmental sciences, interrogation of data using mechanistic models is essential (Baker et al. 2018) to gauge the evidence for/against multiple ecological hypotheses and thus identify the most likely mechanisms controlling observed ecological patterns. In this vein, there are opportunities to integrate the findings from this research into the representation of shrubification in Earth System Models (ESMs) where the nutrient-limited plant growth is poorly represented (or in some cases absent).

7.5 References

Baker, R.E. et al., 2018. Mechanistic models versus machine learning, a fight worth fighting for the biological community? *Biology letters*, 14(5), p.20170660.

Craine, J.M. et al., 2018. Isotopic evidence for oligotrophication of terrestrial ecosystems. *Nature ecology & evolution*, 2(11), pp.1735–1744.

Elmore, A.J., Nelson, D.M. & Craine, J.M., 2016. Earlier springs are causing reduced nitrogen availability in North American eastern deciduous forests. *Nature plants*, 2(10), p.16133.

Guiot, J.L., Boucher, E. & Gea-Izquierdo, G., 2014. Process models and model-data fusion in dendroecology. *Frontiers in Ecology and Evolution*, 2, p.L04705.

Holzkämper, S. et al., 2008. Stable Isotopes in Tree Rings as Proxies for Winter Precipitation Changes in the Russian Arctic over the Past 150 Years. *Geochronometria*, 32(-1), pp.37–46.

McLauchlan, K.K. et al., 2017. Centennial-scale reductions in nitrogen availability in temperate forests of the United States. *Scientific Reports*, 7(1), p.7856.

Mikan, C.J., Schimel, J.P. & Doyle, A.P., 2002. Temperature controls of microbial respiration in arctic tundra soils above and below freezing. *Soil Biology and Biochemistry*, 34(11), pp.1785–1795.

Myers-Smith, I.H. et al., 2015. Climate sensitivity of shrub growth across the tundra biome. *Nature Climate Change*, 5(9), pp.887–891.

Piao, S. et al., 2014. Evidence for a weakening relationship between interannual temperature variability and northern vegetation activity. *Nature Communications*, 5(1), p.1687.

Pullin, A.S. & Stewart, G.B., 2006. Guidelines for Systematic Review in Conservation and Environmental Management. *Conservation Biology*, 20(6), pp.1647–1656.

1

Appendix 1

The Global Pollen Project

Runner up for the *Robert May prize* of the British Ecological Society 2017 for best paper in Methods in Ecology and Evolution.

Martin, A.C. & Harvey, W.J., 2017. The Global Pollen Project: a new tool for pollen identification and the dissemination of physical reference collections S. Goslee, ed. *Methods in Ecology and Evolution*, 8(7), pp.892–897.

Methods in Ecology and Evolution

Methods in Ecology and Evolution 2017, **8,** 892–897 doi: 10.1111/2041-210X.12752

APPLICATION

The Global Pollen Project: a new tool for pollen identification and the dissemination of physical reference collections

Andrew C. Martin* and **William J. Harvey**

Long-Term Ecology Laboratory, Department of Zoology, University of Oxford, South Parks Road, Oxford OX1 3PS, UK

Summary

1. The study of fossil and modern pollen assemblages provides essential information about vegetation dynamics in space and time. A major methodological component of these studies is the identification of pollen grains to plant family, genus and species. This identification is achieved through the use of pollen keys and reference collections of physical specimens, which are regional in scope, disparate and incomplete, slowing the identification process. Reference material is also held in museums and research institutions, where access can be limited. Identification is particularly challenging for those new to the field, such as graduate students.

2. To aid the identification of pollen grains, and provide virtual access to reference material, we present a new online tool: the Global Pollen Project (https://globalpollenproject.org). The project aims to enable people to share and identify pollen grains and through this, will create an open, free and accessible reference library for pollen identification.

3. The online tool has been developed as an open, peer-reviewed database of global pollen, where content and expertise is crowdsourced from across the world. The tool enables: (i) the submission and identification of unknown pollen grains; (ii) the submission and digitisation of existing 'physical' reference collections and (iii) the availability of a free public database of pollen images and their metadata, for use in scientific research and education. The tool connects to external services, including the Global Biodiversity Information Facility and Neotoma Palaeoecology Database, to provide botanical descriptions and occurrence data for each taxon, alongside pollen images and metadata.

4. The database currently holds information for over 1500 species, from Europe, the Americas and Asia. As the collection grows, we envision easier pollen identification, and greater use of the database for novel research on pollen morphology and other characteristics, especially when linked to other palaeoecological databases, such as Neotoma.

Key-words: crowdsourcing, digitisation, dissemination, palynology, pollen, reference-collection

Introduction

Analyses of fossil and modern pollen assemblages provide vital evidence for determining vegetation dynamics in response to environmental change across space and through time. The task of undertaking palynological research can prove challenging, particularly when confronted with the task of identifying grains to genus or species level (Mander & Punyasena 2014). Difficulties arise from the condition and/or preservation of individual grains (Berglund 1986; Bennett & Willis 2002; Pearsall 2015), as well as the availability and accessibility of reference collections with which to compare them. Fast and accurate pollen identification requires a degree of skill that is hard for new researchers to develop if appropriate training and reference material is not at their disposal. Existing pollen reference collections are often kept as collections of slides within research institutions or private collections, which constrains accessibility. Individual researchers and institutions often collect and create their own reference collections that often fail to be shared or archived, and are forgotten, becoming so-called 'dark data' (Heidorn 2008). This issue is not only limited to palynology but also prevalent within other taxonomic fields, including collections held within both public and private institutions. This has led to recent efforts to digitise collections from herbaria to natural history collections (see Brooks *et al.* 2014; Wen *et al.* 2015; iDigBio 2016). We sought to develop a tool that could address the following key aims:

1. to provide virtual access to palynological reference material derived from all regions of the globe,

2. to aid in the identification of pollen grains via education and accessibility;

3. to foster scientific crowdsourcing to improve palynological studies and its use in biodiversity conservation, climate change and anthropogenic impacts on vegetation; and

4. to integrate with supportive material from other global biodiversity and palaeoecological resources.

*Correspondence author. E-mail: andrew.martin@zoo.ox.ac.uk

Here we discuss the development and release of the Global Pollen Project (GPP), a web-based tool that enables digitisation (the upload and sharing of images and metadata in a common format) of pollen reference material. It addresses the aims of access to material, aiding identification and fostering crowdsourcing, by providing an encompassing, evolving peer-reviewed database of pollen through crowdsourcing content and expertise from across the world. By being 'global', we aim to encompass information for all plant taxa around the world, as well as encouraging a world-wide pooling of expertise.

Application framework

The GPP has been designed with the purpose of aiding and disseminating palynological research from within the scientific community as well as the wider public sphere. A key drive in the development of the tool, therefore, was the creation of a flexible underlying framework and an intuitive interface that would encourage use from novices as well as experts. The framework was designed so that users can upload images of pollen grains irrespective of their identification status. If a grain is unidentified, the intention is that its identification can be crowdsourced from other users. Alternatively, users that have well-identified collections can upload their collection digitally with detailed labels. These two inputs of pollen grain images come together to form the GPP's master reference collection.

TECHNICAL IMPLEMENTATION

The GPP is a web application built on Microsoft's.NET Core 1.0 platform with the ASP.NET framework (Microsoft, 2016a), using Entity Framework Core (Microsoft 2016b) with a Microsoft SQL database (Fig. 1). It is currently deployed on Microsoft's Azure cloud infrastructure (Microsoft 2016c) enabling high availability, routine backup and upscaling of resources as the database and image library grows. The application was developed in a decoupled way, such that the web user interface is interchangeable, and the core is not reliant on a specific technical infrastructure.

TAXONOMIC SYSTEM AND TAXONOMIC BACKBONE

Taxonomic organisation of modern and fossil pollen types has been implemented through a hierarchical system relating submitted images to their corresponding plant families, genera and species. New taxa are created automatically when a new user-submitted grain becomes identified, or a slide is digitised for a new taxon. To overcome taxonomic conflicts between collections, we automatically constrain the GPP taxonomy using a dynamic taxonomic backbone. This taxonomy provides an authority on accepted names and synonyms. Any new taxon generated in the GPP must exist in the backbone as an *accepted* taxon. Synonyms will not be accepted and must be entered in accordance with current convention. As changes are made to the dynamic backbone, these are reflected in the GPP taxonomy. The Plant List (2013), the only complete, working list of vascular plant names, is utilised by the GPP as its default taxonomic backbone. The Plant List contains 1 064 035 scientific species names, of which 350 699 are accepted (The Plant List 2013). Palynological morphotypes are often used as a proxy for the presence and abundance of plant taxa. It is important for the integrity of any palynological backbone to be firmly connected to a botanical list, so that changes and amendments made by the scientific community can be tracked through time. Other current palynological lists lack such tracking, thus cannot be used in this way.

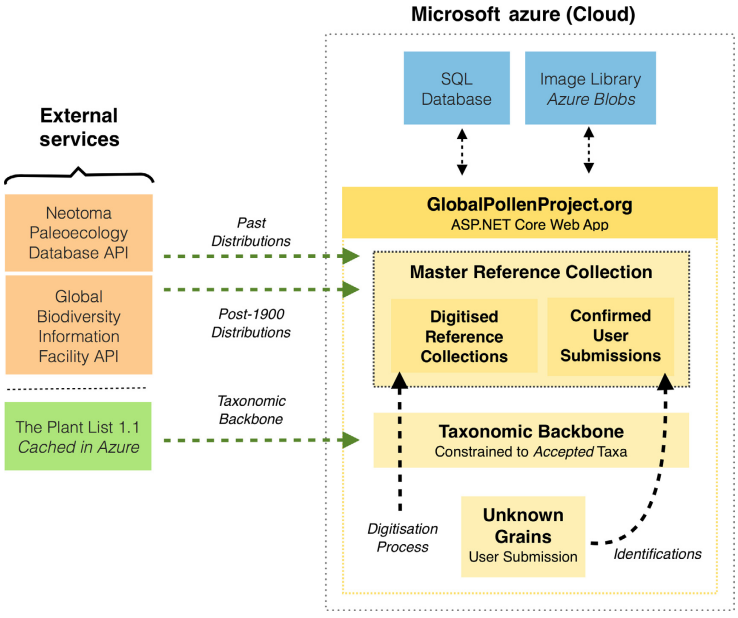

Fig. 1. Integrated framework of the Global Pollen Project. The main infrastructure and functionality is outlined, alongside connections to external services.

USER SYSTEM, PERMISSIONS AND DATA INTEGRITY

The GPP handles users and their permissions to promote data integrity, and limit abuse. Users must provide and validate an email to create an account, and malicious users can be banned, with their contributions subsequently removed. The submission of unknown grains, and their identification, is open to any registered user. If a user disagrees with past identifications of a grain, whether it has gained a confirmed identity or not, they can add another identification and the identity will be recalculated. In this way, the quality of the data increases as more people use it. As the tool is further developed, an improved rating system will be implemented for both users and submissions.

For reference material, the ability to digitise collections is restricted, and rights must be requested using the online form. These requests are handled by database moderators. The quality of digitised material is validated by end users: an image quality rating mechanism is in testing that allows images to be filtered by perceived quality. There is also a reporting mechanism, through which a digitised slide can be flagged as having an identification problem.

User use cases

The web interface of the GPP supports three major use-cases of the tool:

(a) the submission and identification of unknown pollen grains via crowdsourcing;

(b) the submission, digitisation and dissemination of images derived from existing 'physical' reference collections, both modern and fossil; and

(c) the public availability of an integrated global database of pollen images with associated metadata, for use in scientific research and education.

SUBMISSION AND IDENTIFICATION OF UNKNOWN POLLEN GRAINS VIA CROWDSOURCING

Crowdsourcing – the process of obtaining ideas from a wide community – has been implemented within the tool for the identification of pollen grains. Such approaches are already used for the identification of plant, mammal and insect species, e.g. iSpot (Silvertown *et al.* 2015), as well as data collection in the environmental sciences e.g. Zooniverse projects, such as the tropical cyclone project (Hennon *et al.* 2015). To enable crowdsourcing of pollen identification, we implemented mechanisms for uploading unidentified pollen grain images with metadata, group-based identification and community-based competition.

The process of uploading unidentified grains is designed to be fast and thus requires minimal information. The service requires between one and four images of the grain in question, which can be cropped and rotated during the upload. Other information required are the maximum grain diameter (micrometres), and the location from which the grain was collected. Grain diameter provides essential context to grain identification because morphologically similar grains may vary significantly in size (e.g. in the Compositae family). Similarly, spatial context (latitude and longitude) is important for the exclusion of certain taxa during the identification process. The temporal context is currently optional, but in future we envisage this may also be an important filter for excluding certain groups (e.g. extinct species), and for studies of modern non-fossilised pollen (e.g. in pollination research). If the user has a date for the deposition/collection of a given grain, they may input this as additional data in any commonly used convention (e.g. years before present for radiocarbon-dated fossil material, or calendar year for modern samples). Once a grain is uploaded, it is listed on the GPP as unidentified, and is available to the community for identification.

The crowdsourcing grain identification option in the tool was designed to quickly determine confidence the user has in the identification. Identifications can occur at family, genus and species level. For speed of entry, we integrated The Plant List taxonomy so that plant taxa are suggested while typing, and family is auto-filled when a genus is selected (Fig. 2). We defined three requirements to confirm the identity of a grain through crowdsourcing: (i) there are at least three identifications by different users, (ii) there is a minimum agreement of 70% and (iii) the identification is validated by the taxonomic backbone.

To encourage identifications as well as submissions, a scoring system has been included under the header 'Leaderboard'. Unidentified grains are given a base score, which builds over time. This score is given for each taxonomic level identified, such that an identification to genus level (e.g. Betuleaceae – Betula) would gain double points compared with just a family level identification (e.g. Betuleaceae). All users get points. The leaderboard is based on individuals as well as their organisational affiliation, which enables a cross-institutional competitive incentive to the identification process.

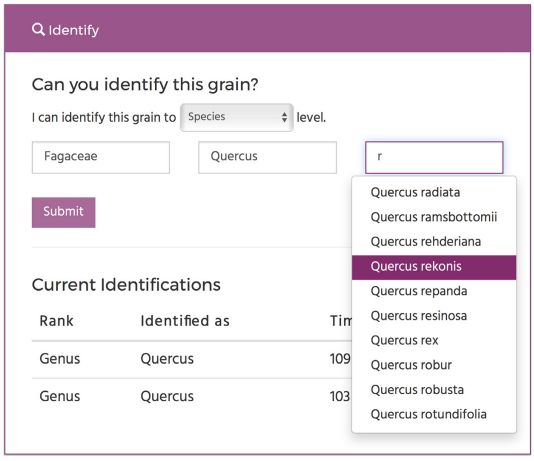

Fig. 2. Identification of an unknown pollen grain, demonstrating the auto-suggestion mechanism of valid taxonomic names, which uses The Plant List as the data source.

DIGITISATION AND DISSEMINATION OF EXISTING 'PHYSICAL' REFERENCE MATERIAL

Pollen reference slides provide an invaluable source of information for pollen grain identification. Many laboratories and funding agencies are now interested in the dissemination of this information to researchers and to the general public. The GPP allows any individual or institution to request digitisation rights, with which they can digitise their offline reference collections and upload onto this platform for dissemination. Any slides digitised in this way appear in the GPP reference collection alongside the user-submitted grains. All reference material is fully attributed to individuals and their institutions, alongside contact information for the associated party. Submitted material is currently under a non-commercial use licence (CC BY-NC 4.0 - https://creativecommons.org/licenses/by-nc/4.0/).

As before, the only information required to upload images is the maximum grain diameter. To aid speed of entry, we also integrated The Plant List (2013) matching in the digitisation interface. To encapsulate the different views of a pollen grain, specifically the rotation and focus that one could obtain from looking down a microscope (Peck 1974), we have developed a 'focus image' function. A z-stack comprising five images of sequential focus levels, taken using a fixed camera, are displayed as a single image that the user can focus through, emulating a light microscope experience (see http://globalpollenproject.org/Reference/Grain/835 as an example of *Agrostemma githago* L.).

A PUBLIC, GLOBAL, INTEGRATED DATABASE OF POLLEN IMAGES AND METADATA

The combination of user-submitted and identified grains along with physical reference collections are collectively presented in the form of a master digital pollen reference collection. These are grains with a 'confirmed' identification and can then be used as both a key for comparative identification, and as a teaching tool (Fig. 3). The database provides various browsing and searching features, and will soon be accessible programmatically. Incorporated into the web interface is data from the Global Biodiversity Information Facility (GBIF) Application Programming Interface (API) to visually depict current distributions of records of individual taxa along with brief descriptions of their habitat and ecology (GBIF 2016). For a given taxon, the user can therefore navigate directly from the GPP to

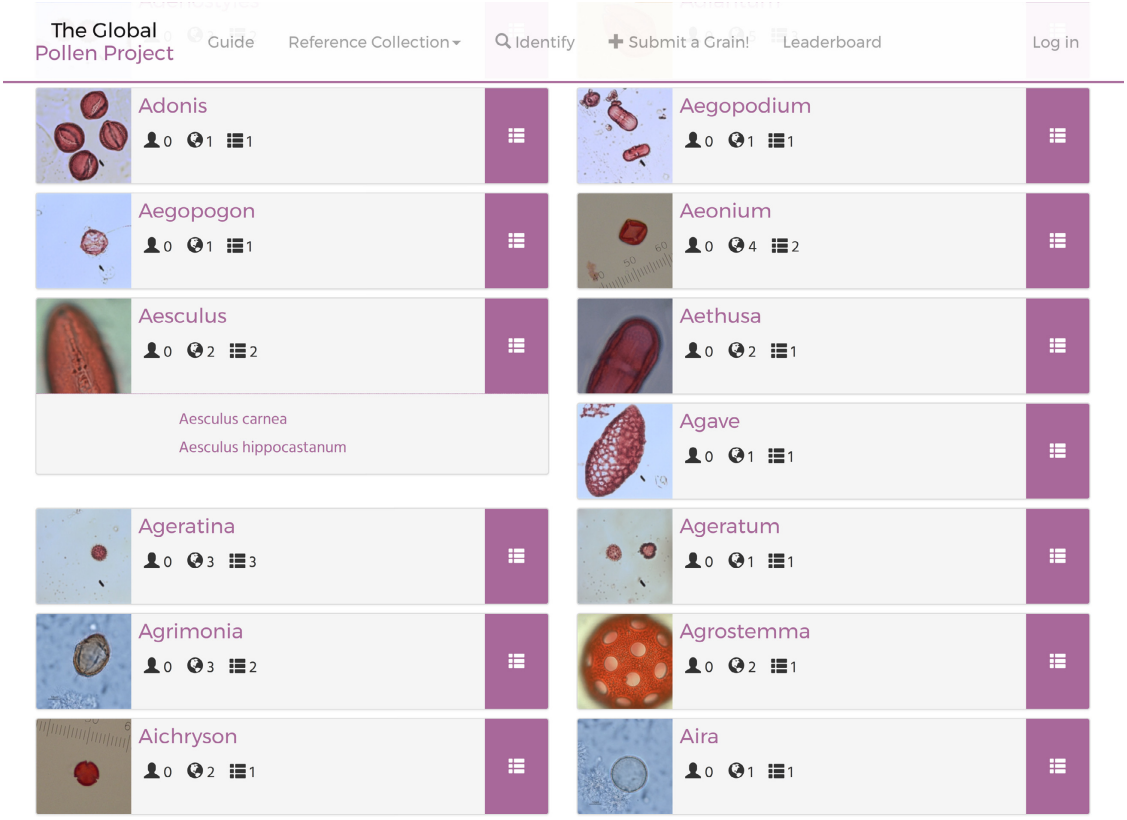

Fig. 3. The web interface for the GPP Master Reference Collection (MRC), organised by genus. The collection can be grouped by family, genus or species. Each taxon is displayed with information generated recursively (for itself and all sub-taxa). Person icon: number of unknown grains that have gained this taxon as their confirmed identification. Globe icon: number of digitised reference slides. List icon: number of taxa directly under this in the hierarchy (species in this case).

GBIF to examine additional information regarding current distribution, classification and description. Taxa in the GPP are also linked directly to corresponding taxon IDs in the Neotoma Palaeoecological Database (Neotoma 2016). Neotoma's API is similarly used to visualise distributions derived from palaeoecological data up to 50 000 years before present, with user-selectable time windows (Fig. 4).

Discussion

There is inherent value in physical palynological collections as well as in their GPP digitised form. Each form has a number of strengths and weaknesses lending to preferential use in education and research. While physical slides may preserve an array of grains from different angles and orientations, and may be physically handled under a microscope, they degrade over time, which could, and has, rendered many collections defunct. Through the process of digitising these physical collections using the GPP protocol, we can preserve and make readily available palynological collections to anyone with a computer and an internet connection. Further added value of the GPP collections compared to physical collections and/or other digital collections is the unique meta-data associated with each GPP slide/grain, which due to its common, indexed, format is inherently search- and sort-able, enabling integration with other databases and platforms such as the TRY plant traits database (Kattge *et al.* 2011). The core framework of the GPP is an open source modular platform that can also be utilised to host and organise other digital collections in other taxonomic groups such as diatoms, Chironomidae, Ostracoda and invertebrates.

The GPP creates new opportunities for research, for example automatic recognition. The image library will be a valuable resource for pollen identification using machine learning approaches. The GPP currently contains over 6000 unique images (when focus images are split) linked directly to botanical taxa. A truly global database of plant pollen images will enable greater power within deep neural network image recognition of pollen grains. Specifically, we suggest that the database promotes image replicates within taxa, which will be crucial to developing morphological pollen recognition using light microscope images.

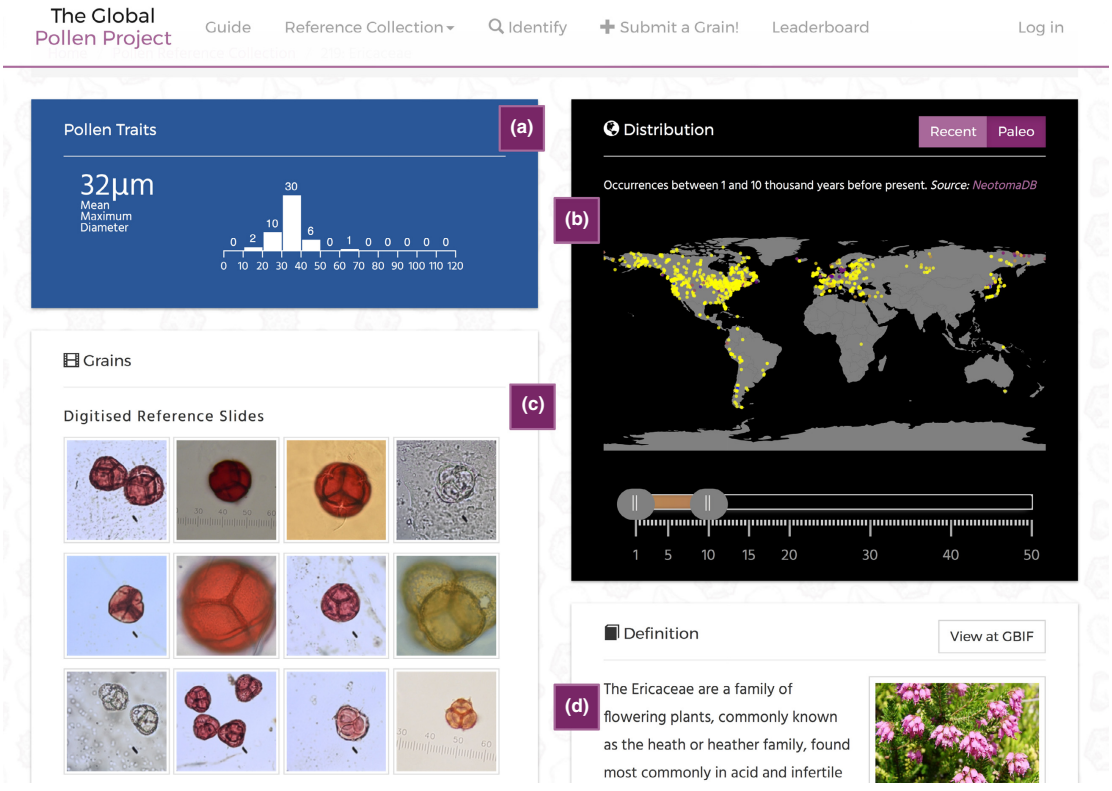

Fig. 4. Ericaceae as an example taxon page in GPP. (a) The pollen traits panel displays recursive trait information. Currently, only maximum grain diameter is collected and displayed as a histogram, alongside the mean value. (b) The distribution panel displaying palaeoecological occurrence data (obtained from the Neotoma Palaeoecological Database) from 1000 to 10 000 years before present. The slider allows user visualisation of changes in the distribution with different time windows. (c) Digitised reference slides are displayed recursively (in this case for all genera and species within Ericaceae). Unknown grains that have gained this identification are shown below digitised reference slides. (d) Botanical information obtained from the Global Biodiversity Information Facility (GBIF). In this case, GBIF returned an image and text summary obtained from Wikipedia. The 'View at GBIF' link connects to Ericaceae on the GBIF website.

Use of the GPP has been growing. Since the GPP was launched in March 2016, 1697 unique users from 86 countries have used the master reference collection (to 15th November 2016), with major use in Scandinavia, Russia, the USA, Canada, Mexico and Brazil. The GPP has also been used in teaching in a university setting, incorporating the tool into lectures and laboratory sessions.

In attempting to maximise the effectiveness of this tool, we have addressed four overarching themes. First, the standardisation of palynological practices, specifically relating to taxonomic nomenclature. Second, the assimilation of resources and collections, often in the form of data that is 'locked away' in physical collections. Third, access for all, providing free tools for the dissemination of collections and data to encourage wider scientific and public interest and use across the globe, particularly in less well-known regions such as the tropics and neotropics. Fourth, use of this collection as a teaching tool. Each aspect of the GPP can be used collectively or individually. The three functions of the GPP: (i) identification of pollen grains, (ii) dissemination of reference collections and (iii) provision of an accessible, global and searchable database, highlight the major areas of expected use within the palynological discipline. Future development of this tool will include the addition of functionality for pollen traits (macro/micro), the ability to rate quality of images, and further development work for eased data access and interoperability.

Authors' contributions

W.J.H. and A.C.M. developed the concept for the GPP; A.C.M. implemented the ideas into a database and web app. Continued revision of the framework was conducted by W.J.H. and A.C.M. The authors contributed equally to the manuscript.

Acknowledgements

The authors would like to give thanks to the reviewers, particularly Jack Williams for his constructive and detailed suggestions. We would also like to thank Kathy Willis and the Oxford Long-Term Ecology Laboratory for their support and contribution of the *European Reference Collection*; Sandra Nogué for her enthusiasm and contributions; Keith Bennett for his early support and contribution of *Pollen of Britain and Ireland*; Leo Petrokofsky for his work digitising collections held in Oxford; and to all others who have already contributed to the database. Funding was awarded by the Natural Environment Research Council (NERC) to digitise the Oxford collections. Additional funding was also awarded by the Oxford NERC Doctoral Training Partnership for maintenance of this database for the next 3 years.

Data accessibility

All source code for the Global Pollen Project is available at Zenodo (doi: 10.5281/zenodo.260180). The latest release is available at https://github.com/AndrewIOM/global-pollen-project.

References

Bennett, K.D. & Willis, K.J. (2002) Pollen. *Tracking Environmental Change Using Lake Sediments: Terrestrial, Algal, and Siliceous Indicators* (eds J.P. Smol, H.J. Birks & W.M. Last), pp. 5–32. Kluver Academic Publishers, Dordrecht, The Netherlands.

Berglund, B.E. (1986) *Handbook of Holocene Palaeoecology and Palaeohydrology*. John Wiley & Sons, Chichester, UK.

Brooks, S.J., Self, A., Toloni, F. & Sparks, T. (2014) Natural history museum collections provide information on phenological change in British butterflies since the late-nineteenth century. *International Journal of Biometeorology*, **58**, 1749–1758.

iDigBio (2016) *iDigBio*. Available at: https://www.idigbio.org/ (accessed 15 December 2016).

GBIF (2016) *The Global Biodiversity Information Facility*. Available at: http://www.gbif.org/ (accessed 16 May 2016).

Heidorn, P.B. (2008) Shedding light on the dark data in the long tail of science. *Library Trends*, **57**, 280–299.

Hennon, C.C., Knapp, K.R., Schreck, C.J. *et al.* (2015) Cyclone Center: can citizen scientists improve tropical cyclone intensity records? *Bulletin of the American Meteorological Society*, **96**, 591–607.

Kattge, J., Díaz, S., Lavorel, S. *et al.* (2011) TRY – a global database of plant traits. *Global Change Biology*, **17**, 2905–2935.

Mander, L. & Punyasena, S. (2014) On the taxonomic resolution of pollen and spore records of Earth's vegetation. *International Journal of Plant Sciences*, **175**, 931–945.

Microsoft (2016a) *ASP.NET Core 1.0.0*. Microsoft Corporation, Seattle, WA, USA. Available at: https://asp.net (accessed 25 July 2016).

Microsoft (2016b) *Entity Framework Core 1.0.0*. Microsoft Corporation, Seattle, WA, USA. Available at: http://efproject.net (accessed 25 July 2016).

Microsoft (2016c) *Microsoft Azure Cloud Platform*. Microsoft Corporation, Seattle, WA, USA. Available at: https://azure.com (accessed 25 July 2016).

Neotoma (2016) *The Neotoma Paleoecological Database*. Available at: http://www.neotomadb.org/ (accessed 16 May 2016).

Pearsall, D.M. (2015) Preservation. *Paleoethnobotany: A Handbook of Procedures*, 3rd edn (ed D.M. Pearsall), pp. 201–203. Left Coast Press, Walnut Creek, CA, USA.

Peck, R.M. (1974) A comparison of four absolute pollen preparation techniques. *New Phytologist*, **73**, 567–587.

Silvertown, J., Harvey, M., Greenwood, R., Dodd, M., Rosewell, J., Rebelo, T., Ansine, J. & McConway, K. (2015) Crowdsourcing the identification of organisms: a case-study of iSpot. *ZooKeys*, **480**, 125.

The Plant List (2013) *Version 1.1*. Available at: http://www.theplantlist.org/ (accessed 23 January 2016).

Wen, J., Ickert-Bond, S.M., Appelhans, M.S., Dorr, L.J. & Funk, V.A. (2015) Collections-based systematics: opportunities and outlook for 2050. *Journal of Systematics and Evolution*, **53**, 477–488.

Received 15 December 2016; accepted 23 January 2017
Handling Editor: Sarah Goslee

Appendix 2

Local Ecological Footprinting Tool

I am third author on this paper. I developed the software framework including the web interface.

Long, Peter R, David Benz, Andrew C Martin, Philip W A Holland, Marc Macias Fauria, Alistair W R Seddon, Randi Hagemann, et al. "LEFT—a Web-Based Tool for the Remote Measurement and Estimation of Ecological Value Across Global Landscapes." *Methods in Ecology and Evolution* 9, no. 3 (March 1, 2018): 571–79. doi:10.1111/2041-210X.12924.

LEFT – a Web-Based tool for the Remote Measurement and Estimation of Ecological Value Across Global Landscapes

7.6 Abstract

The overall aim in the development of the Local Ecological Footprinting Tool (LEFT) was to design a web-based tool that could provide quickly obtained quantitative data on ecological risk to assist landowners when making land-use change decisions.

The Local Ecological Footprinting Tool works for almost any region in the world and uses freely available satellite imagery, biotic and abiotic data from existing global databases, models and algorithms to deliver a customised report for a selected area within one hour of job submission.

Biotic data automatically obtained for a selected landscape includes terrestrial vertebrate and plant species occurrence data, information on their conservation status and remotely sensed vegetation productivity. Abiotic information obtained includes temperature, precipitation, water availability, insolation, topography, elevation, distribution of urban infrastructure and location of wetlands.

The tool performs a number of analyses on the biotic and abiotic data to produce maps for the selected area at a 30 m resolution depicting land cover type, numbers of globally threatened terrestrial vertebrate and plant species, beta-diversity of terrestrial vertebrates and plants, habitat intactness, wetland habitat connectivity, numbers of migratory species and vegetation resilience. Results are also aggregated to produce a summary map demonstrating areas of high and low ecological risk across the selected area.

The Local Ecological Footprinting Tool has been designed to be intuitive to use, requiring no specialised software or user expertise. Input is extremely easy and requires the user to highlight the

area of interest on a map or using grid co-ordinates. Output is delivered via the web application and comprises a customised PDF containing the maps and a zip file of geographical information system (GIS) data for the area requested. Users may run an unlimited number of LEFT analyses and download reports free of charge. In addition to the free tool described in this paper, there is also a paid service: individual LEFT analyses can be upgraded for a charge to allow access to the geographically subsetted datasets generated for each report. These data are supplied as a zip file containing raster datasets for the layers in the LEFT analysis in GeoTIFF format. These can be opened and queried in a GIS software package.

Full text available online

Appendix 3

Shrub Nutrient Modelling Code

The following Bristlecone F# scripts were used to conduct analysis in Chapters 3, 4, and 5.

Shrub Nitrogen Model 1 (Chapter 3)

```
#r "../packages/NETStandard.Library.NETFramework/build/net461/lib/netstandard.dll"
#load "../packages/Bristlecone/bristlecone.fsx"
#load "components/components.fsx"
#r "../packages/Bristlecone.Dendro/lib/netstandard2.0/bristlecone.Dendro.dll"

////////////////////////////////////////////////
/// Yuribei `Salix lanata` Shrub - Nitrogen Interactions
////////////////////////////////////////////////

// Shrub ring width modelled with a single
// resource limitation.

open Bristlecone
open Bristlecone.ModelSystem
open Bristlecone.Dendro
open Bristlecone.Dendro.PlantIndividual
open Bristlecone.Data
open Bristlecone.Workflow.Orchestration

// 1. Configure Options
// ----------------------------

module Options =
    let resultsDirectory = "/Users/andrewmartin/Desktop/Bristlecone Results/YuribeiAn
nual-Filzbach"
    let chains = 3
    let endWhen = Optimisation.EndConditions.afterIteration 100000
    let logger = Logging.Console.logger(1000)
    let engine =
        Bristlecone.mkContinuous
        |> Bristlecone.withContinuousTime Integration.MathNet.integrate
        |> Bristlecone.withOutput logger
        |> Bristlecone.withCustomOptimisation (Optimisation.MonteCarlo.SimulatedAnnea
ling.fastSimulatedAnnealing 0.0001 false
            { Optimisation.MonteCarlo.SimulatedAnnealing.AnnealSettings<float>.Defaul
t with
                BoilingAcceptanceRate = 0.85
                HeatRamp = (fun t -> t + sqrt t); TemperatureCeiling = Some 500.
                HeatStepLength = Optimisation.EndConditions.afterIteration 1000
                AnnealStepLength = (fun x -
> Optimisation.MonteCarlo.SimulatedAnnealing.EndConditions.improvementCount 5000 250
x || Optimisation.EndConditions.afterIteration 10000 x) })

    let orchestrator = OrchestrationAgent(logger, System.Environment.ProcessorCount,
false)


// 2. Create Hypotheses
// ----------------------------

module BaseEquations =

    /// Cumulative stem biomass [dBs/dt]
    let biomass b n r gammab geom f : float =
        b * r * (f n) * geom(b) - gammab * b

    let soilNitrogen n b gamman y geom f feedback : float =
        y - (geom(b) * b * (f n)) - gamman * n + feedback(b)

    let soilNitrogenNoUptake n b gamman y feedback : float =
        y - gamman * n + feedback(b)


let ``base model`` maxGrowthRate nLimitation nitrogenFeedback additionalParameters =

    /// Cumulative stem biomass [b].
    let dbsdt' (b:float) n gammab r maxGrowthRate limit =
        match limit with
        | Some l -> BaseEquations.biomass b n (r * 1000.) gammab maxGrowthRate l
        | None -> BaseEquations.biomass b n r gammab maxGrowthRate (fun _ -> 1.)
```

```
    /// Bioavailable soil nitrogen [N]
    let dndt' bs n lambda gamman maxGrowthRate feedback limit =
        match limit with
        | Some l -
> BaseEquations.soilNitrogen n bs gamman lambda maxGrowthRate l feedback
        | None -> BaseEquations.soilNitrogenNoUptake n bs gamman lambda feedback

    /// Bristlecone function for dBs/dt
    let dbsdt p _ bs (e:Environment) =
        dbsdt' bs ((e.[code "N"]) |> ModelComponents.Proxies.d15NtoAvailability)
            (p |> Pool.getEstimate "gamma[b]") ((p |> Pool.getEstimate "r")) (maxGrow
thRate p) (nLimitation p)

    /// Bristlecone function for dN/dt
    let dndt p _ n (e:Environment) =
        dndt' (e.[code "bs"]) (n |> ModelComponents.Proxies.d15NtoAvailability)
            (p |> Pool.getEstimate "lambda") (p |> Pool.getEstimate "gamma[n]") (maxG
rowthRate p) (nitrogenFeedback p) (nLimitation p)

    /// Measurement (Size) variable: stem radius
    let stemRadius lastRadius lastEnv env =
        let oldCumulativeMass = lookup lastEnv "bs"
        let newCumulativeMass = lookup env "bs"
        if (newCumulativeMass - oldCumulativeMass) > 0.
        then newCumulativeMass |> ModelComponents.Proxies.toRadiusMM
        else lastRadius

    { Equations  = [ code "bs",        dbsdt
                     code "N",         dndt ] |> Map.ofList
      Measures   = [ code "x",         stemRadius ] |> Map.ofList
      Parameters = [ // for nitrogen dynamics
                     code "lambda",    parameter PositiveOnly   0.001 0.500   // Rate
 of nitrogen replenishment
                     code "gamma[n]",  parameter PositiveOnly   0.001 0.200   // Loss
 rate of nitrogen
                     // for shrub physiology
                     code "gamma[b]",  parameter PositiveOnly   0.001 0.200   // Loss
 rate of biomass
                     // for likelihood function
                     code "rho",       parameter Unconstrained  -
0.50 0.500   // Covariance between growth and nitrogen
                     code "sigma[x]",  parameter PositiveOnly   0.001 0.100   // Stan
dard deviation of x (biomass)
                     code "sigma[y]",  parameter PositiveOnly   0.001 0.100   // Stan
dard deviation of y (nitrogen)
                   ] |> List.append additionalParameters |> Map.ofList
      Likelihood = ModelLibrary.Likelihood.bivariateGaussian "x" "N" }

let hypotheses =

    // [A] N may limited growth via combined N-
limitations on (a) photosynthetic and (b) uptake rates
    let limitationModes =
        [ (fun p -
> ModelComponents.GrowthLimitation.hollingDiscModelDual ((p |> Pool.getEstimate "a")
/ 1000.)  ((p |> Pool.getEstimate "r") * 1000.) (p |> Pool.getEstimate "h") 10.),
          [ code "a",      parameter PositiveOnly   0.100 0.400          // N-
uptake efficiency
            code "h",      parameter PositiveOnly   0.100 0.400
            code "r",      parameter PositiveOnly   0.500 1.000 ]     // N-
handling time (including uptake and incorporation)
          (fun p -
> ModelComponents.GrowthLimitation.linear ((p |> Pool.getEstimate "a") / 1000.) 10.),

          [ code "a",      parameter PositiveOnly   0.001 0.010
            code "r",      parameter PositiveOnly   0.100 1.000 ]        // N-
uptake efficiency
          (fun _ -> ModelComponents.GrowthLimitation.none),
          [ code "r",       parameter PositiveOnly   0.500 1.000 ] ]

    // [B] Loss of plant material may feedback into the soil pool of available nitrog
en (instant)
```

```
    let feedbackModes =
        [ (fun _ -> ModelComponents.FeedbackToSoil.none), []
          (fun p -
> ModelComponents.FeedbackToSoil.withBiomassLoss ((p |> Pool.getEstimate "alpha") / 1
00.) (p |> Pool.getEstimate "gamma[b]") ),
          [ code "alpha",  parameter PositiveOnly   0.01 1.00 ] ]    // N-
recycling efficiency

    // [C] A plant may be subject to mechanical constraints on its maximum size
    let geometricModes =
        [  (fun p -> ModelComponents.GeometricConstraint.none), []
           (fun p -
> ModelComponents.GeometricConstraint.chapmanRichards ((p |> Pool.getEstimate "k") *
1000.)),
          [ code "k",  parameter PositiveOnly   3.00 5.00 ] ]     // Asymptotic biom
ass (grams)

    List.combine3 geometricModes limitationModes feedbackModes
    |> List.map (fun ((growth,gp),(limit,lp),(feedback,fp)) ->
        ``base model`` growth limit feedback (List.concat [lp; fp; gp]))

// 2. Load Real Data and Estimate
// ------------------------------

let shrubs =
    let yuribei = Data.PlantIndividual.loadRingWidths (__SOURCE_DIRECTORY__ + "/../da
ta/yamal-rw.csv")
    let d15N = Data.PlantIndividual.loadLocalEnvironmentVariable (__SOURCE_DIRECTORY_
_ + "/../data/yuribei-d15N-imputed.csv")
    yuribei
    |> Seq.map (fun s -> (s.Identifier.Value, s))
    |> Seq.keyMatch d15N
    |> Seq.map (fun (_,plant,d15N) -> PlantIndividual.zipEnv (code "N") plant d15N)
    |> Seq.toList

let getStartValues (startDate:System.DateTime) (plant:PlantIndividual) =
    let initialRadius =
        match plant.Growth with
        | RingWidth s ->
            match s with
            | Absolute c -> c.Head |> fst |> removeUnit
            | Cumulative c ->
                let start = (c |> TimeSeries.trimStart (startDate - System.TimeSpan.F
romDays(366.))).Values |> Seq.head |> removeUnit
                // printfn "Start cumulative growth = %f" start
                start
            | Relative _ -> invalidOp "Not implemented"
        | _ -> invalidOp "Not implemented 2"
    let initialMass = initialRadius |> removeUnit |> ModelComponents.Proxies.toBiomas
sMM
    let initialNitrogen = plant.Environment.[code "N"].Head |> fst
    [ (code "x", initialRadius)
      (code "N", initialNitrogen)
      (code "bs", initialMass) ] |> Map.ofList

let workPackages shrubs hypotheses engine saveDirectory =
    seq {
        for s in shrubs do

            // 1. Arrange the subject and settings
            let shrub = s |> PlantIndividual.toCumulativeGrowth
            let common = shrub |> PlantIndividual.keepCommonYears
            let startDate = (common.Environment.[code "N"]).StartDate |> snd
            let startConditions = getStartValues startDate shrub
            let e = engine |> Bristlecone.withConditioning (Custom startConditions)

            // 2. Setup batches of dependent analyses
            for h in [ 1 .. hypotheses |> List.length ] do
                for _ in [ 1 .. Options.chains ] do
                    yield async {
                            // A. Compute result
                            let result = Bristlecone.PlantIndividual.fit e Options.en
dWhen hypotheses.[h-1] common |> fst
```

```
                            // B. Save to file
                            Bristlecone.Data.EstimationResult.saveAll saveDirectory s
.Identifier.Value h 1 result
                            return result }
    }

// Orchestrate the analyses
let work = workPackages shrubs hypotheses Options.engine Options.resultsDirectory
let run() = work |> Seq.iter (OrchestrationMessage.StartWorkPackage >> Options.orches
trator.Post)
```

Regional Shrub Nutrient Model (Chapter 4)

```
#r "../packages/NETStandard.Library.NETFramework/build/net461/lib/netstandard.dll"
#load "../packages/Bristlecone/bristlecone.fsx"
#load "components/components.fsx"
#r "../packages/Bristlecone.Dendro/lib/netstandard2.0/Bristlecone.Dendro.dll"
#load "components/temperature.fsx"

////////////////////////////////////////////////
/// Long-Term N-Shrub relations in Yamal, Russia
////////////////////////////////////////////////

// This script completes model-fitting and model-selection
// for 24 shrub individuals. Models for nitrogen limitation,
// temperature limitation, and size-related asymptotes are
// included.

open Bristlecone
open Bristlecone.ModelSystem
open Bristlecone.Dendro
open Bristlecone.Dendro.PlantIndividual
open Bristlecone.Workflow.Orchestration
open Bristlecone.Diagnostics.ModelComponents

// .NET Core requires this workaround to bind to MathNet. Hopefully will be fixed in
3.0 RTM.
let x = MathNet.Numerics.Random.MersenneTwister()


// 1. Configure Options
// ----------------------------

module Options =
    let resultsDirectory = "/Users/andrewmartin/Desktop/Bristlecone Results/Paper3-
Repeated-Final/"
    let chains = 3
    let endWhen = Optimisation.EndConditions.afterIteration 100000
    let logger = Logging.Console.logger 1000 //Logging.RealTimeTrace.graphWithConsole
 60. 10000
    let engine =
        Bristlecone.mkContinuous
        |> Bristlecone.withContinuousTime Integration.MathNet.integrate
        |> Bristlecone.withOutput logger
        // |> Bristlecone.withTunedMCMC [ Optimisation.MonteCarlo.TuneMethod.Covarian
ceWithScale 0.100, 1000, Optimisation.EndConditions.afterIteration 100000 ]
        // |> Bristlecone.withCustomOptimisation (Optimisation.MonteCarlo.Filzbach.fi
lzbach filzbachOptions)
```

```
        // |> Bristlecone.withCustomOptimisation (Optimisation.MonteCarlo.adaptiveMet
ropolis 0.250 500)
        |> Bristlecone.withCustomOptimisation (Optimisation.MonteCarlo.SimulatedAnnea
ling.fastSimulatedAnnealing 0.01 true
            { Optimisation.MonteCarlo.SimulatedAnnealing.AnnealSettings<float>.Defaul
t with
                InitialTemperature = 100.
                TemperatureCeiling = Some 100.
                HeatRamp = (fun t -> t + 5.00)
                BoilingAcceptanceRate = 0.85
                HeatStepLength = Optimisation.EndConditions.afterIteration 1000
                TuneLength = 1000
                AnnealStepLength = (fun x -
> (*Optimisation.MonteCarlo.SimulatedAnnealing.EndConditions.improvementCount 5000 25
0 x ||*) Optimisation.EndConditions.afterIteration 10000 x) }) //(Optimisation.EndCon
ditions.afterIteration 10000) })
    let orchestrator = OrchestrationAgent(logger, System.Environment.ProcessorCount,
false)


// 2. Create Hypotheses
// ----------------------------

module BaseEquations =

    /// Cumulative stem biomass [dBs/dt]
    let biomass b n r gammab geom f tempEffect cLog : float =
        if r > 100000. then nan
        else
            cLog "growthRate" (b * r * (f n) * geom(b) * tempEffect)
            cLog "biomassLossRate" (gammab * b)
            cLog "nUptake" (f n)
            cLog "geometryEffect" (geom(b))
            cLog "tLimitation" (tempEffect)
            cLog "nLimitation" (r * (f n))
            cLog "nAndtempLimitation" (r * (f n) * tempEffect)
            b * r * (f n) * geom(b) * tempEffect - gammab * b

    let soilNitrogen n b gamman y geom f feedback tempEffect cLog : float =
        cLog "plantSoilFeedback" (feedback(b))
        cLog "abioticReplenishment" y
        cLog "nEnvironmentalLoss" (-gamman * n)
        cLog "nUseByPlant" ((geom(b) * b * (f n) * tempEffect))
        y - (geom(b) * b * (f n) * tempEffect) - gamman * n + feedback(b)

    let soilNitrogenNoUptake n b gamman y feedback cLog : float =
        cLog "plantSoilFeedback" (feedback(b))
        cLog "abioticReplenishment" y
        cLog "nEnvironmentalLoss" (-gamman * n)
        cLog "nUseByPlant" 0.
        y - gamman * n + feedback(b)


let ``base model`` maxGrowthRate nLimitation nitrogenFeedback tempEffect additionalPa
rameters (cLog:IComponentLogger<float>) =

    /// Cumulative stem biomass [b].
    let dbsdt' t (b:float) n gammab r maxGrowthRate limit tLimit =
        match limit with
        | Some l -
> BaseEquations.biomass b n (r * 1000.) gammab maxGrowthRate l tLimit (fun name l -
> cLog.StoreValue name t l |> ignore)
        | None -> BaseEquations.biomass b n r gammab maxGrowthRate (fun _ -
> 1.) tLimit (fun name l -> cLog.StoreValue name t l |> ignore)
```

```
    /// Bioavailable soil nitrogen [N]
    let dndt' t bs n lambda gamman maxGrowthRate feedback limit tLimit =
        match limit with
        | Some l -
> BaseEquations.soilNitrogen n bs gamman lambda maxGrowthRate l feedback tLimit (fun
name l -> cLog.StoreValue name t l |> ignore)
        | None -
> BaseEquations.soilNitrogenNoUptake n bs gamman lambda feedback (fun name l -
> cLog.StoreValue name t l |> ignore)

    /// Bristlecone function for dBs/dt
    let dbsdt p t bs (e:Environment) =
        dbsdt' t bs ((e.[ShortCode.create "N"]) |> ModelComponents.Proxies.d15NtoAvai
lability)
            (p |> Pool.getEstimate "gamma[b]") ((p |> Pool.getEstimate "r")) (maxGrow
thRate p) (nLimitation p) (tempEffect p e)

    /// Bristlecone function for dN/dt
    let dndt p t n (e:Environment) =
        dndt' t (e.[ShortCode.create "bs"]) (n |> ModelComponents.Proxies.d15NtoAvail
ability)
            (p |> Pool.getEstimate "lambda") (p |> Pool.getEstimate "gamma[n]") (maxG
rowthRate p) (nitrogenFeedback p) (nLimitation p) (tempEffect p e)

    /// Measurement (Size) variable: stem radius
    let stemRadius lastRadius lastEnv env =
        let oldCumulativeMass = lookup lastEnv "bs"
        let newCumulativeMass = lookup env "bs"
        if (newCumulativeMass - oldCumulativeMass) > 0.
        then
            // This clause mandates that stem radius can never decrease.
            let newRadius = newCumulativeMass |> ModelComponents.Proxies.toRadiusMM
            if newRadius > lastRadius then newRadius else lastRadius
        else lastRadius

    { Equations  = [ code "bs",        dbsdt
                     code "N",         dndt ] |> Map.ofList
      Measures   = [ code "x",         stemRadius ] |> Map.ofList
      Parameters = [ // for nitrogen dynamics
                     code "lambda",    parameter PositiveOnly   0.100 2.000   // Rate
 of nitrogen replenishment
                     code "gamma[n]",  parameter PositiveOnly   0.001 5.000   // Loss
 rate of nitrogen
                     // for shrub physiology
                     code "gamma[b]",  parameter PositiveOnly   0.001 0.200   // Loss
 rate of biomass
                     // for likelihood function
                     code "rho",       parameter Unconstrained  -
0.50 0.500   // Covariance between growth and nitrogen
                     code "sigma[x]",  parameter PositiveOnly   0.100 1.200   // Stan
dard deviation of x (biomass)
                     code "sigma[y]",  parameter PositiveOnly   0.250 0.750   // Stan
dard deviation of y (nitrogen)
                   ] |> List.append additionalParameters |> Map.ofList
      Likelihood = ModelLibrary.Likelihood.bivariateGaussian "x" "N" }


let hypotheses : (IComponentLogger<float> -> ModelSystem) list =

    // [A] N may limited growth via combined N-
limitations on (a) photosynthetic and (b) uptake rates
    let limitationModes =
```

```
        [ (fun p -
> ModelComponents.GrowthLimitation.hollingDiscModelDual ((p |> Pool.getEstimate "a")
/ 1000.) ((p |> Pool.getEstimate "r") * 1000.) ((p |> Pool.getEstimate "h") / 1.) 5.0
0),
           [ code "a",      parameter PositiveOnly   0.100 5.000          // N-
uptake efficiency
             code "h",      parameter PositiveOnly   0.001 0.250
             code "r",      parameter PositiveOnly   1.000 10.00 ]      // N-
handling time (including uptake and incorporation)
          (fun p -
> ModelComponents.GrowthLimitation.linear ((p |> Pool.getEstimate "a") / 1000.) 5.00)
,
           [ code "a",      parameter PositiveOnly   0.001 0.010
             code "r",      parameter PositiveOnly   1.000 10.00 ]        // N-
uptake efficiency
          (fun _ -> ModelComponents.GrowthLimitation.none),
           [ code "r",       parameter PositiveOnly  1.000 10.00 ] ]

    // [B] Loss of plant material may feedback into the soil pool of available nitrog
en (instant)
    let feedbackModes =
        [ (fun _ -> ModelComponents.FeedbackToSoil.none), []
          (fun p -
> ModelComponents.FeedbackToSoil.withBiomassLoss ((p |> Pool.getEstimate "alpha") / 1
00.) (p |> Pool.getEstimate "gamma[b]") ),
          [ code "alpha",  parameter PositiveOnly   0.001 0.100 ] ]    // N-
recycling efficiency

    // [C] A plant may be subject to mechanical constraints on its maximum size
    let geometricModes =
        [  (fun p -> ModelComponents.GeometricConstraint.none), []
           (fun p -
> ModelComponents.GeometricConstraint.chapmanRichards ((p |> Pool.getEstimate "k") *
1000.)),
           [ code "k",  parameter PositiveOnly   3.00 5.00 ] ]     // Asymptotic biom
ass (grams)

    // [D] Net photosynthetic rate is temperature-dependent
    let temperature =
        [ (fun _ -> ModelComponents.Temperature.none), []
          (fun p e -
> ModelComponents.Temperature.arrheniusAlt 1. (p |> Pool.getEstimate "Ea") (lookup e
"T[max]")),
           [ code "Ea",             parameter PositiveOnly 10.00 30.00  ] ]

    List.combine4 temperature geometricModes limitationModes feedbackModes
    |> List.map (fun ((temperature,tp),(growth,gp),(limit,lp),(feedback,fp)) ->
        ``base model`` growth limit feedback temperature (List.concat [lp; fp; gp; tp
]))


// 3. Load Real Data and Estimate
// ------------------------------

open FSharp.Data

// 1. Load in ring widths
let rw = Bristlecone.Data.PlantIndividual.loadRingWidths (__SOURCE_DIRECTORY__ + "/..
/data/yamal-rw.csv")

// 2. Load in temperature data
type TemperatureData = CsvProvider<"/Users/andrewmartin/Projects/GitHub-
Projects/shrub-nutrient-modelling/data/yamal-mean-temperatures.csv">
```

```
let summerTemperature =
    let maxTemperatures = TemperatureData.Load "/Users/andrewmartin/Projects/GitHub-
Projects/shrub-nutrient-modelling/data/yamal-mean-temperatures.csv"
    maxTemperatures.Rows
    |> Seq.groupBy(fun r -> r.Station)
    |> Seq.map(fun (station,r) -> station, r |> Seq.map(fun r -
> ( float r.JJA + 273.15, System.DateTime.Create 31 12 r.Year)) |> TimeSeries.fromObs
ervations)
    |> Seq.toList

// 2. Define common timeline for three year bins
// Read in yuribei annual data and regional 3-yearly data
type Regional15N = CsvProvider<"/Users/andrewmartin/Projects/GitHub-Projects/shrub-
nutrient-modelling/data/yamal-d15N-lowres.csv">
type YuribeiD15N = CsvProvider<"/Users/andrewmartin/Projects/GitHub-Projects/shrub-
nutrient-modelling/data/yuribei-d15N-imputed.csv">

let bins = seq { 1900 .. 3 .. 2018 }
let regionalD15N = Regional15N.Load (__SOURCE_DIRECTORY__ + "/../data/yamal-d15N-
lowres.csv")
let yuribeiD15N = YuribeiD15N.Load (__SOURCE_DIRECTORY__ + "/../data/yuribei-d15N-
imputed.csv")

// 3. Lower resolution of data where it is higher resolution than bins.
// - Determine the period that each reading represents
// - Where time-points are repeated, find the average
// - Calculate the weighted average of each period (mixture)

/// Converts input data into 3-year binned d15N and increment data
let lowerResolution (plant:PlantIndividual) =

    printfn "Plant is %A" plant

    let growth =
        match plant.Growth with
        | PlantIndividual.PlantGrowth.RingWidth x ->
            match x with
            | Absolute rw -> rw
            | Cumulative(_) -> failwith "Not Implemented"
            | Relative(_) -> failwith "Not Implemented"
        | _ -> failwith "Not implemented"

    let isotopeByBin =
        bins
        |> Seq.choose(fun binStart ->
            let lowResBins =
                regionalD15N.Rows
                |> Seq.where(fun n -> n.Shrub = plant.Identifier.Value)
                |> Seq.where(fun n -
> n.BinLatest <= (binStart + 2) && n.BinOldest >= binStart)
                |> Seq.map(fun r -> (r.BinOldest, r.BinLatest, r.D15N))
                |> Seq.toList

            // These are complete (pre-interpolated) TODO do this in code instead
            let highResBins =
                yuribeiD15N.Rows
                |> Seq.where(fun n -> n.``Plant Code`` = plant.Identifier.Value)
                |> Seq.where(fun n -
> n.Date.Year <= (binStart + 2) && n.Date.Year >= binStart)
                |> Seq.map(fun r -
> (r.Date.Year, r.Date.Year, (float r.``Predictor 2``) ))
                |> Seq.toList

            let allData =
```

```
                highResBins
                |> Seq.append lowResBins
                |> Seq.sortBy (fun (s,_,_) -> s)
                |> Seq.filter(fun (_,_,x) -> not <| System.Double.IsNaN x)

            // printfn "All data is %A" allData
            // printfn "Low data is %A" lowResBins
            // printfn "High data is %A" highResBins

            if allData |> Seq.isEmpty then None
            else
                // Weighted average is:
                // Get the ring increment for the whole bin and times isotope value
                // Average by these values
                try
                    let weightedAverage =
                        let weights =
                            let increments = allData |> Seq.map (fun (start,en,_) -
> [ start .. en ] |> List.sumBy(fun y -
> growth |> TimeSeries.findExact (System.DateTime(y, 12, 31)) |> fst |> removeUnit ))
                            let totalIncrement = increments |> Seq.sum
                            increments |> Seq.map(fun i -> i / totalIncrement)
                        printfn "Weights are %A" weights
                        allData
                        |> Seq.zip weights
                        |> Seq.averageBy(fun (weight,(s,e,d15n)) -> d15n * weight )
                    Some (binStart + 2, weightedAverage)
                with | _ -> None )
        |> Seq.toList
    isotopeByBin



/// Converts input data into 3-year binned d15N and increment data
let threeYearToAnnual (plant:PlantIndividual) =

    printfn "Plant is %A" plant

    let growth =
        match plant.Growth with
        | PlantIndividual.PlantGrowth.RingWidth x ->
            match x with
            | Absolute rw -> rw
            | Cumulative(_) -> failwith "Not Implemented"
            | Relative(_) -> failwith "Not Implemented"
        | _ -> failwith "not implemented"

    let (isotopeByBin:(int*float) list list) =
        bins
        |> Seq.choose(fun binStart ->
            let lowResBins =
                regionalD15N.Rows
                |> Seq.where(fun n -> n.Shrub = plant.Identifier.Value)
                |> Seq.where(fun n -
> n.BinLatest <= (binStart + 2) && n.BinOldest >= binStart)
                |> Seq.map(fun r -> (r.BinOldest, r.BinLatest, r.D15N))

            let highResBins =
                yuribeiD15N.Rows
                |> Seq.where(fun n -> n.``Plant Code`` = plant.Identifier.Value)
                |> Seq.where(fun n -
> n.Date.Year <= (binStart + 2) && n.Date.Year >= binStart)
                |> Seq.map(fun r -
> (r.Date.Year, r.Date.Year, (float r.``Predictor 2``) ))
```

```
            let allData =
                highResBins
                |> Seq.append lowResBins
                |> Seq.sortBy (fun (s,_,_) -> s)
                |> Seq.filter(fun (_,_,x) -> not <| System.Double.IsNaN x)

            if allData |> Seq.isEmpty then None
            else
                match highResBins |> Seq.length with
                | i when i >= 0 && i < 3 ->
                    try
                        let weightedAverage =
                            let weights =
                                let increments = allData |> Seq.map (fun (start,en,_)
 -> [ start .. en ] |> List.sumBy(fun y -
> growth |> TimeSeries.findExact (System.DateTime(y, 12, 31)) |> fst |> removeUnit ))
                                let totalIncrement = increments |> Seq.sum
                                increments |> Seq.map(fun i -> i / totalIncrement)
                            printfn "Weights are %A" weights
                            allData
                            |> Seq.zip weights
                            |> Seq.averageBy(fun (weight,(s,e,d15n)) -
> d15n * weight )
                        Some <| ([ binStart .. binStart + 2 ] |> List.map (fun y -
> y, weightedAverage))
                    with | _ -> None
                | _ ->
                    highResBins
                    |> Seq.map(fun (x,y,z) -> (x, z) )
                    |> Seq.toList
                    |> Some )
        |> Seq.toList
    List.concat isotopeByBin


let shrubs =
    rw
    |> List.filter(fun s -> regionalD15N.Rows |> Seq.exists(fun x -
> x.Shrub = s.Identifier.Value ) || yuribeiD15N.Rows |> Seq.exists(fun x -
> x.``Plant Code`` = s.Identifier.Value ))
    |> List.map(fun plant ->
        let isotope3Year =
            threeYearToAnnual plant
            //lowerResolution plant
            |> List.map (fun (x,y) -> (y, System.DateTime(x, 12, 31)))
            |> TimeSeries.fromObservations
        plant |> PlantIndividual.zipEnv (code "N") isotope3Year )

let shrubs2 =
    rw
    |> List.filter(fun s -> regionalD15N.Rows |> Seq.exists(fun x -
> x.Shrub = s.Identifier.Value ) || yuribeiD15N.Rows |> Seq.exists(fun x -
> x.``Plant Code`` = s.Identifier.Value ))
    |> List.map(fun plant ->
        let data = lowerResolution plant
        data
        |> List.map(fun (y,f) ->
            printfn "%s,%i,%f" plant.Identifier.Value y f
        ))
shrubs
|> List.map(fun x -
> printfn "[%s] Res = %A" x.Identifier.Value x.Environment.[code "N"].Resolution)
```

```
let getStartValues (startDate:System.DateTime) (plant:PlantIndividual) =
    let initialRadius =
        match plant.Growth with
        | PlantIndividual.PlantGrowth.RingWidth s ->
            match s with
            | GrowthSeries.Absolute c -> c.Head |> fst |> removeUnit
            | GrowthSeries.Cumulative c ->
                let start = (c |> TimeSeries.trimStart (startDate - System.TimeSpan.F
romDays(366.))).Values |> Seq.head |> removeUnit
                // printfn "Start cumulative growth = %f" start
                start
            | GrowthSeries.Relative _ -> invalidOp "Not implemented"
        | _ -> invalidOp "Not implemented 2"
    let initialMass = initialRadius |> removeUnit |> ModelComponents.Proxies.toBiomas
sMM
    let initialNitrogen = plant.Environment.[ShortCode.create "N"].Head |> fst
    let initialT = plant.Environment.[code "T[max]"] |> TimeSeries.findExact startDat
e |> fst
    [ (code "x", initialRadius)
      (code "N", initialNitrogen)
      (code "T[max]", initialT)
      (code "bs", initialMass) ] |> Map.ofList

let enforceMinimumRadius minSize plant =
    let bounded =
        match plant.Growth with
        | RingWidth rw ->
            match rw with
            | Cumulative g ->
                g
                |> TimeSeries.toObservations
                |> Seq.skipWhile (fun (x,_) -> x < minSize)
                |> TimeSeries.fromObservations
                |> Cumulative
            | _ -> invalidOp "Not implemented"
        | _ -> invalidOp "Not implemented"
    { plant with Growth = bounded |> RingWidth }

let tailGrowth plant =
    let bounded =
        match plant.Growth with
        | RingWidth rw ->
            match rw with
            | Cumulative g ->
                g
                |> TimeSeries.toObservations
                |> Seq.tail
                |> TimeSeries.fromObservations
                |> Cumulative
            | _ -> invalidOp "Not implemented"
        | _ -> invalidOp "Not implemented"
    { plant with Growth = bounded |> RingWidth }


// The `EstimationEngine` must be configured for each shrub:
// - Each shrub requires a custom starting condition based on its
//   time-series.
// - Each shrub requires clipping to a custom timebound before fitting.
let fit engine endCondition s hypothesis =
    let tMax =
        if s.Identifier.Value.Contains "S8"
```

```
        then summerTemperature |> Seq.find(fun (s,_) -
> s = "Hoseda Hard") // A Varandei shrub
        else summerTemperature |> Seq.find(fun (s,_) -
> s = "Marre Sale") // A Yamal shrub
    let shrub = s |> PlantIndividual.toCumulativeGrowth |> enforceMinimumRadius 1.53<
mm> |> PlantIndividual.zipEnv (code "T[max]") (snd tMax)
    // printfn "Shrub = %A" shrub
    let common = shrub |> tailGrowth |> PlantIndividual.keepCommonYears |> PlantIndiv
idual.zipEnv (code "T[max]") (snd tMax)
    // printfn "Common = %A" common
    let startDate = (common.Environment.[ShortCode.create "N"]).StartDate |> snd
    let startConditions = getStartValues startDate shrub
    let e = engine |> Bristlecone.withConditioning (Custom startConditions)
    Bristlecone.PlantIndividual.fit e endCondition hypothesis common

let saveLog (cLog:IComponentLogger<float>) (h:int) plantCode (guid:System.Guid) =
    let filePath = (sprintf "%sbristlecone-%s-%i-components-
%s.csv" Options.resultsDirectory plantCode h (guid.ToString()))
    if System.IO.File.Exists filePath then System.IO.File.Delete filePath
    use csv = System.IO.File.AppendText filePath
    let x = cLog.GetAll()
    for m in x do
        for ts in m.Value do
            csv.WriteLine (sprintf "%s,%f,%.16e" m.Key ts.Key ts.Value)

let workPackages shrubs hypotheses engine saveDirectory =
    seq {
        for s in shrubs do
            for h in [ 1 .. hypotheses |> List.length ] do
                for _ in [ 1 .. Options.chains ] do
                    yield async {
                            let result = fit engine Options.endWhen s (hypotheses.[h-
1] (PassThrough() :> IComponentLogger<float>)) |> fst
                            Bristlecone.Data.EstimationResult.saveAll saveDirectory s
.Identifier.Value h 100 result
                            return result }
    }

// Orchestrate the analyses
let work = workPackages (shrubs |> Seq.where(fun x -
> x.Environment.[code "N"].Resolution <> TemporalResolution.Variable)) hypotheses Opt
ions.engine Options.resultsDirectory
let run () =
    work |> Seq.iter (OrchestrationMessage.StartWorkPackage >> Options.orchestrator.P
ost)
```

Seasonal model with snow dynamics (Chapter 5)

```
#r "../packages/NETStandard.Library.NETFramework/build/net461/lib/netstandard.dll"
// #r "../packages/MathNet.Numerics.FSharp/lib/netstandard2.0/MathNet.Numerics.FSharp
.dll"
#load "../packages/Bristlecone/bristlecone.fsx"
#r "../packages/Bristlecone.Dendro/lib/netstandard2.0/bristlecone.Dendro.dll"

#load "components/components.fsx"
#load "components/temperature.fsx"
#load "components/snow.fsx"

//////////////////////////////////////////////////
/// Yamal Salix lanata Shrub - Nitrogen Interactions
//////////////////////////////////////////////////

open Bristlecone
open Bristlecone.ModelSystem
open Bristlecone.Dendro
open Bristlecone.Dendro.PlantIndividual
open Bristlecone.Workflow.Orchestration
open Bristlecone.Diagnostics.ModelComponents

// .NET Core requires this workaround to bind to MathNet. Hopefully will be fixed in
3.0 RTM.
let x = MathNet.Numerics.Random.MersenneTwister()

// 1. Configure Options
// ----------------------------

module Options =
    let resultsDirectory = "/Users/andrewmartin/Desktop/Bristlecone Results/Paper2-
Snow-Short-Reformulated4/"
    let endWhen = Optimisation.EndConditions.afterIteration 25000
    let chains = 1
    let thin = 50
    let engine =
        Bristlecone.mkContinuous
        |> Bristlecone.withContinuousTime Integration.MathNet.integrate
        // |> Bristlecone.withTunedMCMC [ Optimisation.MonteCarlo.TuneMethod.Covarian
ceWithScale 0.250, 500, Optimisation.EndConditions.afterIteration 75000 ]
        |> Bristlecone.withCustomOptimisation (Filzbach.filzbachCauchy
            { TuneAfterChanges = 50
              MaxScaleChange = 100.00
              MinScaleChange = 0.0010
              BurnLength = Optimisation.EndConditions.afterIteration 25000 })

    let orchestrator = OrchestrationAgent(engine.LogTo, System.Environment.ProcessorC
ount, false)
    let latitude = 68.91    // Yuribei North
    let longitude = -70.23  // Yuribei West
    let timezone = "Asia/Yekaterinburg"    // Yuribei is in Yekaterinburg Time


// 2. Create Hypotheses
// ----------------------------

module BaseEquations =

    let biomass b n r gammab geom f (protectionEffect:float) tempEffect lightEffect c
Log : float =

        cLog "stem" (b |> ModelComponents.Proxies.toRadiusMM |> ModelComponents.Proxi
es.shrubHeightCm)
        cLog "biomassGrowth" (b * r * (f n) * geom(b) * tempEffect * lightEffect)
        cLog "biomassLoss" (gammab * (1. - protectionEffect) * b)
```

```
        b * r * (f n) * geom(b) * tempEffect * lightEffect - gammab * (1. - protectio
nEffect) * b

    let soilNitrogen n b gamman y geom f feedback tempEffect lightEffect (protectionE
ffect:float) cLog : float =

        cLog "nReplenishment" y
        cLog "nUptake" (geom(b) * b * (f n) * tempEffect * lightEffect)
        cLog "nLoss" (gamman * n + feedback(b) * (1. - protectionEffect))

        y - (geom(b) * b * (f n) * tempEffect * lightEffect) - gamman * n + feedback(
b) * (1. - protectionEffect)

    // Newton's law of cooling / Fourier's law
    let soilTemperature soilT ambientT conductivity =
        if conductivity > 1. || conductivity < 0.05 then nan
        else - conductivity * (soilT - ambientT)


let ``base model`` maxGrowthRate nLimitation nitrogenFeedback nReplenishment protecti
onEffect temperatureDependency soilConductivity additionalParameters (cLog:IComponent
Logger<float>) ((startDate:System.DateTime),latitude,longitude,timeZone) =

    let limit p =
        match nLimitation p with
        | Some l -> l
        | None -> invalidOp "N limitation is required for this model."

    /// Light limitation effect (linear between 0 and 1).
    /// Light is cached in an object to avoid unnecessary computation.
    let lightFn = Sunrise.DayLengthCache(latitude, longitude, timeZone)
    let seasonalLight t =
        let date = startDate.AddMonths (int t)
        date |> lightFn.GetLight |> Sunrise.dayFraction

    /// Cumulative biomass [B].
    let dbsdt' (b:float) n gammab r maxGrowthRate limit protectionEffect tempEffect d
ayLength =
        BaseEquations.biomass b n (r * 1000.) gammab maxGrowthRate limit protectionEf
fect tempEffect dayLength

    /// Bioavailable soil nitrogen [N]
    let dndt' bs n gamman maxGrowthRate feedback limit nReplenishment tempEffect dayL
ength protectionEffect =
        BaseEquations.soilNitrogen n bs gamman nReplenishment maxGrowthRate limit fee
dback tempEffect dayLength protectionEffect

    /// Soil temperature [T_s]
    let dtsdt' ts ta conductivity =
        BaseEquations.soilTemperature ts ta conductivity

    /// Bristlecone function for dBs/dt
    let dbsdt p t bs (e:Environment) =

        cLog.StoreValue "protectionEffect" t ((protectionEffect p e)) |> ignore
        cLog.StoreValue "biomass" t bs |> ignore
        cLog.StoreValue "temperature-limit-on-
photosynthesis" t (temperatureDependency p e) |> ignore

        (dbsdt' bs ((lookup e "N") |> ModelComponents.Proxies.d15NtoAvailability)
            (p |> Pool.getEstimate "gamma[b]") (p |> Pool.getEstimate "r") (maxGrowth
Rate p) (limit p) (protectionEffect p e) (((temperatureDependency p e))) (seasonalLig
ht t)) (fun s f -> cLog.StoreValue s t f |> ignore)
```

```
    /// Bristlecone function for dN/dt
    let dndt p t n (e:Environment) =
        dndt' (lookup e "bs") (n |> ModelComponents.Proxies.d15NtoAvailability)
            (p |> Pool.getEstimate "gamma[n]") (maxGrowthRate p) (nitrogenFeedback p)
 (limit p) ((nReplenishment p e)) (temperatureDependency p e) (seasonalLight t) (prot
ectionEffect p e) (fun s f -> cLog.StoreValue s t f |> ignore)

    /// Bristlecone function for dTs/dt
    let dtsdt p t ts (e:Environment) =

        cLog.StoreValue "daylight" t (seasonalLight t) |> ignore
        cLog.StoreValue "conductivity" t (soilConductivity p e) |> ignore
        cLog.StoreValue "soilT" t (ts + (dtsdt' ts (lookup e "Tair") (soilConductivit
y p e))) |> ignore

        dtsdt' ts (lookup e "Tair") (soilConductivity p e)

    /// Measurement (Size) variable: stem radius
    let stemRadius lastRadius lastEnv env =
        let oldCumulativeMass = lookup lastEnv "bs"
        let newCumulativeMass = lookup env "bs"
        if (newCumulativeMass - oldCumulativeMass) > 0.
        then
            // This clause mandates that stem radius can never decrease.
            let newRadius = newCumulativeMass |> ModelComponents.Proxies.toRadiusMM
            if newRadius > lastRadius then newRadius else lastRadius
        else lastRadius

    /// Bristlecone function for dr/dt
    { Equations  = [ code "bs",        dbsdt
                     code "N",         dndt
                     code "Tsoil",     dtsdt ] |> Map.ofList
      Measures   = [ code "x",         stemRadius ] |> Map.ofList
      Parameters = [ code "lambda",    parameter PositiveOnly   0.050 0.500   // N-
replenishment rate
                     code "r",         parameter PositiveOnly   2.000 8.000   // Intr
insic growth rate
                     code "gamma[b]",  parameter PositiveOnly   0.001 0.010   // Loss
 rate of biomass
                     code "gamma[n]",  parameter PositiveOnly   0.001 0.010   // Loss
 rate of nitrogen
                     code "rho",       parameter Unconstrained  -
0.50 0.500   // Covariance between growth and nitrogen
                     code "sigma[x]",  parameter PositiveOnly   0.001 0.500   // Stan
dard deviation of x (biomass)
                     code "sigma[y]",  parameter PositiveOnly   0.001 0.500   // Stan
dard deviation of y (nitrogen)
                    ] |> List.append additionalParameters |> Map.ofList
      Likelihood = ModelLibrary.Likelihood.bivariateGaussian "x" "N" }

module NReplenishment =

    let linear lambda = lambda

    // let temperatureDependent a ea soilTemperature =
    //     ModelComponents.Temperature.arrhenius a ea soilTemperature

    /// The universal gas constant in J mol-1 K-1
    let gasConstant = 8.314

    /// An Arrhenius function to represent temperature limitation on growth.
    /// Form of equation from paper: https://pubag.nal.usda.gov/download/13565/PDF.
    /// Temperature limitation is between 0 and 1.
```

```
    /// When temperature increases above 25 degrees Celsius, temperature limitation =
 1.
    let temperatureLimitation preExp activationEnergy temperature =
        preExp * (min (System.Math.E ** ((1000. * activationEnergy * (temperature - 2
98.)) / (298. * gasConstant * temperature))) 1.)

// The snow protection function requires height, but this computes very slowly.
// Here is a lookup table to make this faster (only approximate).

let biomassToHeight' =
    let x = [ 1. .. 5. .. 100000. ] |> List.map (fun x -
> x, x |> ModelComponents.Proxies.toRadiusMM |> ModelComponents.Proxies.shrubHeightCm
)
    List.append x [(System.Double.MaxValue, nan)]

let biomassToHeight biomass =
    let h = biomassToHeight' |> List.tryFind(fun (b,_) -> b > biomass)
    match h with
    | Some h -> h |> snd
    | None -> nan

type NestedComponent<'value> = {
    Parameters: Parameter list
    Function: ParameterPool -> Environment -> 'value
}


let hypotheses =

    // [A] Snow insulates soils, which increases the efficiency of N-
mineralising microbes.
    let nitrogenReplenishment =
        [ // 1. Linear rate not affected by soil temperatures
          (fun p _ -> ModelComponents.Temperature.Conductivity.linear 1.),
          (fun p _ -
> ModelComponents.Temperature.NitrogenReplenishment.linear (p |> Pool.getEstimate "la
mbda")), []
          // 2. Temperature-dependent microbial activity
          (fun p _ -
> ModelComponents.Temperature.Conductivity.linear 1.), //ModelComponents.Temperature.
Conductivity.linear (p |> Pool.getEstimate "condct")),
          (fun p e -
> NReplenishment.temperatureLimitation (p |> Pool.getEstimate "lambda") (p |> Pool.ge
tEstimate "soilEa") (lookup e "Tsoil")),
            [ code "soilEa",        parameter PositiveOnly   5.000 10.00 ]
          // 3. Temperature-dependent microbial activity, with a snow-
insulation effect on soil temperatures
          (fun p e -
> ModelComponents.Temperature.Conductivity.snowConductivity (p |> Pool.getEstimate "c
ondct") (lookup e "snowDepth") ),
          (fun p e -
> NReplenishment.temperatureLimitation (p |> Pool.getEstimate "lambda") (p |> Pool.ge
tEstimate "soilEa") (lookup e "Tsoil")),
            [ code "soilEa",    parameter PositiveOnly   20.00 30.00
              code "condct",    parameter PositiveOnly   0.001 0.200 ] ]

    // [B] Increased snow levels protect shrub biomass from storm and other damage.
    let snowProtection =
        [ (fun _ _ -> ModelComponents.SnowProtection.none), []
          (fun p e -
> ModelComponents.SnowProtection.withShrubHeight (p |> Pool.getEstimate "spe") (looku
p e "bs" |> biomassToHeight) (lookup e "snowDepth")),
            [ code "spe",        parameter PositiveOnly   0.001 1.000 ] ]
```

```
    // [C] Net photosynthetic rate is temperature-dependent
    let temperature =
        [ (fun _ -> ModelComponents.Temperature.none), []
          (fun p e -
> NReplenishment.temperatureLimitation 1. (*(p |> Pool.getEstimate "A")*) (p |> Pool.
getEstimate "Ea") (lookup e "Tair")),
           [ //code "A",              parameter PositiveOnly 5.00 20.0
             code "Ea",             parameter PositiveOnly 30.00 40.00  ] ]

    // [D] N may limited growth via combined N-
limitations on (a) photosynthetic and (b) uptake rates
    let limitationModes =
        [ (fun p -
> ModelComponents.GrowthLimitation.hollingDiscModelDual ((p |> Pool.getEstimate "a")
/ 1000.) ((p |> Pool.getEstimate "r") * 1000.) ((p |> Pool.getEstimate "h") / 1.) 5.0
0),
           [ code "a",      parameter PositiveOnly   0.100 5.000          // N-
uptake efficiency
             code "h",      parameter PositiveOnly   0.001 0.250 ]
          (fun p -
> ModelComponents.GrowthLimitation.linear ((p |> Pool.getEstimate "a") / 1000.) 10.),

           [ code "a",      parameter PositiveOnly   0.010 0.100] ]       // N-
uptake efficiency

    // [E] Loss of plant material may feedback into the soil pool of available nitrog
en (instant)
    let feedbackModes =
        [ (fun p -
> ModelComponents.FeedbackToSoil.withBiomassLoss ((p |> Pool.getEstimate "alpha") / 1
00.) (p |> Pool.getEstimate "gamma[b]") ),
          [ code "alpha",  parameter PositiveOnly   0.001 0.002 ]
          (fun _ -> ModelComponents.FeedbackToSoil.none), [] ]    // N-
recycling efficiency

    // [F] A plant may be subject to mechanical constraints on its maximum size
    let geometricModes =
        [  (fun p -
> ModelComponents.GeometricConstraint.chapmanRichards ((p |> Pool.getEstimate "k") *
1000.)),
           [ code "k",  parameter PositiveOnly   3.00 5.00 ]
           (fun p -
> ModelComponents.GeometricConstraint.none), [] ]     // Asymptotic biomass (grams)

    // Create all combinations of H1-H5
    List.combine6 geometricModes feedbackModes limitationModes nitrogenReplenishment
snowProtection temperature
    |> List.map (fun ((growth,gp),(feedback,fp),(limit,lp),(conduct,replace,rp), (sno
w,sp), (temp,tp)) ->
        ``base model`` growth limit feedback replace snow temp conduct (List.concat [
lp; fp; gp; rp; sp; tp]))


// 3. Load Real Data and Estimate
// ------------------------------
// A. Daily air temperature data from Marre Sale weather station.
// B. Daily snow depth data from earth observation.

open FSharp.Data

[<Literal>]
let ClimateUrl = __SOURCE_DIRECTORY__ + "/../data/marre-sale-meantemp.csv"
[<Literal>]
let SnowUrl = __SOURCE_DIRECTORY__ + "/../data/yuribei-snow-depth.csv"
```

```
type DailyTemperature = CsvProvider<ClimateUrl>
type DailySnowDepth = CsvProvider<SnowUrl>

let monthlyTemperatures =
    let meanTemperatures = DailyTemperature.Load ClimateUrl
    meanTemperatures.Rows
    |> Seq.map(fun r -
> ( (if System.Double.IsNaN r.``T[avg]`` then None else Some (r.``T[avg]`` + 273.15))
, r.Date))
    |> TimeSeries.fromObservations
    |> TimeSeries.interpolate
    |> TimeSeries.generalise (Months 1) (fun x -> x |> Seq.averageBy fst)

let monthlySnow =
    let snowDepths = DailySnowDepth.Load SnowUrl
    snowDepths.Rows
    |> Seq.map(fun (r:DailySnowDepth.Row) -> (if  (float r.MeanSnowDepth) = -
9999. then None else Some <| float r.MeanSnowDepth), r.DATE)
    |> TimeSeries.fromObservations
    |> TimeSeries.interpolate // Need to interpolate dates
    |> TimeSeries.generalise (Months 1) (fun x -> x |> Seq.averageBy fst)

let growthMap fn plant =
    match plant with
    | RingWidth rw ->
        match rw with
        | Absolute rws -
> rws |> TimeSeries.toObservations |> Seq.map fn |> TimeSeries.fromObservations |> Ab
solute |> RingWidth
        | _ -> invalidOp "Not implemented"
    | _ -> invalidOp "Not implemented"

// b) Load shrub individual data + environment
let shrubs =
    let yuribei = Data.PlantIndividual.loadRingWidths (__SOURCE_DIRECTORY__ + "/../da
ta/yamal-rw.csv")
    let d15N = Data.PlantIndividual.loadLocalEnvironmentVariable (__SOURCE_DIRECTORY_
_ + "/../data/yuribei-d15N-imputed.csv")
    yuribei
    |> Seq.map (fun s -> s.Identifier.Value, s)
    |> Seq.keyMatch d15N
    |> Seq.map (fun (_,d15N,plant) ->
        // Custom: move RW and d15N measurements to end of September (from end of Dec
ember)
        let p = {plant with Growth = plant.Growth |> growthMap (fun (x,t) -
> (x, t - System.TimeSpan.FromDays 92.)) }
        let n = d15N |> TimeSeries.toObservations |> Seq.map(fun (x,t) -
> (x, t - System.TimeSpan.FromDays 92.)) |> TimeSeries.fromObservations
        PlantIndividual.zipEnv (code "N") n p
        |> PlantIndividual.zipEnv (code "Tair") monthlyTemperatures
        |> PlantIndividual.zipEnv (code "snowDepth") monthlySnow )
    |> Seq.toList


/// How to generalise `getStartValues` for Bristlecone or
/// Bristlecone.Dendro?
///
/// - A. Determine if start time - 1 (what time-
step?) is present. If so, use this. Otherwise, repeat start value.
/// - B. For PlantIndividual, must interpret the type of growth series.
/// - C. When doing allometric model, must set start mass as allometric transform.
let getStartValues (startDate:System.DateTime) (plant:PlantIndividual) =
    let initialRadius =
```

```
        match plant.Growth with
        | PlantIndividual.PlantGrowth.RingWidth s ->
            match s with
            | GrowthSeries.Absolute c -> c.Head |> fst |> removeUnit
            | GrowthSeries.Cumulative c ->
                let start = (c |> TimeSeries.trimStart (startDate - System.TimeSpan.F
romDays(366.))).Values |> Seq.head |> removeUnit
                printfn "Start cumulative growth = %f" start
                start
            | GrowthSeries.Relative _ -> invalidOp "Not implemented"
        | _ -> invalidOp "Not implemented 2"
    let initialMass = initialRadius |> removeUnit |> ModelComponents.Proxies.toBiomas
sMM
    let initialNitrogen = plant.Environment.[code "N"].Head |> fst
    let initialAirT = plant.Environment.[code "Tair"].Head |> fst
    let initialSnow = plant.Environment.[code "snowDepth"].Head |> fst
    [ code "x", initialRadius
      code "N", initialNitrogen
      code "Tair", initialAirT
      code "Tsoil", initialAirT
      code "snowDepth", initialSnow
      code "bs", initialMass ] |> Map.ofList

/// How to generalise the `fit` function?
/// - Start Date = common 'variables' (as opposed to environmental data). Codes can b
e got from ModelSystem.
/// - End Date = common 'variables' (as opposed to environmental data).
/// - Ensure that start values are present (at t-1, including for env variables).
let fit s hypothesis engine =
    let shrub = s |> PlantIndividual.toCumulativeGrowth
    let common =
        shrub
        |> PlantIndividual.keepCommonYears
    let startDate = (common.Environment.[code "N"]).StartDate |> snd
    let endDate = (common.Environment.[code "N"]) |> TimeSeries.endDate
    let shrubWithHighResEnvironment =
        common
        |> PlantIndividual.zipEnv (code "Tair") (monthlyTemperatures |> TimeSeries.bo
und (startDate - System.TimeSpan.FromDays 366.) endDate)
        |> PlantIndividual.zipEnv (code "snowDepth") (monthlySnow |> TimeSeries.bound
 (startDate - System.TimeSpan.FromDays 366.) endDate) // TODO Bristlecone should stan
dardise environmental time-series of varying length
    let startConditions = getStartValues startDate shrub
    let e = engine |> Bristlecone.withConditioning (Custom startConditions)
    Bristlecone.PlantIndividual.fit e Options.endWhen (hypothesis (startDate,Options.
latitude,Options.longitude,Options.timezone)) shrubWithHighResEnvironment

let setupHypothesis s hypothesis =
    let shrub = s |> PlantIndividual.toCumulativeGrowth
    let common = shrub |> PlantIndividual.keepCommonYears
    let startDate = (common.Environment.[code "N"]).StartDate |> snd
    hypothesis (startDate,Options.latitude,Options.longitude,Options.timezone)


/// Use this type in Bristlecone itself.
type WorkPackage = Async<EstimationResult>

/// How to generalise this function?
/// - It is just a nested set of commands.
let workPackages shrubs hypotheses engine saveDirectory =
    seq {
        for s in shrubs do
            for h in [ 1 .. hypotheses |> List.length ] do
                for _ in [ 1 .. Options.chains ] do
```

```
                    if h = 12 || h = 24 then
                        yield async {
                                let cLog = PassThrough()
                                let result = fit s (hypotheses.[h-1] cLog) engine
                                Bristlecone.Data.EstimationResult.saveAll saveDirecto
ry s.Identifier.Value h Options.thin (result |> fst)
                                return result |> fst }
    }

// Orchestrate the analyses
let shrubsWithIsotope = [ "YUSL03A"; "YUSL05A"; "YUSL26A"; "YUSL29A"; "YUSL39A" ]
let work = workPackages (shrubs |> Seq.where(fun s -
> shrubsWithIsotope |> List.contains s.Identifier.Value)) hypotheses Options.engine O
ptions.resultsDirectory |> Seq.toList

let run () =
    work |> Seq.map(fun x -
> x,System.Random().Next()) |> Seq.sortBy snd |> Seq.map fst |> Seq.iter (Orchestrati
onMessage.StartWorkPackage >> Options.orchestrator.Post)
```

Supporting Script: Components

```
module ModelComponents

#r "../../packages/Bristlecone/lib/netstandard2.0/Bristlecone.dll"
#load "constants.fsx"

open Bristlecone

let pi = System.Math.PI

module NiklasAndSpatz_Allometry =

    let nthroot n A =
        let rec f x =
            let m = n - 1.
            let x' = (m * x + A/x**m) / n
            match abs(x' - x) with
            | t when t < abs(x * 1e-9) -> x'
            | _ -> f x'
        f (A / double n)

    /// Gives the basal radius in centimeters of a stem/branch given its length in ce
ntimeters. Function from Niklas and Spatz (2004).
    /// The basal radius is always positive.
    let basalRadius k5 k6 stemLength =
        max (100. * (( 0.01 * stemLength + k6) / k5) ** (3. / 2.) / 2.) 1e-06

    /// Inverse equation of basalRadius, rearranged using Wolfram Alpha
    /// http://www.wolframalpha.com/input/?i=solve+r+%3D+100*((0.01*h%2Bk_6)%2Fk_5)%5
E(3%2F2)%2F2+for+h
    /// The stem length is always positive.
    let stemLength k5 k6 radius =
        max (2. * ((nthroot 3. 2.) * 5. ** (2./3.) * k5 * radius ** (2./3.) - 50. * k
6)) 1e-06

module Götmark2016_ShrubModel =

    /// Total shrub volume given height and number of stems
    let shrubVolume b a rtip p lmin k5 k6 n h =
```

```
        let radius = NiklasAndSpatz_Allometry.basalRadius k5 k6
        let mainStemVolume =
            match radius h with
            | r when r > rtip -
> n * pi * h * ((radius h) ** 2. + (radius h) * rtip + rtip ** 2.) / 3.
            | _ -> n * pi * h * rtip ** 2.

        let mutable volume = mainStemVolume
        let mutable k = 0.

        while (p ** k * h > lmin * 2./3.) do
            let volToAdd =
                match (p ** k * h < lmin) with
                | true ->
                    match (b * 3. * p * (p ** k * h - 2. * lmin / 3.) > rtip) with
                    | true ->
                        n * a * (a + 1.) ** (float k) * pi * 3. * p * (p ** k * h - 2
. * lmin / 3.) * ((radius (3. * p * (p ** k * h - 2. * lmin / 3.))) * (radius (3. * p
 * (p ** k * h - 2. * lmin / 3.)) * rtip + rtip ** 2.)) / 3.
                    | false ->
                        n * a * (a + 1.) ** (float k) * 3. * p * (p ** k * h - 2. * l
min / 3.) * pi * rtip ** 2.
                | false ->
                    match (radius (p ** (k + 1.) * h) > rtip) with
                    | true ->
                        n * a * (a + 1.) ** (float k) * pi * p ** (k + 1.) * h * ((ra
dius (p ** (k+1.) * h)) ** 2. + (radius (p ** (k + 1.) * h)) * rtip + rtip ** 2.) / 3
.
                    | false ->
                        n * a * (a + 1.) ** (float k) * p ** (k + 1.) * h * pi * rtip
 ** 2.

            volume <- volume + volToAdd
            k <- k + 1.

        k, volume


module Allometrics =

    open Götmark2016_ShrubModel

    let mass woodDensity volume =
        volume * woodDensity

    let massToVolume woodDensity mass =
        mass / woodDensity

    let shrubBiomass b a rtip p lmin k5 k6 n woodDensity radius =
        radius
        |> NiklasAndSpatz_Allometry.stemLength k5 k6
        |> shrubVolume b a rtip p lmin k5 k6 n |> snd
        |> mass woodDensity

    let shrubRadius b a rtip p lmin k5 k6 n woodDensity mass =
        let findRadius volume =
            let v x = x |> NiklasAndSpatz_Allometry.stemLength k5 k6 |> shrubVolume b
 a rtip p lmin k5 k6 n |> snd
            let f = (fun x -> (v x) - volume )
            Statistics.RootFinding.bisect 0 200 f 0.01 100.00 1e-
8 // Assumption that shrub radius is between 0.01 and 100.0cm.
        mass
        |> massToVolume woodDensity
```

```
        |> findRadius

    let shrubHeight k5 k6 radius =
        radius |> NiklasAndSpatz_Allometry.stemLength k5 k6


module GrowthLimitation =

    /// **Description**
    ///
    /// A function that represents the efficiency of two simultaneous
    /// processes. The combined processes have a single 'handling time',
    /// which represents the rate at which the processes occur.
    ///
    /// **Parameters**
    ///   * `a` - efficiency of process A
    ///   * `b` - efficiency of process B
    ///   * `h` - integrated handling time / rate of process A+B
    ///   * `min` - a level of resource at which the resultant process is `> 1e-12`
    let hollingDiscModelDual a b h min =
        Some <| fun r ->
            if (a * min) / (1. + (a * b * h * min)) < 1e-12 then nan
            else (a * r) / (1. + (a * b * h * r))

    /// A rearranged version of a Monod model that represents
    /// a single, saturating process.
    ///   * `a` - efficiency of the process
    ///   * `h` - handling time / rate of the process
    let hollingDiscModel a h min =
        Some <| fun r ->
            if (a * min) / (1. + (a * h * min)) < 1e-12 then nan
            else (a * r) / (1. + (a * h * r))

    let hollingSimple a h min =
        Some <| fun r ->
            if (a * min) / (1. + (h * min)) < 1e-12 then nan
            else (a * r) / (1. + (h * r))

    /// TEST: An integrated supply and use model
    let saturatingSupplySaturatingGrowth r a b h rootMass =
        Some <| fun resource -
> (a * r * rootMass * resource) / (1. + a * b * r * rootMass * resource + a * h * res
ource)

    /// Monod model once saturation has been reached
    let linear (a:float) min =
        Some <| fun r -> if a * min < 1e-12 then nan else a * r

    /// The resource enforces no limitation on growth, and is negated
    let none = None

    /// **Description**
    /// A monotonically increasing function of a resource `r`.
    /// **Parameters**
    ///   * `h` - soil resource concentration required for growth at half the maximum
 rate
    ///   * `r` - the current resource concentration
    let michaelisMenten h (r:float) =
        r / (h + r)

    /// From Jabot and Pottier 2012
    let monod k (r:float) =
        r / (k + r)
```

```
module AbioticResource =

    /// **Description**
    /// A standard chemostat-type model for replenshment of an abiotic resource.
    /// **Parameters**
    ///   * `d` - a rate constant
    ///   * `s` - resource concentration of the inflow
    ///   * `n` - the current resource concentration
    let chemostat d s (n:float) =
        d * (s - n)


module Proxies =

    /// Radius in millimetres
    let toBiomassMM radiusMM =
        radiusMM / 10. |> Allometrics.shrubBiomass Constants.Allometrics.b Constants.
Allometrics.a Constants.Allometrics.rtip Constants.Allometrics.p Constants.Allometric
s.lmin Constants.Allometrics.k5 Constants.Allometrics.k6 Constants.Allometrics.number
OfStems Constants.Allometrics.salixWoodDensity

    /// Biomass in grams.
    let toRadiusMM biomassGrams =
        if System.Double.IsNaN biomassGrams || System.Double.IsInfinity biomassGrams
|| System.Double.IsNegativeInfinity biomassGrams then nan
        else
            let radiusCm = biomassGrams |> Allometrics.shrubRadius Constants.Allometr
ics.b Constants.Allometrics.a Constants.Allometrics.rtip Constants.Allometrics.p Cons
tants.Allometrics.lmin Constants.Allometrics.k5 Constants.Allometrics.k6 Constants.Al
lometrics.numberOfStems Constants.Allometrics.salixWoodDensity
            radiusCm * 10.

    /// d15N to N availability. From Craine 2009, as shown in Craine 2015 (Plant and
Soil).
    /// Assuming d15N is a linear index of N availability, the minimum supported valu
e of d15N is -3.09, as 0 N availability.
    let d15NtoAvailability d15N =
        (100. * d15N + 309.) / 359.

    let shrubHeightCm radiusMM =
        radiusMM / 10. |> Allometrics.shrubHeight Constants.Allometrics.k5 Constants.
Allometrics.k6


module GeometricConstraint =

    /// Linear growth rate in dM/dt form.
    let none _ = 1.

    /// A dM/dt form of the von Bertalanffy monomollecular growth function, where M =
 mass.
    let vonBertalanffy k m =
        (k / m)

    /// The dM/dt form of the Chapman-Richards growth function, where M = mass.
    let chapmanRichards k m =
        (1. - (m / k))


module FeedbackToSoil =

    let none b : float = 0. * b
    let withBiomassLoss alpha gammab b : float = alpha * b * gammab
```

```
module Constants

module Allometrics =

    // Empirically-derived parameters:
    let k5 = 19.98239 // Allometric fit to Yamal shrub BD-
length data #1 (in centimetres)
    let k6 = 0.42092 // Allometric fit to Yamal shrub BD-
length data #2 (in centimetres)

    // Constants from the literature:
    let a = 2. // the number of child branches added to previous branches (including
the tops of the stems) for a shrub
    let p = 0.5 // the length of a child branch as a proportion of its parent branch/
stem
    let lmin = 20. //cm. the length at which a stem or branch gets child branches
    let rtip = 0.1 //cm. the radius of the outermost tip of a stem or branch
    let b = 0.0075 // the ratio of the basal radius of a stem or branch and its lengt
h
    let salixWoodDensity = 0.5 // g / cm3 (from internet)
    let numberOfStems = 2.2
```

```
module ModelComponents.SnowProtection

let none = 0.

let withShrubHeight (protectionEffect:float) shrubHeightCentimetres snowMass =
    (snowMass * protectionEffect) / (shrubHeightCentimetres + (snowMass * protectionE
ffect))

/// Fraction of the year that is snow-free
let snowCoverLimitsPhotosynthesis snowFreeDays =
    float snowFreeDays / 365.

let linear (protectionEffect:float) snowMass =
    protectionEffect * snowMass
```

```
module ModelComponents.Temperature

// NB The parameter A is our parameter 'r' or 'Q', hence its absence from the below e
quations.
let none _ = 1.
let linear a t = a * t

/// Activation energy is in KJ rather than J
let arrhenius a ea t = a * System.Math.E ** (- ((ea * 1000.) / (8.314 * t)))

/// The universal gas constant in J mol-1 K-1
let gasConstant = 8.314

/// An Arrhenius function to represent temperature limitation on growth.
/// Form of equation from paper: https://pubag.nal.usda.gov/download/13565/PDF.
/// Temperature limitation is between 0 and 1.
/// When temperature increases above 25 degrees Celsius, temperature limitation = 1.
let arrheniusAlt preExp activationEnergy temperature =
    preExp * (min (System.Math.E ** ((1000. * activationEnergy * (temperature - 298.)
) / (298. * gasConstant * temperature))) 1.)

module Soil =

    // Soil temperature is a function of a flux between summer and winter mean temper
atures.
    // The flux is moderated by a snow regulation factor.
    // Snow depth = snow mass / snow density.
    // BUT, here the density effect is collapsed down into the insulation factor, lea
ving one term to be estimated.

    /// See: 10.1002/2016JG003725
    let snowMassEffect insulationFactor snow =
        System.Math.E ** (-insulationFactor * snow)

    /// Fouriers Law for heat flux
    let localHeatFlux outsideTemp insideTemp conductivity : float =
        - conductivity * (outsideTemp - insideTemp)

module Conductivity =

    let linear conductivity = conductivity

    let snowConductivity insulationFactor snowDepth =
        snowDepth
        |> Soil.snowMassEffect insulationFactor


module NitrogenReplenishment =

    let linear lambda = lambda

    let temperatureDependent a ea conductivity summerTemp winterTemp =
        conductivity
        |> Soil.localHeatFlux summerTemp winterTemp // The temperature difference in
winter (with snow insulation effect)
        |> (fun heatFlux -> summerTemp + heatFlux)
        |> arrheniusAlt a ea

    let temperatureDependentSnowInsulation a ea insulationFactor snowMass summerTemp
winterTemp =
        snowMass
        |> Soil.snowMassEffect insulationFactor
        |> fun con -> temperatureDependent a ea con summerTemp winterTemp
```